ACS 11,360

AD A072656

THIS DOCUMENT IS BEST QUALITY PRACTICABLE.
THE COPY FURNISHED TO DDC CONTAINED A
SIGNIFICANT NUMBER OF PAGES WHICH DO NOT
REPRODUCE LEGIBLY.

LEVEL II

CLOSED LOOP FIRE CONTROL SYSTEM
FINAL REPORT

CONTRACT NO. DAAA25-74-C0609

DDC FILE COPY

THIS DOCUMENT IS BEST QUALITY PRACTICABLE.
THE COPY FURNISHED TO DDC CONTAINED A
SIGNIFICANT NUMBER OF PAGES WHICH DO NOT
REPRODUCE LEGIBLY.

AUG 10 1979

NOVEMBER 1976

PREPARED FOR

U.S. ARMY
FRANKFORD ARSENAL
PHILADELPHIA
PENNSYLVANIA

This document has been approved
for public release and sale; its
distribution is unlimited.

AUTHORS

W.S. ARMSTRONG
P. BRIGGS
G.C. QUON

GENERAL ELECTRIC

79 08 06 140

AIRCRAFT EQUIPMENT DIVISION BINGHAMTON, NEW YORK

DISCLAIMER NOTICE

THIS DOCUMENT IS BEST QUALITY
PRACTICABLE. THE COPY FURNISHED
TO DDC CONTAINED A SIGNIFICANT
NUMBER OF PAGES WHICH DO NOT
REPRODUCE LEGIBLY.

C

(6

CLOSED LOOP FIRE CONTROL SYSTEM

(9

FINAL REPORT

CONTRACT NO. DAAA25-74-C0609

(15)

(11 NOVEMBER 1976

(12) 224p.

DDC
AUG 10 1979
C

PREPARED FOR

U.S. ARMY
FRANKFORD ARSENAL
PHILADELPHIA
PENNSYLVANIA

This document has been approved for public release and sale; its distribution is unlimited.

AUTHORS

(10 W.S. ARMSTRONG
P. BRIGGS
G.C. QUON

GENERAL ELECTRIC Co.

AIRCRAFT EQUIPMENT DIVISION BINGHAMTON, NEW YORK

TABLE OF CONTENTS

Section Page

1.0 INTRODUCTION 1-1

2.0 SYSTEM FORMULATION 2-1
2.1 Overview 2-1
2.2 Summary of Kalman Estimator Characteristics 2-1
2.3 Operational Considerations 2-6
2.4 Design of the Partitioned Kalman Estimator for the CLFCS 2-15
2.5 Open Loop Fire Control Computation 2-59
2.6 Closed Loop Fire Control Computation 2-66

3.0 CLOSED LOOP FIRE CONTROL SOFTWARE 3-1
3.1 Overview 3-1
3.2 Organization 3-1
3.3 Page Zero Variables and Constants 3-3
3.4 Executive and Aircraft Estimator 3-3
3.5 Line of Sight Estimator Subroutine 3-5
3.6 Line of Sight Gain Subroutine 3-5
3.7 Open Loop Fire Control Subroutine 3-5
3.8 Closed Loop Fire Control Subroutine 3-6
3.9 Interrupt Service Subroutine 3-6
3.10 Air Data Subroutine 3-6
3.11 Flight Recorder Subroutine 3-12
3.12 CDC Debug Routine 3-16
3.13 Arithmetic Subroutines 3-17
3.14 Loader Routines 3-17
3.15 Variable Array Section 3-17

4.0 CLOSED LOOP FIRE CONTROL HARDWARE 4-1
4.1 Overview 4-1
4.2 Computer Interface Unit 4-5
4.3 Inertial Measurement Unit and Electronics 4-16

Accession For
NTIS GRA&I ☑
DDC TAB ☐
Unannounced ☐
Justification
By
Distribution/
Availability Codes
Dist | Avail and/or special
A

TABLE OF CONTENTS (Cont'd)

Section Page

5.0 FLIGHT TEST PLAN 5-1
5.1 Introduction 5-1
5.2 CLFCS Flight Test Philosophy 5-2
5.3 Recommendations for Flight Test Management 5-4
5.4 Overall System Performance Metric 5-11
5.5 Weapon System Deployment 5-12

6.0 CLFCS ACCEPTANCE TEST 6-1
6.1 Software Test Summary and Results 6-1
6.2 Simulation Method for Software Test 6-2
6.3 Demonstration of Closed Loop Function on Aircraft 6-11
6.4 Hardware Test of Computer Interface Unit 6-11
6.5 Alignment and Calibration of Inertial Measurement Unit 6-18

7.0 ELECTROMAGNETIC INTERFERENCE REPORT 7-1

7.1 Grounding System 7-1
7.2 Suppression Devices 7-3
7.3 Cable Design 7-4
7.4 Package Shielding 7-5
7.5 Special Circuits 7-5

8.0 RELIABILITY REPORT 8-1
8.1 Results 8-1
8.2 Assumptions 8-1
8.3 Discussion of Results 8-1
8.4 Analysis 8-2

Appendix

A Kalman Estimator Terminology, Process Equations and Computational Flow A-1
B Kalman Estimator Analysis Program (KEAP-II) B-1
C Helicopter Flight Path Simulation C-1
D Open and Closed Loop Fire Control Simulation D-1
E Safety Statement E-1

LIST OF ILLUSTRATIONS

Figure Page

2-1 Closed Loop Fire Control Software Organization 2-2

2-2 Illustration of Target Engagements Used for CLFCS Design and Analysis 2-13

2-3 Illustration of Acceleration Build-Up and Decay Function 2-14

2-4 Illustration of Coordinate Frames 2-16

2-5 First Order Gauss - Markov Process Relabionships 2-33

2-6 Aircraft Angular Velocity Estimation Uncertainty 2-53

2-7 Aircraft Linear Acceleration Uncertainty 2-54

2-8 Aircraft Linear Velocity Uncertainty 2-55

2-9 Vertical Axis Direction Uncertainty 2-56

2-10 Target State Estimator Performance Comparison Gain Updates 1/1 Frame Versus 1/5 Frame 2-58

2-11 Angular Strikepoint Error vs Range Error 2-67

2-12 Illustration of the Operation of the Modified Closed Loop Fire Control Algorithm 2-69

2-13 The Relationship Between Range Bias Error and Strikepoint Error - Horizontal Plane View 2-70

2-14 Closed Loop Fire Control Subroutine Sequence 2-73

3-1 Executive Flow in a Packed Format 3-3

3-2 Executive Flow Chart 3-4

3-3 CLFC Subroutine Flow Chart 3-7

4-1 CLFCS Aircraft Installation 4-2

4-2 Console Cabinet 4-3

4-3 Computer Interface Unit Functional Block Diagram 4-6

4-4 Computer Interface Unit 4-7

4-5 Inertial Measurement Unit 4-17

4-6 IMU Electronics Assembly 4-18

4-7 Gyro Block Diagram 4-20

4-8 Control Logic and Signal Generator 4-21

4-9 Timing and Control 4-23

4-10 Gyro Spin Motor Sequence 4-24

LIST OF TABLES (Cont'd).

Tables Page

2-26 Target State Estimator - Observation Noise Parameters 2-50
2-27 Ballistics of the M-56 Projectile.................................. 2-60
2-28 Average Projectile Velocity vs Time of Flight...................... 2-63
2-29 Verification of Open Loop Fire Control Accuracy 2-65
2-30 Backward Integration Algorithm 2-75

3-1 Memory Map 3-2
3-2 CLFC Subroutine Symbol Descriptions 3-8
3-3 Input Signals Services by Interrupt Routine 3-9
3-4 Air Data Scale Factors 3-10
3-5 Mode Zero Record 3-13
3-6 Mode 1 Record 3-15
3-7 Arithmetic Subroutines 3-17
3-8 General Electric Memory Loader 3-18
3-9 Frankford Arsenal Memory Loader 3-19

4-1 Analog Inputs 4-8
4-2 Discrete Inputs 4-10
4-3 I/O Channel Code Assignment 4-14
4-4 Interrupt Register Code.. 4-15
4-5 Summary of Gyro Characteristics 4-19
4-6 Summary of Accelerometer Characteristics 4-19

6-1 Accuracy Assessment for the Closed Loop Firing Burst 6-4
6-2 Verification of Open Loop Fire Control Accuracy 6-6
6-3 Verification of Closed Loop Algorithm 6-7
6-4 Fire Control Solution at Time T=24 Seconds Data Block #134_8 6-8
6-5 Fire Control Solution at Time T=27 Seconds Data Block #256_8 6-9
6-6 Fire Control Solution at Time T=30 Seconds Data Block #420_8 6-10
6-7 Analog Inputs 6-14
6-8 Simulated Gyro Input 6-15
6-9 Analog Input Test Settings 6-16

LIST OF TABLES

Tables Page

2-1 Survey of Aircraft State Estimator Design 2-3

2-2 Survey of Aircraft State Estimator Performance 2-3

2-3 Survey of Target State Estimator Design 2-4

2-4 Survey of Performance of Target State Estimator 2-5

2-5 Timing of Engagement Events - Pop Up/Standoff Attack Target Range = 5000 ft = 1524M 2-7

2-6 Observability of the Elevation Strikepoint Error Component. 2-10

2-7 Sight Train Limitation 2-10

2-8 Aircraft Performance Assumptions 2-11

2-9 Description of Engagements Assumed for Kalman Estimator Design and Simulation 2-12

2-10 Timing of Engagement Events - Veer-Off Attack 2-15

2-11 Aircraft State Estimator - True State Array 2-24

2-12 Aircraft State Estimator - Estimated State Array 2-25

2-13 Aircraft State Estimator - Observation Array 2-27

2-14 Aircraft State Estimator - State Transition Process 2-29

2-15 Aircraft State Estimator - State to Observation Conversion Process 2-31

2-16 Aircraft State Estimator - State Excitation Process 2-34

2-17 Aircraft State Estimator - Observation Noise Parameters. 2-37

2-18 Fixed Gun Estimator Design Methodology. 2-40

2-19 Listing of Selected Fixed Gain Elements for a Practicable Aircraft State Estimator Design 2-41

2-20 Target State Estimator - True State Array 2-43

2-21 Target State Estimator - Estimated State Array 2-44

2-22 Target State Estimator - Observation Array 2-44

2-23 Target State Estimator - Transition Process 2-46

2-24 Target State Estimator - State to Observation Conversion Process 2-47

2-25 Target State Estimator - State Excitation Process Parameters 2-48

LIST OF ILLUSTRATIONS (Cont'd).

Figure		Page
4-11	Pulse Torqued Loop and Spin Motor Drive	4-25
4-12	Three Level Contactor	4-26
5-1	Proposed Target/Flight Path Relationships	5-6
5-2	Proposed Target Engagement Alternatives	5-8
5-3	Target and Aircraft Coordinate Sets	5-10
5-4	Illustration of Three Potential System Comparison in the CLFCS Flight Test	5-11
5-5	Performance Histogram for a Generic Ensemble of Passes	5-13
6-1	Illustration of Check Problem Geometry	6-2
6-2	CLFCS Effectiveness	6-3
6-3	Software Test Information Path	6-5
6-4	CLFCS Test Set	6-12
6-5	Calibration and Alignment Test Setup	6-25
6-6	Yaw Gyro Average Counts/Rev. at 15°/Sec vs Temperature	6-30

LIST OF TABLES (Cont'd).

Tables		Page
6-10	Specified Results from A/D Inputs	6-17
6-11	Specified D/A Outputs	6-17
6-12	A/D Test Data - D. C. Inputs	6-19
6-13	A/D Test Data - Pitch and Roll, Positive Angles	6-20
6-14	A/D Test Data - Pitch and Roll, Negative Angles	6-21
6-15	A/D Test Data - Sightline Data, Zero Elevation Angle	6-22
6-16	A/D Test Data - Sightline Data, Non Zero Elevation Angle	6-23
6-17	D/A Converter Test Data - Lead Angle Outputs	6-24
6-18	IMU Data - One Revolution at Various Rates	6-27
6-19	IMU Data - Various Rates for 60 Second Intervals	6-28
6-20	Summary of Gyro Calibration Data	6-29
6-21	Summary of Gyro Alignment Data	6-29
6-22	IMU Data - Buffered Accelerometer Outputs (Volts)	6-31
8-1	Component Failure Rates for the Computer Interface Unit	8-5
8-2	Component Failure Rates for the IMU Electronics Assy	8-6
8-3	Component Failure Rates for the In[illegible]al Measurement Unit	8-7

Section 1
INTRODUCTION

The principal objective of the Closed Loop Fire Control System (CLFCS) program is to assess the feasibility of incorporating first burst strikepoint observations into the fire control solution for improved second burst effectiveness. Fundamentally, the problem is to deduce from a strikepoint observation at time t_2 the bias components of the fire control error which existed at the instant of firing, t_1, where $t_2 - t_1$ is an interval slightly greater than the projectile time of flight.

Among the specific sources of fire control bias error which the CLFCS concept seeks to reduce or eliminate are:

- Range estimation error,
- Velocity estimation error, including wind and target velocity
- Gun boresight error.

In general, the CLFCS is capable of removing any error component whose correlation time is long in comparison with the bullet time of flight.

The system which has been designed incorporates Kalman aircraft and target state estimators. These provide the basis for an optimized open loop firing solution and the accurate estimation of the true target sightline existing at the instant of strikepoint observation. This latter capability involves the interpolation between target sightings prior to and after the strikepoint sighting by means of the target state estimator transition process. The closed loop fire control function is thereby dependent upon the accurate linear and angular velocity outputs of the aircraft state estimator.

Should the tactical situation preclude the expenditure of the time required for a strikepoint error observation, the open loop fire control solution affords an improved effectiveness in comparison with existing AH-1 gunnery systems. This is mainly due to the superior measurement and estimation of aircraft velocity.

Section 2

FORMULATION OF THE CLOSED LOOP FIRE CONTROL SYSTEM

2.1 OVERVIEW

In agreement with the approach presented in the Technical Proposal (Reference 1), the system formulation consists of the following four segments:

- Aircraft state estimator
- Target state estimator
- Open loop fire control computations
- Closed loop fire control computations

The relationship among these is illustrated by Figure 2-1.

This section is organized into subsections which summarize the characteristics of the aircraft and target state estimators, review certain tactical considerations which provide a basis for CLFCS design, convey the details of the design and performance of the estimators, and set forth the details of the open and closed loop fire control computations.

2.2 SUMMARY OF KALMAN ESTIMATOR CHARACTERISTICS

2.2.1 AIRCRAFT STATE ESTIMATOR

Table 2-1 lists the prominent design features of the aircraft state estimator, and Table 2-2 gives an overall indication of its performance.

The output of the aircraft state estimator consists of 12 state variables describing the angular velocity, linear acceleration, linear velocity, and vertical axis direction in vehicle coordinates. It utilizes a constant gain matrix, which alleviates the computational burden on the CDC 469 processor in such a fashion that a full-up software capability exists immediately after power is applied (or restored after an interruption) to the CLFCS.

Table 2-2 conveys an appreciation for the overall performance of the aircraft state estimator. Both the input sensor errors and the estimator output errors are exprssed in terms of the resultant of the rms errors appearing in each of three axes of information. The error attenuation column places in evidence the fact that the estimator affords a significant improvement (over 2 to 1) in the critical aircraft linear velocity variable. A comparison of the performance of the aircraft state estimator with full Kalman gain computation with that of the fixed gain version reveals that the simplification to fixed gains increases the output errors by only about 10%.

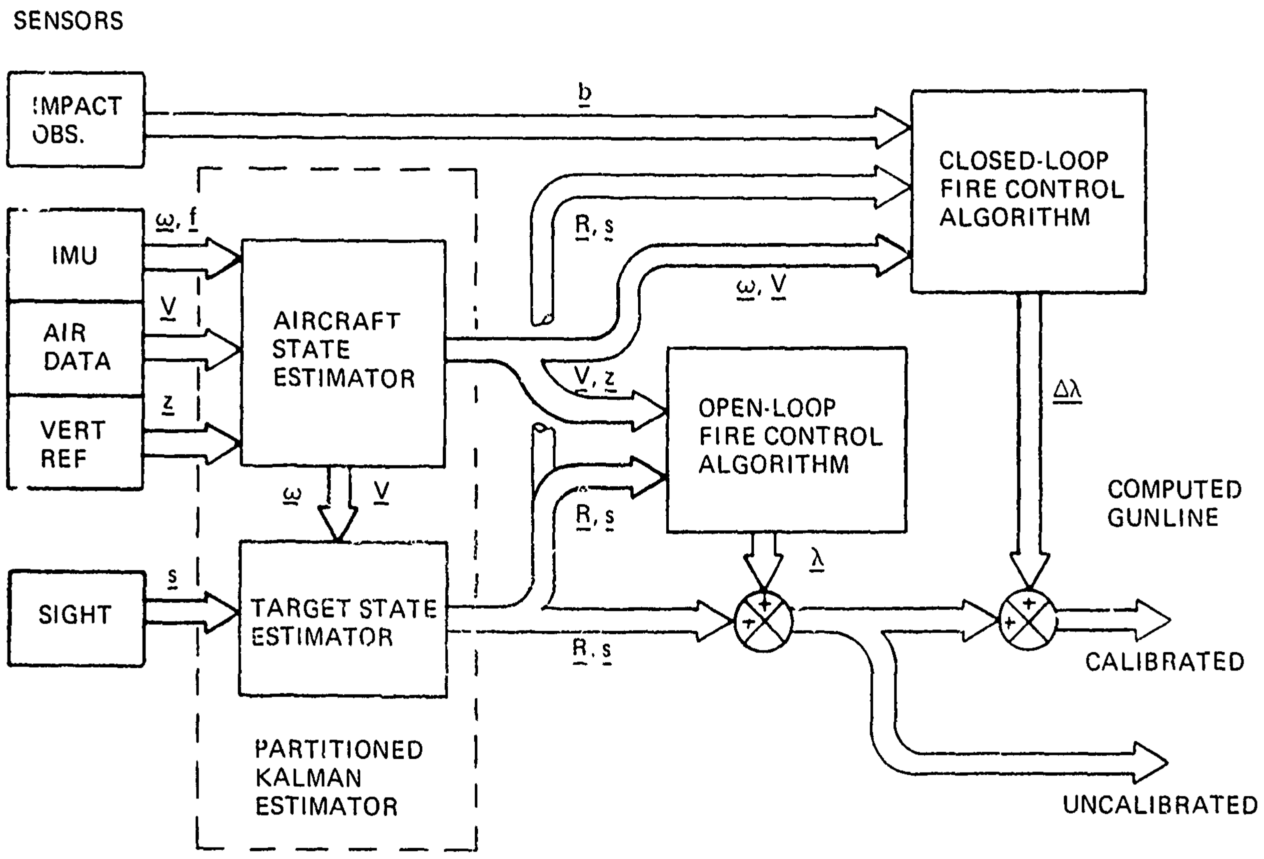

SENSORS
IMPACT OBS.
b
IMU
ω, f
AIR DATA
V
VERT REF
z
SIGHT
s
AIRCRAFT STATE ESTIMATOR
ω
V
TARGET STATE ESTIMATOR
PARTITIONED KALMAN ESTIMATOR
R, s
ω, V
V, z
R, s
R, s
CLOSED-LOOP FIRE CONTROL ALGORITHM
OPEN-LOOP FIRE CONTROL ALGORITHM
Δλ
λ
+
+
+
+
COMPUTED GUNLINE
CALIBRATED
UNCALIBRATED

Figure 2-1. Closed Loop Fire Control Software Organization

TABLE 2-1

SURVEY OF AIRCRAFT STATE ESTIMATOR DESIGN

TYPE - Fixed gain Kalman, 12 output state variables, 12 input observations

OUTPUT STATE VARIABLES

- Aircraft angular velocity
- Aircraft linear acceleration
- Aircraft linear velocity (inertially augmented airspeed)
- Vertical axis direction in aircraft coordinates

GAIN MATRIX

- Total of 31 gains
- Primary, diagonal gains - 12
- Off-diagonal gains - 19

TABLE 2-2

SURVEY OF AIRCRAFT STATE ESTIMATOR PERFORMANCE

State Information	Sensors	Sensor Errors	Output Errors*	Error Attenuation Ratio
Aircraft Angular Velocity	Rate Integrating Gyroscopes	1.22 mrad/sec	0.746 mrad/sec	1/1.64 = -4.3 dB
Aircraft Linear Acceleration	Linear Accelerometers	0.416 ft/sec^2	0.254 ft/sec^2	1/1.64 = -4.3 dB
Aircraft Linear Velocity	Air Data System	31.9 ft/sec	15.1 ft/sec	1/2.11 = -6.5 dB
Vertical Axis Direction	Pitch/Roll Gyro	33.9 mrad	11.8 mrad	1/2.87 = -9.2 dB

---

* All errors are resultant rms over three axes.

2.2.2 TARGET STATE ESTIMATOR

Tables 2-3 and 2-4 summarize the design features and performance of the target state estimator.

The target state estimator utilizes the full Kalman gain update algorithm, but operated at a rate of 6 updates per second in comparsion with the main frame rate of 30 per second. This allows the significant burden of the gain computations to be dispersed over 5 frames, thereby reducing the total amount of computation to be executed each frame. The sacrifice in performance is shown to be insignificant.

In the case of the target state estimator, the principal advantage of on-line Kalman gain computation is that it automatically accommodates the wide variations in target/aircraft geometries

TABLE 2-3

SURVEY OF TARGET STATE ESTIMATOR DESIGN

TYPE - Kalman with on-line gain computation, 4 output states, 6 auxiliary states, 3 input observations

OUTPUT STATE VARIABLES

- Estimated target line-of-sight direction cosines relative to aircraft coordinate frame.
- Range, based upon updating an initial pilot estimate by kinematic processes within the estimator.

GAIN MATRIX

- 10 rows, 3 columns - 30 elements.
- Execution of gain update algorithms distributed over 5 main frame iterations - i.e., 6 gain updates/sec.

TABLE 2-4

SURVEY OF PERFORMANCE OF TARGET STATE ESTIMATOR

State Information	Sensors	Sensor Errors	Output Errors	Error Attenuation Ratio
Los Direction Cosines	Pantographic Sight	9.80 mrad*	3.82 mrad*	1/2.56 = -8.2 dB
Range	None	500 ft**	410 ft	1/1.22 = -1.7 dB

---

* Los errors are resultant rms over three axes.

** Assumed error in initial estimate.

which are found to require significant adjustment in the gain values. The development of empirical adjustment rules for a set of fixed gains was found to be difficult and of questionable validity over the full operation envelope.

The target state estimator has 4 primary state variables describing the target line-of-sight (LOS) direction and range relative to a vehicle coordinate frame. The only observations are the LOS direction cosines so that the updating of range from an initial handset value is based upon kinematic processes within the target state estimator combined with the estimate of velocity furnished by the aircraft state estimator

Auxiliary state variables describe the error in the velocity output of the aircraft state estimator as a measure of the relative velocity of the aircraft with respect to a possibly moving target, and also the lowband errors in the pantographic sight direction cosines, which result largely from gunner tracking error.

Table 2-4 shows that the target state estimator is quite successful in attenuating the tracking error introduced by the gunner. The error attenuation ratio is about 2.5 to 1, in fact. This reflects directly into an improvement in gunnery effectiveness in comparison with existing AH-1 fire control systems, including the "J" version, which do not incorporate a target state estimator, but rather use the sight outputs in their unfiltered form.

2.3 OPERATIONAL CONSIDERATIONS

The designs of both the aircraft and target state estimators are based upon certain assumptions regarding the magnitudes of the linear and angular motions of the AH-1 aircraft during CLFCS deployment. Moreover, there are certain operational constraints which should be placed in evidence.

2.3.1 CLFCS DEPLOYMENT CONSTRAINTS

2.3.1.1 Nap-of-the-Earth Flight Environment

The evolution of armed helicopter tactics has progressed toward increased emphasis of the nap-of-the-earth (NOE) flight regime characterized by:

- 3 to 5 ft ground clearance
- Relatively low speed, below 60 knots in most cases
- Minimum exposure above foliation and terrain masks.

For strict adherence to the NOE flying doctrine, an obvious, but not necessarily appropriate, CLFCS deployment sequence would be as follows:

- NOE navigation to a selected attack point.
- Pop-up to an altitude barely sufficient to acquire the target LOS and at a range of about 5000 ft (1524 m).
- Fire a short, precisely aimed initial burst, observe the strikepoint and incorporate into the fire control solution.
- Fire one or more calibrated bursts.
- Assess target damage.
- Return to terrain/foliation mask and depart target area.

2.3.1.2 Exposure Time

Table 2-5 imparts some appreciation for the probable timing of the above listed engagement events. The long exposure time to enemy air defenses is obvious. A reduction in range to

TABLE 2-5

TIMING OF ENGAGEMENT EVENTS - POP-UP/STANDOFF ATTACK

TARGET RANGE = 5000 FT = 1524 M

0	Pop-up from terrain/foliation mask
5	Gunner handsets range estimate, acquires precise target track, depresses trigger for initial, short firing burst (time-of-flight ≈ 3 sec).
6	Trigger released.
8	First round impacts target area. Gunner breaks target track and begins to acquire burst controid.
9	Last round impacts.
10	Gunner completes burst centroid acquisition and keys CLFCS computer for incorporation of strikepoint error into fire control solution.
12	Gunner reacquires target, depresses trigger for calibrated firing burst.
14	Trigger released.
15	First round impacts.
17	Last round impacts. Gunner assesses damage.
20	Aircraft returns to terrain/foliation mask and departs target area.

4000 ft (1219 m) reduces the time-of-flight to about 2 sec, and hence the overall duration of the engagement to 18 sec. However, the vulnerability to enemy air defense systems is increased. Increasing the range to 6000 ft (1829 m) increases the time-of-flight to about 4 sec and the duration of the engagement to 22 sec. This degrades the effectiveness of the M-56 20 mm round and does not significantly alter the vulnerability of the aircraft.

It might be proposed that the aircraft return to mask between the two firing bursts, but this would often prevent the gunner from accurately observing the bullet strikepoints, due, for example, to the merging or movement of the dust, smoke, or debris. Also, if the target area is well foliated or marshy, the gunner must actually perceive the impacts as they occur since there is no persistent indication of their location. Accordingly, we feel that there is no alternative to the aircraft remaining exposed during the entire engagement episode.

2.3.1.3 The Observation of the Elevation Strikepoint Error Component

A second problem to be recognized is the difficulty of observing the elevation component of the strikepoint error from very low altitudes with respect to the target. Assuming as a case typical of the NOE flight environment that the aircraft and target are at the same altitude, the M-56 20 mm projectile angle of fall at 5000 ft range is about 4.4°. This means that a 500 ft range error, considered typical for the initial handset estimate, would produce a 39 ft strikepoint error in elevation - sufficient to cause the projectile to entirely miss the target, falling short or long by the amount of the range error, assuming an otherwise perfect fire control solution. But, if the aircraft and target are co-altitude, this very substantial strikepoint error would not be observable unless the target were located on a hillside.

In general, there appear to be two alternative solutions to this problem:

- Measure range with a laser and thereby reduce the range uncertainty to 50 ft or less, and the resulting elevation strikepoint error to 4 ft or less.
- Operate at a significant altitude above the target - about 10% of slant range is found to be an appropriate altitude advantage.

In that the prototype CLFCS does not include a rangefinder, it is recommended that the second approach be incorporated into the flight test plan. This will permit the elevation component of the strikepoint error to be observed and the appropriate compensation for it to be incorporated into the calibrated burst fire control solution. However, it is also recommended that future versions of the CLFCS include a laser rangefinder so as to facilitate operation in the NOE environment.

2.3.1.4 Limited Train Capability of the Pantographic Sight

Use of the pantographic sight at train angles above 50° from the aircraft's longitudinal reference axis becomes difficult and uncomfortable. An upper limit to the sight train angle is understood to be 80° (not to be confused with the mechanical limit of 110°). This limitation restricts the aircraft maneuvers which may be executed during a target engagement.

2.3.1.5 Summary of Target Engagement Assumptions

The key target engagement assumptions, which bear upon the design of the prototype CLFCS and its deployment in future flight tests, are now summarized.

Although the pop-up/standoff engagement described in Section 2.3.1.1 and Table 2-5 adheres to the NOE flying doctrine, the 20 sec exposure time in hovering flight and within the effective range of a potential enemy air defense threat appears to unnecessarily compromise aircraft survivability. Therefore, the CLFCS has been designed to accommodate reasonable linear and angular motions of the aircraft during the target engagement, subject, of course, to the train limitation of the pantographic sight. Although the flight test of the CLFCS should include hovering attacks, offset straight-line and veer-off attacks may also be utilized.

Tables 2-6 and 2-7 summarize the considerations of aircraft altitude above the target for elevation strikepoint observability and of the sight train limitation. The aircraft and target state estimators have been designed and simulated for offset straight-line and veer-off courses in which the altitude of the aircraft above the target is 500 ft or more and the maximum resultant angle between the LOS and the aircraft's longitudinal reference axis is about 85°; this angle includes both the elevation and train components.

2.3.2 AIRCRAFT PERFORMANCE ASSUMPTIONS

Table 2-8 summarizes the assumptions made relative to the aircraft linear and angular motions which could occur during an attack episode. These are based upon the premise that the tactical use of the CLFCS could involve the maintenance of a substantial aircraft velocity to counteract the prolonged exposure to a potential air defense threat.

Although the simulated target engagements used in the process of designing the aircraft and target state estimators are based upon the assumptions listed in Table 2-8, this in nowise precludes the use of hover attacks as part of the prototype CLFCS flight test.

TABLE 2-6

OBSERVABILITY OF THE ELEVATION STRIKEPOINT ERROR COMPONENT

ALTITUDE ADVANTAGE OF AIRCRAFT RELATIVE TO TARGET

- The altitude of the aircraft above the target = H
- The slant range = R
- To render the elevation component of bullet impact error observable, $(H/R) > 0.10$

JUSTIFICATION

- ΔE = Elevation impact error - Angular miss
- ΔR = Range impact error - Linear miss
- $\Delta E \approx \left(\frac{\Delta R}{R + \Delta R}\right) E \approx \left(\frac{\Delta R}{R + \Delta R}\right) \left(\frac{H}{R}\right)$
- With $\left(\frac{\Delta R}{R + \Delta R}\right) = \left(\frac{H}{R}\right) = 0.1$, $\Delta E = 0.010$ rad, which is marginally observable

TABLE 2-7

SIGHT TRAIN LIMITATION

SPECIFICATION OF THE LIMITATION

- The train angle between the longitudinal reference axis of the aircraft and the target LOS should not exceed 80° during CLFCS deployment.

IMPLICATION - Restricted Target Engagement Options

- Pop-up/stand-off at 5-6 kft - High vulnerability to AA attack
- Veer-off engagement with long range/low angle-off target acquisition - Fire control problem for AA made more difficult, aircraft/target separation increased at end of engagement - veer-off must be delayed and must be very mild to accommodate sight limit.

TABLE 2-8

AIRCRAFT PERFORMANCE ASSUMPTIONS

APPLICABILITY - Approach to attack point, attack, and escape from target area.

AIRCRAFT STATE VARIABLES

- Nominal Aircraft Velocity = 200 ft/sec = 118.5 knots
- Maximum Aircraft Velocity = 250 ft/sec = 148.1 knots
- Nominal Aircraft Attitude: Roll = 0°
  Pitch = -6°
- Maximum Load Factor = 2 g's
- Maximum Angular Velocities: Roll = 40 deg/sec
  Pitch = 10 deg/sec
  Yaw = 15 deg/sec

2.3.3 DESCRIPTION OF TARGET ENGAGEMENTS

The straight-line and veer-off engagements selected for use in the design and analysis of the aircraft and target state estimators are described in Table 2-9 and illustrated in Figure 2-2. The particular manner in which these were used is discussed in detail in Section 2.4.

As indicated in Table 2-9, the build-up and decay of aircraft acceleration in the veer-off attack is not abrupt. Rather, it follows an exponential function which is illustrated Figure 2-3. This is believed to simulate the procedure the pilot would use to implement a direction change.

A plausible CLFCS deployment episode is portrayed in Table 2-10, which lists the time, range, and total LOS angle (essentially the resultant of elevation and train) for each of the key engagement events. Time is calculated from the initiation of the engagement, as shown in Figure 2-2.

TABLE 2-9

DESCRIPTION OF ENGAGEMENTS ASSUMED FOR KALMAN ESTIMATOR DESIGN AND SIMULATION

STRAIGHT-LINE COURSE - Used for design

- Initial target range = 10 kft
- Initial target angle = 10°
- Constant velocity = 200 ft/sec
- Constant altitude = 500 ft

VEER-OFF COURSE - Used for simulation

- Same initial conditions as straight-line course - Velocity heading = -10°
- At 22.5 sec initiate climbing veer-off away from target with exponential build-up of path curvature and longitudinal acceleration
- At 32.5 sec initiate roll-out into straight, climbing flight path with exponential decay of acceleration
- Outgoing leg - velocity = 240 ft/sec, Heading = -51°, Climb angle = 21°

In Sections 2.5.3 and 2.6.5 a compressed version of the engagement episode described by Table 2-10 is utilized for verification of the open and closed loop fire control algorithms. In it the first firing burst occurs at 24 sec and the second, at 30 sec. These firing times are selected so that both bursts occur during the period of significant aircraft angular velocity.

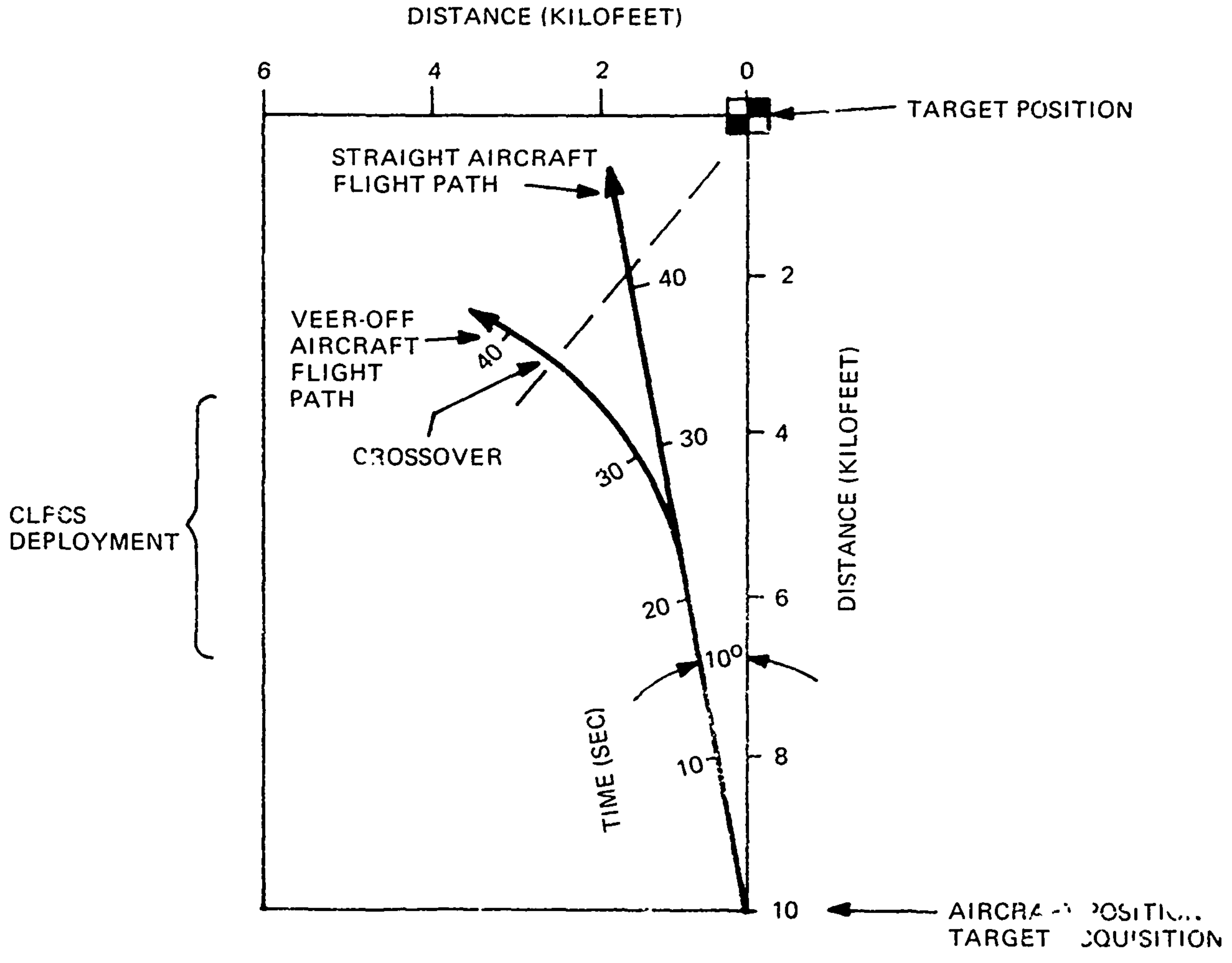
DISTANCE (KILOFEET)
6
4
2
0
TARGET POSITION
STRAIGHT AIRCRAFT FLIGHT PATH
40
2
VEER-OFF AIRCRAFT FLIGHT PATH
40
CROSSOVER
30
4
30
DISTANCE (KILOFEET)
CLFCS DEPLOYMENT
20
6
10°
TIME (SEC)
10
8
10
AIRCRA POSITI
TARGET QUISITION

Figure 2-2. Illustration of Target Engagements Used for CLFCS Design and Analysis

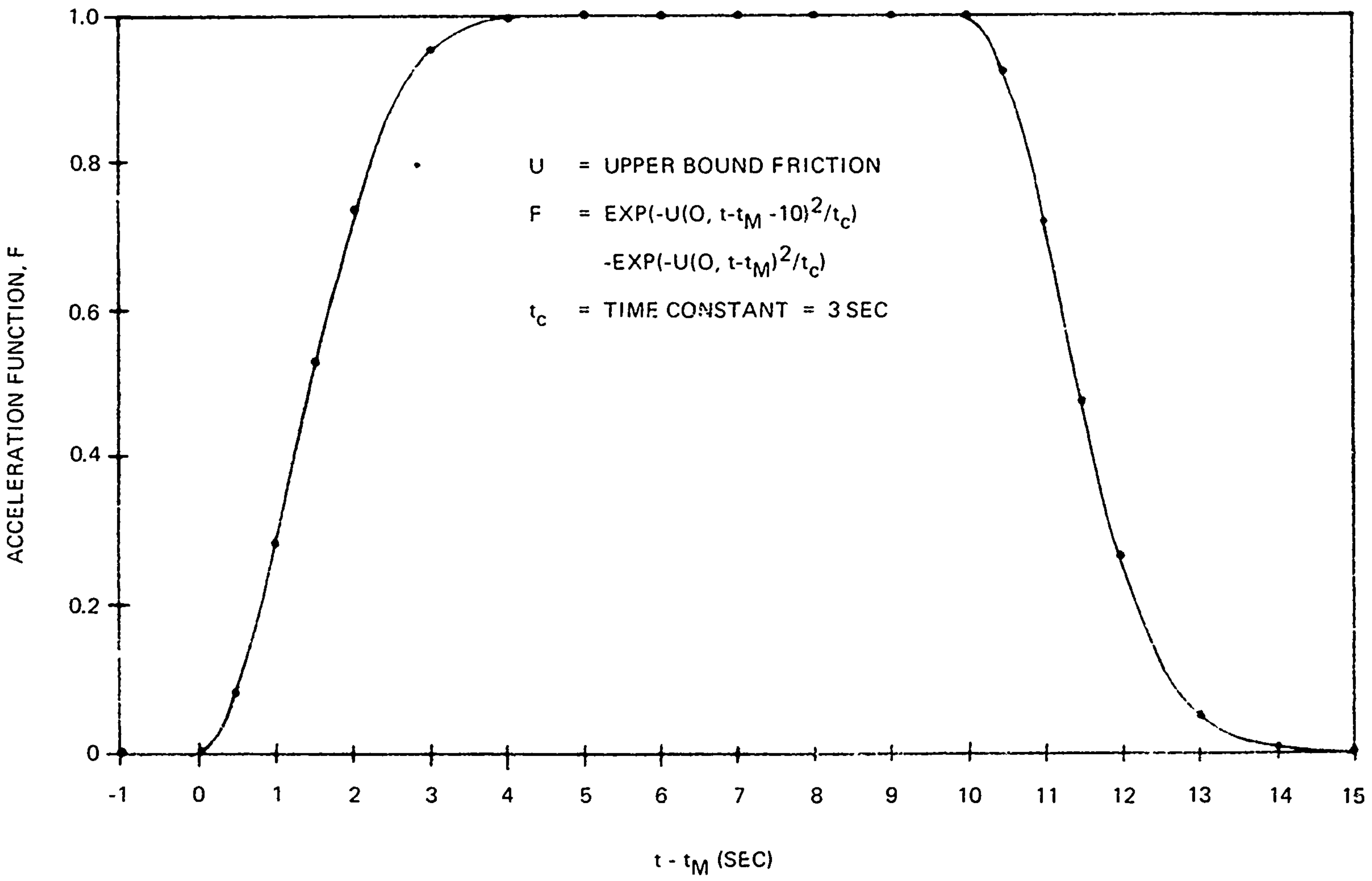

Figure 2-3. Illustration of Acceleration Build-Up and Decay Function

TABLE 2-10

TIMING OF ENGAGEMENT EVENTS - VEER-OFF ATTACK

Time (Sec)	Range (Kft)	Total Los Angle (Deg)	Event
20	6.12	16.5	Trigger depressed for uncalibrated open-loop firing burst. Time-of-flight ≈ 4 sec.
21	5.93	17.0	Trigger released.
24	5.36	19.8	First round impacts.
25	5.18	23.4	Last round impacts.
26	5.00	28.2	Gunner breaks target track.
28	4.66	39.1	Gunner acquires burst centroid.
30	4.38	51.2	Gunner reacquires target.
31	4.27	57.7	Trigger depressed for calibrated firing burst. Time-of-flight ≈ 2 sec.
33	4.11	71.3	Trigger released. First round impacts.
35	4.05	85.3	Last round impacts.

2.4 DESIGN OF THE PARTITIONED KALMAN ESTIMATOR FOR THE CLFCS

2.4.1 COORDINATE FRAMES

The three coordinate frames utilized in the mathematical formulation of the CLFCS are illustrated in Figure 2-4. They are defined below.

2.4.1.1 Pseudo-Geographic Reference Coordinate Frame

The pseudo-geographic reference coordinate frame is defined as a matter of convenience for the purpose of developing the basic dynamic relationships for the aircraft and target state transition processes. Its axes are

$\underline{x}$ = Horizontal azimuth reference axis (e.g., North)
$\underline{y}$ = Horizontal axis orthogonal to $\underline{x}$ (e.g., West)
$\underline{z}$ = Vertical axis pointing upward ($\underline{z} = \underline{x} \times \underline{y}$)

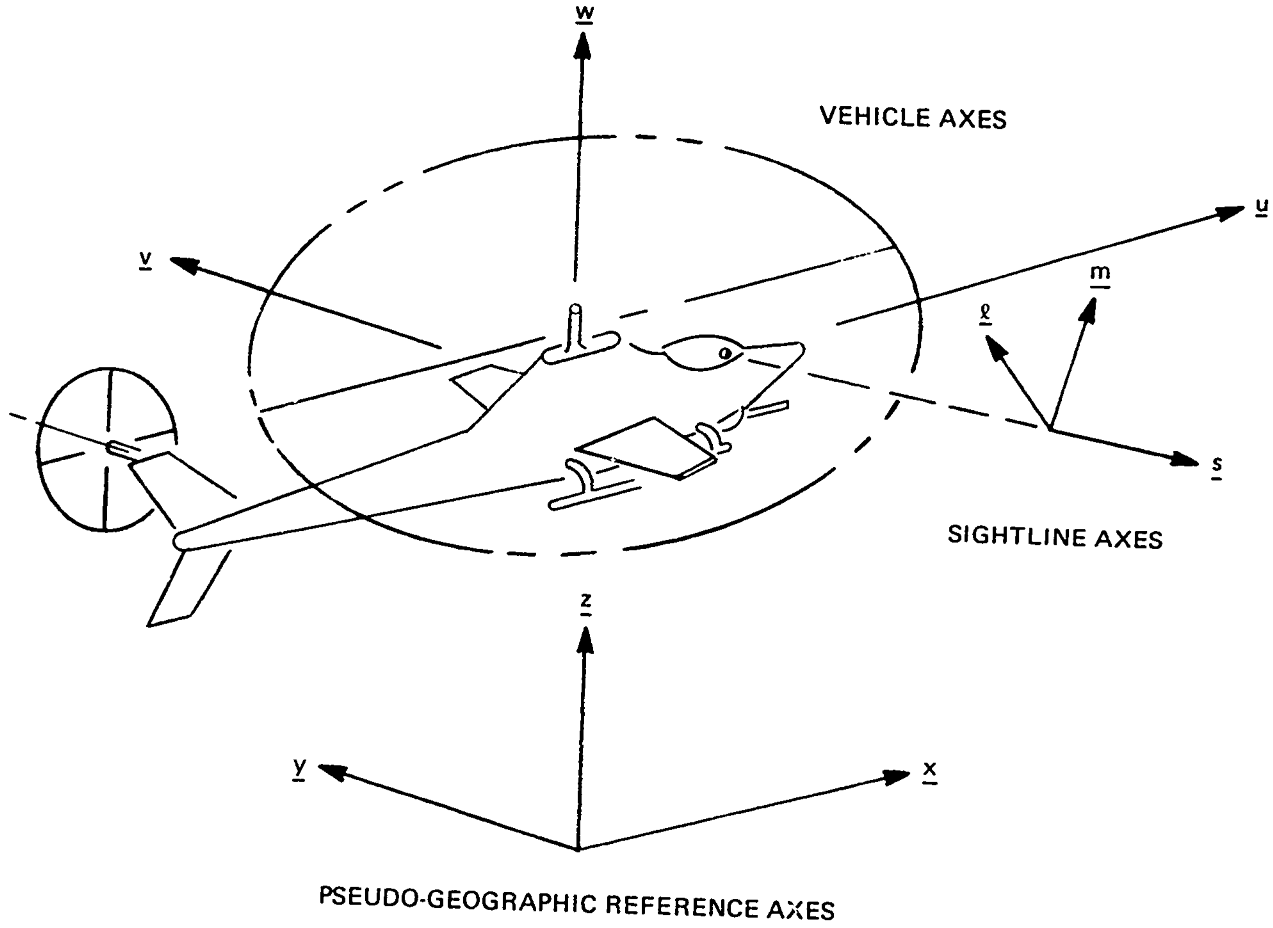
w
VEHICLE AXES
u
v
m
ℓ
s
SIGHTLINE AXES
z
y
x
PSEUDO-GEOGRAPHIC REFERENCE AXES

Figure 2-4. Illustration of Coordinate Frames

The effect of gyro bias drift and earth rate are considered insignificant in the CLFCS, which means that $\underline{x}\ \underline{y}\ \underline{z}$ need not be defined as an absolute inertial reference frame. In the case of an aircraft moving at 200 ft/sec, a two-earth rate angular velocity uncertainty (30^0/hr) contributes a 0.39 ft. uncertainty in aircraft position after 20 seconds. As will be shown in the sequel, the aircraft state estimator incorporates terms which compensate for the relatively large angular velocity uncertainties resulting from gyro misalignment.

2.4.1.2 Vehicle Coordinate Frame

This is the principal coordinate frame in the CLFCS formulation. Its axes are defined as follows.

$\underline{u}$ = Longitudinal reference axis.

$\underline{v}$ = Lateral axis in the plane of the aircraft's deck, orthogonal to $\underline{u}$, and extending to the left.

$\underline{w}$ = Normal axis, mutually perpendicular to $\underline{u}$ and $\underline{v}$, and extending upward.

All sensor information is furnished to the aircraft and target state estimators in the vehicle coordinate frame. In particular, the sensor elements of the CLFCS inertial measurement unit (IMU) are aligned to $\underline{u}$, $\underline{v}$, and $\underline{w}$. Indeed, the sensitive axes of the IMU represent the physical embodiment of the $\underline{u}\ \underline{v}\ \underline{w}$ axis set.

2.4.1.3 Sightline Coordinate Frame

Although the pantographic sight does not possess definite gimbal axes, it is helpful in describing the motion of the LOS to establish a sightline axis set. Let

$\underline{s}$ = Unit vector along the LOS

$\underline{\ell}$ = The effective elevation gimbal axis of the LOS, orthogonal to $\underline{s}$, lying in the $\underline{u}$ - $\underline{v}$ plane, and extending to the left.

$\underline{m}$ = The effective traverse gimbal axis of the LOS; $\underline{m} = \underline{s} \times \underline{\ell}$.

2.4.2 FUNDAMENTAL DYNAMIC RELATIONSHIPS

The transition processes for the aircraft and target state estimators are based upon dynamic relationships which describe the most probable behavior of the aircraft and target. These are now developed for each of the principal elements of state.

2.4.2.1 Aircraft Angular Velocity

In the case of a fixed wing aircraft, a strong coupling exists between the angular and linear motion states because the behavior of the aircraft is essentially coordinated - that is, changes in the direction of the velocity vector are implemented by altering the magnitude and direction of the lift vector, with lateral acceleration maintained close to zero. This coupling can be exploited so as to improve the estimation of aircraft state. Although the behavior of a helicopter at a significant velocity (i.e., above 40 knots) is similar to that of a fixed wing aircraft, it seems inappropriate to assume coordination, since at lower velocities the helicopter pilot can implement sideward and backward translations without rotating the aircraft. Hence, for the sake of accommodating all possible flight conditions, the design of the aircraft state estimator is based upon the proposition that the angular and linear motion states of the helicopter can vary independently.

According to this assumption, the output of each of the IMU gyros is regarded as correct, except for a lowband error process. The Kalman filter develops estimates of each of these errors rather than the entire amount of the angular velocity. The sum of the estimated error and the associated gyro output then represents the angular velocity of the aircraft.

To further articulate this arrangement, let the following be defined.

$\omega_{u\,v\,w}$ = True aircraft angular velocity vector

$\hat{\omega}_{u\,v\,w}$ = Estimated value of $\omega_{u\,v\,w}$

$\tilde{\omega}_{u\,v\,w}$ = Measured value of $\omega_{u\,v\,w}$; i.e., the outputs of the IMU gyros

$\Delta\omega_{u\,v\,w}$ = $\omega_{u\,v\,w} - \tilde{\omega}_{u\,v\,w}$

= The error in the IMU gyro readings

$\Delta\hat{\omega}_{u\,v\,w}$ = Estimated value of $\Delta\omega_{u\,v\,w}$

The Kalman filter develops values for the components of $\Delta\hat{\omega}_{u\,v\,w}$. These are then added to the measured components outside of the filter loop to reconstruct the total angular velocity estimate.

$$\hat{\omega}_{u\,v\,w} = \tilde{\omega}_{u\,v\,w} + \Delta\hat{\omega}_{u\,v\,w} \tag{1}$$

2.4.2.2 Aircraft Linear Acceleration

An arrangement similar to that described in Section 2.4.2.1 is used for the estimation of aircraft linear acceleration. Let the following be defined.

$a_{u\,v\,w}$ = True aircraft linear acceleration

$\hat{a}_{u\,v\,w}$ = Estimated value of $a_{u\,v\,w}$

$z_{u\,v\,w}$ = True vertical axis direction relative to $\underline{u}\ \underline{v}\ \underline{w}$

$\hat{z}_{u\,v\,w}$ = Estimated value of $z_{u\,v\,w}$

$f_{u\,v\,w}$ = True specific force from the IMU accelerometers

= $-a_{u\,v\,w} - g\,z_{u\,v\,w}$

$\tilde{f}_{u\,v\,w}$ = Measured specific force

$\Delta f_{u\,v\,w}$ = $f_{u\,v\,w} - \tilde{f}_{u\,v\,w}$

= The error in the IMU accelerometer readings

$\Delta\hat{f}_{u\,v\,w}$ = Estimated value of $\Delta f_{u\,v\,w}$

The actual output of the Kalman filter is $\Delta\hat{f}_{u\,v\,w}$. Reconstruction of $\hat{a}_{u\,v\,w}$ is according to

$$\hat{a}_{u\,v\,w} = -\tilde{f}_{u\,v\,w} - g\,\hat{z}_{u\,v\,w} - \Delta\hat{f}_{u\,v\,w} \tag{2}$$

and takes place outside of the filter loop

2.4.2.3 Aircraft Linear Velocity

Updating the aircraft linear velocity in the rotating $\underline{u}\ \underline{v}\ \underline{w}$ coordinate frame involves the estimated values of both the angular velocity and linear acceleration. In addition to the variables defined above in Section 2.4.2.1 and 2.4.2.2., let

$\hat{V}_{u\,v\,w}$ = Estimated aircraft velocity, which is actually inertially augmented airspeed.

$\dfrac{d\hat{V}_{u\,v\,w}}{dt}$ = The derivative of $\hat{V}_{u\,v\,w}$ as computed in the rotating $\underline{u}\ \underline{v}\ \underline{w}$ frame.

The velocity transition process is based upon the relationship

$$\frac{d\hat{V}_{uvw}}{dt} = a_{uvw} - \hat{\omega}_{uvw} \times \hat{V}_{uvw} \tag{3}$$

In this equation, $\hat{a}_{uvw}$ represents the acceleration of the aircraft relative to the reference $\underline{x}\,\underline{y}\,\underline{z}$ coordinate frame, but as expressed in terms of its $\underline{u}\,\underline{v}\,\underline{w}$ components. The term $(\hat{\omega}_{uvw} \times \hat{V}_{uvw})$ represents the apparent velocity change which is produced by the rotation of the $\underline{u}\,\underline{v}\,\underline{w}$ axis set.

Given a value for $\hat{V}_{uvw}(t)$, the value at time $t + \Delta t$ is, to a first-order approximation,

$$\hat{V}_{uvw}(t + \Delta t) = \hat{V}_{uvw}(t) + \Delta t \left[\hat{a}_{uvw}(t) - \hat{\omega}_{uvw}(t) \times \hat{V}_{uvw}(t)\right] \tag{4}$$

2.4.2.4 Vertical Axis Direction

Since the vertical axis direction remains constant relative to the reference $\underline{x}\,\underline{y}\,\underline{z}$ coordinate frame, its apparent rate of change in the $\underline{u}\,\underline{v}\,\underline{w}$ axis set is due only to the rotation of $\underline{u}\,\underline{v}\,\underline{w}$. Following the same pattern as in Section 2.4.2.3, let

$$\frac{d\hat{z}_{uvw}}{dt} = \text{The derivative of } \hat{z}_{uvw} \text{ as computed in the rotating } \underline{u}\,\underline{v}\,\underline{w} \text{ frame.}$$

Then

$$\frac{d\hat{z}_{uvw}}{dt} = -\hat{\omega}_{uvw} \times \hat{z}_{uvw} \tag{5}$$

The transition from time t to time $t + \Delta t$ is approximated by

$$\hat{z}_{uvw}(t + \Delta t) = \hat{z}_{uvw}(t) - \Delta t \left[\hat{\omega}_{uvw}(t) \times \hat{z}_{uvw}(t)\right] \tag{6}$$

2.4.2.5 Line-of-Sight Direction and Range

Beyond its role as part of the target state estimator, the transition process for LOS direction and range is important for two reasons.

- It perpetuates the estimate of target state through periods of obscuration.

- It perpetuates the estimate of target state through periods of gunner closed loop fire control activity.

As exhibited by Tables 2-5 and 2-10, there will be an interval of several seconds during an engagement when the gunner is perceiving the centroid of the burst strikepoints, acquiring this point with the pantographic sight, signalling the computer when burst acquisition has been accomplished, and reacquiring the target. It is conceivable that at any point during this period the need for continued fire on the target may arise. The target state estimator and CLFCS fire control computations are so designed that a viable fire control solution exists at all times during the engagement. This assures that the gun is continuously aimed, according to the best estimate of target position, regardless of whether the gunner is tracking the target at any particular instant.

The expected value of target velocity is zero. Hence, the rate of change of target LOS direction and range, as expressed in the $\underline{u}\ \underline{v}\ \underline{w}$ vehicle coordinate frame, is determined by aircraft linear and angular velocity, as established by the aircraft state estimator. Provision is made for stochastic quantities which describe the error between the estimated aircraft velocity and the true velocity of the aircraft relative to the target.

In addition to the variables defined above in Sections 2.4.2.1 through 2.4.2.4, let the following be defined.

$\underline{R}$ = Position vector of the target relative to the aircraft; with $|\underline{R}| = R$, we may say that $\underline{R} = R\,\underline{s}$.

$\Delta \underline{V}$ = Pseudo target velocity.

$\frac{d\underline{R}}{dt}$ = Derivative of the components of $\underline{R}$ in the rotating $\underline{u}\ \underline{v}\ \underline{w}$ coordinate frame.

Concerning the pseudo target velocity, if $\underline{V}^*$ is the velocity of the aircraft relative to a possibly moving target, then

$$\underline{V}^* = \hat{\underline{V}} - \Delta \underline{V} \tag{7}$$

where we recall that $\hat{\underline{V}}$ is the estimated aircraft velocity, being actually the inertially augmented airspeed.

The rate of change of $\underline{R}$ in the rotating $\underline{u}\ \underline{v}\ \underline{w}$ coordinate frame is given by

$$\frac{d\underline{R}}{dt} = -\underline{V}^{*} - \underline{\omega} \times \underline{R}$$

With

$$\underline{R} = R\,\underline{s}$$

and

$$\dot{R} = -\underline{V}^{*} \cdot \underline{s}$$

then the rate of change in $\underline{s}$ is given by

$$\frac{d\underline{s}}{dt} = -\frac{\underline{V}^{*} + \dot{R}\underline{s}}{R} - \underline{\omega} \times \underline{s} \tag{8}$$

Converting equation (8) into a transition equation for the estimate of LOS direction in $\underline{u}\ \underline{v}\ \underline{w}$ coordinates, we have the following:

$$V^{*}_{u\,v\,w}(t) = \hat{V}_{u\,v\,w}(t) - \Delta \hat{V}_{u\,v\,w}(t) \tag{9}$$

$$\dot{R}(t) = -V^{*}_{u\,v\,w}(t) \cdot \hat{s}_{u\,v\,w}(t) \tag{10}$$

$$\hat{s}_{u\,v\,w}(t+\Delta t) = \hat{s}_{u\,v\,w}(t) - \Delta t \left[\frac{V^{*}_{u\,v\,w}(t) + \dot{R}(t)\,\hat{s}_{u\,v\,w}(t)}{\hat{R}(t)} + \hat{\omega}_{u\,v\,w}(t) \times \hat{s}_{u\,v\,w}(t) \right] \tag{11}$$

The accompanying transition equation for range is

$$\hat{R}(t+\Delta t) = \hat{R}(t) + \Delta t\, \dot{R}(t) \tag{12}$$

2.4.3 KALMAN ESTIMATION NOMENCLATURE AND PROCESS EQUATIONS

The Kalman estimator formulation employed in the design of the aircraft and target state estimators is essentially that of Nahi, Reference 1. Appendix A sets forth all the generally applicable nomenclature, process equations, computational flow, and block diagrams. The particulars of the estimator designs are given in Sections 2.4.4 and 2.4.5 below.

The elements of the formulation of the aircraft and target state estimators include specifications for the following:

- The true state array
- The estimated state array
- The observation array
- The state transition process
- The state to observation conversion process
- The state excitation process
- The observation noise process
- The initial state vector and estimation error covariance values
- The generation of the gain matrix

The exposition of both the aircraft and target state estimators will follow this outline.

The results of the analysis of the estimator designs is presented in Section 2.4.6. This analysis has been accomplished using versions of the Kalman Estimator Analysis Program (KEAP II) described in Appendix B.

2.4.4 AIRCRAFT STATE ESTIMATOR DESIGN

2.4.4.1 True State Array

The true state array in this case describes the actual flight condition of the helicopter. This is in contrast to the estimated state array, which describes the approximate flight condition as developed from sensor readings. The 12 elements of the true state array are defined in Table 2-11.

2.4.4.2 Estimated State Array

The composition of the estimated state array differs in two important respects from that of the true state array:

- State variables 1 through 6 represent the estimated values of the lowband errors in the gyro and accelerometer readings rather than the angular velocity and linear acceleration components as in Table 2-11.

- The estimated state array includes auxiliary variables required for the generation of lowband observation noise components.

The elements of the estimated state array are defined in Table 2-12. The auxiliary state variables 13 through 24 are required only during the process of designing the fixed gain aircraft estimator; they are not present in the operational CLFCS as mechanized in the CDC 469 computer.

TABLE 2-11.

AIRCRAFT STATE ESTIMATOR - TRUE STATE ARRAY

$x_1 = \omega_u =$ Angular velocity about $\underline{u}$ (mrad/sec)

$x_2 = \omega_v =$ Angular velocity about $\underline{v}$ (mrad/sec)

$x_3 = \omega_w =$ Angular velocity about $\underline{w}$ (mrad/sec)

$x_4 = a_u =$ Linear acceleration along $\underline{u}$ (ft/sec^2)

$x_5 = a_v =$ Linear acceleration along $\underline{v}$ (ft/sec^2)

$x_6 = a_w =$ Linear acceleration along $\underline{w}$ (ft/sec^2)

$x_7 = V_u =$ Velocity along $\underline{u}$ (ft/sec)

$x_8 = V_v =$ Velocity along $\underline{v}$ (ft/sec)

$x_9 = V_w =$ Velocity along $\underline{w}$ (ft/sec)

$x_{10} = z_u =$ Vertical axis direction cosine along $\underline{u}$ (mrad)

$x_{11} = z_v =$ Vertical axis direction cosine along $\underline{v}$ (mrad)

$x_{12} = z_w =$ Vertical axis direction cosine along $\underline{w}$ (mrad)

TABLE 2-12.

AIRCRAFT STATE ESTIMATOR - ESTIMATED STATE ARRAY

Principal State Variables

$\hat{x}_1 = \Delta\hat{\omega}_u =$ Estimated value of the lowband error in the measurement of ω_u (mrad/sec)

$\hat{x}_2 = \Delta\hat{\omega}_v =$ Estimated value of the lowband error in the measurement of ω_v (mrad/sec)

$\hat{x}_3 = \Delta\hat{\omega}_w =$ Estimated value of the lowband error in the measurement of ω_w (mrad/sec)

$\hat{x}_4 = \Delta\hat{f}_u =$ Estimated value of the lowband error in the measurement of the specific force along the u axis (ft/sec^2)

$\hat{x}_5 = \Delta\hat{f}_v =$ Estimated value of the lowband error in the measurement of the specific force along the v axis (ft/sec^2)

$\hat{x}_6 = \Delta\hat{f}_w =$ Estimated value of the lowband error in the measurement of the specific force along the w axis (ft/sec^2)

$\hat{x}_7 = \hat{V}_u =$ Estimated value of V_u (ft/sec)

$\hat{x}_8 = \hat{V}_v =$ Estimated value of V_v (ft/sec)

$\hat{x}_9 = \hat{V}_w =$ Estimated value of V_w (ft/sec)

$\hat{x}_{10} = \hat{z}_u =$ Estimated value of z_u (mrad)

$\hat{x}_{11} = \hat{z}_v =$ Estimated value of z_v (mrad)

$\hat{x}_{12} = \hat{z}_w =$ Estimated value of z_w (mrad)

Auxiliary State Variables

$\hat{x}_{13} = \delta\omega_u =$ Lowband observation noise on the measurement of ω_u (mrad/sec)

$\hat{x}_{14} = \delta\omega_v =$ Lowband observation noise on the measurement of ω_v (mrad/sec)

$\hat{x}_{15} = \delta\omega_w =$ Lowband observation noise on the measurement of ω_w (mrad/sec)

TABLE 2-12 (Continued)

$\hat{x}_{16} = \delta f_u =$ Lowband observation noise on the measurement of the specific force component along $\underline{u}$ (ft/sec^2)

$\hat{x}_{17} = \delta f_v =$ Lowband observation noise on the measurement of the specific force component along $\underline{v}$ (ft/sec^2)

$\hat{x}_{18} = \delta f_w =$ Lowband observation noise on the measurement of the specific force component along $\underline{w}$ (ft/sec^2)

$\hat{x}_{19} = \delta V_u =$ Lowband observation noise on the measurement of V_u (ft/sec)

$\hat{x}_{20} = \delta V_v =$ Lowband observation noise on the measurement of V_v (ft/sec)

$\hat{x}_{21} = \delta V_w =$ Lowband observation noise on the measurement of V_w (ft/sec)

$\hat{x}_{22} = \delta z_u =$ Lowband observation noise on the measurement of z_u (mrad)

$\hat{x}_{23} = \delta z_v =$ Lowband observation noise on the measurement of z_v (mrad)

$\hat{x}_{24} = \delta z_w =$ Lowband observation noise on the measurement of z_w (mrad)

2.4.4.3 Observation Array

The composition of the observation array is similar to that of the true state array. Its elements are defined in Table 2-13.

In the case of the IMU gyro outputs, it is convenient to employ the angular increment turned about a given axis rather than the angular velocity because the gyros are equipped with digital, pulse torqued readout circuits.

TABLE 2-13.

AIRCRAFT STATE ESTIMATOR - OBSERVATION ARRAY

$y_1 = \tilde{\theta}_u =$ Angular increment about $\underline{u}$ corresponding to a measurement of the quantity $\omega_u \Delta t$ (mrad/frame)

$y_2 = \tilde{\theta}_v =$ Angular increment about $\underline{v}$ corresponding to a measurement of the quantity $\omega_v \Delta t$ (mrad/frame)

$y_3 = \tilde{\theta}_w =$ Angular increment about $\underline{w}$ corresponding to a measurement of the quantity $\omega_w \Delta t$ (mrad/frame)

$y_4 = \tilde{f}_u =$ Specific force along $\underline{u}$ corresponding to a measurement of $(-a_u - gz_u)$ (ft/sec^2)

$y_5 = \tilde{f}_v =$ Specific force along $\underline{v}$ corresponding to a measurement of $(-a_v - gz_v)$ (ft/sec^2)

$y_6 = \tilde{f}_w =$ Specific force along $\underline{w}$ corresponding to a measurement of $(-a_w - gz_w)$ (ft/sec^2)

$y_7 = \tilde{V}_u =$ Measurement of V_u (ft/sec)

$y_8 = \tilde{V}_v =$ Measurement of V_v (ft/sec)

$y_9 = \tilde{V}_w =$ Measurement of V_w (ft/sec)

$y_{10} = \tilde{z}_u =$ Measurement of z_u (mrad)

$y_{11} = \tilde{z}_v =$ Measurement of z_v (mrad)

$y_{12} = \tilde{z}_w =$ Measurement of z_w (mrad)

2.4.4.4 State Transition Process

Referring to Appendix A, the generalized, nonlinear state process is characterized by the matrix equation

$$\underline{x}_{k+1} = \Phi(\underline{x}_k) + B\ \underline{u}_k \tag{13}$$

The state transition process, Φ, is a set or vector of equations operating on the present state at iteration k to yield a forecasted state for iteration k + 1. The partial derivatives of Φ with respect to the elements of $\underline{x}$ and evaluated at $\underline{x}_k$ comprise the state transition matrix, A (see Appendix A, Section A.1). This matrix constitutes a linearized description of the behavior of the system in the region of state space close to the point $\underline{x}_k$. As seen in Appendix A, Section A.2, the state transition matrix is required for the propagation of covariance as part of the gain computation. Its elements may either be determined by explicitly differentiating the transition process equations or by numerical differentiation. The former approach was utilized in the CLFCS program.

The transition process equations are listed in Table 2-14. Note that x_1^* through x_6^* are dummy variables which reconstruct the components of ω_{uvw} and a_{uvw} for use in subsequent transition equations. The terms in curly brackets are elements of the vector $B\underline{u}$; they are not part of the transition process, but are included to show how the disturbance process, $\underline{u}$, enters into the various elements of state. The mathematical name of each variable and its units are listed as part of Table 2-14.

The action of the aircraft state estimator can cause the estimate of the vertical axis vector, $\hat{z}_{uvw}$, to depart from unit value. The selected technique for maintaining $|z_{uvw}| = 1$ is to normalize it near the close of each computer frame. The following equations are utilized:

$$Q = 1000/\sqrt{\bar{x}_{10}(k+1)^2 + \bar{x}_{11}(k+1)^2 + \bar{x}_{12}(k+1)^2}$$

$$\bar{x}_{10}(k+1) = Q\ \bar{x}_{10}(k+i)$$

$$\bar{x}_{11}(k+1) = Q\bar{x}_{11}(k+1)$$

$$\bar{x}_{12}(k+1) = Q\ \bar{x}_{12}(k+1)$$

TABLE 2-14

AIRCRAFT STATE ESTIMATOR - STATE TRANSITION PROCESS

$\bar{x}_1(k+1) = (1 - \alpha_1 \Delta t)\,\hat{x}_1(k) + \{\alpha_1 \Delta t\ u_1\}$	- $\Delta\hat{\omega}_u$ (mrad/sec)
$\bar{x}_2(k+1) = (1 - \alpha_1 \Delta t)\,\hat{x}_2(k) + \{\alpha_1 \Delta t\ u_2\}$	- $\Delta\hat{\omega}_v$ (mrad/sec)
$\bar{x}_3(k+1) = (1 - \alpha_1 \Delta t)\,\hat{x}_3(k) + \{\alpha_1 \Delta t\ u_3\}$	- $\Delta\hat{\omega}_w$ (mrad/sec)
$\bar{x}_4(k+1) = (1 - \alpha_2 \Delta t)\,\hat{x}_4(k) + \{\alpha_2 \Delta t\ u_4\}$	- $\Delta\hat{f}_u$ (ft/sec^2)
$\bar{x}_5(k+1) = (1 - \alpha_2 \Delta t)\,\hat{x}_5(k) + \{\alpha_2 \Delta t\ u_5\}$	- $\Delta\hat{f}_v$ (ft/sec^2)
$\bar{x}_6(k+1) = (1 - \alpha_2 \Delta t)\,\hat{x}_6(k) + \{\alpha_2 \Delta t\ u_6\}$	- $\Delta\hat{f}_w$ (ft/sec^2)
$x_1^* = \hat{x}_1(k) + y_1(k)/\Delta t$	- $\hat{\omega}_u$ (mrad/sec)
$x_2^* = \hat{x}_2(k) + y_2(k)/\Delta t$	- $\hat{\omega}_v$ (mrad/sec)
$x_3^* = \hat{x}_3(k) + y_3(k)/\Delta t$	- $\hat{\omega}_w$ (mrad/sec)
$x_4^* = -\hat{x}_4(k) - y_4(k) - 32.17\ \hat{x}_{10}(k)/1000.$	- $\hat{a}_u$ (ft/sec^2)
$x_5^* = -\hat{x}_5(k) - y_5(k) - 32.17\ \hat{x}_{11}(k)/1000.$	- $\hat{a}_v$ (ft/sec^2)
$x_6^* = -\hat{x}_6(k) - y_6(k) - 32.17\ \hat{x}_{12}(k)/1000.$	- $\hat{a}_w$ (ft/sec^2)
$\bar{x}_7(k+1) = \hat{x}_7(k) + \Delta t\,(x_4^* - (x_2^*\,\hat{x}_9(k) - x_3^*\,\hat{x}_8(k))/1000.)$	- $\hat{V}_u$ (ft/sec)
$\bar{x}_8(k+1) = \hat{x}_8(k) + \Delta t\,(x_5^* - (x_3^*\,\hat{x}_7(k) - x_1^*\,\hat{x}_9(k))/1000.)$	- $\hat{V}_v$ (ft/sec)
$\bar{x}_9(k+1) = \hat{x}_9(k) + \Delta t\,(x_6^* - (x_1^*\,\hat{x}_8(k) - x_2^*\,\hat{x}_7(k))/1000.)$	- $\hat{V}_w$ (ft/sec)

TABLE 2-14. (Continued)

$\bar{x}_{10}(k+1) = \hat{x}_{10}(k) - \Delta t\,(x_2^* \hat{x}_{12}(k) - x_3^* \hat{x}_{11}(k))/1000.$	-	$\hat{z}_u$ (mrad)
$\bar{x}_{11}(k+1) = \hat{x}_{11}(k) - \Delta t\,(x_3^* \hat{x}_{10}(k) - x_1^* \hat{x}_{12}(k))/1000.$	-	$\hat{z}_v$ (mrad)
$\bar{x}_{12}(k+1) = \hat{x}_{12}(k) - \Delta t\,(x_1^* \hat{x}_{11}(k) - x_2^* \hat{x}_{10}(k))/1000.$	-	$\hat{z}_w$ (mrad)
$\bar{x}_{13}(k+1) = (1 - \alpha_3 \Delta t)\,\hat{x}_{13}(k) + \left\{ \alpha_3 \Delta t\ u_{13} \right\}$	-	$\delta\omega_u$ (mrad/sec)
$\bar{x}_{14}(k+1) = (1 - \alpha_3 \Delta t)\,\hat{x}_{14}(k) + \left\{ \alpha_3 \Delta t\ u_{14} \right\}$	-	$\delta\omega_v$ (mrad/sec)
$\bar{x}_{15}(k+1) = (1 - \alpha_3 \Delta t)\,\hat{x}_{15}(k) + \left\{ \alpha_3 \Delta t\ u_{15} \right\}$	-	$\delta\omega_w$ (mrad/sec)
$\bar{x}_{16}(k+1) = (1 - \alpha_4 \Delta t)\,\hat{x}_{16}(k) + \left\{ \alpha_4 \Delta t\ u_{16} \right\}$	-	$\delta\ a_u$ (ft/sec^2)
$\bar{x}_{17}(k+1) = (1 - \alpha_4 \Delta t)\,\hat{x}_{17}(k) + \left\{ \alpha_4 \Delta t\ u_{17} \right\}$	-	$\delta\ a_v$ (ft/sec^2)
$\bar{x}_{18}(k+1) = (1 - \alpha_4 \Delta t)\,\hat{x}_{18}(k) + \left\{ \alpha_4 \Delta t\ u_{18} \right\}$	-	$\delta\ a_w$ (ft/sec^2)
$\bar{x}_{19}(k+1) = (1 - \alpha_5 \Delta t)\,\hat{x}_{19}(k) + \left\{ \alpha_5 \Delta t\ u_{19} \right\}$	-	$\delta\ V_u$ (ft/sec)
$\bar{x}_{20}(k+1) = (1 - \alpha_5 \Delta t)\,\hat{x}_{20}(k) + \left\{ \alpha_5 \Delta t\ u_{20} \right\}$	-	$\delta\ V_v$ (ft/sec)
$\bar{x}_{21}(k+1) = (1 - \alpha_5 \Delta t)\,\hat{x}_{21}(k) + \left\{ \alpha_5 \Delta t\ u_{21} \right\}$	-	$\delta\ V_w$ (ft/sec)
$\bar{x}_{22}(k+1) = (1 - \alpha_6 \Delta t)\,\hat{x}_{22}(k) + \left\{ \alpha_6 \Delta t\ u_{22} \right\}$	-	$\delta\ z_u$ (mrad)
$\bar{x}_{23}(k+1) = (1 - \alpha_6 \Delta t)\,\hat{x}_{23}(k) + \left\{ \alpha_6 \Delta t\ u_{23} \right\}$	-	$\delta\ z_v$ (mrad)
$\bar{x}_{24}(k+1) = (1 - \alpha_6 \Delta t)\,\hat{x}_{24}(k) + \left\{ \alpha_6 \Delta t\ u_{24} \right\}$	-	$\delta\ z_w$ (mrad)

2.4.4.5 State to Observation Conversion Process

Referring to Appendix A, the observation process is characterized in general by the equation

$$\underline{y}_k = \Gamma(\underline{x}_k) + D\,\underline{v}_k \tag{15}$$

The conversion process Γ consists of a vector of equations which transform the state array into the observation array. As seen from Appendix A, Section A. 2, the partial derivatives of Γ with respect to the elements of $\underline{x}$ and evaluated at $\underline{x}_k$ comprise the conversion matrix, C (see Appendix A, Section A. 2). This matrix constitutes a linearization of Γ in the vicinity of $\underline{x}_k$.

The equations of the conversion process are listed in Table 2-15. As can be seen, in the case of the aircraft state estimator Γ is linear so that the elements of C can be written down by inspection.

TABLE 2-15

AIRCRAFT STATE ESTIMATOR - STATE TO OBSERVATION CONVERSION PROCESS

$\bar{y}_1(k) = \Delta t\,(\bar{x}_1(k) + \bar{x}_{13}(k)) + y_1(k-1)$	-	$\tilde{\theta}_u$ (mrad/frame)
$\bar{y}_2(k) = \Delta t\,(\bar{x}_2(k) + \bar{x}_{14}(k)) + y_2(k-1)$	-	$\tilde{\theta}_v$ (mrad/frame)
$\bar{y}_3(k) = \Delta t\,(\bar{x}_3(k) + \bar{x}_{15}(k)) + y_3(k-1)$	-	$\tilde{\theta}_w$ (mrad/frame)
$\bar{y}_4(k) = -\bar{x}_4(k) - \bar{x}_{16}(k) + y_4(k-1)$	-	$\tilde{f}_u$ (ft/sec^2)
$\bar{y}_5(k) = -\bar{x}_5(k) - \bar{x}_{17}(k) + y_5(k-1)$	-	$\tilde{f}_v$ (ft/sec^2)
$\bar{y}_6(k) = -\bar{x}_6(k) - \bar{x}_{18}(k) + y_6(k-1)$	-	$\tilde{f}_w$ (ft/sec^2)
$\bar{y}_7(k) = \bar{x}_7(k) + \bar{x}_{19}(k)$	-	V_u (ft/sec)
$\bar{y}_8(k) = \bar{x}_8(k) + \bar{x}_{20}(k)$	-	V_v (ft/sec)
$\bar{y}_9(k) = \bar{x}_9(k) + \bar{x}_{21}(k)$	-	V_w (ft/sec)
$\bar{y}_{10}(k) = \bar{x}_{10}(k) + \bar{x}_{22}(k)$	-	z_u (mrad)
$\bar{y}_{11}(k) = \bar{x}_{11}(k) + \bar{x}_{23}(k)$	-	z_v (mrad)
$\bar{y}_{12}(k) = \bar{x}_{12}(k) + \bar{x}_{24}(k)$	-	z_w (mrad)

Examination of Table 2-15 reveals the entrance of the lowband sensor noises (states $\bar{x}_{13}$ through $\bar{x}_{24}$) into the corresponding observations. By this means, the $(CP_k C^T)$ term in the innovation covariance (see Appendix A, Section A.2) reflects the presence of the lowband sensor noise. The wideband sensor noise, to be discussed in the sequel, is reflected in the (DLD^T) term.

2.4.4.6 State Excitation Process

Referring to Appendix A, Section A.2, and equation (13), the driving function for the state process is a vector of noises, $\underline{u}$. The association of the 24 elements of $\underline{u}$ with the 24 state elements is placed in evidence by Table 2-14; note that u_7 through u_{12} are identically zero, being defined only for the sake of commonality of subscripting.

Again referring to Appendix A, Section A.1, the covariance of $\underline{u}$ is the matrix K.

$$K = \mathrm{Cov}\ (\underline{u}) = \mathrm{Exp}\ (\underline{u}\ \underline{u}^T) \tag{16}$$

The off-diagonal elements of K are zero in the present case, and the diagonal elements are the variances of the elements of $\underline{u}$.

$$\begin{aligned} k_{ij} &= 0,\ i \neq j,\ i=1, 2, \ldots, 24,\ j=1, 2, \ldots, 24 \\ k_{ii} &= \sigma_{u_i}^{\ 2},\ i=1, 2, \ldots, 24 \end{aligned} \tag{17}$$

As we have noted,

$$k_{ii} = 0,\ i=7, 8, \ldots, 12 \tag{18}$$

All of the noise processes defined for the aircraft state estimator represent lowband sensor errors and are of first order with a break frequency α_i rad/sec $(i=1, 2, \ldots, 24)$. The relationships involved in selecting the required input variance for a desired output variance are summarized in Figure 2-5 for the first order process.

Table 2-16 lists the values selected for the RMS values of the lowband sensor errors after filtering, the selected break frequencies, α_i, and the required values of the K-matrix elements corresponding to these choices.

- EXCITED STATE VARIABLE - x
- GAUSSIAN TIME SERIES WITH FLAT SPECTRUM = u
- FIRST ORDER PROCESS SPECTRAL DENSITY FUNCTION

$$\Phi_{XX} = \frac{\Phi_u}{1 + \left(\frac{\omega}{\alpha}\right)^2}$$

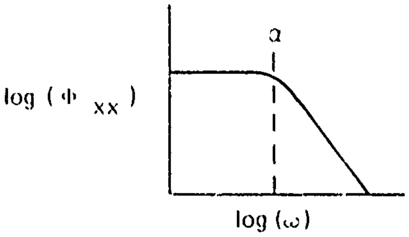

- FORM OF STATE TRANSITION EQUATION

$$x_{k+1} = (1 - \alpha \Delta t)\, x_k + \alpha \Delta t\, u_k$$

- RELATIONSHIP OF INPUT AND OUTPUT VARIANCES

f_s = PROCESSOR SAMPLING FREQUENCY (Hz)

$$\sigma_u^2 = \left(\frac{2 f_s}{\alpha} \right) \sigma_x^2$$

Figure 2-5. First Order Gauss-Markov Process Relationships

The RMS sensor errors were arrived at by analysis of the performance of the particular sensors selected for incorporation into the CLFCS, taking into account such effects as:

- Drifts and Biases
- Scale factor uncertainties
- Errors introduced by sensor misalignments

The errors selected for δz_{uvw} were obtained, in fact, from a simulation of the LSI-9000 vertical gyro over a sequence of straight-line and maneuvering path segments.

The values selected for the break frequencies, α_i, were arrived at through engineering judgment with an appreciation for the dominant driving functions of the several errors. In general, the values of the α_i reflect the probable bandwidth of the measured state variable. That is, for example, the bandwidth of δV_u is expected to be similar to that of V_u.

TABLE 2-16

AIRCRAFT STATE ESTIMATOR - STATE EXCITATION PROCESS PARAMETERS

State Variable(s)	u - Element(s)	RMS Value σ_x	α rad/sec	σ_u^2/σ_x^2	K - Element(s)
$x_{1,2,3} = \Delta\hat{\omega}_{uvw}$	$u_{1,2,3}$	0.5 mrad/sec	$\alpha_1=1$	5.90×10^1	$k_{1,1}=k_{2,2}=k_{3,3} = 14.75$
$x_{4,5,6} = \Delta\hat{f}_{uvw}$	$u_{4,5,6}$	0.17 ft/sec^2	$\alpha_2=1$	5.90×10^1	$k_{4,4}=k_{5,5}=k_{6,6} = 1.705$
$x_{13,14,15} = \delta\hat{\omega}_{uvw}$	$u_{13,14,15}$	0.5 mrad/sec	$\alpha_3=1$	5.90×10^1	$k_{13,13}=k_{14,14}=k_{15,15}=14.75$
$x_{16,17,18} = \delta\hat{a}_{uvw}$	$u_{16,17,18}$	0.17 ft/sec^2	$\alpha_4=1$	5.90×10^1	$k_{16,16}=k_{17,17}=k_{18,18}=1.705$
$x_{19} = \delta\hat{V}_u$	u_{19}	10 ft/sec	$\alpha_5=0.5$	1.19×10^2	$k_{19,19}= 1.190 \times 10^4$
$x_{20} = \delta\hat{V}_v$	u_{20}	20 ft/sec	$\alpha_5=0.5$	1.19×10^2	$k_{20,20} = 4.760 \times 10^4$
$x_{21} = \delta\hat{V}_w$	u_{21}	$\sqrt{10 \text{ ft/sec}}$	$\alpha_5=0.5$	1.19×10^2	$k_{21,21} = 1.190 \times 10^3$
$x_{22} = \delta\hat{z}_u$	u_{22}	16 mrad	$\alpha_6=0.5$	1.19×10^2	$k_{22,22}= 3.046 \times 10^4$
$x_{23} = \delta\hat{z}_v$	u_{23}	16 mrad	$\alpha_6=0.5$	1.19×10^2	$k_{23,23} = 3.046 \times 10^4$
$x_{24} = \delta\hat{z}_w$	u_{24}	8 mrad	$\alpha_6=0.5$	1.19×10^2	$k_{24,24} = 7.616 \times 10^3$

As is evident from Appendix A, Section A. 2, and equation ., the state excitation noise components enter the estimation process via the propagation matrix B. In the present case, the B-matrix is 24 x 24, and its non-zero elements are shown in Table 2-14 (the terms enclosed in curly brackets). They are also listed below for the sake of clarity:

$$b_{1,1} = b_{2,2} = b_{3,3} = \alpha_1 \Delta t , \ \alpha_1 = 1 \text{ rad/sec}$$

$$b_{4,4} = b_{5,5} = b_{6,6} = \alpha_2 \Delta t , \ \alpha_2 = 1 \text{ rad/sec}$$

$$b_{13,13} = b_{14,14} = b_{15,15} = \alpha_3 \Delta t , \ \alpha_3 = 1 \text{ rad/sec}$$

$$b_{16,16} = b_{17,17} = b_{18,18} = \alpha_4 \Delta t , \ \alpha_4 = 1 \text{ rad/sec}$$

$$b_{19,19} = b_{20,20} = b_{21,21} = \alpha_5 \Delta t , \ \alpha_5 = 0.5 \text{ rad/sec}$$

$$b_{22,22} = b_{23,23} = b_{24,24} = \alpha_6 \Delta t , \ \alpha_6 = 0.5 \text{ rad/sec}$$

The values for the α_i are as shown in Table 2-16. All the other elements of the B-matrix not listed above are zero.

2.4.4.7 Observation Noise Process

Referring to Appendix A, Section A. 2, and equation (15), the sensor readings are corrupted by a noise process $\underline{v}$. By definition, the components of $\underline{v}$ are sequentially uncorrelated; that is

$$\text{Exp} (\underline{v}_k \underline{v}^T_{k+m}) = 0, \quad m > 0 \qquad (19)$$

Accordingly, the $\underline{v}$ noise process is wideband in character for a computer iteration rate appropriate to a fire control estimator.

In General Electric's experience, most fire control sensors exhibit substantial lowband error components. In the case of the aircraft state estimator, these have been introduced via state variables $\hat{x}_{13}$ through $\hat{x}_{29}$ driven by sequentially uncorrelated noises u_{13} through u_{24}. The RMS values and bandwidths of the lowband errors are described in Section 2. 4. 4. 6.

The wideband sensor errors introduced through $\underline{v}$ represent thermal noise, quantization/resolution effects, etc., which tend to manifest different values from one computer frame to the next. Somewhat arbitrarily, the variances of the elements of $\underline{v}$ are made equal to the corresponding lowband error variances. Thus, in the case of the IMU gyros, for example, an RMS wideband error of 0.5 mrad/sec is introduced so that the total sensor error, including both lowband and wideband components, is

$$\overline{\delta\omega} = \sqrt{0.5^2 + 0.5^2} = 0.707 \text{ mrad/sec} \tag{20}$$

Referring to Appendix A, Section A.1, the covariance of $\underline{v}$ is denoted L.

$$L = \text{Cov}\ (\underline{v}) = \text{Exp}\ (\underline{v}\,\underline{v}^T) \tag{20}$$

As in the case of the K-matrix, the off-diagonal elements of L are zero and its diagonal elements are the variances of the elements of $\underline{v}$. There is one element of $\underline{v}$ for each of the 12 sensors (see Table 2-13 for a definition of the observation array). Accordingly,

$$\begin{aligned} \ell_{ij} &= 0,\ i = 1, 2, \ldots, 12,\ j = 1, 2, \ldots, 12 \\ \ell_{ii} &= \sigma_{v_i}^2,\ i = 1, 2, \ldots, 12 \end{aligned} \tag{21}$$

Table 2-17 lists the values selected for the elements of L, which are in agreement with the lowband errors listed in Table 2-16.

As is evident from Appendix A, Section A.2, and equation (15), the observation noise components enter the observation process via the propagation matrix D. In the present case, the D matrix is equal to the identity matrix.

$$D = I \tag{22}$$

2.4.4.8 Initial State Vector and Estimation Error Covariance Values

As indicated in Appendix A, Section A.4, the estimation error covariance matrix, $\overline{P}$, must be initially established from input data in order to commence the calculation of the Kalman gain. In general, the values selected for the elements of the initial $\overline{P}$ - matrix should reflect the level of confidence which can be placed in whatever values are chosen for the elements of the initial state vector, $\overline{x}$. The effect on the estimator is to influence the gains during the first few computer frames.

TABLE 2-17.
AIRCRAFT STATE ESTIMATOR - OBSERVATION NOISE PARAMETERS

Observed Variable(s)	$\underline{v}$ - Element(s)	RMS Value σ_v	L-Element (σ_v^2)
$y_{1,2,3} = \tilde{\omega}_{uvw}$	$v_{1,2,3}$	0.50 mrad/sec	$\ell_{1,1} = \ell_{2,2} = \ell_{3,3} = 0.25$
$y_{4,5,6} = \tilde{f}_{uvw}$	$v_{4,5,6}$	0.17 ft/sec^2	$\ell_{4,4} = \ell_{5,5} = \ell_{6,6} = 2.89 \times 10^{-2}$
$y_7 = \tilde{V}_u$	v_7	10 ft/sec	$\ell_{7,7} = 100$
$y_8 = \tilde{V}_v$	v_8	20 ft/sec	$\ell_{8,8} = 400$
$y_9 = \tilde{V}_w$	v_9	$\sqrt{10}$ ft/sec	$\ell_{9,9} = 10$
$y_{10,11} = \tilde{z}_{uv}$	$v_{10,11}$	16 mrad	$\ell_{10,10} = \ell_{11,11} = 256$
$y_{12} = \tilde{z}_w$	v_{12}	8 mrad	$\ell_{12,12} = 64$

States $\bar{x}_{1,2,3}$ represent the estimated values of the lowband gyro errors. Accordingly, the appropriate initial values for them are

$$\bar{x}_1 = \bar{x}_2 = \bar{x}_3 = 0 \tag{23}$$

The RMS value assigned to each of the lowband gyro errors in Table 2-16 is 0.5 mrad/sec, which therefore also reflects the uncertainty in $\bar{x}_{1,2,3}$. On this basis,

$$p_{1,1} = p_{2,2} = p_{3,3} = 0.25 \text{ (mrad/sec)}^2 \tag{24}$$

States $\bar{x}_{4,5,6}$ represent the estimated values of the lowband accelerometer errors. The appropriate initial values for them are

$$\bar{x}_4 = \bar{x}_5 = \bar{x}_6 = 0 \tag{25}$$

and, in agreement with Table 2-16, the uncertainties associated with these values are

$$p_{4,4} = p_{5,5} = p_{6,6} = 0.0289 \ (\text{ft/sec}^2)^2 \qquad (26)$$

States $\bar{x}_{7,8,9}$ represent the aircraft velocity. These state variables are initially set directly from observations $y_{7,8,9}$, which are the velocity outputs of the air data subsystem. In other words, at time t = 0, the values for $y_{7,8,9}$ are placed in the memory locations for $\bar{x}_{7,8,9}$. The uncertainty in each of these values is the resultant of the lowband and wideband sensor error components. Therefore,

$$\begin{aligned} p_{7,7} &= 10^2 + 10^2 = 200 \ (\text{ft/sec})^2 \\ p_{8,8} &= 20^2 + 20^2 = 800 \ (\text{ft/sec})^2 \qquad (27) \\ p_{9,9} &= 10 + 10 = 20 \ (\text{ft/sec})^2 \end{aligned}$$

States $\bar{x}_{10,11,12}$ represent the vertical axis direction and are initially set from observations $y_{10,11,12}$, which are developed from the outputs of the LSI-9000 vertical gyro. The resultants of the lowband and wideband sensor errors for these observations gives

$$\begin{aligned} p_{10,10} = p_{11,11} &= 16^2 + 16^2 = 512 \ \text{mrad}^2 \\ & \qquad\qquad\qquad (28) \\ p_{12,12} &= 8^2 + 8^2 = 128 \ \text{mrad}^2 \end{aligned}$$

States x_{13} through x_{24} are auxiliary variables for the generation of the lowband sensor error components and are assigned initial values of 0. In agreement with the RMS values assigned in Table 2-16, the following initial estimation error covariances are used:

$$\begin{aligned} p_{13,13} = p_{14,14} = p_{15,15} &= 0.25 \ (\text{mrad/sec})^2 \\ p_{16,16} = p_{17,17} = p_{18,18} &= 0.0289 \ (\text{ft/sec}^2)^2 \\ p_{19,19} &= 100 \ (\text{ft/sec})^2 \\ p_{20,20} &= 400 \ (\text{ft/sec})^2 \qquad (29) \\ p_{21,21} &= 10 \ (\text{ft/sec})^2 \\ p_{22,22} = p_{23,23} &= 256 \ \text{mrad}^2 \\ p_{24,24} &= 64 \ \text{mrad}^2 \end{aligned}$$

2.4.4.9 Gain Matrix Computation

Because of the fact that the aircraft state estimator can operate continuously from the point of take-off, or at least from a point significantly before the target engagement, there did not appear to be justification for on-line Kalman gain computation. Experimentation with various estimator designs led to the fixed gain design which is now described.

The aircraft state estimator has 12 principal state variables whose filtered values are to be continuously generated as a basis for the fire control solution (see Table 2-12). Auxiliary state variables 13 through 24 introduce lowband sensor noise into the estimation process, and are therefore not subject to filtering. That is, the gain elements which would normally produce adjustments in these state variables are arbitrarily set to zero. Accordingly, there are potentially 12 x 12 = 144 gain elements of concern in the operational system.

Section 2.3.3 describes two target engagements which were selected as the basis for design and analysis of the CLFCS estimators. Table 2-9 lists the parameters for these two engagements, a straight-line offset attack and a veer-off attack. Table 2-18 summarizes the methodology for designing the fixed gain aircraft state estimator, in which both the straight-line and veer-off attacks are employed.

A key step in the fixed gain design process is the initial sort based upon the result of operating the estimator against the straight-line attack. This involves a ranking of the elements in each row of the gain matrix according to their actual importance in the estimation process.

From Appendix A, Section A.1 and A.2, the fact is evident that the gain matrix, G, operates on the innovation vector $\underline{z} = \underline{y} - \bar{\underline{y}}$. Accordingly, the corrections applied by the filter to the state vector is $G\underline{z}$. In particular, the correction applied to state element i is

$$\Delta x_i = \sum_{j=i}^{12} g_{ij} \; z_j \tag{30}$$

The covariance matrix for $\underline{z}$ is $Q = C\bar{P}C^T + DLD^T$, which is computed as part of the Kalman gain algorithm (see Appendix A, Section A.4). Therefore, the variance of z_j is

$$\sigma_{z_j}^2 = q_{jj} \tag{31}$$

TABLE 2-18.
FIXED GAIN ESTIMATOR DESIGN METHODOLOGY

- Compute the Kalman gains versus time at 30/sec for 40 sec along the straight-line course. Select the gain values at the end of 40 sec for use in the fixed-gain estimator.
- Using the RMS values of the innovation elements (RMS $(z_j) = \sigma_{z_j} = \sqrt{q_{jj}}$)

  $$r_{ij} = 100 \left[g_{ij} \sqrt{q_{jj}} \right] / \left[g_{ii} \sqrt{q_{ii}} \right] \quad , \; j = 1,2,\ldots,12, \; i = 1,2,\ldots,12$$
- In the ith row, the diagonal element receives a ranking of 100%. In most, but not all cases, $r_{ij} \leq r_{ii}$.
- Reject from further consideration any g_{ij} for which $r_{ij} < 1\%$.
- Compute the Kalman gains along the 40 sec veer-off course.
- Reject from further consideration any g_{ij} which exhibits kinematically induced gain variations.
- The net result is a 31 - element fixed gain estimator.

Considering the case where the gain elements, g_{ij}, have reached their steady-state values, the RMS value of each of the 12 contributors to Δx_i is reflected by

$$\sigma_{\Delta x_{ij}} = g_{ij} \; \sigma_{z_j} = g_{ij}\sqrt{q_{jj}} \qquad (32)$$

The individual gains in each row of G are thereby ranked in relation to the diagonal element, and those off-diagonal gains contributing less than 1% to Δx_i on an RMS basis are eliminated.

The second stage of sorting involves the use of the veer-off course which includes maneuvers as described in Section 2.3.3. Gains whose values are modulated by the maneuver are subject to kinematically induced variation and must therefore be eliminated from the fixed gain matrix.

As a consequence of these two stages of sorting, a 31 - gain estimator was developed. Table 2-19 lists the values of the 31 non-zero elements in the 12 x 12 gain matrix.

The satisfactory performance of the fixed gain aircraft state estimator was confirmed using the veer-off attack. The results of this analysis are presented in Section 2.4.6.

TABLE 2-19.

LISTING OF SELECTED FIXED GAIN ELEMENTS FOR A PRACTICABLE AIRCRAFT STATE ESTIMATOR DESIGN

Gain Element & Value	State Element	Innovation Element
G(1, 1)=3.12	ω_u	$\delta\theta_u$
G(1,11)=1.06E-04	ω_u	δz_v
G(2, 2)=G(1, 1)	ω_v	$\delta\theta_v$
G(2, 9)=5.35E-04	ω_v	δV_w
G(2,10)=-9.76E-05	ω_v	δz_u
G(3, 3)=G(1, 1)	ω_w	$\delta\theta_w$
G(3, 8)=-1.22E-05	ω_w	δV_v
G(4, 4)=-.104	a_u	δa_u
G(4, 7)=3.59E-05	a_u	δV_u
G(5, 5)=G(4, 4)	a_v	δa_v
G(5, 8)=8.51E-06	a_v	δV_v
G(6, 6)=G(4, 4)	a_w	δa_w
G(6, 9)=3.77E-04	a_w	δV_w
G(7, 4)=-.0158	V_u	δa_u
G(7, 7)=.0210	V_u	δV_u
G(7,10)=-.00596	V_u	δz_u
G(8, 5)=-.0136	V_v	δa_v
G(8, 8)=.0131	V_v	δV_v
G(8,11)=-.00832	V_v	δz_v
G(9, 6)=-.0179	V_w	δa_w
G(9, 9)=.0281	V_w	δV_w
G(9,12)=-.00359	V_w	δz_w
G(10, 2)=-.258	z_u	$\delta\theta_v$
G(10, 7)=-.0161	z_u	δV_u
G(10,10)=.00676	z_u	δz_u
G(11, 1)=.327	z_v	$\delta\theta_u$
G(11, 8)=-.00563	z_v	δV_v
G(11,11)=.00856	z_v	δz_v
G(12, 6)=.00994	z_w	δa_w
G(12, 9)=-.0241	z_w	δV_w
G(12,12)=.00407	z_w	δz_w

2.4.5 TARGET STATE ESTIMATOR

With the description of the aircraft state estimator as background, the details of the target state estimator design are now presented.

2.4.5.1 Preliminary Discussion

The purpose of the target state estimator is to maintain an accurate representation of the target's position, in terms of both range and LOS direction, with respect to the $\underline{u}\ \underline{v}\ \underline{w}$ vehicle coordinate frame. Continuous measurement of the LOS direction cosines relative to $\underline{u}\ \underline{v}\ \underline{w}$ is obtained from the pantographic sight resolvers while the gunner is actually tracking the target. In the absence of these measurements, while the gunner is engaged in closed loop fire control activity, the LOS direction is perpetuated by the target state estimator transition process.

There is no continuous measurement of target range. The pilot inserts an estimate of range via the range potentiometer on the CLFCS control panel at the instant of target acquisition. The detailed crew activities involved in this are as follows:

- Prior to target acquisition, a value for acquisition range is selected and dialed in by the pilot; an acquisition range of 8.000 to 10.000 ft (2438 m to 3048 m) is considered appropriate.
- As this range is approached, the gunner establishes a LOS track, but does not depress the sight action switch.
- The pilot signals the gunner when the selected acquisition range is attained; the gunner thereupon depresses the action switch.
- This generates a discrete command to the CDC 469 computer to initiate target state estimation, and also initiates slewing of the gun to the continuously updated aiming solution. As part of this, the range pot setting is used to establish an initial range value.

Further discussion of the problem of introducing the initial estimate of range in the flight test environment is contained in Reference 3.

The target state estimator transition process makes use of the angular and linear velocities furnished by the aircraft state estimator. In particular, the linear velocity information provides a basis for updating target range. The introduction of pseudo target velocity auxiliary variables accounts for the probable disparity between the estimated aircraft velocity and its actual velocity relative to the target.

Within the target state estimator, all angular information (direction cosines, angular velocities) is expressed in milliradian units and range information, in kilofeet units. This reduces the range of the error covariance values and thereby diminishes the probability of numerical problems in the fixed point implementation of the target state estimator. Conversion back to standard units (radians, feet, etc.) at the interface with the fire control computations is assumed in the sequel.

2.4.5.2 True State, Estimated State, and Observation Arrays

Tables 2-20, 2-21, and 2-22 define the elements of the true state. estimated state, and observation arrays for the target state estimator.

TABLE 2-20.

TARGET STATE ESTIMATOR - TRUE STATE ARRAY

$x_1 = s_u$	=	Direction cosine of LOS with respect to $\underline{u}$ vehicle axis (mrad)
$x_2 = s_v$	=	Direction cosine of LOS with respect to $\underline{v}$ vehicle axis (mrad)
$x_3 = s_w$	=	Direction cosine of LOS with respect to $\underline{w}$ vehicle axis (mrad)
$x_4 = R$	=	Range (kilofeet)

TABLE 2-21.
TARGET STATE ESTIMATOR - ESTIMATED STATE ARRAY

$\hat{x}_1 = \hat{s}_u$ = Estimated value of s_u (mrad)

$\hat{x}_2 = \hat{s}_v$ = Estimated value of s_v (mrad)

$\hat{x}_3 = \hat{s}_w$ = Estimated value of s_w (mrad)

$\hat{x}_4 = \hat{R}$ = Estimated value of R (kilofeet)

$\hat{x}_5 = \Delta\hat{V}_u$ = Pseudo target velocity along $\underline{u}$ vehicle axis (ft/sec)

$\hat{x}_6 = \Delta\hat{V}_v$ = Pseudo target velocity along $\underline{v}$ vehicle axis (ft/sec)

$\hat{x}_7 = \Delta\hat{V}_w$ = Pseudo target velocity along $\underline{w}$ vehicle axis (ft/sec)

$\hat{x}_8 = \delta\,\hat{s}_u$ = Lowband error in the measurement of s_u (mrad)

$\hat{x}_9 = \delta\,\hat{s}_v$ = Lowband error in the measurement of s_v (mrad)

$\hat{x}_{10} = \delta\,\hat{s}_w$ = Lowband error in the measurement of s_w (mrad)

TABLE 2-22.
TARGET STATE ESTIMATOR - OBSERVATION ARRAY

$y_1 = \tilde{s}_u$ = Measured value of s_u (mrad)

$y_2 = \tilde{s}_v$ = Measured value of s_v (mrad)

$y_3 = \tilde{s}_w$ = Measured value of s_w (mrad)

2.4.5.3 Transition Process

In Section 2.4.2.5, the fundamental dynamic relationships for the target state estimator transition process are set forth. These include the incorporation of pseudo target velocity components, which reflect the difference between the velocity output by the aircraft state estimator and the actual velocity of the aircraft relative to the target.

The angular and linear aircraft velocity components, as they are used in the target state transition process, are denoted as follows:

$\omega_1(k) = \hat{\omega}_u$ = Angular velocity component about $\underline{u}$ axis as output by the aircraft state estimator at frame k.

$\omega_2(k) = \hat{\omega}_v$ = Angular velocity component about $\underline{v}$ axis.

$\omega_3(k) = \hat{\omega}_w$ = Angular velocity component about $\underline{w}$ axis.

$V_1(k) = \hat{V}_u$ = Linear velocity component along $\underline{u}$ axis as output by the aircraft state estimator at frame k.

$V_2(k) = \hat{V}_v$ = Linear velocity component along $\underline{v}$ axis.

$V_3(k) = \hat{V}_w$ = Linear velocity component along $\underline{w}$ axis.

With this, the target state transition process equations are listed in Table 2-23. To maintain the LOS vector at unit value, its components are normalized each computer frame according to the following equations:

$$
\begin{aligned}
Q &= 1000/\sqrt{\bar{x}_1(k+1)^2 + \bar{x}_2(k+1)^2 + \bar{x}_3(k+1)^2} \\
\bar{x}_1(k+1) &= Q\,\bar{x}_1(k+1) \\
\bar{x}_2(k+1) &= Q\,\bar{x}_2(k+1) \\
\bar{x}_3(k+1) &= Q\,\bar{x}_3(k+1)
\end{aligned}
\qquad (33)
$$

TABLE 2-23

TARGET STATE ESTIMATOR - TRANSITION PROCESS

Principal State Variables

$$V_1^*(k) = V_1(k) - \hat{x}_5(k) \qquad (V_u^*,\ \text{ft/sec})$$

$$V_2^*(k) = V_2(k) - \hat{x}_6(k) \qquad (V_v^*,\ \text{ft/sec})$$

$$V_3^*(k) = V_3(k) - \hat{x}_7(k) \qquad (V_w^*,\ \text{ft/sec})$$

$$\dot{R}(k) = -10^{-6}\left(V_1^*(k)\,\hat{x}_1(k) + V_2^*(k)\,\hat{x}_2(k) + V_3^*(k)\,\hat{x}_3(k)\right) \qquad (\dot{R},\ \text{kft/sec})$$

$$\bar{x}_1(k+1) = \hat{x}_1(k) - \Delta t\left((V_1^*(k) + \dot{R}(k)\,\hat{x}_1(k))/\hat{x}_4(k) + 10^{-3}(\omega_2(k)\,\hat{x}_3(k) - \omega_3(k)\,\hat{x}_2(k))\right) \qquad (\hat{s}_u,\ \text{mrad})$$

$$\bar{x}_2(k+1 = \hat{x}_2(k) - \Delta t\left((V_2^*(k) + \dot{R}(k)\,\hat{x}_2(k))/\hat{x}_4(k) + 10^{-3}(\omega_3(k)\,\hat{x}_1(k) - \omega_1(k)\,\hat{x}_3(k))\right) \qquad (\hat{s}_v,\ \text{mrad})$$

$$\bar{x}_3(k+1) = \hat{x}_3(k) - \Delta t\left((V_3^*(k) + \dot{R}(k)\,\hat{x}_3(k))/\hat{x}_4(k) + 10^{-3}(\omega_1(k)\,\hat{x}_2(k) - \omega_2(k)\,\hat{x}_1(k))\right) \qquad (\hat{s}_w,\ \text{mrad})$$

$$\bar{x}_4(k+1) = \hat{x}_4(k) + \Delta t\,\dot{R}(k) \qquad (R,\ \text{kft})$$

Pseudo-Target Velocity Components

$$\bar{x}_5(k+1) = (1 - \alpha_1\Delta t)\,\hat{x}_5(k) - .001\,(\omega_2(k)\,\hat{x}_7(k) - \omega_3(k)\,\hat{x}_6(k) + \left\{\alpha_1\Delta t\,u_1\right\} \qquad (\Delta\hat{V}_u,\ \text{ft/sec})$$

$$\bar{x}_6(k+1) = (1 - \alpha_1\Delta t)\,\hat{x}_6(k) - .001\,(\omega_3(k)\,\hat{x}_5(k) - \omega_1(k)\,\hat{x}_7(k) + \left\{\alpha_1\Delta t\,u_2\right\} \qquad (\Delta\hat{V}_v,\ \text{ft/sec})$$

$$\bar{x}_7(k+1) = (1 - \alpha_1\Delta t)\,\hat{x}_7(k) - .001\,(\omega_1(k)\,\hat{x}_6(k) - \omega_2(k)\,\hat{x}_5(k) + \left\{\alpha_1\Delta t\,u_3\right\} \qquad (\Delta\hat{V}_w,\ \text{ft sec})$$

Lowband Sight Errors

$$\bar{x}_8(k+1) = (1 - \alpha_2\Delta t)\,\hat{x}_8(k) + \left\{\alpha_2\Delta t\ u_4\right\} \qquad (\delta\,\hat{s}_u,\ \text{mrad})$$

$$\bar{x}_9(k+1) = (1 - \alpha_2\Delta t)\,\hat{x}_9(k) + \left\{\alpha_2\Delta t\ u_5\right\} \qquad (\delta\,\hat{s}_v,\ \text{mrad})$$

$$\bar{x}_{10}(k+1) = (1 - \alpha_2\Delta t)\,\hat{x}_{10}(k) + \left\{\alpha_2\Delta t\ u_6\right\} \qquad (\delta\,\hat{s}_w,\ \text{mrad})$$

2.4.5.4 State to Observation Conversion Process

The conversion process equations for the target state estimator are listed in Table 2-24. Note the introduction of the lowband sight error components.

TABLE 2-24.

TARGET STATE ESTIMATOR - STATE TO OBSERVATION CONVERSION PROCESS

$\bar{y}_1 (k) = \bar{x}_1 (k) + \bar{x}_8 (k)$	$(s_u$, mrad)
$\bar{y}_2 (k) = \bar{x}_2 (k) + \bar{x}_9 (k)$	$(s_v$, mrad)
$\bar{y}_3 (k) = \bar{x}_3 (k) + \bar{x}_{10} (k)$	$(s_w$, mrad)

2.4.5.5 State Excitation Process

The state excitation for the target state estimator consists of the pseudo target velocity components, ΔV_{uvw}. Auxiliary variables are also defined for the generation of lowband sight error components, due principally to gunner tracking error.

The pseudo target velocity vector potentially includes all effects which cause the estimated aircraft velocity to differ from the actual velocity of the aircraft relative to the target. The following contributors must therefore be considered:

- The error in $\hat{V}_{uvw}$, considered as inertially augmented airspeed.
- Wind velocity.
- Target velocity.

Accordingly, the break frequency of 1 rad/sec and the variances listed in Table 2-25 reflect the desire to optimize $\hat{V}_{uvw}$ for the estimation of airspeed error.

TABLE 2-25.

TARGET STATE ESTIMATOR - STATE EXCITATION PROCESS PARAMETERS

State Variable	RMS Value σ_x	Frequency α (rad/sec)	$\underline{u}$ - Element	σ_u^2/σ_x^2	K-Element (σ_u^2)
$x_5 = \Delta\hat{V}_u$	20 ft/sec	$\alpha_1 = 1$	u_1	5.9×10^1	$k_{1,1} = 2.36 \times 10^4$
$x_6 = \Delta\hat{V}_y$	20 ft/sec	$\alpha_1 = 1$	u_2	5.9×10^1	$k_{2,2} = 2.36 \times 10^4$
$x_7 = \Delta\hat{V}_w$	10 ft/sec	$\alpha_1 = 1$	u_3	5.9×10^1	$k_{3,3} = 5.90 \times 10^3$
$x_8 = \delta\hat{s}_u$	4 mrad	$\alpha_2 = 4$	u_4	1.4×10^1	$k_{4,4} = 224$
$x_9 = \delta\hat{s}_v$	4 mrad	$\alpha_2 = 4$	u_5	1.4×10^1	$k_{5,5} = 224$
$x_{10} = \delta\hat{s}_w$	4 mrad	$\alpha_2 = 4$	u_6	1.4×10^1	$k_{6,6} = 224$

Contributors to an error $\delta\hat{s}_{uvw}$ in the measurement of the LOS direction by the pantographic sight include gunner tracking error, electro-mechanical sight errors, and optical canopy errors. In considering the magnitude and bandwidth parameters which should be assigned to the overall sighting error, we must recognize that in the CLFCS the sight is being used to establish the target location relative to the $\underline{u}\ \underline{v}\ \underline{w}$ coordinate set for the initial and calibrated firing bursts, and to measure the angular difference between the aimpoint and strikepoint for the initial burst. These measurements are obtained by:

1. A precise sighting on the target, preparatory to the initial firing burst - $(s_1)_{uvw}$.
2. A sighting on the initial burst strikepoint location - $(s_2)_{uvw}$.
3. A second sighting on the target preparatory to firing the calibrated burst - $(s_3)_{uvw}$.

The unit vectors to these three points, $(s_i)_{uvw}$, $i = 1, 2, 3$, define a spherical triangle over which the sight is deployed in relation to the $\underline{u}\ \underline{v}\ \underline{w}$ coordinate set. There is also an elapsed time factor of about 15 to 20 sec which measures the duration of sight deployment. Error constituents which strongly correlate over the spherical triangle traversed by the sight, whose area is of the order of 25° (or about 7% of the area of the entire sphere), and over an interval of about 15 sec, will be common to the three sightings, and thus substantially counteracted by the closed loop fire control function. Accordingly, the residual error, which limits the effectiveness of the CLFCS, is the random error or lack of repeatibility in measuring angular differences of the order of 50° or less.

General Electric obtained data on this part of the sight error, with the result that it was assigned the value listed on Table 2-25. The break frequency of 4 rad/sec was selected according to the rationale that the largest contributor to the random sighting error component would be gunner tracking error, and that this, in turn should be appropriate to a fairly tight tracking loop closure on the part of the gunner.

The state excitation propagation matrix, B, for the target state estimator is 10 x 6. Its non-zero elements are the terms enclosed in curly brackets in Table 2-23, and are listed below:

$$\begin{aligned} b_{5,1} &= b_{6,2} = b_{7,3} = \alpha_1 \Delta t, \quad \alpha_1 = 1 \text{ rad/sec} \\ b_{8,4} &= b_{9,5} = b_{10,6} = \alpha_2 \Delta t, \quad \alpha_2 = 4 \text{ rad/sec} \end{aligned} \qquad (34)$$

All other elements in the B-matrix are zero.

2.4.5.6 Observation Noise Process

In agreement with the rationale set forth in Section 2.4.4.7, wideband sighting errors are introduced via the L-matrix with variances equal to those of the lowband errors described in Table 2-25. The $\underline{v}$ - vector for the target state estimator has 3 components, one for each component of $\tilde{s}_{uvw}$ (see Table 2-22). Hence, L is 3 x 3, with zero off-diagonal elements and diagonal elements as defined in Table 2-26.

The observation noise propagation matrix, D, is equal to the identity matrix.

$$D = I \qquad (35)$$

TABLE 2-26.

TARGET STATE ESTIMATOR - OBSERVATION NOISE PARAMETERS

Observed Variable	$\underline{v}$ - Element	RMS Error σ_v	L-Element (σ_v^2)
$y_1 = \tilde{s}_u$	v_1	4 mrad	$\ell_{1,1} = 16$
$y_2 = \tilde{s}_v$	v_2	4 mrad	$\ell_{2,2} = 16$
$y_3 = \tilde{s}_w$	v_3	4 mrad	$\ell_{3,3} = 16$

2.4.5.7 Initial State Vector and Estimation Error Covariance Values

As was indicated in Section 2.4.4.8, the initial covariance of the estimation error and the initial values selected for the state elements are related. In the case of the target state estimator, the estimates of the LOS direction cosines are initially established directly from the measured values. That is, at time t = 0,

$$\bar{x}_i = y_i, \quad i = 1, 2, 3 \qquad (36)$$

Accordingly, their error covariances are equal to the sum of the lowband and wideband observation noise components.

$$p_{1,1} = p_{2,2} = p_{3,3} = 4^2 + 4^2 = 32 \text{ mrad}^2 \qquad (37)$$

The initial estimate of range is derived from the range pot on the CLFCS Control Panel. The RMS uncertainty in the crew's estimate of range is expected to be $\sqrt{2.5} = 1.6$ kft, so that

$$p_{4,4} = 2.5 \text{ kft}^2 \qquad (38)$$

States x_5 through x_{10} are auxiliary variables for the generation of stochastic processes representing pseudo target velocity and lowband sight errors. They are initially assigned values of 0, and their initial error covariances are as follows, in accordance with Table 2-25:

$$\begin{aligned} p_{5,5} &= p_{6,6} = 400\ (\text{ft/sec})^2 \\ p_{7,7} &= 100\ (\text{ft/sec})^2 \qquad (39) \\ p_{8,8} &= p_{9,9} = p_{10,10} = 16\ (\text{mrad})^2 \end{aligned}$$

2.4.5.8 Gain Matrix Computation

Two aspects of the target state estimation problem militate against the use of a simple form of gain matrix, such as a set of fixed or explicitly varying gains:

- Rapid settling of the estimator, in order to reach a viable aiming solution as quickly as possible after target acquisition, is vital to the overall effectiveness of the CLFCS.
- The ensemble of target engagements encompasses major variations in aircraft/target geometrical and kinematical relationships. Principal among the parameters subject to such variability are target range and the angle between the LOS and the $\underline{u}$ aircraft axis. These variations, either occurring over the course of a given engagement or from one engagement to another, demand significant variations in the optimal filter gains, which are difficult, if not impossible, to reproduce in an explicit gain formulation.

Initial design effort confirmed the existence of the latter problem and prompted consideration of the real-time generation of the Kalman gains. To alleviate the computational burden, it was decided that a reduced gain update rate should be investigated. The dynamics of the gain variability proved to be such that an update rate of 6 per sec, or 1 update every 5 main frames, preserved essentially all of the full Kalman performance capability.

2.4.6 ANALYSIS OF ESTIMATOR PERFORMANCE

The analysis of the performance of the aircraft and target state estimators was accomplished using the target engagements described in Table 2-9, particularly the veer-off engagement. The analysis was carried out using a version of the Kalman Estimator Analysis Program (KEAP II) described in Appendix B.

2.4.6.1 Analysis of the Aircraft State Estimator

Three particular runs of the KEAP program are of significance in presenting the results of the analysis of the aircraft state estimator:

- G1757 - Operation of aircraft state estimator with Kalman gains generated on-line versus the straight-line attack course.
- G1770 - Operation of the aircraft state estimator with Kalman gains generated on-line versus the veer-off attack course.
- G1799 - Operation of the aircraft state estimator with fixed gains (see Table 2-19) versus the veer-off attack course.

The indices of aircraft state estimator performance are the RMS uncertainties in each of the twelve principal state variables (see Table 2-12). These are plotted in Figures 2-6 through 2-9 for each of the three computer runs listed above.

Figures 2-6 and 2-7 indicate that neither the presence of aircraft maneuvers or the use of fixed gains instead of full Kalman gains is expected to have an appreciable effect on the estimation of aircraft angular velocity and linear acceleration. The length of time required for settling of these state variables is about 3 sec.

Figure 2-8 shows that both the presence of aircraft maneuvers and the mode of gain generation influence the ability to estimate linear velocity. The most significant effect appears in the V_v uncertainty, which is improved by about 6 ft/sec when the Kalman gains are generated in the presence of an aircraft maneuver. This occurs to a lesser degree (about 1.5 ft/sec change)

Figure 2-6.

AIRCRAFT ANGULAR VELOCITY ESTIMATION UNCERTAINTY

No. G1757 - KALMAN GAINS VERSUS STRAIGHT COURSE
No. G1770 - KALMAN GAINS VERSUS VEER-OFF COURSE
No. G1799 - CONSTANT GAINS VERSUS VEER-OFF COURSE

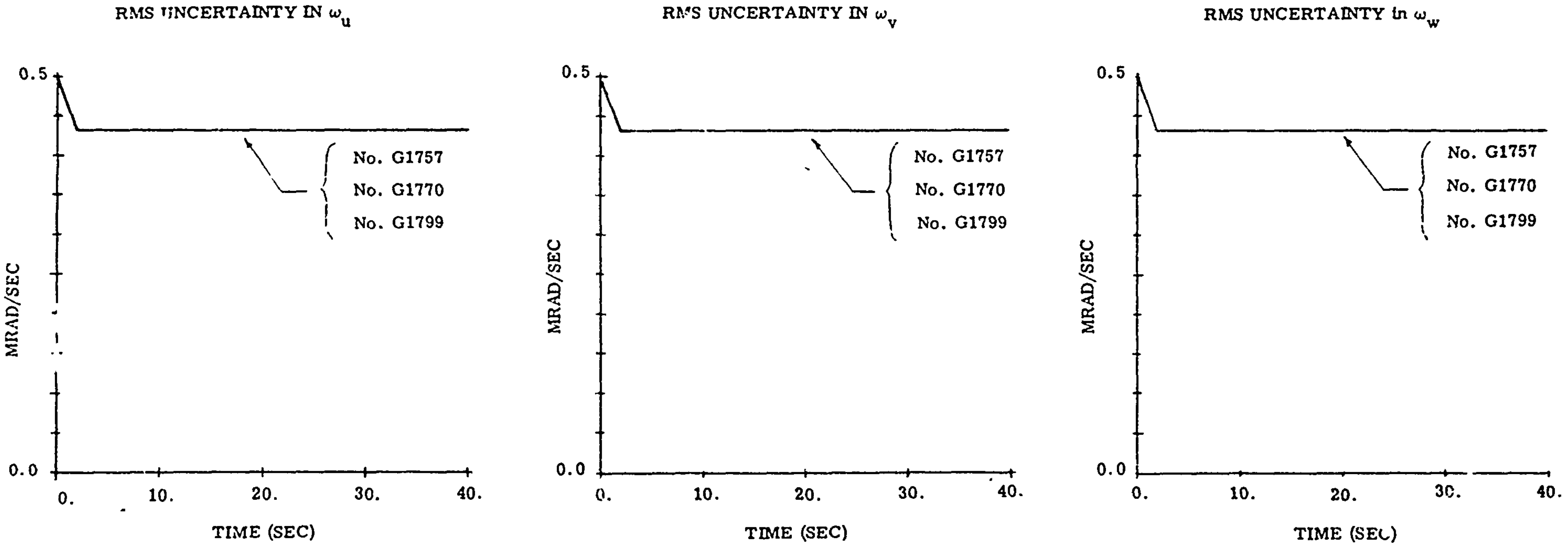

RMS UNCERTAINTY IN ω_u

RMS UNCERTAINTY IN ω_v

RMS UNCERTAINTY in ω_w

Figure 2-7

AIRCRAFT LINEAR ACCELERATION UNCERTAINTY

No. G1757 - KALMAN GAINS VERSUS STRAIGHT COURSE
No. G1770 - KALMAN GAINS VERSUS VEER-OFF COURSE
No. G1799 - CONSTANT GAINS VERSUS VEER-OFF COURSE

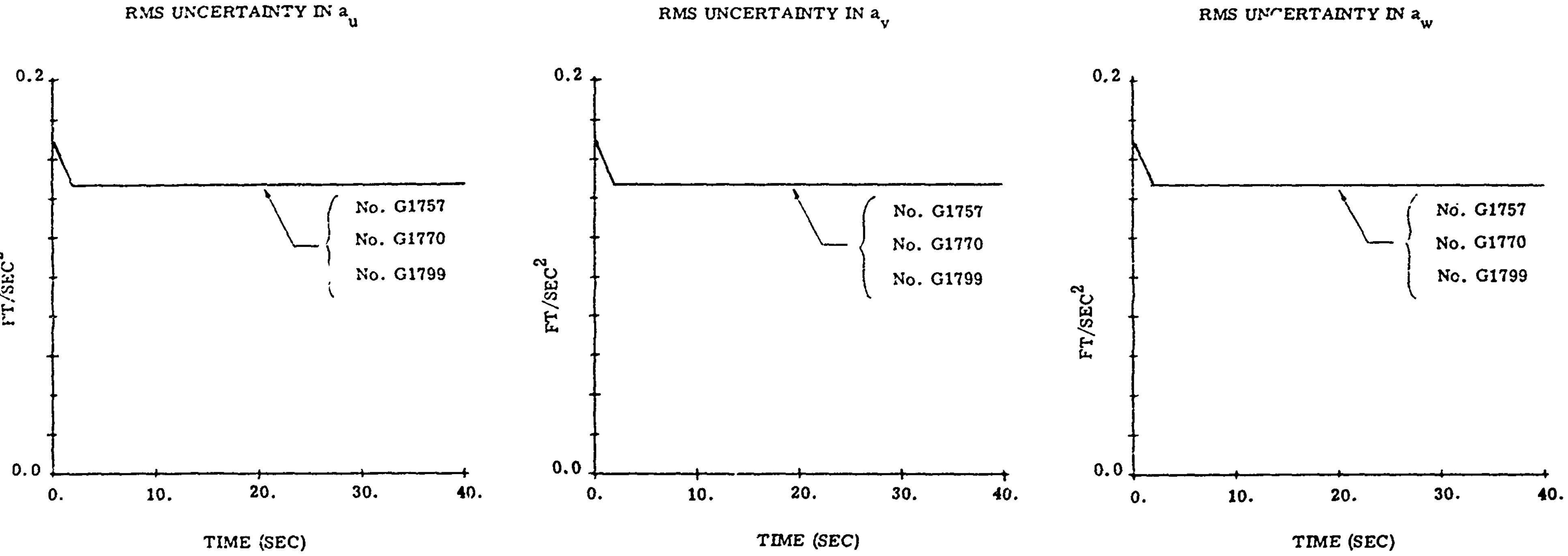

Figure 2-8.

AIRCRAFT LINEAR VELOCITY UNCERTAINTY

No. G1757 - KALMAN GAINS VERSUS STRAIGHT COURSE
No. G1770 - KALMAN GAINS VERSUS VEER-OFF COURSE
No. G1799 - CONSTANT GAINS VERSUS VEER-OFF COURSE

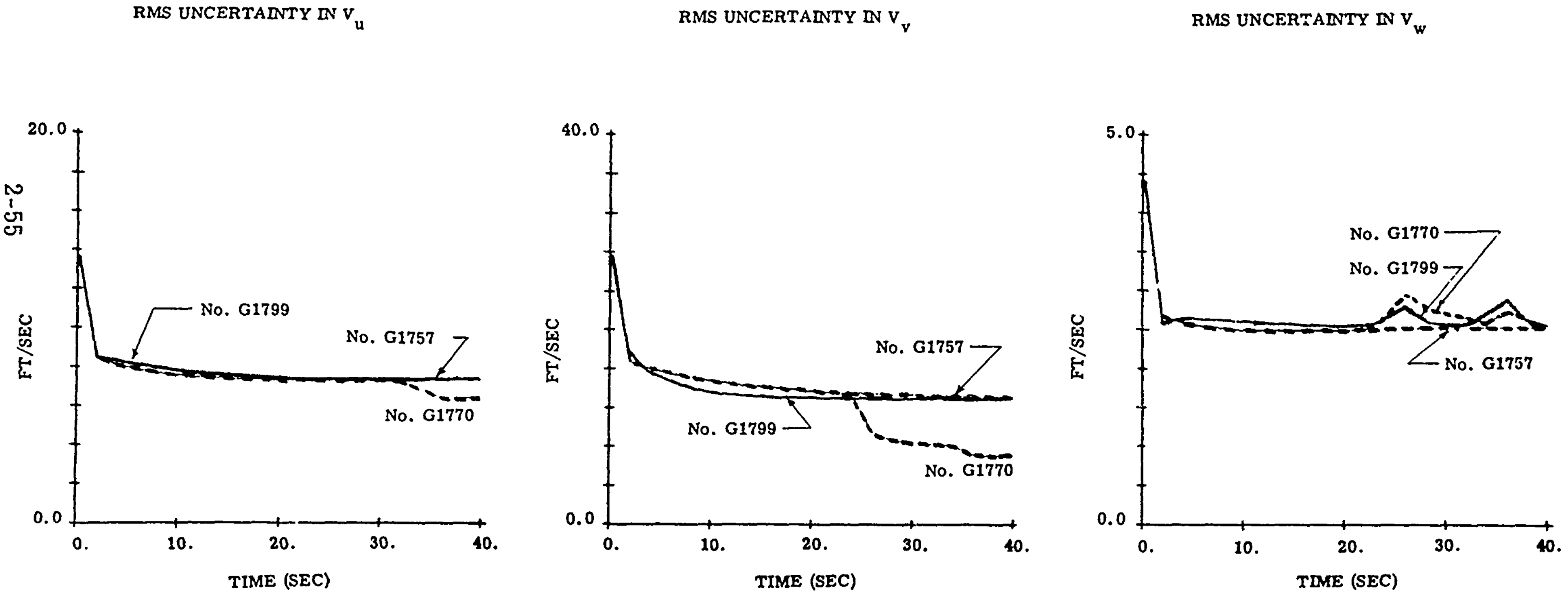

RMS UNCERTAINTY IN V_u — RMS UNCERTAINTY IN V_v — RMS UNCERTAINTY IN V_w

Figure 2-9.

VERTICAL AXIS DIRECTION UNCERTAINTY

No. G1757 - KALMAN GAINS VERSUS STRAIGHT COURSE
No. G1770 - KALMAN GAINS VERSUS VEER-OFF COURSE
No. G1799 - CONSTANT GAINS VERSUS VEER-OFF COURSE

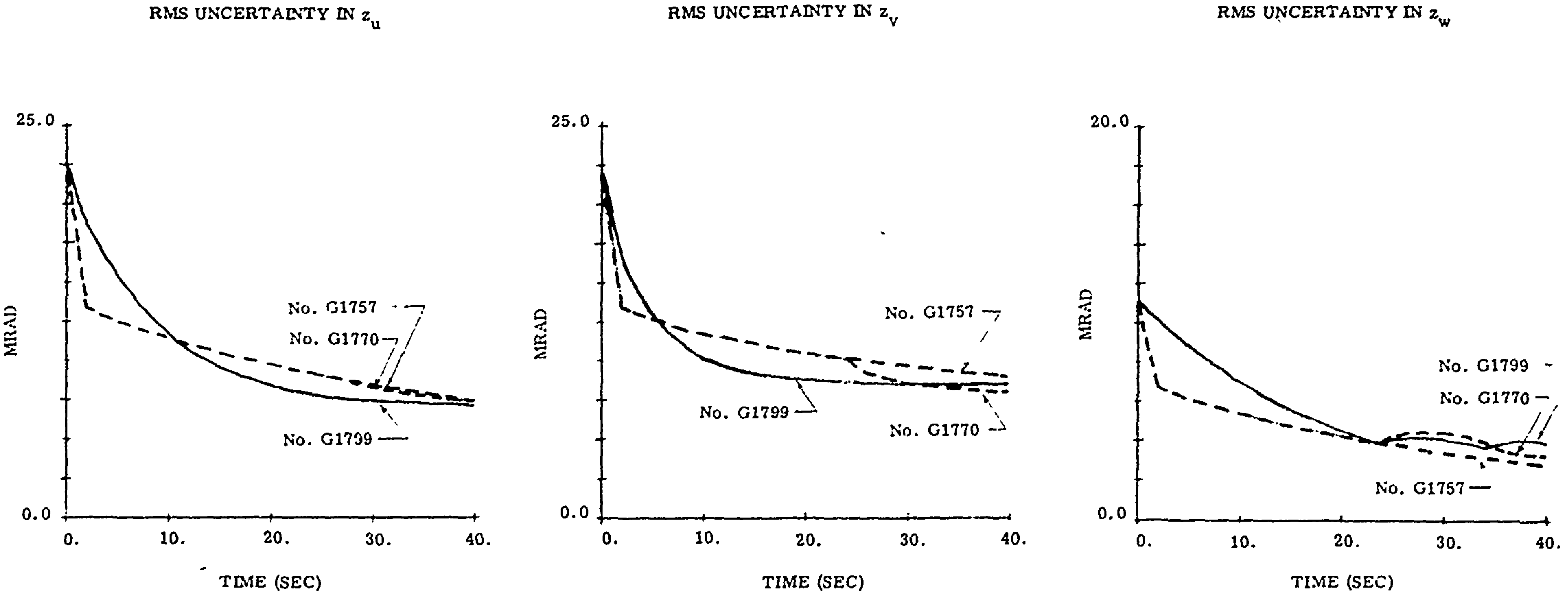

RMS UNCERTAINTY IN z_u

RMS UNCERTAINTY IN z_v

RMS UNCERTAINTY IN z_w

in the case of V_u. The estimation of V_w is less effected by the use of fixed versus Kalman gains than by the mere presence of the maneuver, which slightly degrades the quality of the estimate (about 0.5 ft/sec change).

The principal effect evident in Figure 2-9 is the superior settling time afforded by the use of Kalman gains. In comparison, the effect of the maneuver is of the order of 1.5 mrad or less. Since the aircraft state estimator will normally be allowed to run continuously, settling time is not an important issue insofar as CLFCS effectiveness is concerned. The accuracy of knowledge of the vertical axis direction required for 20 mm gunnery is about 1°, and this level of uncertainty is reached in less than 10 sec with the fixed gain estimator, and in about 2 sec with Kalman gains. Therefore, if it should be necessary to restart the aircraft state estimator in flight, a fully viable output for gunnery purposes will be available in about 10 sec.

2.4.6.2 Analysis of the Target State Estimator

The performance of the target state estimator was assessed for the veer-off attack described in Table 2-9 and Figure 2-2. The engagement was carried through the crossover event to assure that the onset of crossover kinematics would not cause estimator instability or other anomalous behavior. This was done in spite of the fact that the pantographic sight cannot be comfortably deployed beyond a train angle of about 80°.

The principal matter of concern in the analysis of the target state estimator is the comparison of its performance with Kalman gains updated once per 5 computer frames (operational system) versus once per frame (performance baseline system).

Figure 2-10 shows the resultant RMS uncertainty in LOS direction and the RMS uncertainty in range plotted as a function of time. For the critical stage of the run, which lies between 15 and 30 sec and corresponds to the period of CLFCS deployment, the difference between the two gain update rates is insignificant. It becomes appreciable, particularly with respect to range estimation, at crossover, and then subsides after crossover. This indicates that the crossover kinematics are inducing rapid changes in the Kalman gains, which the reduced update rate has difficulty in following. Nevertheless, the performance of the target state estimator with gain updates once per 5 computer frames is judged to be perfectly adequate for application to the CLFCS.

Figure 2-10.

TARGET STATE ESTIMATOR PERFORMANCE COMPARISON

GAIN UPDATES 1/1 FRAME VERSUS 1/5 FRAMES

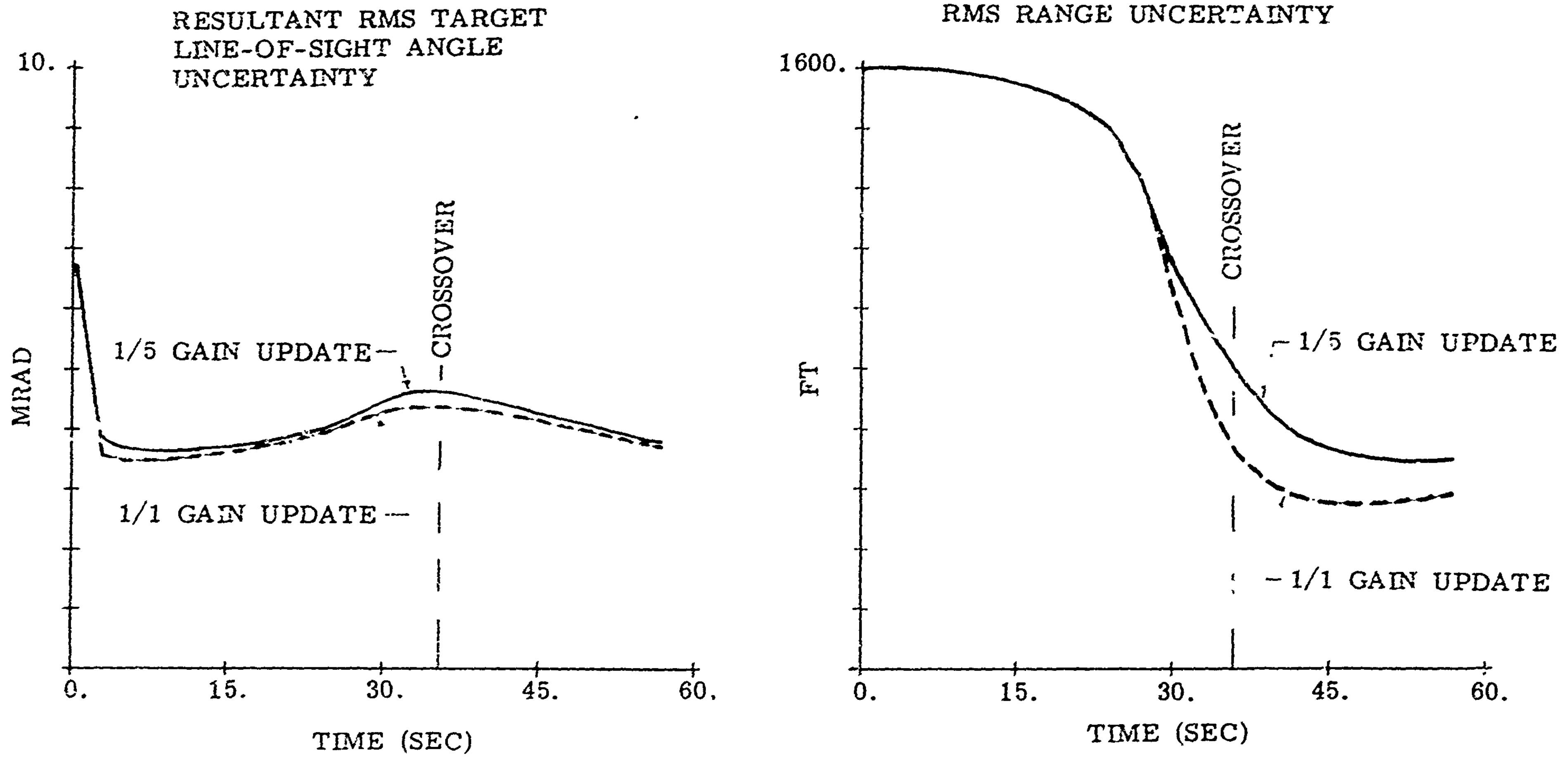

2.5 OPEN LOOP FIRE CONTROL COMPUTATION

The objective of the open loop fire control computations (as distinguished from closed loop fire control) is to position the gun in the best way possible on the basis of the outputs of the aircraft and target state estimators. This assures a maximum first burst kill probability and also provides for the maintenance of a viable gun pointing solution through all phases of the attack, including the period of strikepoint observation by the gunner.

The discussion of the open loop fire control computation is divided into three parts:

- Fitting time of flight and gravity drop expressions to the 20 mm M-56 ballistics.
- Developing the gun orders for positioning the weapon.
- Verification of accuracy.

2.5.1 BALLISTICS OF THE M-56 PROJECTILE

Table 2-27 lists the slant range (R_S) and gravity drop (R_Z) corresponding to times of flight (T_F) ranging from 0 to 4.5 sec.

2.5.1.1 Time of Flight Equation

To determine the correct angular relationship between the gun axis and the target sightline, an estimate of the projectile time of flight is required. The principal use in helicopter gunnery is to determine the magnitude of gravity drop.

Let the following variables be defined:

B = Projectile muzzle velocity = 3320 ft/sec

C_1 = Drag parameter

R = Range-rate (negative of the component of aircraft velocity along the sightline)

ρ_g/ρ_o = Air density ratio

TABLE 2-27
BALLISTICS OF THE M-56 PROJECTILE

T_F (sec)	R_S (ft)	R_Z (ft)
0	0.0	0.0
0.5	1405.4	3.6
1.0	2432.3	13.2
1.5	3216.1	27.6
2.0	3838.0	46.3
2.5	4368.8	69.8
3.0	4855.9	99.1
3.5	5309.8	134.1
4.0	5735.8	174.8
4.5	6137.4	220.9

Conditions:
Aircraft velocity = 0
Aircraft altitude = 0 (Sea Level)
Gun position = Horizontal

A form for the time of flight equation which is compatible with the drag characteristics of supersonic projectiles is:

$$T_F = \frac{R_S}{(B - R) - \frac{C_1}{2}\sqrt{B - \dot{R}}\ R_S} \tag{40}$$

For an optimized fit to the M-56 ballistics of Table 2-27, the value of C_1 is selected to be

$$C_1 = 10.3998 \times 10^{-3}\ \rho_g/\rho_o \tag{41}$$

The data of Table 2-27 corresponds to $\rho_g/\rho_o = 1$. The appearance of ρ_g/ρ_o in the expression for C_1 reflects the reduction in drag with increased aircraft altitude.

It is convenient to define

$$B_1 = \frac{C_1}{2} \sqrt{B - \dot{R}} \tag{42}$$

so that

$$T_F = \frac{R_S}{(B - R) - B_1 R_S} \tag{43}$$

2.5.1.2 Gravity Drop Equation

A form for the gravity drop equation which is descriptive of the flight of supersonic projectiles and compatible with the time of flight equation (40) is as follows:

$$R_Z = q\, T_F^{\,2}/2, \quad q = q_1 - q_2\,(\rho_g/\rho_o)\, T_F \tag{44}$$

An optimized fit to the M-56 ballistic data of Table 2-27 is achieved by the selection

$$\begin{aligned} q_1 &= 27.6746 \text{ ft/sec}^2 \\ q_2 &= 0.176772 \text{ ft/sec}^3 \end{aligned} \tag{45}$$

Using equations (40), (41), (44) and (45) in combination, it is determined that the RMS deviation between the ballistic model and the data of Table 2-27 is 1.07 mrad.

2.5.2 DERIVATION OF GUN ORDERS

Let the following additional variables be defined:

$\underline{g}$ = Gunline direction

$\underline{s}$ = Sightline direction

$\Delta \underline{g}$ = Differential gun orders
= $\underline{g} - \underline{s}$

$\underline{V}$ = Airspeed vector

$\underline{W}$ = Wind velocity vector

$\underline{z}$ = Vertical axis direction

$\underline{B}$ = Bullet position vector

$\underline{R}$ = $R\underline{s}$ = Target position vector

It is possible to show that the position of the bullet relative to the launching point, as a function of time of flight, is

$$\underline{B} = \frac{(B\underline{g} + \underline{V})\,T_F}{1 + B_1 T_F} + \underline{W}T_F - (qT_F^{\,2}\ 2)\underline{z} \tag{46}$$

Since it is desired that the bullet impact the target, 1st

$$\underline{B} = R\underline{s} \tag{47}$$

Also, let

$$\underline{g} = \underline{s} + \Delta\underline{g},\ R_z = qT_F^{\,2}\ 2 \tag{48}$$

Then equation (47) becomes

$$R\underline{s} = \frac{(B - \dot{R})T_F\,\underline{s}}{1 + B_1\,T_F} + \frac{(B\Delta\underline{g} + \underline{V} + \dot{R}\underline{s})T_F}{1 + B_1\,T_F} + \underline{W}T_F - R_z\underline{z} \tag{49}$$

It can be shown from equation (43) that

$$R = \frac{(B - \dot{R})T_F}{1 + B_1 T_F} \tag{50}$$

Solving for the differential gun order by transposing terms in equation (49)

$$\Delta \underline{g} = \frac{(1 + B_1 T_F)(-\underline{W} T_F + R_z \underline{z})}{B T_F} - \frac{\underline{V} + R \underline{s}}{B} \tag{51}$$

$$= \left(\frac{B - \dot{R}}{B}\right)\left(\frac{-\underline{W} T_F + R_z \underline{z}}{R}\right) - \frac{V + \dot{R} \underline{s}}{B} \tag{51}$$

In the CLFCS, the input data required for estimating wind velocity are not available. The open loop fire control solution is therefore based upon the assumption of zero wind velocity. Accordingly, the solution for the differential gun orders actually implemented is

$$\Delta \underline{g} = \left(\frac{B - \dot{R}}{B}\right)\left(\frac{R_z}{R}\right) - \frac{\underline{V} + \dot{R} \underline{s}}{B} \tag{52}$$

As may be seen from equation (51), the effect of wind velocity normal to the sightline is to induce a bullet strikepoint error which varies according to the ratio (T_F/R). This is the inverse of the average projectile velocity, which is shown in Table 2-28 for $T_F = 2, 3$, and 4 sec.

In the case of firing from hover, the angular deflections induced by a 10 ft/sec wind velocity at 2, 3, and 4 sec times of flight are 5.2, 6.2, and 7.0 mrad, respectively. The closure of the aircraft on the target occurring over the interval between the initial calibration firing burst and the second calibrated burst is not likely to reduce the time of flight by more than a second.

TABLE 2-28

AVERAGE PROJECTILE VELOCITY VS TIME OF FLIGHT

T_F (sec)	AVERAGE PROJECTILE VELOCITY (ft/sec)
2.0	1919
3.0	1619
4.0	1434

Also, typically, the direction of fire will not rotate relative to the wind direction by more than a few degrees. Therefore, the fact is evident that the deflection induced by a steady wind may be regarded as a substantially constant angular effect. The wind velocity itself will tend to correlate strongly over periods of 10 to 20 sec. Hence, windage is included among those strikepoint error contributors which are amenable to compensation via closed loop fire control.

2.5.2.1 Control of Gun Position

It is desired that the computer output a set of differential gun orders which are such that when added to the unfiltered electrical sight outputs the gun will be positioned correctly. By this means, if the computer should fail, the gun can be slaved directly to the sight without system reconfiguration.

Let the following variables be defined:

$\hat{s}_{uvw}$ = Estimated target line of sight direction cosines

$\overset{w}{s}_{uvw}$ = Unfiltered target line of sight direction cosines obtained directly from the sight

The desired gun direction is then given by

$$g_{uvw} = \hat{s}_{uvw} + \Delta g_{uvw} \qquad (53)$$

and the differential gun orders which should be added to the sight outputs, by

$$\begin{aligned} \Delta g^*_{uvw} &= g_{uvw} - \overset{w}{s}_{uvw} \\ &= g_{uvw} + s_{uvw} - \overset{w}{s}_{uvw} \qquad (54) \end{aligned}$$

2.5.3 VERIFICATION OF ACCURACY

In Section 2.3.3 a veer-off target engagement is described which has been utilized for demonstration of the performance of the aircraft and target state estimators. An episode from this same engagement provides the basis for a numerical check of the accuracy of the open loop fire control solution defined above.

Specifically, at the t = 24 sec point in the veer-off engagement an open loop firing burst is assumed to occur. Gun position is established by the open loop fire control algorithm embodied in equations (52) and (54) on the presumption of ideal velocity and range inputs. The bullet impact point corresponding to this solution is determined by evaluating equation (46) for incremented values of time of flight until the approximate point is discovered (to within 0.1 ft) at which the bullet passes through the horizontal plane containing the target. The strikepoint error is then calculated in terms of both horizontal and angular miss.

The computations described above are executed by a time shared computer program "GQGUN", a listing of which is contained in Appendix D. The output listing pertinent to the open loop fire control solution is shown in Table 2-29.

THIS PAGE IS BEST QUALITY PRACTICABLE
FROM COPY FURNISHED TO DDC

TABLE 2-29

VERIFICATION OF OPEN LOOP FIRE CONTROL ACCURACY

```
GQGUN          08:55EST      11/23/76

FIRST FIRING CONDITION

OPEN LOOP FIRE CONTROL DATA
TARGET SIGHTLINE DIRECTION COSINES:
SU= 0.940513 RAD
SV=-0.335301 RAD
SW=-5.31038E-2 RAD
EST RANGE= 5351.23 FT
EST RANGE-RATE=-187.596 FT/SEC
DRAG COEF= 0.303177 1/SEC
EST TF= 2.85082 SEC
EST GRAV DROP= 110.331 FT
COMPUTED LEAD ANG.
DU=-8.83213E-3
DV=-2.08215E-2
DW= 1.31927E-2
COMPUTED GUNLINE DIRECTION COSINES:
GU= 0.933502 RAD
GV=-0.356729 RAD
GW=-3.09837E-2 RAD
GUN ELEV=-3.99243E-2 RAD
GUN TRAIN= 0.36507 RAD

STRIKEPOINT DATA
ACTUAL TF= 2.846 SEC
DBX= 4.05188 FT
DBY=-0.824959 FT
DBZ= 2.35596E-2 FT

HORIZ MISS= 4.13501 FT

ANGULAR MISS= 3.34579E-2 MRAD
```

The angular miss relative to the target sightline is calculated to be 0.083 mrad, and the linear miss on the horizontal ground plane is 4.1 ft. This means that in actual operation only a minor part of the strikepoint error in the open loop firing burst can be ascribed to the open loop fire control algorithm itself. The major part will be due to errors in the estimated state variable input, to the algorithm; namely, range and velocity.

Because the CLFCS does not incorporate an active rangefinder, the range estimation error at the instant of the open loop firing burst may be quite large. Specifically, the error in the initial crew estimate of range at the commencement of the engagement can be as great as 40%. The target state estimator displays some capability to reduce this initial error during the period of target tracking preparatory to the open loop firing burst (see Figure 2-10). Nevertheless, a 25% error in range can still exist at that point in the engagement. Figure 2-11 shows the variation in the angular strikepoint error as a function of range error. The error sensitivity relationship is approximately 10 mrad of strikepoint error per 1000 ft of range error.

Wind is the main contributor to velocity estimation error, and the strikepoint error resulting therefrom is strongly a function of the orientation of the wind velocity vector relative to the target sightline. A velocity error of 20 ft/sec normal to the sightline will produce approximately 6 mrad of angular miss.

Bias errors in the estimates of range and velocity are among the effects which the closed loop fire control algorithm is designed to counteract. The formulation of this algorithm is now described in detail.

2.6 CLOSED LOOP FIRE CONTROL COMPUTATIONS

Figure 2-1 portrays the overall organization of the CLFCS software. As shown in this figure, the closed loop fire control algorithm absorbs target state information and the direction cosines of the centroid of the open loop firing burst impacts, as observed by the gunner utilizing the pantographic sight. Its output is a set of gun corrections which counteract the errors which existed in the open loop fire control solution when the initial burst was fired. These errors include:

- Gun boresight error
- Range bias error
- Velocity bias error

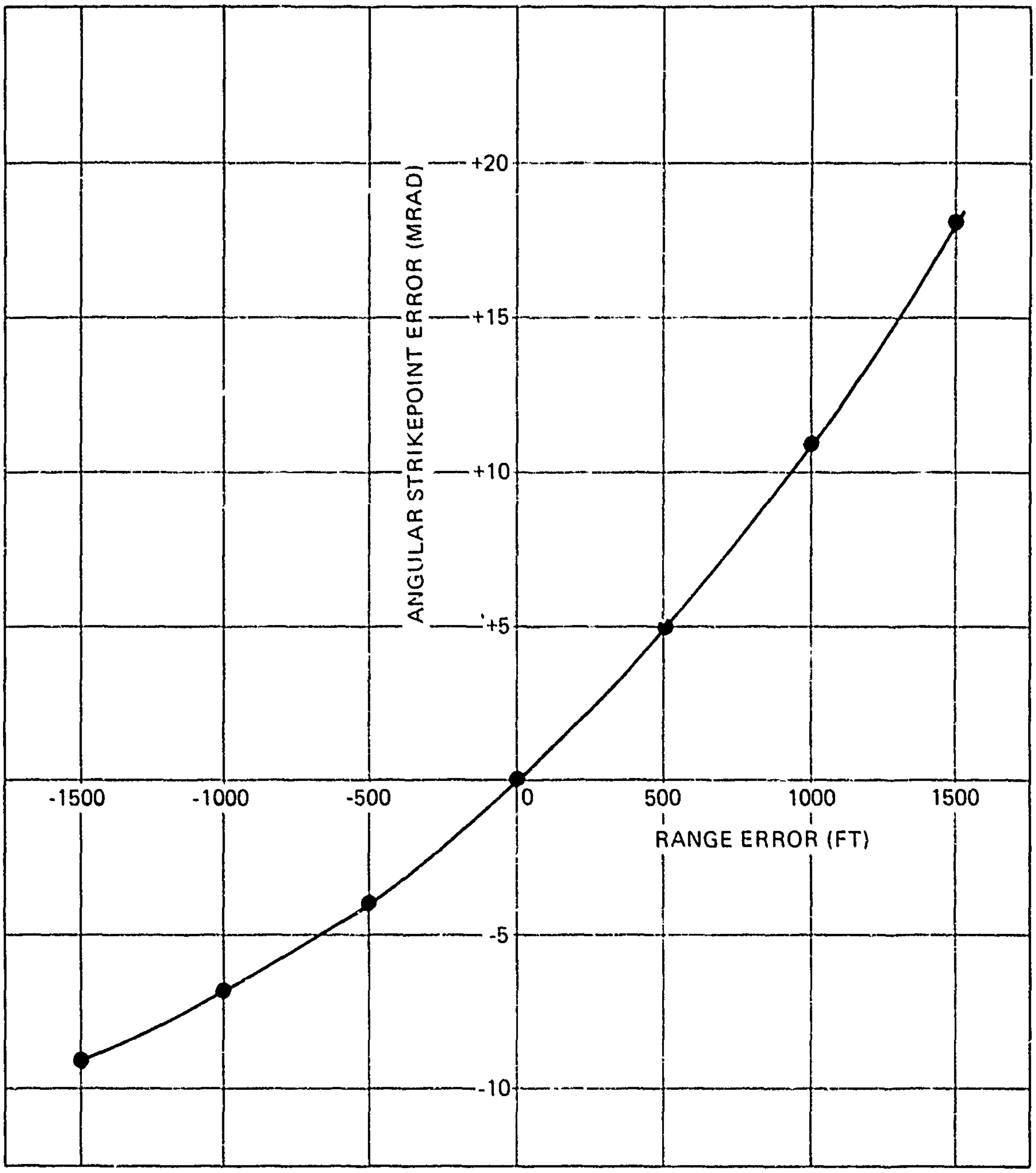

- OPEN LOOP FIRING CONDITION
- RANGE ≈ 5400 FT

Figure 2-11. Angular Strikepoint Error VS Range Error

A key feature of the closed loop fire control algorithm now to be described in an interpolation scheme for developing an accurate estimate of the target sightline at the instant the gunner makes the bullet strikepoint observation.

2.6.1 OVERALL PHILOSOPHY AND EVENT TIMING

Figure 2-12 illustrates the operation of the closed loop fire control algorithm, particularly with respect to the timing of the engagement events.

After a period of tracking the target (approximately 3 sec), the gunner depresses the trigger at time t_1 for a short ($\sim$ 1 sec) initial firing burst. Target tracking is continued through the bullet time of flight until time t_2.

Figure 2-13 shows that the bullet impact event will occur after a time of flight, T_f, which falls within the following range:

$$.95\hat{T}_F < T_F < 1.50\,\hat{T}_F$$

where $\hat{T}_F$ is the estimated time of flight used in the initial aiming solution. Accordingly, although the estimated time of flight may be in error insofar as the target is concerned, it will generally be a good indication of the actual time of flight to the strikepoint. The CLFCS computer can therefore predict fairly well when it is appropriate for the gunner to break track with the target and begin acquiring the strikepoint.

At time t_2, the computer signals the gunner that the target track may be broken. It is imperative that the gunner maintain precise tracking through this event, and then acquire the strikepoint as soon as possible thereafter.

When he has acquired the strikepoint, the gunner depresses the ABC (Acquire Burst Centroid) switch at time t_3. This signals the computer to capture the sight resolver outputs as a measure of strikepoint angular position. Precise pointing of the sight with respect to the burst centroid is essential.

As rapidly as possible, the gunner reacquires the target at time t_4. When he has a precise point established, he releases the ABC switch. At time t_5, after a short period of tracking, the second burst is fired, which is a calibrated burst.

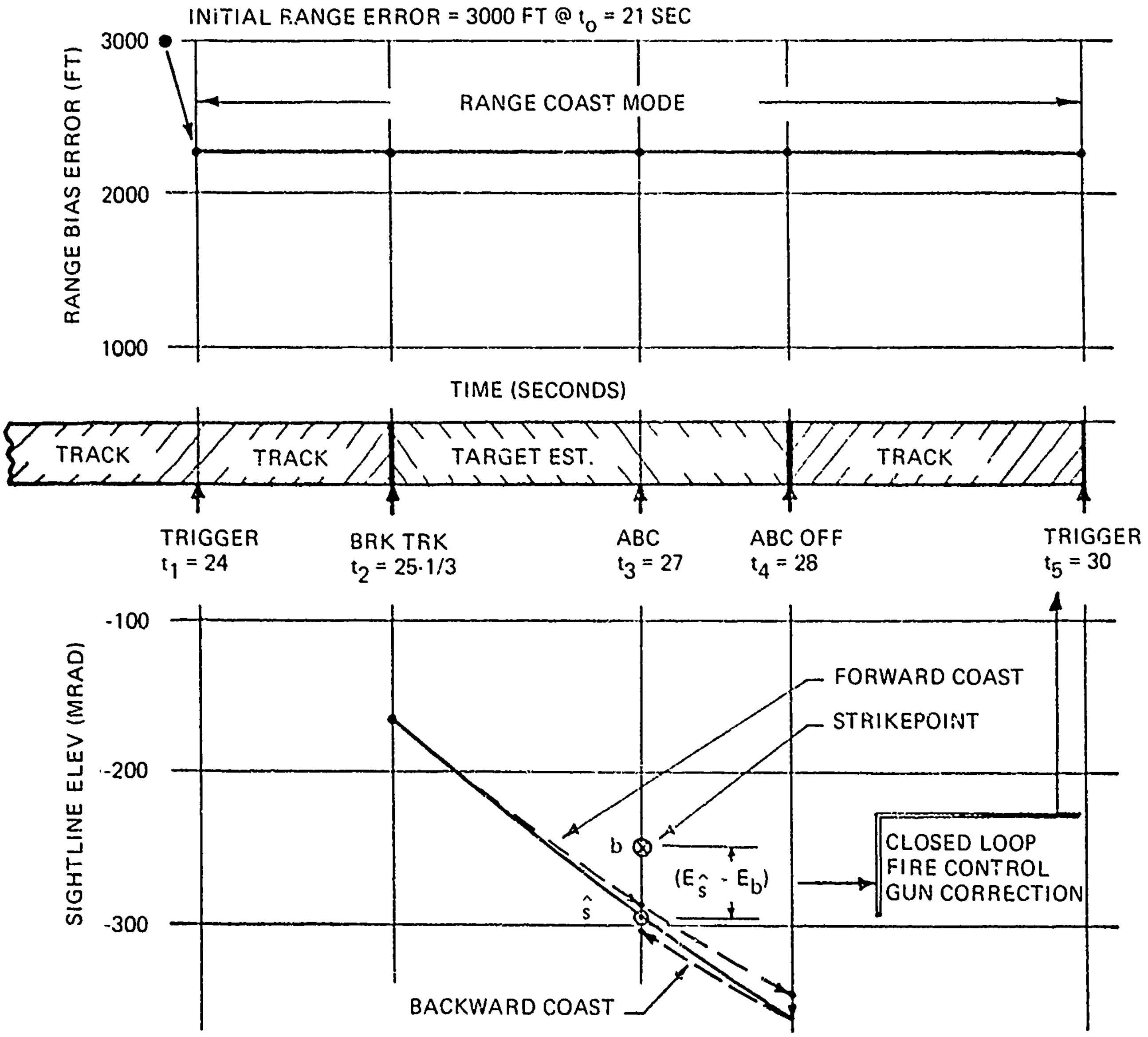

Figure 2-12. Illustration of the Operation of the Modified Closed Loop Fire Control Algorithm

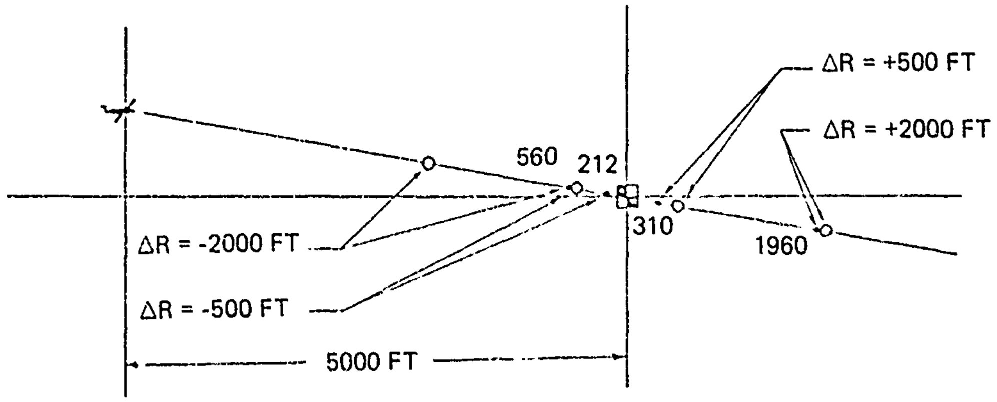

Figure 2-13. The Relationship Between Range Bias Error and Strikepoint Error - Horizontal Plane View

2.6.2 TARGET STATE ESTIMATED MODES

For time $t < t_1$, the target state estimator is in its normal mode of operation with all gains active.

For time $t_1 \leq t \leq t_5$, the gains which are associated with the estimation of range (the entire fourth row) are set to zero. This is to prevent competition between the target state estimator and the closed loop fire control algorithm in compensating for any error which may exist in the range estimate at time t_1.

At time t_2 the target state estimator enters a full coast mode with all gains set to zero. By virtue of precise target tracking during the interval $t_1 \leq t \leq t_2$, the estimated and true versions of the target sightline are assumed to be equal. However, due to range and velocity bias errors, the extrapolated sightline diverges from the true for $t_3 \leq t \leq t_4$, as illustrated in Figure 2-12. The state of the extrapolated target sightline at time t_3 is captured by the computer for use in the closed loop fire control algorithm.

At time t_4, the target state estimator returns to the range only coast mode; that is, all gains except those in the fourth row are active.

2.6.3 CLOSED LOOP FIRE CONTROL ALGORITHM DESCRIPTION

The closed loop fire control algorithm references the observed strikepoint location to the location of the target. Accordingly, a precise measure of the target location at time t_3 is required. Since the gunner is not tracking the target at this instant, interpolation of target sightline information from times t_3 and t_4 are required.

Let the following variables be defined:

$\overset{w}{\underline{s}}(t)$ = Unfiltered sight direction cosines at time t

$\hat{\underline{s}}(t)$ = Estimated target sightline at time t

$\underline{s}(t)$ = True target sightline at time t

The extrapolated sightline at time t_3 $\hat{\underline{s}}(t_3)$, differs significantly from the true because of range and velocity bias errors. However, by developing a second estimate, extrapolated backwards from time t_4, a reduction of this error is possible. Let the forward extrapolated value be designated $\hat{\underline{s}}_F(t_3)$ and the backward by $\hat{\underline{s}}_B(t_3)$.

By storing the linear and angular velocities of the aircraft over the time interval $t_3 \leq t \leq t_4$, and assuming that $\overset{w}{\underline{s}}(t_4) = \underline{s}(t_4)$ by virtue of precise pointing of the sight by the gunner, the backward extrapolation of the target sightline from t_4 to t_3 can be implemented. As illustrated in Figure 2-12, this extrapolation follows a path parallel to that of the forward extrapolation. It is evident that the average of $\hat{\underline{s}}_F(t_3)$ and $\hat{\underline{s}}_B(t_3)$ provides an accurate measure of $\underline{s}(t_3)$; especially if

$$t_3 - t_2 \approx t_4 - t_3.$$

Let

$$\hat{\underline{s}}(t_3) = \frac{1}{2}[\hat{\underline{s}}_F(t_3) + \hat{\underline{s}}_B(t_3)]$$

where this averaging will actually be implemented in terms of the elevation and train angles associated with $\hat{\underline{s}}_F(t_3)$ and $\hat{\underline{s}}_B(t_3)$ rather than in terms of the direction cosines. The detailed steps are given in the sequel.

The observed sightline to the burst centroid or strikepoint is designed $\underline{b}$, and the difference

$$\delta \underline{g} = \hat{\underline{s}}(t_3) - \underline{b}$$

measures the gun error existing at time t_1, provided the aircraft neither rotates nor translates excessively during the interval $t_1 < t < t_3$. This difference may be applied directly to the correction of the gun orders at time t_5.

In the [illegible] mechanization described in the sequel, the computation and application of δg is [illegible] in terms of elevation and train angles.

2.6.4 DETAILED ALGORITHM STEPS

The following 17 steps impact the details of the closed loop fire control algorithm, including program logic. The steps are summarized in the CLFC Subroutine Sequence Chart of Figure 2-14.

1. Detect the time t_1 event. Set the target state estimator gains in the fourth row (i.e., those affecting the estimate of range) equal to zero.

2. Using the estimated value of time of flight, $\hat{T}_F$, compute

   $$t_2 = t_1 + K\hat{T}_F$$

   where K is to be initially set to a value of 0.95, but it must be adjustable during flight test.

3. The gunner continues precise tracking of the target over the interval $t_1 < t < t_2$. Having defined the time t_2 event, signal the gunner to break target track via the flashing ready-to-fire light. Discontinue flashing after about 1 sec to avoid interference with the acquisition of the strikepoint.

4. Also at t_2, commence target state estimator forward coast with all gains set to zero.

5. Detect the closure of the ABC switch, defining the t_3 event. Capture the sight direction cosines and define them to be the strikepoint vector b_{uvw}. If $\overset{w}{s}_{uvw}(t_3)$ is the unfiltered sight output at time t_3, then

   $$b_{uvw} = \overset{w}{s}_{uvw}(t_3)$$

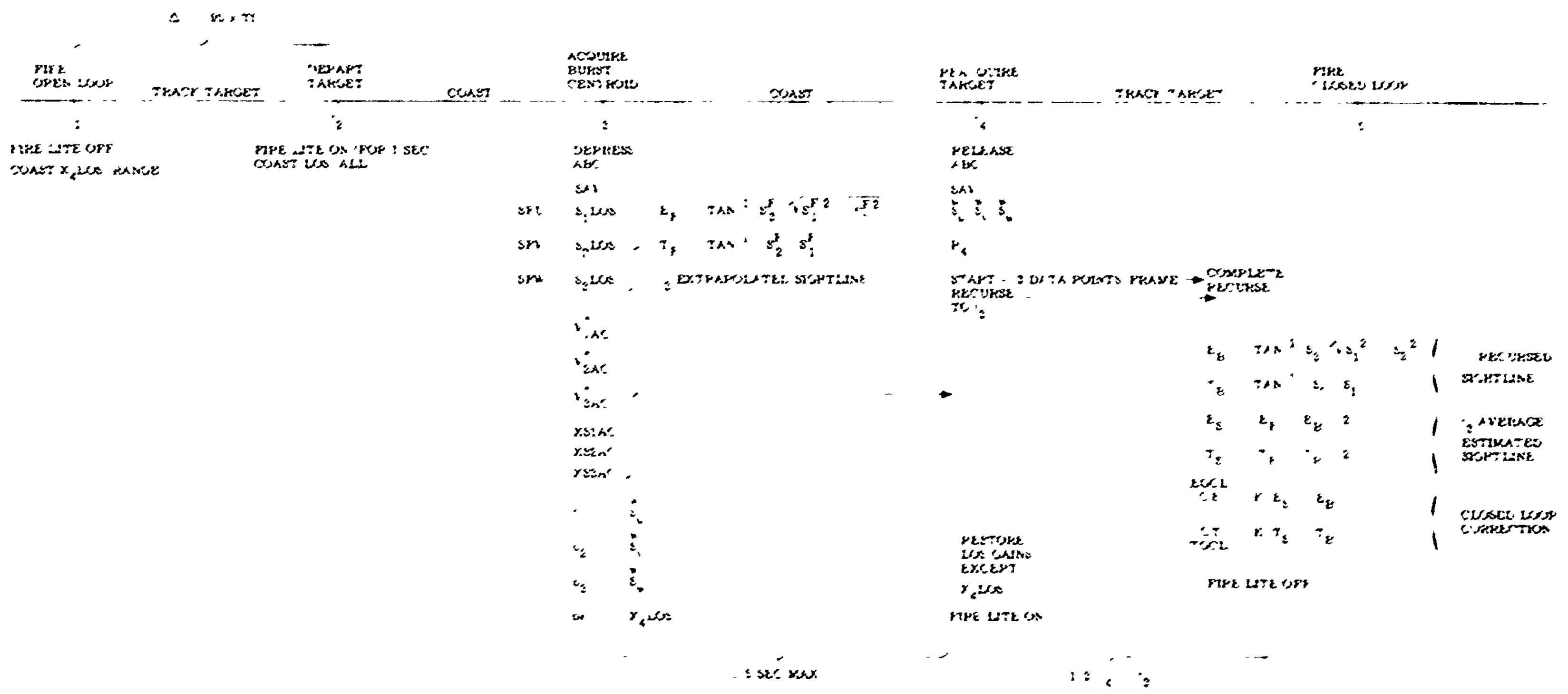
FIRE OPEN LOOP
TRACK TARGET
DEPART TARGET
COAST
ACQUIRE BURST CENTROID
COAST
REACQUIRE TARGET
TRACK TARGET
FIRE CLOSED LOOP
FIRE LITE OFF
COAST X_4LOS RANGE
FIRE LITE ON FOR 1 SEC
COAST LOS ALL
DEPRESS ABC
SAV
RELEASE ABC
EXTRAPOLATED SIGHTLINE
START - 3 DATA POINTS FRAME
RECURSE
COMPLETE RECURSE
RECURSED SIGHTLINE
AVERAGE ESTIMATED SIGHTLINE
CLOSED LOOP CORRECTION
RESTORE LOS GAINS EXCEPT X_4LOS
FIRE LITE ON
FIRE LITE OFF
5 SEC MAX

Figure 2-14. Closed Loop Fire Control Subroutine Sequence

6. Also at t_3, capture the extrapolated target sightline direction cosines, $\hat{s}_{uvw}(t_3)$. These are given a distinct label for future use.

$$s_{Fu}(t_3) = \hat{s}_u(t_3)$$

$$s_{Fv}(t_3) = \hat{s}_v(t_3)$$

$$s_{Fw}(t_3) = \hat{s}_w(t_3)$$

The subscript "F" designates the forward coasted value of the target sightline, as distinct from the backward coasted value defined below.

7. Also at t_3, commence storage of $V^*_{1,2,3}$ and $\omega_{1,2,3}$ as used in the target state estimator transition process. This storage process continues until the event t_4 when the ABC switch is released.

8. Detect the event t_4 (release of ABC switch), which signals the fact that the gunner has re-established a precise target point. Capture the unfiltered sight direction cosines $\overset{w}{s}_{uvw}(t_4)$. Stop the target state estimator forward coast and return it to its normal mode of operation except for the estimation of range. That is, reactivate all gains except for those in the fourth row; these should be maintained at zero.

9. Also at t_4, commence a backward coast of the target state transition process using the algorithm listed in Table 2-30. Initialize this process with the unfiltered sight direction cosines, $\overset{w}{s}_{uvw}(t_4)$, and the estimated range, $\hat{R}(t_4)$, resulting from the forward coast of the target state over $t_2 \le t \le t_4$. Using the nomenclature of Table 2-31, set

$$S1 = \overset{w}{s}_u(t_4),$$

$$S2 = \overset{w}{s}_v(t_4),$$

$$S3 = \overset{w}{s}_w(t_4),$$

$$R = \hat{R}(t_4).$$

With k_3 and k_4 designating the computer frames corresponding to times t_3 and t_4, and $V^*_{1,2,3}(k)$ and $\omega_{1,2,3}(k)$, the stored linear and angular velocity data, the backward coast algorithm of Table 2-31 is to be executed for $K = k_4 - 1, k_4 - 2, k_4 - 3, \ldots, k_3$; that is, for $k_4 - k_3$ recursions.

10. At the completion of the backward coast process, capture the extrapolated target sightline direction cosines.

$$s_{Bu}(t_3) = S1$$

$$s_{Bv}(t_3) = S2$$

$$s_{Bw}(t_3) = S3$$

TABLE 2-30

BACKWARD INTEGRATION ALGORITHM

```
      DRS       =   0
      DS1S      =   0
      DS2S      =   0
      DS3S      =   0
      DO 25 I   =   1, 2
      RDOT      =   (V1 * S1 + V2 * S2 + V3 * S3)
      DR        =   - DT * RDOT
      R         =   R + DR - DRS
      DS1       =   DT * ((V1 + RDOT * S1)/R + (W2 * S3 - W3 * S2))
      DS2       =   DT * ((V2 + RDOT * S2)/R + (W3 * S1 - W1 * S3))
      DS3       =   DT * ((V3 + RDOT * S3)/R + (W1 * S2 - W2 * S1))
      S1        =   S1 + DS1 - DS1S
      S2        =   S2 + DS2 - DS2S
      S3   =    =   S3 + DS3 - DS3S
      DRS       =   DR
      DS1S      =   DS1
      DS2S      =   DS2
      DS3S      =   DS3
25 CONTINUE
      Q         =   1.0/SQRT (S1 ** 2 + S2 ** 2 + S3 ** 2)
      S1        =   Q * S1
      S2        =   Q * S2
      S3        =   Q * S3
```

11. Compute the elevation and train angles for both $s_{Fuvw}(t_3)$ and $s_{Buvw}(t_3)$. The algorithms required for this step are

$$E = \mathrm{Tan}^{-1} \left(s_w / \sqrt{s_u^{\,2} + s_v^{\,2}} \right)$$

$$T = \mathrm{Tan}^{-1} \left(-s_v / s_u \right)$$

Using these algorithms, values for E_F, T_F, E_B, and T_B are obtained.

12. Compute the average elevation and train angle according to

$$E_s = \frac{1}{2}(E_F + E_B), \qquad T_s = \frac{1}{2}(T_F + T_B)$$

13. Compute the elevation and train of the strikepoint

$$E_b = \mathrm{Tan}^{-1} \left(b_w / \sqrt{b_u^2 + b_v^2}\right)$$

$$T_b = \mathrm{Tan}^{-1} (-b_v / b_u)$$

14. Compute the gun corrections in elevation and train

$$\delta E_g = K_1 (E_s - E_b)$$

$$\delta T_g = K_2 (T_s - T_b)$$

The adjustable coefficients K_1 and K_2 are to be initially set to 1.0.

NOTE: The computational steps following are to be executed continuously.

15. Continuously compute the elevation and train of the gun position commanded by the open loop fire control algorithm.

$$E_g = \mathrm{Tan}^{-1} \left(g_w / \sqrt{g_u^2 + g_v^2}\right)$$

$$T_g = \mathrm{Tan}^{-1} (-g_v \; g_u)$$

16. Add the closed loop fire control corrections.

$$E^*_g = E_g + \delta E_g$$

$$T^*_g = T_g + \delta T_g$$

For operation prior to the point in time when δE_g and δT_g have been developed from the strikepoint observation these quantities should be set to zero.

17. Compute the direction cosines of the calibrated gunline.

$$g^*_u = \cos E^*_g \cos T^*_g$$

$$g^*_v = - \cos E^*_g \sin T^*_g$$

$$g^*_w = \sin E^*_g$$

These are continuously transmitted to the gun servos.

2.6.5 DEMONSTRATION OF PERFORMANCE

The numerical check problem to demonstrate the closed loop algorithm is included in Section 6.1, Software Test Summary and Results.

Section 3

CLOSED LOOP FIRE CONTROL SOFTWARE

3.1 OVERVIEW

The closed loop fire control system formulation has been programmed for the CDC 469 mini computer in assembly level language. All assemblies have been accomplished at Frankford Arsenal and the latest assembly on October 8, 1976 is permanently saved on magnetic tape at Frankford Arsenal. File names and control card information pertinent to the October 8, 1976 Assembly are recorded on the DAY File at the end of the listing. The assembled program is stored on two reels of blue mylar tape dated October 8, 1976 and is loaded into the CDC 469 8K memory by Frankford Arsenal's software controlled memory loader.

3.2 ORGANIZATION

The realtime software in the CDC 469 Computer consists of the following sections:

1. Page zero variables/constants
2. Executive/aircraft estimator
3. Line of sight estimator subroutine
4. Line of sight gain subroutine
5. Open loop fire control subroutine
6. Closed loop fire control subroutine
7. Interrupt service subroutine
8. Air data subroutine
9. Flight Recorder subroutine
10. CDC debug routine
11. Arithmetic subroutines (square root, sin, cos, arc tan, long shift, initial 0, initial 1, matrix multiply).

12. Loader routines

13. Variable array section

The locations in CDC 469 memory for each section is shown in Table 3-1.

TABLE 3-1

MEMORY MAP

SECTION DESCRIPTION	IDENTIFYING NAME	MEMORY LOCATIONS (OCTAL)
Page Zero	PAGE 0	000000 to 000377
Executive Aircraft Estimator	EXEC START A. C ESTIMATOR	010407 to 011467
Line of Sight Estimator	LOSEST	0007567 to 010264
Line of Sight Gain Computation	LOS GAIN (TOG1. TOG2. TOG3. TOG4. TOG5)	000400 to 007017
Open Loop Fire Control Computation	OLFC	011664 to 012131
Closed Loop Fire Control Computation	CLFC	012132 to 013051
Interrupt Service Subroutine	INTR	007442 to 007512
Air Data Computations	AIR DATA	011470 to 011663
Flight Recorder Subroutine	FLT REC	013052 to 013331
CDC Debug Routine	DEBUG	017060 to 017777
Arithmetic Subroutines	INIT0	010265 to 010327
	INIT1	007020 to 007116
	LSQRT	007400 to 007441
	LSHFT	007513 to 007520
	MATM	007521 to 007566
	SIN COS	013372 to 013413
	ATAN	013332 to 013371
Variable Arrays		013734 to 017056

3.3 PAGE ZERO VARIABLES AND CONSTANTS

Most common variables, constants and scaling factors are stored in this section. The mode control variables are also located in this area. All page zero data is directly accessible by any program instruction throughout memory. The page zero data of interest with scaling included, is listed in Table 3-6 as part of the Flight Recorder Subroutine.

3.4 EXECUTIVE AND AIRCRAFT ESTIMATOR

The executive is the routine which controls all logic and timing functions, all subroutine calls and input/output operations. The executive flow chart is shown in Figure 3-2. Closed Loop Fire Control System modes are input by the executive in a packed format (Figure 3-1) and unpacked into flag words. The flag words are then used to activate or deactivate the various computational subroutines which supports the particular mode.

The Aircraft Estimator is an integral part of the executive and is always active at power on to the Closed Loop or Open Loop switch positions of the Pilot's Control Panel. All timing is based on a real time clock (30 Hz) which the executive synchronizes to at power on. The worst case instruction execution timing is 26 milliseconds out of a total time available of 33.3 milliseconds.

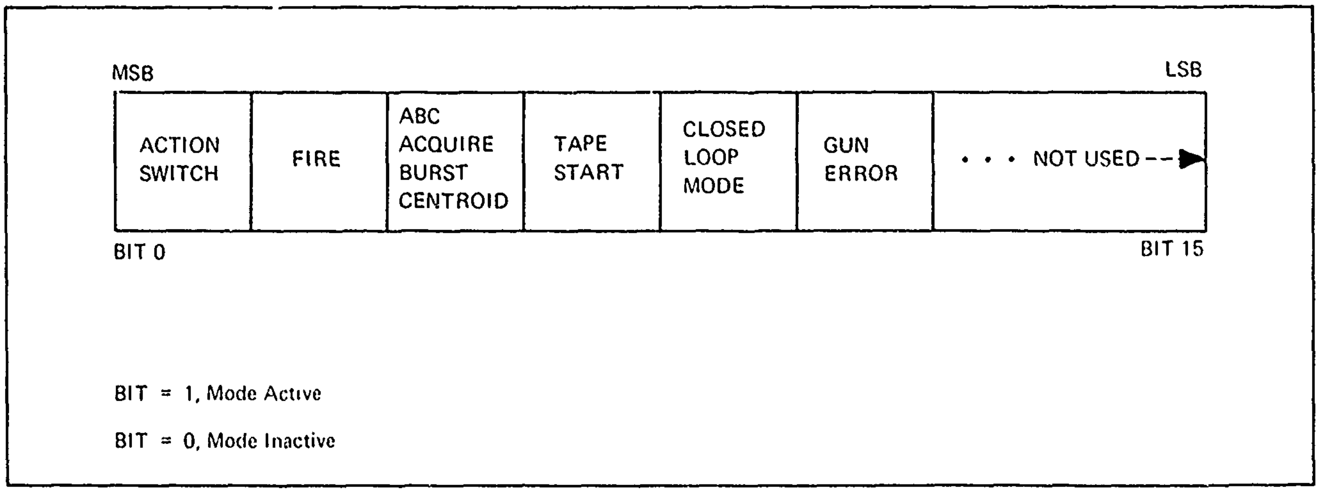
MSB
LSB
ACTION SWITCH
FIRE
ABC ACQUIRE BURST CENTROID
TAPE START
CLOSED LOOP MODE
GUN ERROR
• • • NOT USED
BIT 0
BIT 15
BIT = 1, Mode Active
BIT = 0, Mode Inactive

Figure 3-1. Executive Flow in a Packed Format

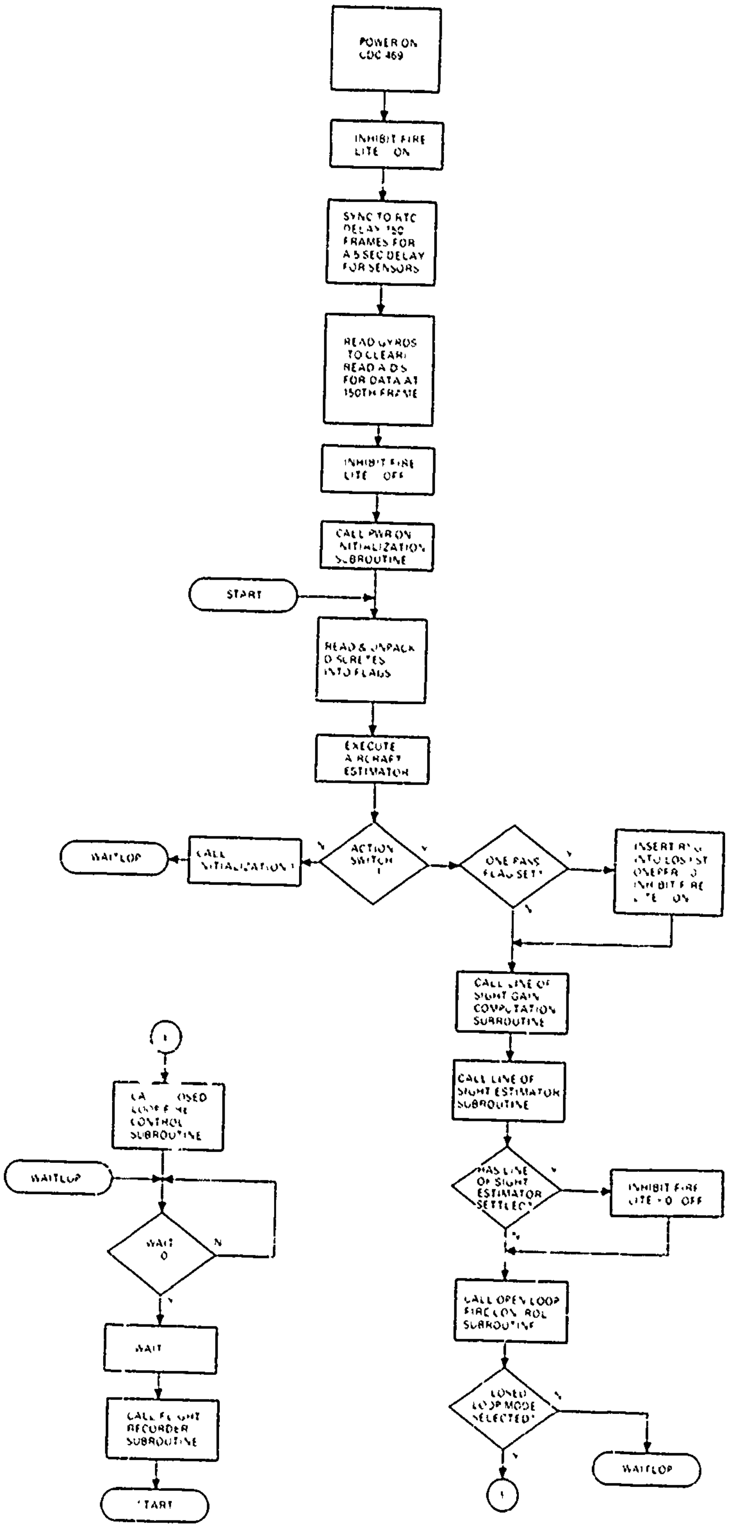
POWER ON
CDC 469
INHIBIT FIRE LITE ON
SYNC TO RTC DELAY 150 FRAMES FOR A 5 SEC DELAY FOR SENSORS
READ GYROS TO CLEAR; READ A/D'S FOR DATA AT 150TH FRAME
INHIBIT FIRE LITE OFF
CALL PWR ON INITIALIZATION SUBROUTINE
START
READ & UNPACK DISCRETES INTO FLAGS
EXECUTE AIRCRAFT ESTIMATOR
ACTION SWITCH 1
N
Y
CALL INITIALIZATION 1
WAITLOP
ONE PASS FLAG SET?
Y
N
INSERT RNG INTO LOS EST ONEPFR 0 INHIBIT FIRE LITE ON
CALL LINE OF SIGHT GAIN COMPUTATION SUBROUTINE
CALL LINE OF SIGHT ESTIMATOR SUBROUTINE
HAS LINE OF SIGHT ESTIMATOR SETTLED?
Y
N
INHIBIT FIRE LITE = 0 OFF
CALL OPEN LOOP FIRE CONTROL SUBROUTINE
CLOSED LOOP MODE SELECTED?
N
Y
WAITLOP
1
1
CALL CLOSED LOOP FIRE CONTROL SUBROUTINE
WAITLOP
WAIT 0
N
Y
WAIT
CALL FLIGHT RECORDER SUBROUTINE
START

Figure 3-2. Executive Flow Chart

The discrete inputs, discrete output to the fire inhibit light of the sight, and the digital to analog output to the turret servo are directly serviced by program instructions in the executive. The gyro digital inputs and the analog to digital inputs are initiated by the executive but are tied to the interrupt system and are serviced by the interrupt service routine. When all program instructions are completed, the executive stays in a wait loop until the real time clock causes an interrupt to the beginning of the executive.

3.5 LINE OF SIGHT ESTIMATOR SUBROUTINE

This subroutine is active when the action switch is on. It continually computes and maintains an estimate of the line of sight and range to the target. At action switch on, range from the range pot of the Pilot's Control Panel is inserted once. The gunner sight line direction cosines are continuously inserted during the time this subroutine is active. A detailed description of the formulation of this subroutine is included in paragraph 2.4.5.

3.6 LINE OF SIGHT GAIN SUBROUTINE

This subroutine is also active when the action switch is on. It computes the thirty gains required by the Line of Sight estimator. The subroutine is sub divided into five modules. One module is executed for each execution of the complete executive. The complete gain computations requires 166.666 milliseconds. A set of new gain values are computed every five executions of the executive. A description of the formulation of this subroutine is included in paragraph 2.4 5.8.

3.7 OPEN LOOP FIRE CONTROL SUBROUTINE

This subroutine is active when the action switch is on. It computes the lead angles, adds in any closed loop fire control corrections and computes the differential gun orders that are output to the turret. The relative air density ρ/ρ_0 is computed by the following method:

$$PP = \rho/\rho_0 = KPP \cdot PS/TA$$

where KPP = 19.605. The formulation of the open loop computation is described in Subsection 2.5.

3.8 CLOSED LOOP FIRE CONTROL SUBROUTINE

This subroutine is active when the action switch is on and the system mode switch on the pilot's control panel is in the closed loop position. It uses the fire and acquire burst centroid discretes, the aircraft estimator outputs and the line of sight estimator inputs and outputs to compute a fire control correction based on first burst strikepoint observations. The forumlation of the closed loop computation is described in Subsection 2.6. The subroutine flow chart is found in Figure 3-3, with supportive nomenclature in Table 3-2.

3.9 INTERRUPT SERVICE SUBROUTINE

This routine services any hardware interrupts that are initiated by the executive. The real time clock, the gyros and the analog to digital signals are tied to the interrupt system. When an interrupt occurs the program instruction address is forced to the interrupt service routine and the interrupting device is determined and serviced. The program address is then returned to the address at the time the interrupt occurred. Table 3-3 shows the signals and addresses in memory serviced by this routine. Table 3-4 shows the scaling terms applied to the input signals. A description of the interface of this routine with the associated hardware is provided in paragraph 4.2.5.

3.10 AIR DATA SUBROUTINE

This subroutine is active at power on to the closed loop fire control system. It converts and scales raw input signals to the proper engineering units used in the computer. Table 3-4 lists the variables computed by this subroutine which have direct scaling of the form

$$X' = AX + B$$

where X is the input as a result of the Interrupt Service Subroutine. A and B are the scaling value and offset, respectively, that produce X' in the desired engineering units with the desired resolution.

Other inputs have more complex scaling algorithms and are described in the following paragraphs.

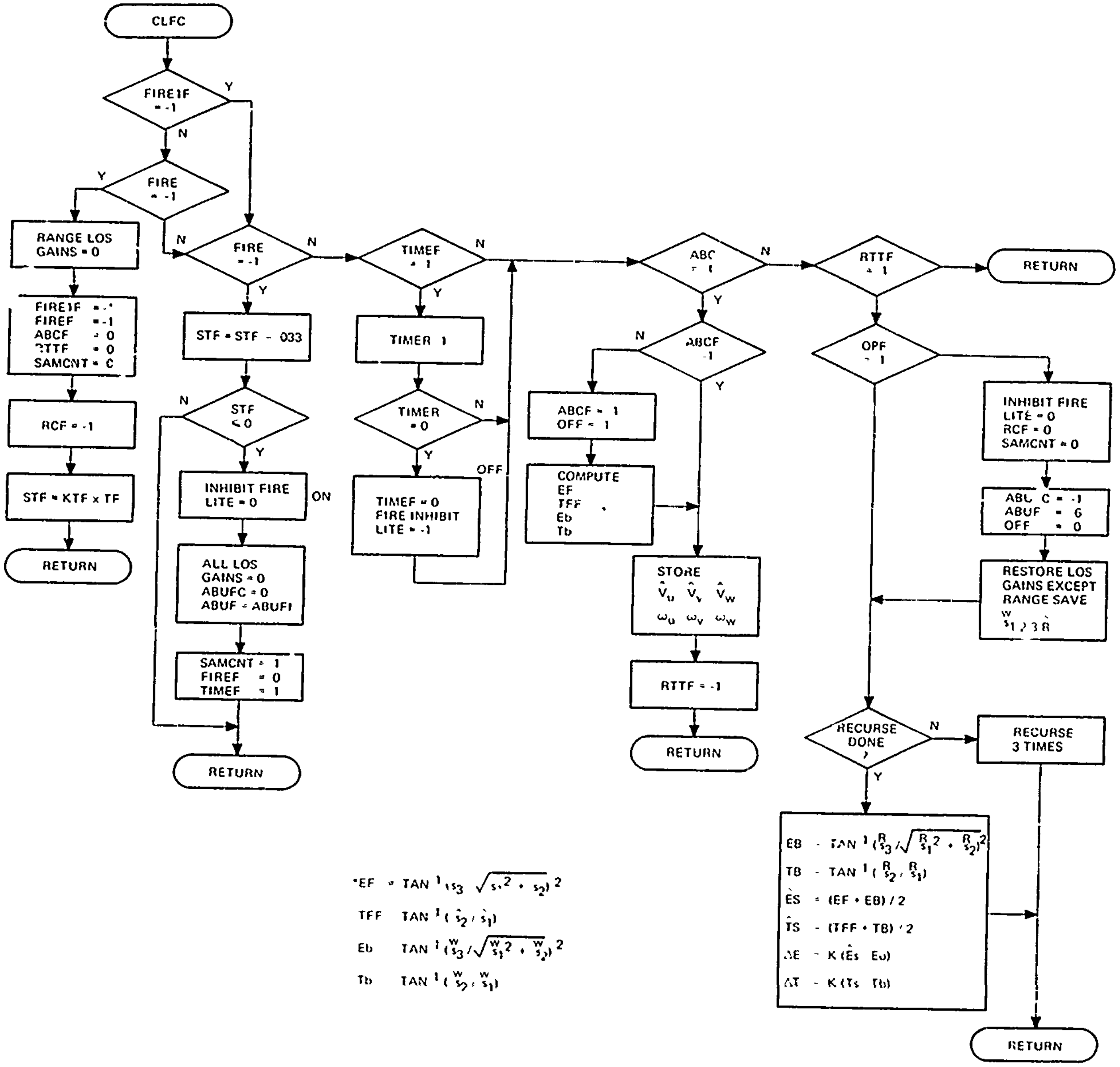
CLFC
FIREIF = -1
Y
N
FIRE = -1
Y
N
RANGE LOS GAINS = 0
FIREIF = -1
FIREF = -1
ABCF = 0
RTTF = 0
SAMCNT = 0
RCF = -1
STF = KTF x TF
RETURN
FIRE = -1
N
Y
STF = STF - 033
STF ≤ 0
N
Y
INHIBIT FIRE LITE = 0
ON
ALL LOS GAINS = 0
ABUFC = 0
ABUF = ABUFI
SAMCNT = 1
FIREF = 0
TIMEF = 1
RETURN
TIMEF = 1
N
Y
TIMER 1
TIMER = 0
N
Y
OFF
TIMEF = 0
FIRE INHIBIT LITE = -1
ABC = 1
N
Y
ABCF = 1
N
Y
ABCF = 1
OFF = 1
COMPUTE
EF
TFF *
Eb
Tb
STORE
$\hat{V}_u$ $\hat{V}_v$ $\hat{V}_w$
ω_u ω_v ω_w
RTTF = -1
RETURN
RTTF = 1
RETURN
OFF = 1
INHIBIT FIRE LITE = 0
RCF = 0
SAMCNT = 0
ABUC = -1
ABUF = 6
OFF = 0
RESTORE LOS GAINS EXCEPT RANGE SAVE ${}^{w}s_{1,2,3}$ $\dot{R}$
RECURSE DONE ?
N
Y
RECURSE 3 TIMES
EB = TAN^{-1}(${}^{R}s_3/\sqrt{{}^{R}s_1^2 + {}^{R}s_2^2}$)
TB = TAN^{-1}(${}^{R}s_2/{}^{R}s_1$)
$\hat{E}S$ = (EF + EB)/2
$\hat{T}S$ = (TFF + TB)/2
ΔE = K($\hat{E}$s - Eb)
ΔT = K(Ts - Tb)
RETURN

$${}^*EF = TAN^{-1}(\dot{s}_3/\sqrt{\dot{s}_1^2 + \dot{s}_2^2})$$

$$TFF = TAN^{-1}(\dot{s}_2/\dot{s}_1)$$

$$Eb = TAN^{-1}({}^{w}s_3/\sqrt{{}^{w}s_1^2 + {}^{w}s_2^2})$$

$$Tb = TAN^{-1}({}^{w}s_2/{}^{w}s_1)$$

Figure 3-3. CLFC Subroutine Flow Chart

TABLE 3-2

CLFC SUBROUTINE SYMBOL DESCRIPTIONS

NAME	DESCRIPTION
FIREIF	One Pass Flag for Fire
FIRE	Fire Discrete
FIREF	Flag to Control Indication of End of Scaled Time of Flight
ABCF	Acquire Burst Centroid Flag - First Pass Only
RTTF	Flag to Control Execution of Recursion Computations
SAMCNT	Coast Line of Sight Estimator Flag
RCF	Coast Range in Line of Sight Estimator Flag
STF	Scaled Time of Flight
ABUFC	Velocity and Angular Rate Buffer Counter
ABUF	Velocity and Angular Rate Buffer Address
TIMEF	Flag to Control Execution of Fire Inhibit Light Computations
TIMER	Delay Counter
OPF	One Pass Flag for Recursion Computations
ABC	Acquire Burst Centroid Discrete
EF	ELEV Estimated at ABC
TFF	TRAIN Estimated at ABC
Eb	ELEV Measured at ABC
Tb	TRAIN Measured at ABC
Vuvw	Estimated Velocities
Wuvw	Estimated Angular Rates
EB	Recursed ELEV of Strikepoint
TB	Recursed TRAIN of Strikepoint
$\hat{E}S$	Average ELEV at Fire
$\hat{T}S$	Average TRAIN at Fire
ΔE	Closed Loop Correction ELEV
ΔT	Closed Loop Correction TRAIN

TABLE 3-3

INPUT SIGNALS SERVICED BY INTERRUPT ROUTINE

MEMORY LOCATION	NAME	DESCRIPTION
225	GYROX	GYROX - Incremental Roll Rate (1/30 Sec)
226	GYROY	GYROY - Incremental Pitch Rate (1/30 Sec)
227	GYROZ	GYROZ - Incremental Yaw Rate (1/30 Sec)
014514	CHAN0	AU - Acceleration u
014515	CHAN1	AV - Acceleration v
014516	CHAN2	AW - Acceleration w
014517	CHAN3	STHETA - Sin Pitch
014520	CHAN4	CTHETA - Cos Pitch
014521	CHAN5	SPHI - Sin Roll
014522	CHAN6	CPHI - Cos Roll
014523	CHAN7	PS - Static Pressure
014524	CHAN8	TA - Air Temp
014525	CHAN9	PD - Differential Pressure
014526	CHAN10	SU - Sightline u
014527	CHAN11	SV - Sightline v
014530	CHAN12	SW - Sightline w
014531	CHAN13	Est. Range - Estimated Range
014532	CHAN14	SPARE - Not Used
014533	CHAN15	SPARE - Not Used

TABLE 3-4
AIR DATA SCALE FACTORS

					SCALE FACTOR APPLIED TO INPUT FROM A/D			OFFSET		
LOC	VARIABLE	SCALE	DESCRIPTION	DIMENSION	LOC	NAME	SCALE	LOC	NAME	SCALE
254	PS	B - 9	Static Air Pressure	lbs/in^2	274	SCPS	B + 2	244	OFFPS	B - 9
315	TA	B - 9	Temperature Absolute	K^o	275	SCTA	B + 2	245	OFFTA	B - 9
255	PD	B - 5	Differential Air Pressure	lbs/in^2	273	SCPD	B + 6	-	-	-
324	VELU	B - 8	Aircraft u Axis Velocity	ft/sec				-	-	-
325	VELV	B - 8	Aircraft v Axis Velocity	ft/sec	-	-	-	-	-	-
326	VELW	B - 8	Aircraft w Axis Velocity	ft/sec	-	-	-	-	-	-
276	SCU	B - 10	Sightline u	milliradians	-	-	-	-	-	-
277	SCV	B - 10	Sightline v	milliradians	-	-	-	-	-	-
300	SCW	B - 10	Sightline w	milliradians	-	-	-	-	-	-
361	ZU	B - 10	Aircraft Vertical u	milliradians	-	-	-	-	-	-
362	ZV	B - 10	Aircraft Vertical v	milliradians	-	-	-	-	-	-
363	ZW	B - 10	Aircraft Vertical w	milliradians	-	-	-	-	-	-
102	ACCU	B - 6	Aircraft Acceleration u	ft/sec^2	011661	SACCU	B + 3	-	-	-
103	ACCV	B - 6	Aircraft Acceleration v	ft/sec^2	011662	SACCV	B + 3	-	-	-
104	ACCW	B - 6	Aircraft Acceleration w	ft/sec^2	011663	SACCW	B + 3	-	-	-
225	GYROX	B - 6	Incremental Gyro Roll Rate	MR/1/30 sec	036	SGX	B0	-	-	-
226	GYROY	B - 6	Incremental Gyro Pitch Rate	MR/1/30 sec	037	SGY	B0	-	-	-
227	GYROZ	B - 6	Incremental Gyro Yaw Rate	MR/1/30 sec	040	SGZ	B0	-	-	-

The software computes airspeed of the aircraft according to the following relations:

$$\mathrm{VELU} = \left(\frac{\mathrm{KVxTA \times PD}}{\mathrm{PS}}\right)^{1/2}$$

$$\mathrm{VELV} = 0$$

$$\mathrm{VELW} = \mathrm{KC \times VELU}^2$$

Where KV = 6177.5647B -13 (Loc 241)

KC = 0.0004284999B +8 (Loc 235)

Relative air density ρ/ρ_0 is computed in the Open Loop Fire Control Subroutine.

The sightline direction cosine signals are subject to variations caused by fluctuations on the 400 Hz carrier (reference voltage). Variations are also caused by demodulator ripple in the a-c to d-c conversions. Normalization solves these problems by extracting the pure sine and cosine terms according to the following:

$$\mathrm{CHAN10} = \mathrm{Su} = \mathrm{K\ Cos\ E\ Cos\ T}$$

$$\mathrm{CHAN11} = \mathrm{Sv} = \mathrm{K\ Cos\ E\ Sin\ T}$$

$$\mathrm{CHAN12} = \mathrm{Sw} = \mathrm{K\ Sin\ E}$$

Where K is proportional to the reference voltage; the nominal value for K is 28,330.

The normalized sightline direction cosines are

$$\mathrm{SCu} = \tilde{\mathrm{S}}\mathrm{u} = \mathrm{Su}/\sqrt{\mathrm{Su}^2 + \mathrm{Sv}^2 + \mathrm{Sw}^2}$$

$$\mathrm{SCv} = \tilde{\mathrm{S}}\mathrm{v} = -\mathrm{Sv}/\sqrt{\mathrm{Su}^2 + \mathrm{Sv}^2 + \mathrm{Sw}^2}$$

$$\mathrm{SCw} = \tilde{\mathrm{S}}\mathrm{w} = -\mathrm{Sw}/\sqrt{\mathrm{Su}^2 + \mathrm{Sv}^2 + \mathrm{Sw}^2}$$

where: where:

CHAN10, 11, 12 = Suvw = Electrically measured sightline direction cosines.

SCuvw = $\tilde{\mathrm{S}}$uvw = Normalized observed values of sightline direction cosines.

The aircraft attitude signals, pitch and roll, are subject to variations caused by fluctuations on the 400 Hz carrier (reference voltage). Variations are also caused by demodulator ripple in the a-c to d-c conversion. Normalization of these signals is accomplished and the direction of the vertical vector with respect to the airframe is determined according to the following:

$$Zu = \text{Sin}\ \theta / (\text{Sin}^2\ \theta + \text{Cos}^2\ \theta)^{1/2}$$

$$Zv = (\text{Cos}\ \theta\ (\text{Sin}^2\ \theta + \text{Cos}^2\ \theta)^{1/2})\ (\text{Sin}\ \phi\ (\text{Sin}^2\ \phi + \text{Cos}^2\ \phi)^{1/2})$$

$$Zw = (\text{Cos}\ \theta\ (\text{Sin}^2\ \theta + \text{Cos}^2\ \theta)^{1/2})\ (\text{Cos}\ \phi\ (\text{Sin}^2\ \phi + \text{Cos}^2\ \phi)^{1/2})$$

where

Sin θ = CHAN3
Cos θ = CHAN4
Sin ϕ = CHAN5
Cos ϕ = CHAN6

are the measured input signals from the A/D.

3.11 FLIGHT RECORDER SUBROUTINE

The Flight Recorder Subroutine stores real time data on the flight recorder. This subroutine is activated by the executive when the tape start switch is turned on at the pilot's control panel. There are two modes of operation, mode zero and mode one. The mode select flag resides in page zero, address 230_8. An octal 000000_8 will select mode zero and an octal 177777_8 will select mode one operation. The number of tape starts is recorded in the variable TAPECNT in location 55_8 of page zero. This variable is used to record the target pass number. Each time the tape start switch on the pilot's control panel is cycled from off to on, this variable increments by one. It is "OR ed" into the packed discretes variable PDISC at location 247_8, and is therefore stored by the flight recorder.

3.11.1 MODE ZERO OPERATION

Mode zero operation stores the same seven words of data every computer iteration in a storage buffer. At the end of the seventh iteration, the 49 words in the buffer plus one index word is output to the flight recorder. In order to record more data, the action switch flag is monitored for the inactive state, when this occurs a different set of data is stored in the storage buffer. Table 3-5 shows the data set being recorded in mode zero.

TABLE 3-5

MODE ZERO RECORD

COMPUTER ITERATION	WORD NO.	VARIABLE (ACTION SW ON)	LOC. (OCTAL)	SCALE	VARIABLE (ACTION SW OFF)	LOC. (OCTAL)	SCALE
-	0	Index Word	-	-	-	-	-
n	1	Discretes	247	-	Discretes	247	-
	2	XH10AC (sin θ)	340	B-10 mr.	XH10AC (sin θ)	340	B-10 mr.
	3	$\frac{XH11AC}{XH12AC}$ (tan ϕ)	-	B0 rad.	$\frac{XH11AC}{XH12AC}$ (tan ϕ)	-	B0 rad.
	4	$\frac{XH2LOS}{XH1LOS}$ (LOS tan T)	-	B0 rad.	TS (AVE LOS TRAIN AT ABC)	041	B-1 rad.
	5	XH3LOS (LOS sin ELEV)	345	B-10 mr.	ES (AVE LOS ELEV AT ABC)	272	B-1 rad.
	6	TG (GUN TRAIN)	252	B-1 rad.	TSP (BULLET TRAIN STRIKEPOINT)	314	B-1 rad.
	7	EG (GUN ELEV)	251	B-1 rad.	ESP (BULLET ELEV STRIKEPOINT)	313	B-1 rad.
n + 1	8	Discretes	247	-	Discretes	247	-
	9	XH10AC (sin θ)	340	B-10 mr.	XH10AC (sin θ)	340	B-10 mr.
	10	$\frac{XH11AC}{XH12AC}$ (tan ϕ)	-	B0 rad	$\frac{XH11AC}{XH12AC}$ (tan ϕ)		B0 rad
	11	$\frac{XH2LOS}{XH1LOS}$ (LOS tan T)	-	B0 rad	TS (AVE LOS TRAIN AT ABC)	041	B-1 rad
	12	XH3LOS (LOS sin ELEV)	345	B-10 mr.	ES (AVE LOS ELEV AT ABC)	272	B-1 rad
	13	TG (GUN TRAIN)	252	B-1 rad	TSP (BULLET TRAIN STRIKEPOINT)	314	B-1 rad
	14	EG (GUN ELEV)	251	B-1 rad	ESP (BULLET ELEV STRIKEPOINT)	313	B-1 rad
n + 2	15	Discretes	247	-	Discretes	247	-
	16	XH10AC (sin θ)	340	B-10 mr.	XH10AC (sin θ)	340	B-10 mr.
	17	$\frac{XH11AC}{XH12AC}$ (tan ϕ)	-	B0 rad	$\frac{XH11AC}{XH12AC}$ (tan ϕ)	-	B0 rad
	18	$\frac{XH2LOS}{XH1LOS}$ (LOS tan T)	-	B0 rad	TS (AVE LOS TRAIN AT ABC)	041	B-1 rad
	19	XH3LOS (LOS sin E)	345	B-10 mr.	ES (AVE LOS ELEV AT ABC)	272	B-1 rad
	20	TG (GUN TRAIN)	252	B-1 rad	TSP (BULLET TRAIN STRIKEPOINT)	314	B-1 rad
	21	EG (GUN ELEV)	251	B-1 rad	ESP (BULLET ELEV STRIKEPOINT)	313	B-1 rad
n + 3	22	Discretes	247	-	Discretes	247	-
	23	XH10AC (sin θ)	340	B-10 mr.	XH10AC (sin θ)	340	B-10 mr.
	24	$\frac{XH11AC}{XH12AC}$ (tan ϕ)	-	B0 rad	$\frac{XH11AC}{XH12AC}$ (tan ϕ)	-	B0 rad
	25	$\frac{XH2LOS}{XH1LOS}$ (LOS tan T)	-	B0 rad	TS (AVE LOS TRAIN AT ABC)	041	B-1 rad
	26	XH3LOS (LOS sin E)	345	B-10 mr.	ES (AVE LOS ELEV AT ABC)	272	B-1
	27	TG (GUN TRAIN)	252	B-1 rad	TSP (BULLET TRAIN STRIKEPOINT)	314	B-1
	28	EG (GUN ELEV)	251	B-1 rad	ESP (BULLET ELEV STRIKEPOINT)	313	B-1 rad

TABLE 3-5 (Continued)

COMPUTER ITERATION	WORD NO.	VARIABLE (ACTION SW ON)	LOC. (OCTAL)	SCALE	VARIABLE (ACTION SW OFF)	LOC (OCTAL)	SCALE
	29	Discretes	247_8	-	Discretes	247_8	-
	30	XH10AC (θ)	340_8	B-10 mr.	XH10AC (sin θ)	340	B-10 mr.
	31	$\frac{XH11AC}{XH12AC}$ (tan ϕ)	-	B0 rad	$\frac{XH11AC}{XH12AC}$ (tan ϕ)	-	B0 rad
n + 4	32	$\frac{XH2LOS}{XH1LOS}$ (LOS tan T)	-	B0 rad	TS (AVE LOS TRAIN AT ABC)	041	B-1 rad
	33	XH3LOS (LOS sin E)	345	B-10 mr.	ES (AVE LOS ELEV AT ABC)	272	B-1 rad
	34	TG (GUN TRAIN)	252	B-1 rad	TSP (BULLET TRAIN STRIKEPOINT)	314	B-1 rad
	35	EG (GUN ELEV)	251	B-1 rad	ESP (BULLET ELEV STRIKEPOINT)	313	B-1 rad
	36	Discretes	247	-	Discretes	247_8	-
	37	XH10AC (sin θ)	340	B-10 mr.	XH10AC (sin θ)	340	B-10 mr.
	38	$\frac{XH11AC}{XH12AC}$ (tan ϕ)	-	B0 rad	$\frac{XH11AC}{XH12AC}$ (tan ϕ)	-	B0 rad
n + 5	39	$\frac{XH2LOS}{XH1LOS}$ (LOS tan T)	-	B0 rad	TS (AVE LOS TRAIN AT ABC)	041	B-1 rad
	40	XH3LOS (LOS sin E)	345	B-10 mr.	ES (AVE LOS ELEV AT ABC)	272	B-1 rad
	41	TG (GUN TRAIN)	252	B-1 rad	TSP (BULLET TRAIN STRIKEPOINT)	314	B-1 rad
	42	EG (GUN ELEV)	251	B-1 rad	ESP (BULLET ELEV STRIKEPOINT)	313	B-1 rad
	43	Discretes	247	-	Discretes	247	-
	44	XH10AC (sin θ)	340	B-10 mr.	XH10AC (sin θ)	340	B-10 mr.
	45	$\frac{XH11AC}{XH12AC}$ (tan ϕ)	-	B0 rad	$\frac{XH11AC}{XH12AC}$ (tan ϕ)	-	B0 rad
n + 6	46	$\frac{XH2LOS}{XH1LOS}$ (LOS tan T)	-	B0 rad	TS (AVE LOS TRAIN AT ABC)	041	B-1 rad
	47	XH3LOS (LOS sin E)	345	B-10 mr.	ES (AVE LOS ELEV AT ABC)	272	B-1 rad
	48	TG (GUN TRAIN)	252	B-1 rad	TSP (BULLET TRAIN STRIKEPOINT)	314	B-1 rad
	49	EG (GUN ELEV)	251	B-1 rad	ESP (BULLET ELEV STRIKEPOINT)	313	B-1 rad

3.11.2 MODE ONE OPERATION

Mode one operation does not store any variables in memory. It outputs 49 words plus one index word at the end of every seventh computer iteration. Table 3-6 shows the data recorded in this mode.

TABLE 3-6
MODE 1 RECORD

	VARIABLE	(OCTAL) LOC.	SCALE	DESCRIPTION
1	-	150	-	Index Word
2	PDISC	247	-	Packed Discretes and Tape Start Count
3	GYROX	225	B-6 MR	Incremental ang. rate Roll 1/30 sec
4	GYROY	226	B-6 MR	Incremental ang. rate Pitch 1/30 sec
5	GYROZ	227	B-6 MR	Incremental ang. rate Yaw 1/30 sec
6	ACCU	102	B-6 ft/sec^2	Measured aircraft acceleration u
7	ACCV	103	B-6 ft/sec^2	Measured aircraft acceleration v
8	ACCW	104	B-6 ft/sec^2	Measured aircraft acceleration w
9	VELU	324	B-8 ft/sec	Measured aircraft velocity u
10	VELV	325	B-8 ft/sec	Measured aircraft velocity v
11	VELW	326	B-8 ft/sec	Measured aircraft velocity w
12	ZU	361	B-10 MR	Aircraft vertical u
13	ZV	362	B-10 MR	Aircraft vertical v
14	ZW	363	B-10 MR	Aircraft vertical w
15	SCU	276	B-10 MR	Measured sight line u
16	SCV	277	B-10 MR	Measured sight line v
17	SCW	300	B-10 MR	Measured sight line w
18	PS	254	B-9 lbs/in^2	Static air pressure
19	PD	255	B-5 lbs/in^2	Differential air pressure
20	TA	315	B-9 k^o	Temperature absolute
21	XS1AC	022	B-11 MR	Aircraft ang. rate u
22	XS2AC	023	B-11 MR	Aircraft ang. rate v
23	XS3AC	024	B-11 MR	Aircraft ang. rate w
24	XH4AC	332	B-1 ft/sec^2	Estimated error specific force u
25	XH5AC	333	B-1 ft/sec^2	Estimated error specific force v
26	XH6AC	334	B-1 ft/sec^2	Estimated error specific force w
27	XH7AC	335	B-8 ft/sec	Estimated velocity aircraft u
28	XH8AC	336	B-8 ft/sec	Estimated velocity aircraft v
29	XH9AC	337	B-8 ft/sec	Estimated velocity aircraft w
30	XH10AC	340	B-10 MR	Estimated aircraft zu
31	XH11AC	341	B-10 MR	Estimated aircraft zv

TABLE 3-6 (Continued)

	VARIABLE	(OCTAL) LOC.	SCALE	DESCRIPTION
32	XH12AC	342	B-10 MR	Estimated aircraft zw
33	XH1LOS	343	B-10 MR	Estimated sight line u
34	XH2LOS	344	B-10 MR	Estimated sight line v
35	XH3LOS	345	B-10 MR	Estimated sight line w
36	XH4LOS	346	B-4 Kft	Estimated tgt range
37	RDOT	257	B-0 Kft/sec	Range rate
38	TF	317	B-3 sec	Time of flight
39	Q	256	B-5 ft/sec^2	Grav. acceleration
40	GU	217	B-10 MR	Estimated sight line u + "lead angle" u
41	GV	220	B-10 MR	Estimated sight line v + "lead angle" v
42	GW	221	B-10 MR	Estimated sight line w + "lead angle" w
43	TGCL	127	B-1 rad	Closed loop correction-train
44	EGCL	266	B-1 rad	Closed loop correction-elevation
45		230	-	Dummy
46	SGYROX	301	B-6 MR	Summed values of GYROX over last flight recorder dump
47	SGYROY	302	B-6 MR	Summed values of GYROY over last flight recorder dump
48	SGYROZ	303	B-6 MR	Summed values of GYROZ over last flight recorder dump
49		230	-	Dummy
50		230	-	Dummy

3.12 CDC DEBUG ROUTINE

This is a Control Data Corporation generated utility program which is included in the closed loop system tape. It is tied to the ASR 33 Teletype and may be used to dump or change memory locations in the CDC 469. This program resides in memory location 17060_8 to 17777_8. The starting address is 17136_8. This program may be destroyed by the closed loop fire control subroutine if the time between ABC (acquire Burst Centroid) and reacquisition of the target exceeds 6 seconds.

3.13 ARITHMETIC SUBROUTINES

There are eight arithmetic utility subroutines which are used by the system software. The following Table 3-7 lists the names and locations in memory.

TABLE 3-7
ARITHMETIC SUBROUTINES

NAME	LOCATION	DESCRIPTION
LSQRT	7400_8 to 7441_8	Square root subroutine
SIN	013372 to 013413	Sine and cosine subroutine
ATAN	013332 to 013371	Arctangent subroutine
LSHFT	7513_8 to 7520_8	Double precision shift subroutine
MATM	7521_8 to 7566_8	Matrix multiply subroutine
INITO	010265 to 010327	Power on initialization subroutine
INITI	007020 to 007116	Line of sight inactive initialization subroutine

3.14 LOADER ROUTINES

There are two software memory loaders for the system. Each has to be hand entered into memory via the console. The General Electric generated loader resides in memory locations 7314_8 to 7377_8 (Starting Address = 7314). This loader reads a special binary format tape. It is used to read the G. E. test tape for testing system operation on the ground. The second loader, made by Frankford Arsenal, is used to load ASCII formated tape. It is used to load the Closed Loop Fire Control System tape. It resides in memory at location 7237_8 to 7312_8 (Starting Address = 7237_8). Table 3-8 lists the G. E. Loader and Table 3-9 lists the Frankford Arsenal Loader.

3.15 VARIABLE ARRAY SECTION

The variable array section extends from location 13734_8 to 17056_8 in CDC 469 memory. Included in the section are the arrays used in the line of sight gain computations, the expected state array for the line of sight computation, analog to digital input array, the aircraft expected state array and gains, temporary gain storage array, the flight recorder buffer array, and the storage buffer for the closed loop fire control subroutine.

TABLE 3-8

GENERAL ELECTRIC MEMORY LOADER

```
7314    006 001    LIS 1
7315    014 177    ENR         177B  10B
7316    104 010    LS          1  10B          Make 377B - start addr code
7317    004 301    INC         1  10B
7320    015 507    ENR         107B  13B
7321    105 413    LS          1  13B          Make 217B - stop code
7322    005 701    INC         1  13B
7323    014 417    ENR         17B  11B        Mask data
7324    013 400    ENR         0, 7            Setup for pack subr
7325    015 374    ENR         -4  12B
7326    142 000    OUT         0  4            Advance 1 frame
7327    000 417    SRJ         Read, 17B       Get a frame in R4
7330    007 357
7331    004 144    SKEQ        4  10B          = 377B?
7332    010 326    ENP         * -4            No        Try again
7333    000 416    SRJ         Pack  16B       Yes       Next 4 frames = Address in R5
7334    007 363
7335    040 405    LDR         5, 1            Put address in R1 (index)
7336    000 416    SRJ         Pack  16B       Get data
7337    007 363
7340    072 400    STR  X      0  5            Store via R1
7341    053 000    LDR  X      0  6            Read back to verify STORE
7342    002 546    SKEQ        6 5             R6 = R5?
7343    010 343    ENP         *               Stop - bad store - check NRDO
7344    000 701    INC         1  1            [illegible]d  bump R6 address
7345    142 000    OUT         0  4            [illegible]me
7346    000 417    SRJ         Read, 17B       Re[illegible]frame
7347    007 357
7350    004 104    SKNE        4, 10B          = 377B?
7351    010 333    ENP         * -16B          Yes, get address
7352    005 504    SKNE        4, 13B          No  ck for stop code = 217_8
7353    010 353    ENP         *               Yes = 217B  stop
7354    000 416    SRJ         Pack + 3, 16B   No ≠ 217B, continue
7355    007 366
7356    010 340    ENP         * -16B          Go get data
7357    162 004    Read INP    4, 4            Read 1 frame
7360    002 061         PJP    * +2, 4
7361    010 357         ENP    * -2
7362    000 017         RTN    17B
7363    142 000    Pack OUT    0, 4            Advance 1 frame
7364    000 417         SRJ    Read, 17B       Read 1 frame
7365    007 357         Read
7366    002 271         AND    11B, 4          Mask data to R4
7367    103 404         Ado    4,7             Build word in R7
7370    005 301         INC    1, 12B
7371    005 062         PJP    * +3, 12B       Exit when R12B = pos.
7372    003 723         LS   4,7               4 BITS
7373    010 363         ENP  * -10B
7374    042 407         LDR  7,5               Transfer word to R5
7375    013 400         ENR  0,7               Reinitialize for nxt call
7376    015 374         ENR  -4,12B
7377    000 016         RTN  16B
```

TABLE 3-9

FRANKFORD ARSENAL MEMORY LOADER

```
7237   013 067            ENR 67B, 6        ASCII for 7B
7240   013 457            ENR 57B, 7
7241   006 001            LIS 1             R1 - index register
7242   014 006            ENR 6, 8          6 character test
7243   017 407            ENR 7, 15         To convert ASCII to octal
7244   015 400            ENR 0, 11         Clear word accumulator
7245   016 000            ENR 0, 12         Initialize character count
7246   142 000   STARTR   OUT 0, 4          Advance reader 1 frame
7247   162 012            INP 10, 4         Input character
7250   005 061            PJP * +2, 10      Jump if ready
7251   010 006            ENP * -2          Loop for ready
7252   014 577            ENR 177B, 9       Convert to 7 bit ASCII
7253   005 271            AND 9, 10
7254   104 453            ENR 053B, 9
7255   005 111            SKNE 9, 10        Skip if not +
7256   010 035            ENP ENTERWD       (ENTERWD at 3035)
7257   014 456            ENR 056B, 9
7260   005 111            SKNE 9, 10        Skip if not
7261   010 046            ENP SET X         (SETX at 3046)
7262   003 172            SKLE 10, 6        Check to see
7263   010 005            ENP STARTR        if character input is 0 - 7
7264   003 532            SKGT 10, 7        (octal ).  If not
7265   010 005            ENP STARTR        input next character.
7266   006 150   STORE    SKEQ 8, 12        Skip if too many characters
7267   010 030            ENP * +2
7270   010 027            ENP * +0
7271   005 277            AND 15, 10        Convert ASCII to octal
7272   005 722            LS 3, 11          Shift word store to accept character
7273   105 412            ADD 10, 11        Add char. to word store.
7274   006 301            INC 1, 12         Increment character count
7275   010 005            END STARTR        Go back and input next character
7276   006 150   ENTERWD  SKEQ 8, 12        Skip if correct (6) number
7277   010 036            ENP * +0          Of characters to be stored
7300   007 041            NJP * +2, 14      If R14 = —, verify mode
```

TABLE 3-9 (Continued)

```
7301   075 400           STR, X, 0, 11       Store word
7302   056 400           LDR, X, 0, 13       Load for verify
7303   006 553           SKEQ 11, 13         Verify stored count
7304   010 043           ENP * +0            Halt if not verified
7305   000 701           INC 1, 1            Increment index register
7306   010 003           ENP STARTR - 2      Next character
7307   006 150   SET X   SKEQ 8, 12          Skip if correct (6) number
7310   010 047           ENP * +10           of characters to set
7311   040 413           TRF 11, 1           Index reg.
7312   010 003           ENP STARTR - 2      Next character
```

Section 4

CLOSED LOOP FIRE CONTROL SYSTEM HARDWARE

4.1 OVERVIEW

The hardware developed on the Closed Loop Fire Control contract includes the following. All items except Items 4 and 5 have been installed on the AH-1G Helicopter SN 15003, which was at this facility from October 1975 to June 1976. The installation of these items on the aircraft is shown in Figure 4-1.

1. Computer Interface Unit (CIU), GE Assy 293E268G1

   This unit houses the Control Data Corporation (CDC) Model 469 Processor, a power supply and eight printed circuit boards. The boards include A/D and D/A conversion, digital control, console interface, and flight recorder interface.

2. Inertial Measurement Unit (IMU), GE Assy 123D6654G1

   This unit houses three rate integrating gyros, three accelerometers, and a sensor buffer printed circuit board.

3. Inertial Measurement Unit (IMU) Electronics, GE Assy 293E269G1

   This unit houses a power supply and six printed circuit boards. The boards include gyro electronics and digital control.

4. Program Console Unit (PCU), GE Assy 123D6446G1

   This unit includes two printed circuit boards for Processor/Programmer's Console Interface. It resides within the Console Cabinet, GE Assy 123D7231, shown in Figure 4-2.

5. Flight Recorder Ground Unit, GE Assy 123D5802G1

   This is a GFE item originally developed on the MWFCS program. The unit transfers data from the GFE Flight Recorder to cassette tapes, which become permanent storage for flight test data. The unit may then be used to dump selected data from the cassettes to a Hewlett Packard 2115A Computer for processing.

6. Control Panel, GE Assy 123D6891G1

   This unit will allow the pilot to control the various operating modes of the CLFCS, including instrumentation commands and estimated range input.

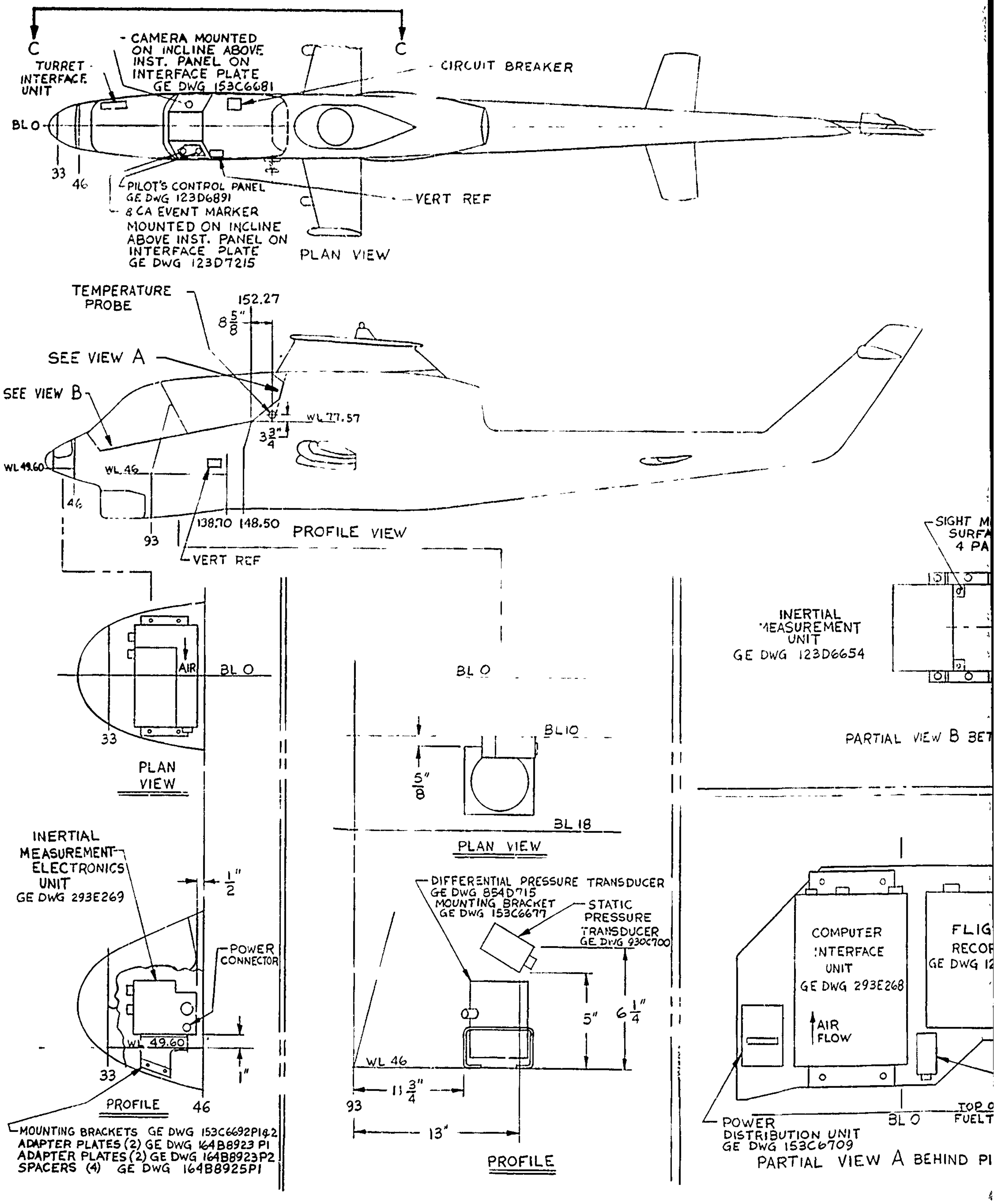
C
C
CAMERA MOUNTED ON INCLINE ABOVE INST. PANEL ON INTERFACE PLATE GE DWG 153C6681
TURRET INTERFACE UNIT
CIRCUIT BREAKER
BL O
33
46
PILOT'S CONTROL PANEL GE DWG 123D6891
8 CA EVENT MARKER MOUNTED ON INCLINE ABOVE INST. PANEL ON INTERFACE PLATE GE DWG 123D7215
VERT REF
PLAN VIEW
TEMPERATURE PROBE
152.27
8 5/8"
SEE VIEW A
SEE VIEW B
WL 77.57
3 3/4"
WL 49.60
WL 46
46
93
138.70
148.50
PROFILE VIEW
VERT REF
SIGHT M
SURFA
4 PA
AIR
BL O
33
PLAN VIEW
BL O
BL 10
5/8"
BL 18
PLAN VIEW
INERTIAL MEASUREMENT UNIT GE DWG 123D6654
PARTIAL VIEW B BET
INERTIAL MEASUREMENT ELECTRONICS UNIT GE DWG 293E269
1/2"
POWER CONNECTOR
WL 49.60
1"
33
46
PROFILE
MOUNTING BRACKETS GE DWG 153C6692P1&2
ADAPTER PLATES (2) GE DWG 164B8923 P1
ADAPTER PLATES (2) GE DWG 164B8923P2
SPACERS (4) GE DWG 164B8925P1
DIFFERENTIAL PRESSURE TRANSDUCER GE DWG 854D715
MOUNTING BRACKET GE DWG 153C6677
STATIC PRESSURE TRANSDUCER GE DWG 930C700
5"
6 1/4"
WL 46
11 3/4"
93
13"
PROFILE
COMPUTER INTERFACE UNIT GE DWG 293E268
AIR FLOW
FLIG
RECOR
GE DWG 12
POWER DISTRIBUTION UNIT GE DWG 153C6709
BL O
TOP O
FUELT
PARTIAL VIEW A BEHIND PI

Figure 4-1. CLFCS Aircraft Installation

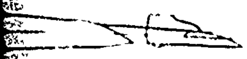

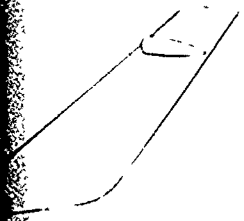

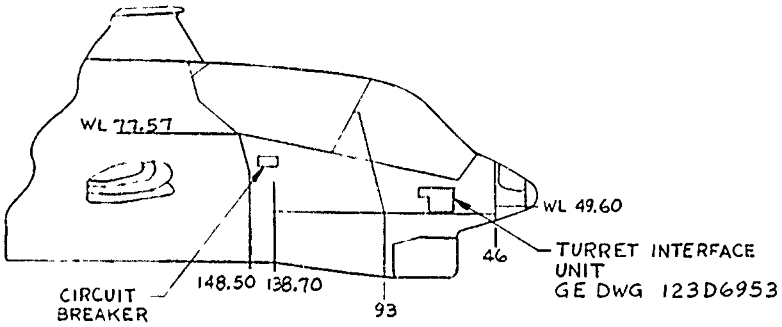
WL 77.57
WL 49.60
TURRET INTERFACE UNIT GE DWG 123D6953
46
CIRCUIT BREAKER
148.50
138.70
93

PARTIAL VIEW C-C
ROTATED 180°

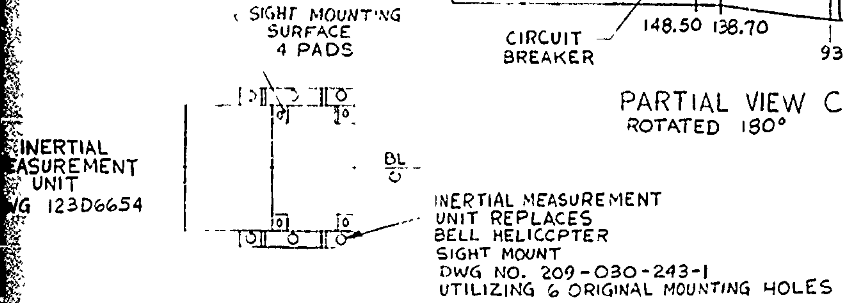
SIGHT MOUNTING SURFACE 4 PADS
INERTIAL
EASUREMENT
UNIT
G 123D6654
BL 0
INERTIAL MEASUREMENT UNIT REPLACES BELL HELICOPTER SIGHT MOUNT DWG NO. 209-030-243-1 UTILIZING 6 ORIGINAL MOUNTING HOLES

PARTIAL VIEW B BETWEEN GUNNER'S FEET

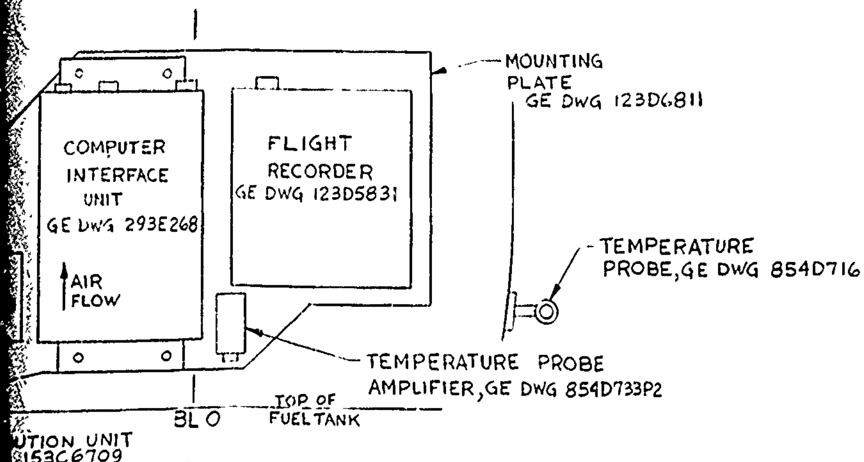
MOUNTING PLATE GE DWG 123D6811
COMPUTER INTERFACE UNIT GE DWG 293E268
AIR FLOW
FLIGHT RECORDER GE DWG 123D5831
TEMPERATURE PROBE, GE DWG 854D716
TEMPERATURE PROBE AMPLIFIER, GE DWG 854D733P2
BL 0
TOP OF FUEL TANK
UTION UNIT
153C6709

RTIAL VIEW A BEHIND PILOTS HEAD

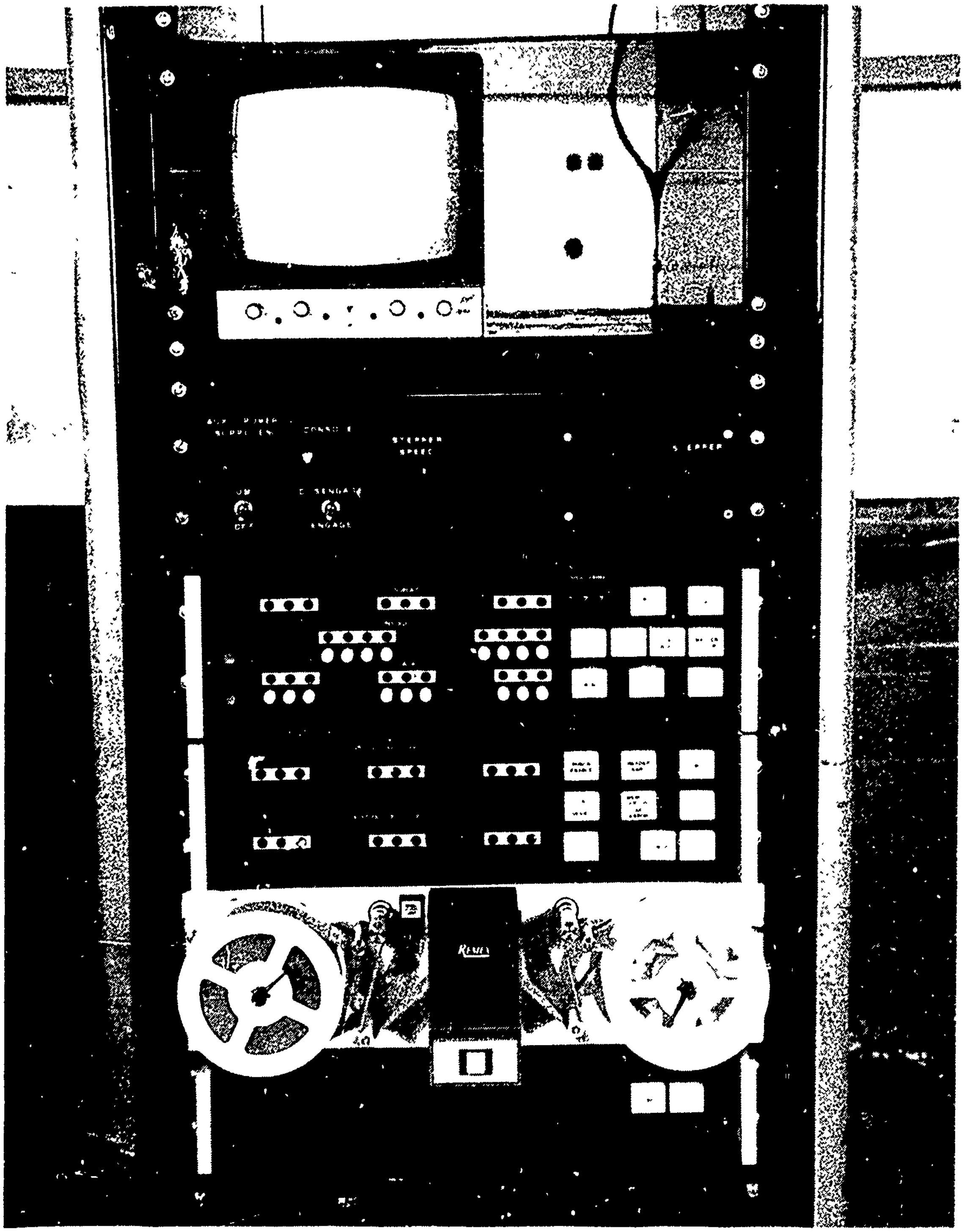

Figure 4-2. Console Cabinet

7. Air Data Sensors

Air Data Sensors will be installed as inputs to the CIU.

Absolute Temperature Probe, GE 854D716P1
Absolute Temperature Amplifier, GE 854D733P2
Static Pressure Transducer, GE 930C700P1
Dynamic Pressure Transducer, GE 854D715P1

The total system design includes 14 board designs, 17 boards to be fabricated.

In addition to the previous items, the following GFE items will be installed on the aircraft.

1. XM97 Turret and 20 MM Gun
2. Improved Pantograph Sight
3. Turret Electronics Unit
4. Gun Control Unit
5. Sight Stabilization Unit
6. Turret Circuit Breaker
7. Turret Interface Unit
8. Pilot Control Panel
9. Gunner Control Panel
10. Flight Recorder
11. Camera and Fiber Optics
12. Camera Film Marker Electronics
13. Vertical Reference Unit

Items 2, 4 and 7 of the above GFE have been modified to meet the interface requirements of the CLFCS.

Control Data Corporation peripheral equipment supplied by Frankford Arsenal for use with the CDC 469 Processor includes the following, which have been packaged in the Console Cabinet, GE Assy 123D7231, shown in Figure 4-2.

1. Programmer's Console with Video Monitor
2. Punched Tape Memory Loader
3. Teletype Controller

4.2 COMPUTER INTERFACE UNIT

This section presents a description of the Computer-Interface Unit (see Figure 4-4) discussing its functions, operation at a block diagram level, and its interconnection with other system components. The functional block diagram for this hardware is found in Figure 4-3.

The Computer-Interface Unit (CIU) provides five functions:

1. Translates aircraft system information into a digital format for use in the general purpose digital processor.
2. Performs necessary computational tasks to provide lead angles or lead angles plus closed loop corrections to the aircraft weapon system.
3. Translates the digital quantities representing lead angles generated by the general purpose digital processor into analog correction signals to command the gun turret to a desired position.
4. Provides a discrete to the sight/turret subsystem to inhibit the firing of the weapon at times when the processor has not arrived at a valid solution.
5. Provides digital data to be recorded on a flight recorder which will aid in evaluating the performance of the airborne fire control system.

4.2.1 ANALOG SIGNAL CONDITIONING

The aircraft sensors provide various forms of analog signals which must be conditioned and converted to a digital format to be compatible with the general purpose computer. The definition of the analog signal types and their multiplexed analog to digital channel assignments are listed in Table 4-1. For the following description, reference may be made to the functional block diagram in Figure 4-3.

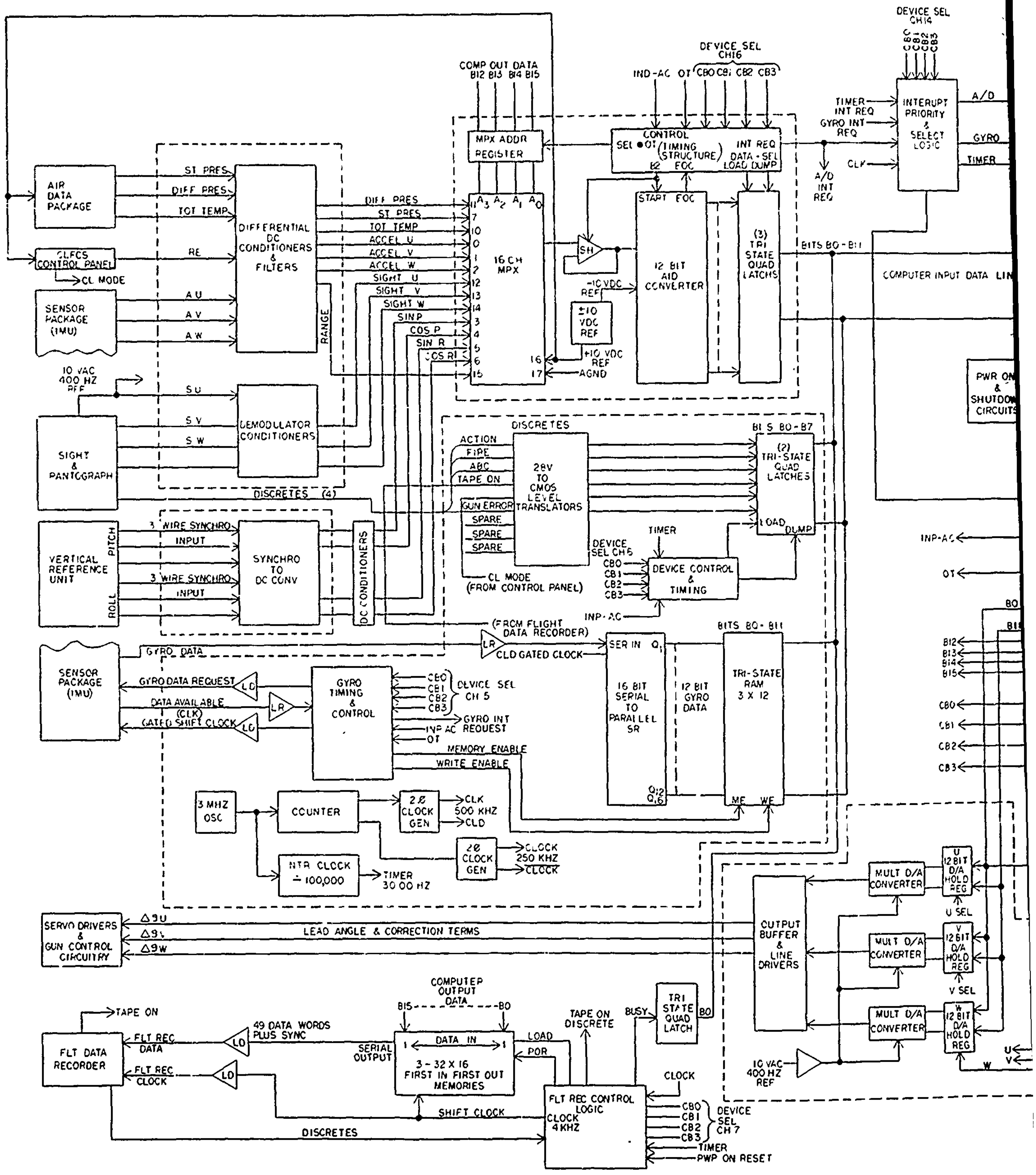

DEVICE SEL CH14
CB0 CB1 CB2 CB3
DEVICE SEL CH16
IND-AC OT CB0 CB1 CB2 CB3
COMP OUT DATA B12 B13 B14 B15
TIMER INT REQ
GYRO INT REQ
CLK
INTERUPT PRIORITY & SELECT LOGIC
A/D
GYRO
TIMER
MPX ADDR REGISTER
CONTROL SEL OT (TIMING STRUCTURE) INT REQ DATA-SEL LOAD DUMP
B2 EOC
A/D INT REQ
AIR DATA PACKAGE
ST PRES
DIFF PRES
TOT TEMP
CLFCS CONTROL PANEL
RE
CL MODE
SENSOR PACKAGE (IMU)
AU
AV
AW
DIFFERENTIAL DC CONDITIONERS & FILTERS
RANGE
DIFF PRES
ST PRES
TOT TEMP
ACCEL U
ACCEL V
ACCEL W
SIGHT U
SIGHT V
SIGHT W
SIN P
COS P
SIN R
COS R
A3 A2 A1 A0
16 CH MPX
SH
START EOC
12 BIT A/D CONVERTER
(3) TRI STATE QUAD LATCHS
BITS B0-B11
COMPUTER INPUT DATA LIN
-10 VDC REF
±10 VDC REF
+10 VDC REF
AGND
10 VAC 400 HZ REF
SU
SV
SW
DEMODULATOR CONDITIONERS
SIGHT & PANTOGRAPH
DISCRETES (4)
PWR ON & SHUTDOW CIRCUITS
DISCRETES
ACTION
FIRE
ABC
TAPE ON
GUN ERROR
SPARE
SPARE
SPARE
28V TO CMOS LEVEL TRANSLATORS
BITS B0-B7
(2) TRI-STATE QUAD LATCHES
LOAD DUMP
TIMER
DEVICE SEL CH5
CB0 CB1 CB2 CB3
DEVICE CONTROL & TIMING
CL MODE (FROM CONTROL PANEL)
INP-AC
OT
VERTICAL REFERENCE UNIT
PITCH
ROLL
3 WIRE SYNCHRO INPUT
3 WIRE SYNCHRO INPUT
SYNCHRO TO DC CONV
DC CONDITIONERS
(FROM FLIGHT DATA RECORDER)
LR
CLD GATED CLOCK
BITS B0-B11
SENSOR PACKAGE (IMU)
GYRO DATA
GYRO DATA REQUEST
DATA AVAILABLE (CLK)
GATED SHIFT CLOCK
LD
LR
GYRO TIMING & CONTROL
CB0 CB1 CB2 CB3
DEVICE SEL CH 5
GYRO INT REQUEST
INP AC
OT
MEMORY ENABLE
WRITE ENABLE
SER IN Q1
16 BIT SERIAL TO PARALLEL SR
Q12 Q16
12 BIT GYRO DATA
TRI-STATE RAM 3 X 12
ME WE
B12 B13 B14 B15
CB0 CB1 CB2 CB3
3 MHZ OSC
COUNTER
2Ø CLOCK GEN
CLK 500 KHZ
CLD
2Ø CLOCK GEN
CLOCK 250 KHZ
CLOCK
NTR CLOCK ÷ 100,000
TIMER 30.00 HZ
SERVO DRIVERS & GUN CONTROL CIRCUITRY
Δ9U
Δ9V
Δ9W
LEAD ANGLE & CORRECTION TERMS
OUTPUT BUFFER & LINE DRIVERS
MULT D/A CONVERTER
MULT D/A CONVERTER
MULT D/A CONVERTER
U 12 BIT D/A HOLD REG
U SEL
V 12 BIT D/A HOLD REG
V SEL
W 12 BIT D/A HOLD REG
10 VAC 400 HZ REF
U
V
W
B0
TAPE ON
FLT DATA RECORDER
FLT REC DATA
FLT REC CLOCK
49 DATA WORDS PLUS SYNC
LD
LD
COMPUTER OUTPUT DATA
B15 B0
DATA IN
SERIAL OUTPUT
3-32 X 16 FIRST IN FIRST OUT MEMORIES
LOAD
POR
TAPE ON DISCRETE
BUSY
TRI STATE QUAD LATCH
B0
CLOCK
FLT REC CONTROL LOGIC
CLOCK 4 KHZ
SHIFT CLOCK
DISCRETES
CB0 CB1 CB2 CB3
DEVICE SEL CH 7
TIMER
PWR ON RESET

Figure 4-3. Computer Interface Unit Functional Block Diagram

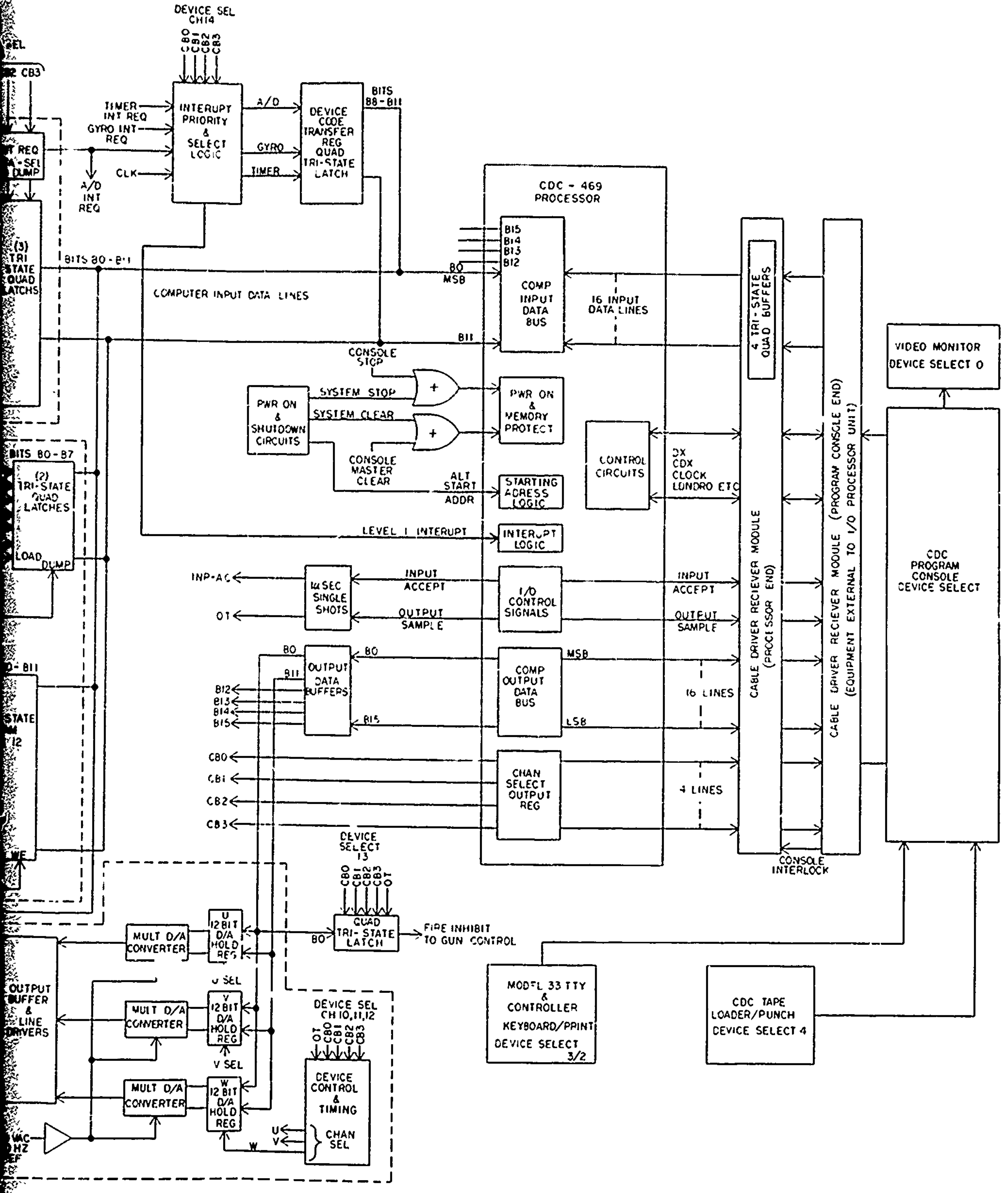
DEVICE SEL CH14
CB0 CB1 CB2 CB3
SEL
CB3
INT REQ
A/D-SEL DUMP
TIMER INT REQ
GYRO INT REQ
CLK
A/D INT REQ
INTERUPT PRIORITY & SELECT LOGIC
A/D
GYRO
TIMER
DEVICE CODE TRANSFER REG QUAD TRI-STATE LATCH
BITS B8-B11
(3) TRI STATE QUAD LATCHS
BITS B0-B11
COMPUTER INPUT DATA LINES
CDC - 469 PROCESSOR
B15
B14
B13
B12
B0 MSB
COMP INPUT DATA BUS
16 INPUT DATA LINES
B11
CONSOLE STOP
PWR ON & SHUTDOWN CIRCUITS
SYSTEM STOP
SYSTEM CLEAR
PWR ON & MEMORY PROTECT
CONSOLE MASTER CLEAR
ALT START ADDR
STARTING ACRESS LOGIC
CONTROL CIRCUITS
DX CDX CLOCK LONDRO ETC
LEVEL 1 INTERUPT
INTERUPT LOGIC
4 TRI-STATE QUAD BUFFERS
CABLE DRIVER RECIEVER MODULE (PROCESSOR END)
CABLE DRIVER RECIEVER MODULE (PROGRAM CONSOLE END) (EQUIPMENT EXTERNAL TO I/O PROCESSOR UNIT)
VIDEO MONITOR DEVICE SELECT 0
CDC PROGRAM CONSOLE DEVICE SELECT
BITS B0-B7
(2) TRI-STATE QUAD LATCHES
LOAD
DUMP
INP-AC
OT
14 SEC SINGLE SHOTS
INPUT ACCEPT
OUTPUT SAMPLE
I/O CONTROL SIGNALS
INPUT ACCEPT
OUTPUT SAMPLE
B0
B11
OUTPUT DATA BUFFERS
B12
B13
B14
B15
COMP OUTPUT DATA BUS
MSB
LSB
16 LINES
B0-B11
STATE
12
CB0
CB1
CB2
CB3
CHAN SELECT OUTPUT REG
4 LINES
CONSOLE INTERLOCK
WE
DEVICE SELECT 13
CB0 CB1 CB2 CB3 OT
QUAD TRI-STATE LATCH
B0
FIRE INHIBIT TO GUN CONTROL
MULT D/A CONVERTER
U 12 BIT D/A HOLD REG
U SEL
V 12 BIT D/A HOLD REG
V SEL
W 12 BIT D/A HOLD REG
OUTPUT BUFFER & LINE DRIVERS
DEVICE SEL CH 10,11,12
OT CB0 CB1 CB2 CB3
DEVICE CONTROL & TIMING
U
V
W
CHAN SEL
VAC
HZ
EF
MODEL 33 TTY & CONTROLLER KEYBOARD/PRINT DEVICE SELECT 3/2
CDC TAPE LOADER/PUNCH DEVICE SELECT 4

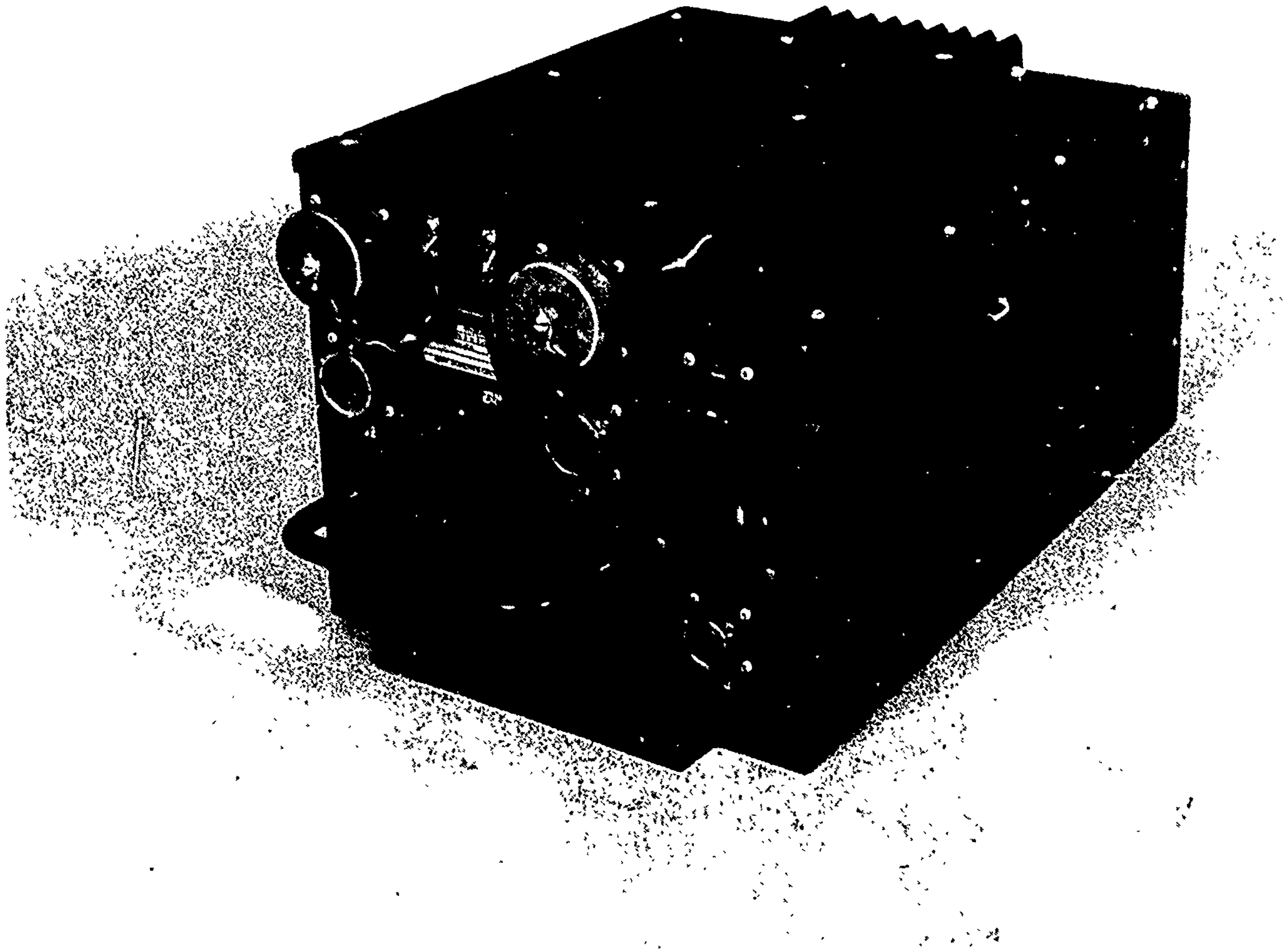

Figure 4-4. Computer Interface Unit

TABLE 4-1

ANALOG INPUTS

CHANNEL NO.	SIGNAL NAME	SIGNAL TYPE
0	Acceleration U	DC
1	Acceleration V	DC
2	Acceleration W	DC
3	Sin Pitch	3-Wire Synchro
4	Cos Pitch	
5	Sin Roll	3-Wire Synchro
6	Cos Roll	
7	Static Pressure	DC
10	Ambient Temperature	DC
11	Differential Pressure	DC
12	Sight U	AC
13	Sight V	AC
14	Sight W	AC
15	Range Estimate	DC
16	10 VDC Reference	DC
17	Analog Ground	DC

The vertical reference signals, pitch and roll, are received in the CIU in 3-wire synchro format. These signals are processed by a 2-channel synchro to direct current sine/cosine converter, and the resulting four signals are thereafter treated as DC inputs. This converter utilizes a Scott-T input, thereby offering DC isolation in its interface with the vertical reference.

The DC signals are received by differential amplifiers utilizing active filters with a break frequency of 3 hertz and a 40 db/decade attenuation. The break frequency, a decade below the A/D sampling rate of 30 hertz, was chosen to minimize measurement errors produced by the aliasing of signal frequencies equal to or greater than one half the sampling rate. The low frequency filters for the three accelerometer signals are resident in the sensor package external to the CIU; within the CIU differential amplifiers utilizing passive T-filters with a 500 hertz break frequency and 20 db/decade slope attenuate line noise that may have been introduced. Range Estimate is generated by a manually set potentiometer. Since it is not time-varying, it is given the same DC conditioning within the CIU as the accelerometer signals.

The three AC signals from the sighting station are first buffered by differential amplifiers, then converted to DC through a phase sensitive demodulator. The signals are then conditioned by active filters similar to those for the DC inputs, attenuating the demodulator ripple by 130 db.

4.2.2 A/D CONVERSION

The fourteen analog signals in buffered DC format are tied to the inputs of a sixteen channel multiplexer. In addition an internal 10 volt DC reference and analog ground are tied to the remaining two multiplexer channels for test purposes. Any of the sixteen signals may be made available to the sample and hold amplifier input to the A/D by software control. The appropriate four bit code representing the octal multiplexer channel number defined in Table 3-1 is output from the digital processor (CDC 469) on output data lines bits 12 through 15, and Device Code 16B is addressed. The sample and hold then samples the desired input, and holds its analog value constant long enough for the successive approximation A/D converter to make its conversion. The converted digital value is then clocked into a set of tri-state latches to be made available to the CDC 469.

4.2.3 DISCRETE INPUTS

At the beginning of each computer iteration (1/30 second) the Interrupt Clock sets the present values of the Discrete Inputs into a set of tri-state latches. Since the discretes are at a 28 VDC level at the input to the CIU, each requires a 28 VDC to CMOS level translator prior to being fed to the tri-state latches. The CDC-469 packs the discretes into the first eight digits of a computer word. For instrumentation purposes, the CDC 469 also utilizes the last eight bits of the same word to store the output of a software counter which indicates the number of times the flight recorder has been set in motion. The assignment of the bit locations for the discrete word is given in Table 4-2. The discrete word may be found at computer location 247.

TABLE 4-2
DISCRETE INPUTS

BIT LOCATION	SIGNAL NAME	LOGIC INVERSION	DESCRIPTION
0	ACTION	Yes	Indicates that gun is being commanded to follow sight.
1	FIRE	Yes	Indicates that weapon is firing.
2	ABC	Yes	Acquire Burst Centroid. Indicates that sight is directed toward impacts rather than the target.
3	TAPE ON	Yes	Indicates that flight recorder is in motion. CIU hardware delays discrete by 2 sec. to allow transport to achieve regulated speed prior to recording.
4	CL MODE	Yes	Commands computer to apply closed loop corrections to second firing within one engagement. Otherwise second firing will have open loop solution only.
5	GUN ERROR	No	Indicates that gain is not servoed to commanded position or that computer has not arrived at valid solution or that computer is signaling gunner to break track.
6	DISC 6	Yes	Spare discrete electrically held at logic level "1".
7	DISC 7	Yes	Spare discrete electrically held at logic level "1".
8	B8	No	Software counter output representing the number of times the flight recorder has been set in motion. This will be the file number assigned to a continuous block of recorded data. The MSB is B8, the LSB is B15.
9	B9	No	
10	B10	No	
11	B11	No	
12	B12	No	
13	B13	No	
14	B14	No	
15	B15	No	

4.2.4 ANGULAR RATE INPUTS

Aircraft angular rates are presented to the CIU from the Inertial Measurement Unit (IMU). The IMU utilizes three rate integrating gyros aligned along the aircraft body axes. Each gyro is in a pulse torquing loop with pulse rate a measure of inertia rates and pulse count a measure of angular position. The net clockwise/counterclockwise pulse count is stored in a counter. Upon request from the CIU, the IMU will sample all their counters, store this information in a transfer register, reset the counters to zero, and signal the CIU that the data is available. The data available signal initiates three 16-bit data word transfers, the 12 least significant bits of each being tangible gyro data. The transfer of data from the IMU to CIU is made in serial format at a 500 kHz clock rate. Once the first word is received at the CIU, it is stored in a random access memory (i.e., external to the CDC 469) and the second transfer begins. This process is again repeated and finally the data is transferred from the random access memory to the CDC 469 in three input operations.

4.2.5 CDC 469 COMPUTER INTERFACE UNIT COMMUNICATION

A conventional interrupt system with the CDC 469 initiating all service has been utilized to control the data flow between the general purpose digital processor and the CIU interface circuitry.

In the previous sections, it was simply stated that data was transferred to the processor. To understand the mechanism of this operation, a discussion of the first iteration following a power-on situation will follow.

Once power is applied to the system, a master clear pulse from the CIU forces the CDC 469 to its starting address where a short power-on routine initializes the processor to the correct program location. At the same time a power-on reset pulse within the CIU conditions its interface boards to the start condition. The CDC 469 has two preset starting addresses. Normally the processor goes to the cold start starting address 10400. However, at power-up a timer in the CIU hardware detects whether the power had been interrupted for greater or less than 2.5 seconds. For an interruption of less than 2.5 seconds, the CIU activates the alternate starting address line to the CDC 469, and the processor is forced to location 11000.

A countdown of the CIU 3 MHz oscillator is now underway, and 1/30 of a second later the 30 Hz interrupt clock generates an interrupt request. Upon recognition of this interrupt, the processor begins its computational tasks. For a cold start situation, the first software task is to time out a delay of 150 iterations of the 30 Hz interrupt clock, or 5 seconds. This delay allows time for the gyros in the IMU to spin up to speed.

All interfacing service is initiated by the processor; at a time determined by the processor software, a request for I/O data is made. The interface system responds to this request by initiating one of several operations depending on which data is requested.

The request for A/D data is accomplished by selecting the A/D device controller, which is assigned DEVICE SEL 16, using an output data instruction. The data transferred to the A/D selects the desired multiplexer channel to be converted, and initiates the conversion process. Once this output instruction is completed, the processor is free to return to computation. The conversion of one piece of A/D data will now take 100 μsec to complete, and upon completion a request for service will be sent to the processor using a level one interrupt, and the interrupt code for the A/D converter, listed in Table 4-4, is loaded into the device code transfer register. Upon answering the interrupt request, the processor reads the transfer register, detects which driver interrupted it, and jumps to the service routine for that device, which in this case is the A/D converter. The data is then read from the A/D and the service request is reset. After completion of the service routine, the processor will return to its normal computational mode. The software may initiate another A/D data request, or, if the 16 word A/D data buffer is satisfied, gyro data from the IMU may now be requested. The servicing of the gyro's is similar to that of the A/D with the exception that three 16 bit words will now be taken sequentially.

The interface system was designed and built with a three level priority technique which complied with Control Data Corporation documentation. The system would handle simultaneous interrupt requests with the following order of hardwired priority:

1. Interrupt Clock
2. Gyro
3. A/D Converter

For other than simultaneous requests, the devices are serviced on a first-come, first serve basis. In either event, overlapping service requests are stored in the interface logic until service is available. However, contrary to CDC documentation, the CDC 469 could not handle any service request if there is another interrupt pending. Therefore it is imperative that the software be designed to guarantee that each interrupt be serviced before another is initiated.

In addition to the A/D and gyro inputs are the discrete inputs. Since all discrete data (Table 4-2) is packed into one 16-bit word, it need not operate on an interrupt basis. Shortly after the interrupt clock is serviced, the software selects the discrete device (channel 6) and reads the data which has been clocked into a storage register.

The functional block diagram of Figure 4-3 shows that the data transferred to the processor is organized on a common bus system. Each input device, i.e., the A/D, gyros, discretes, and transfer register, places its data on this bus through tri-state quad latches which only become active when that particular device is selected. The CIU utilizes twelve of the possible sixteen bits of the input data bus, with the remaining four bits forced to zero by means of open circuit logic convention.

4.2.6 D/A CONVERTER

After processing the various pieces of data and arriving at a solution for gun order corrections to the original sight command position, a set of three D/A converters is utilized to translate this data into a form acceptable to the gun turret system. At a time determined by the software, U, V, or W axis correction signals are sent from the processor out over the output data bus to the selected D/A converter. Each of the converters function as a separate output device; the channel code assignments are listed in Table 4-3. The selected converter stores the output data in a 12-bit holding register and within 10 μ second converts this data to a 400 Hz amplitude scaled signal which is sent to the command inputs of the gun turret resolver chain, to be summed with the improved pantograph sight output vector to generate a desired gun position command. As long as the software has a valid open loop solution, the D/A outputs will be updated at the software iteration rate of 30 Hz, otherwise the outputs will be clamped to zero.

4.2.7 FLIGHT RECORDER

The CIU has a subfunction of data logging such that a selected set of parameters may be recorded in flight for use in the system evaluation and/or troubleshooting. The selected data is transferred from the processor to first in - first out (FIFO) memories. The transfer from the FIFO's in the CIU to the government furnished flight recorder is set at a bit rate of about 4 kHz, or 4 msec per 16-bit word. Weighing this rate against the 30 Hz processor iteration rate and the available software space, a limited flexibility in recording mode relating recording rate to number of variables recorded was established. In software controlled Mode 0, seven parameters from one iteration are stored in a software buffer, followed by the same seven parameters for

TABLE 4-3

I/O CHANNEL CODE ASSIGNMENTS

CHANNEL NUMBER	DEVICE	CHANNEL CODE			
		CB0	CB1	CB2	CB3
0	Video Monitor	0	0	0	0
1	Programmer's Console	0	0	0	1
2	Teletype (Print)	0	0	1	0
3	Teletype (Keyboard)	0	0	1	1
4	Memory Loader	0	1	0	0
5	Gyro Inputs	0	1	0	1
6	Discretes	0	1	1	0
7	Flight Recorder	0	1	1	1
10	D/A Channel U	1	0	0	0
11	D/A Channel V	1	0	0	1
12	D/A Channel W	1	0	1	0
13	Fire Inhibit	1	0	1	1
14	Transfer Register Device Control	1	1	0	0
15	(Spare)	1	1	0	1
16	A/D Converter	1	1	1	0
17	(Spare)	1	1	1	1

TABLE 4-4
INTERRUPT REGISTER CODE

INTERRUPT NUMBER	DEVICE	INTERRUPT CODE			
		B9	B9	B10	B11
220	A/D Converter	1	0	0	1
240	Gyro Inputs	1	0	1	0
300	Interrupt Clock	1	1	0	0

the next iteration. After the seventh iteration, the 7x7 or 49 words plus an index code word (record marker) are transferred to the FIFO's at a rate of about 2.5 μsec per word, or 125 μsec total. The FIFO then shifts out data serially to the recorder, taking about 6 processor iterations to complete the 50 word record. A clock gap then appears on the data line indicating the end of the record, then at the beginning of the 8th iteration, when the FIFO's are loaded with another 50 words, another shift out occurs. Mode 0 is assumed in the software assembly. If Mode 1 is desired, a key-in must be executed from the console after the assembly has been loaded. In Mode 1, 49 words from our iteration are transferred to the recorder every 7 iterations, resulting in an increased number of parameters measured at the expense of sampling rate. A listing of the parameters recorded is given in Tables 3-5 and 3-6.

4.2.8 PROGRAMMER'S CONSOLE TO PROCESSOR BUFFERING

The CDC 469 processor utilizes C-MOS drivers for its data and control signals, so provisions are necessary for operation in the console controlled mode with the long cables inherent with flight line conditions. Each cable connection from the processor to the programmer's console, and vice versa, includes a a line driver/receiver pair, with one half of the pair resident in the CIU and the other in the Console Interface Unit, which is mounted in the console cabinet. Provision is made to deactivate the receivers in the CIU during normal operation so that the undriven inputs will not interfere with proper operation.

4.3 INTERTIAL MEASUREMENT UNIT AND ELECTRONICS

4.3.1 INTRODUCTION

The hardware dedicated to inertial measurement has been packaged in two chassis. The Inertial Measurement Unit (IMU) contains 3 rate integrating gyros and 3 accelerometers, orthogonally mounted and aligned to the uvw axis of the aircraft. The IMU Electronics Assembly contains power supplies and supportive electronics for the sensors, in particular for the gyros. These gyros and accelerometers provide body-bound sensor outputs for computation of inertial position and velocities.

The two chassis are shown in Figures 4-5 and 4-6, which are photographs taken during the test phase. The IMU is shown attached to its alignment fixture.

The gyro is a Honeywell GG1111LC02 subminiature rate integrating gyro used in a pulse torquing loop with pulse rate a measure of inertial rates and pulse count a measure of angular position relative to some previous position. Specifications for this gyro are listed in Table 4-5.

The SUNDSTRAND QA1000 - S5 servo accelerometer provides the three axis acceleration outputs. Its significant characteristics are listed in Table 4-6.

The basic principle involved in the pulse torqued loop is that the average current into the gyro torque motor coil required to null the signal generator output is proportional to the angular rate at which the gyro is being rotated about its sensitive axis. If this average current is provided by pulses of accurately known amplitude and duration, then each pulse is equivalent to an increment in angular position. The total change in angular position over a given time interval is obtained by counting these pulses in any up-down binary counter. Thus the accumulated angular change is available in digital form to be transmitted to the digital processor.

Figure 4-7 shows the complements of hardware required for the 3 channel, pulse torqued loop configuration. Common circuitry is shared for the control functions, computer interface logic, and signal generator excitation, while separate electronics for each channel is required for the remainder. Figure 4-8 shows the common circuitry.

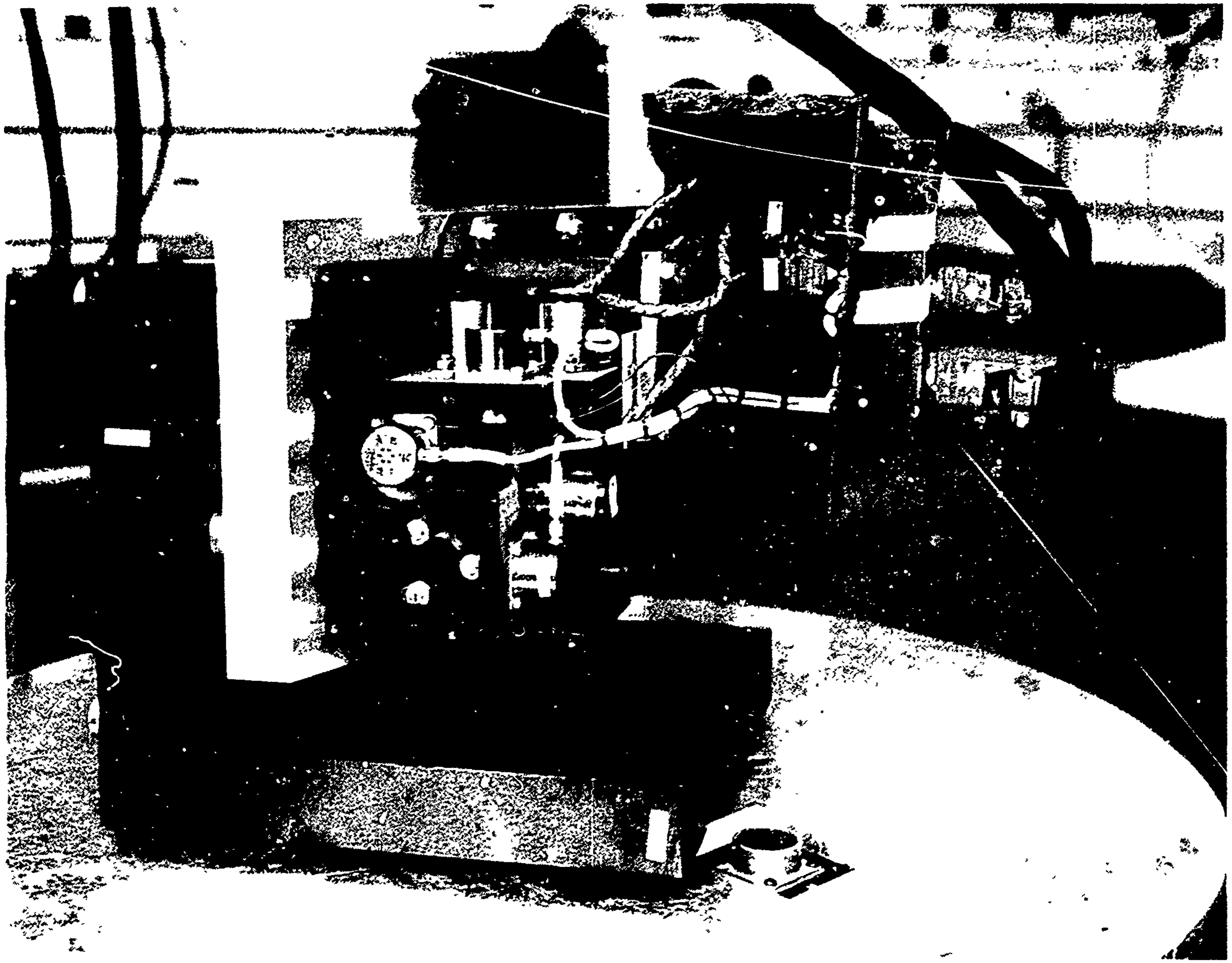

Figure 4-5. Inertial Measurement Unit

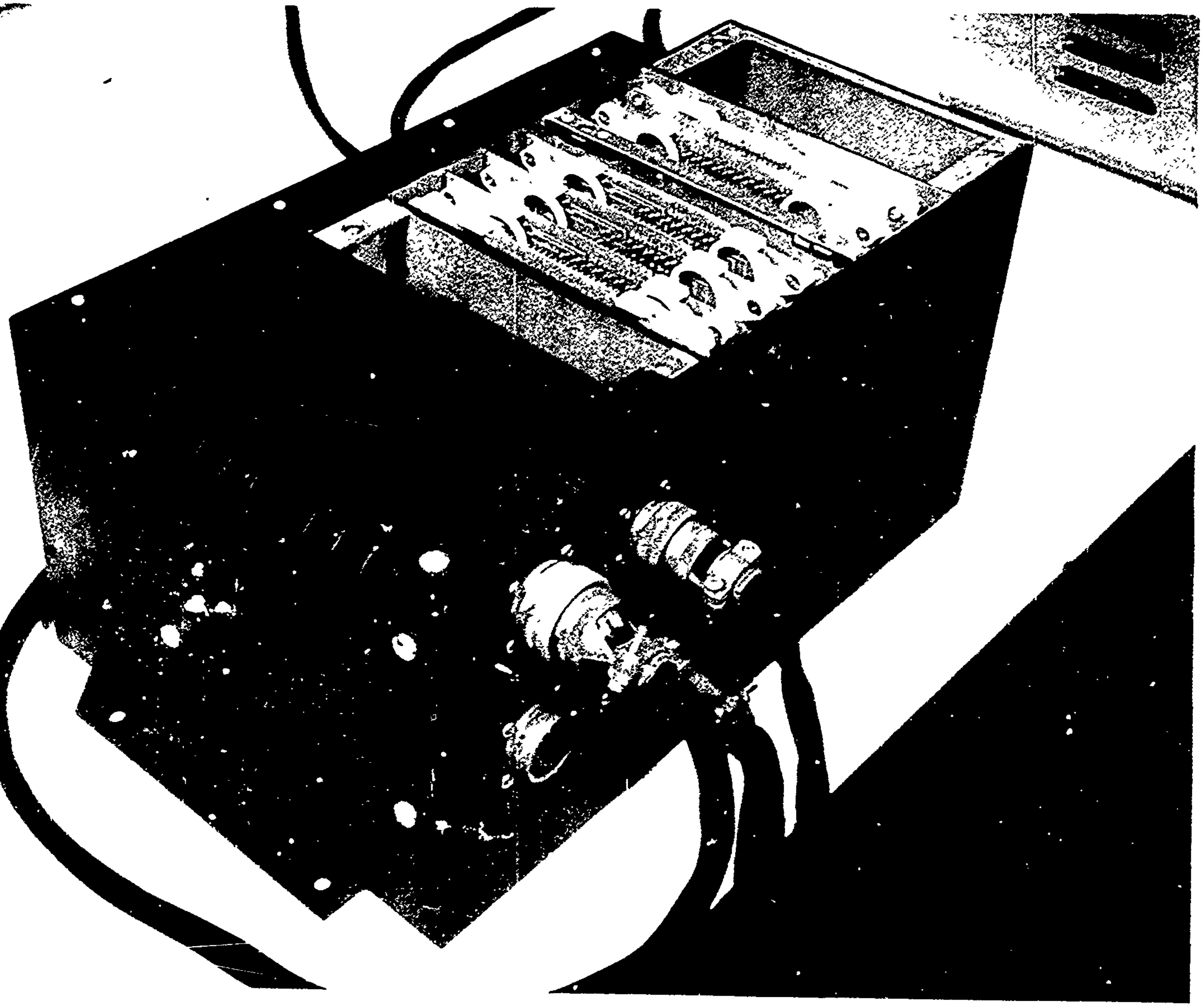

Figure 4-6. IMU Electronics Assembly

TABLE 4-5
SUMMARY OF GYRO CHARACTERISTICS

Type	Rate Integrating
Manufacturer and Model	Honeywell Model GG1111LC02
Size	1.19 inch diameter x 2.5 inches long
Maximum Rate	200 deg/sec
Random Drift	12 deg/hr
g Sensitivity	25 deg/hr/g vector
Scale Factor	1 deg/sec/mA
Sensitivity	24 volts/rad
Linearity	< 0.1% FS
Time Constant	1.5 msec max
Spin Motor Power	7 volts rms, 2 phase, 900 Hz sine
Signal Generator Voltage	20 volts rms, 4 kHz

TABLE 4-6
SUMMARY OF ACCELEROMETER CHARACTERISTICS

Type	Servo, Low - g Linear
Manufacturer and Model	SUNSTRAND QA1000 - S5
Size	1.0 inch diameter x 1.5 inches long
Range	± 10g
Zero Unbalance	± 0.005 g typical, ± 0.010g max
Thermal Zero Shift	75 micro-g/°F
Scale Factor	1.000 volt/g
Linearity	20 micro-g to 0.07g 0.03% of point above 0.07g
Excitation	± 15 VDC, 40 mA maximum

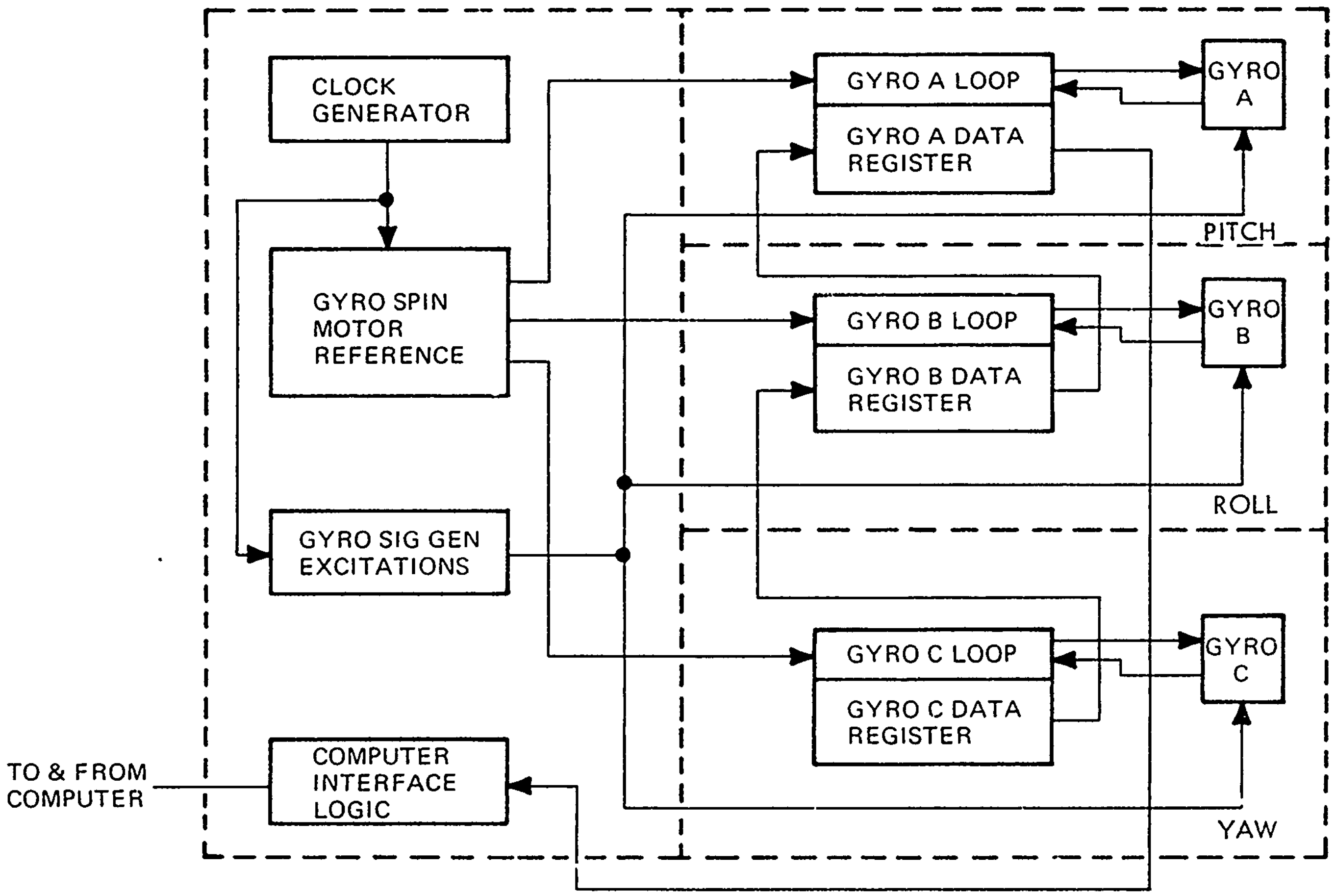
CLOCK GENERATOR
GYRO SPIN MOTOR REFERENCE
GYRO SIG GEN EXCITATIONS
COMPUTER INTERFACE LOGIC
TO & FROM COMPUTER
GYRO A LOOP
GYRO A DATA REGISTER
GYRO A
PITCH
GYRO B LOOP
GYRO B DATA REGISTER
GYRO B
ROLL
GYRO C LOOP
GYRO C DATA REGISTER
GYRO C
YAW

Figure 4-7. Gyro Block Diagram

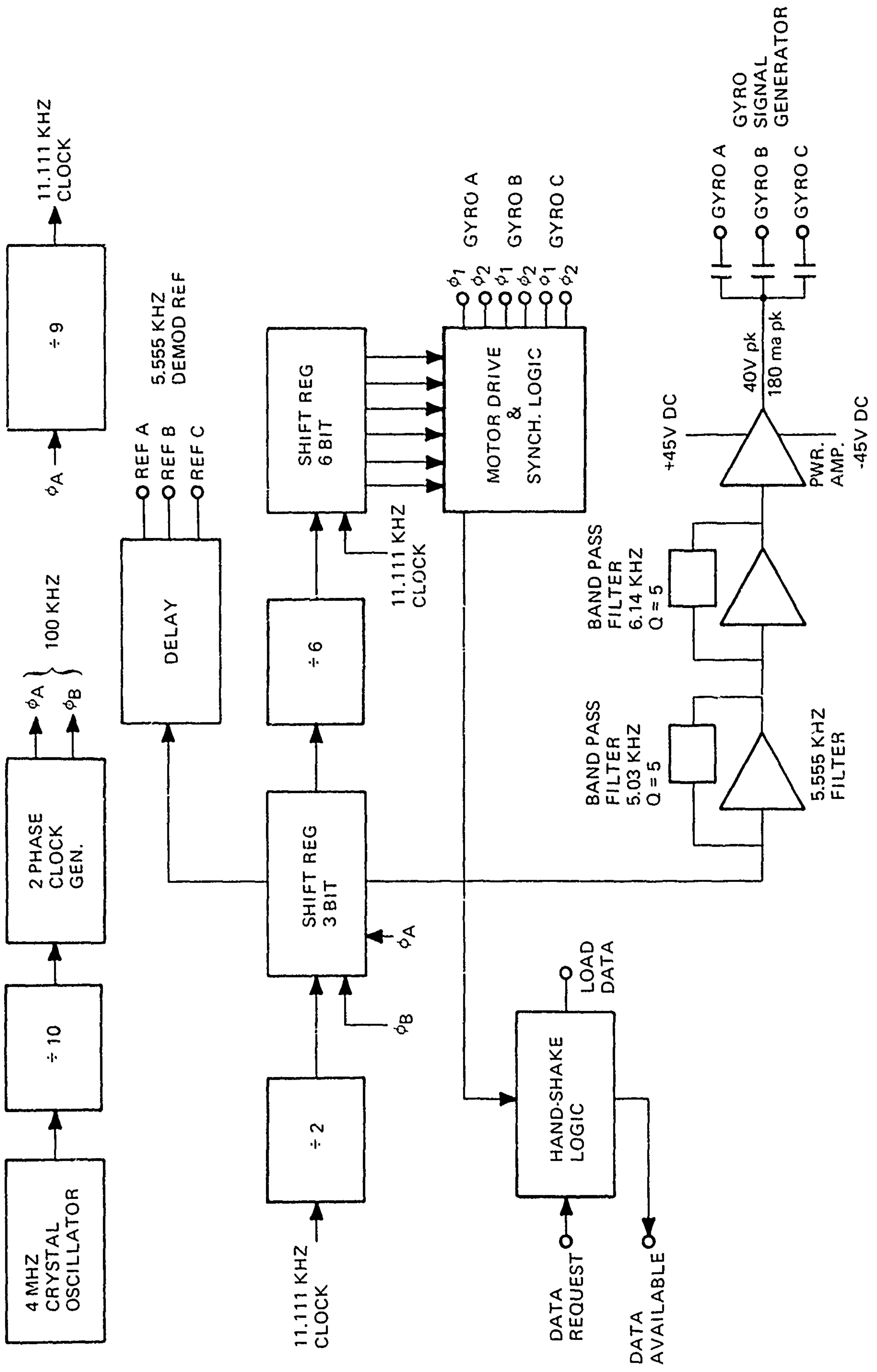
4 MHZ CRYSTAL OSCILLATOR
÷ 10
2 PHASE CLOCK GEN.
ϕ_A
ϕ_B
100 KHZ
÷ 9
ϕ_A
11.111 KHZ CLOCK
DELAY
REF A
REF B
REF C
5.555 KHZ DEMOD REF
11.111 KHZ CLOCK
÷ 2
SHIFT REG 3 BIT
ϕ_B
ϕ_A
÷ 6
SHIFT REG 6 BIT
11.111 KHZ CLOCK
MOTOR DRIVE & SYNCH. LOGIC
ϕ_1
ϕ_2
ϕ_1
ϕ_2
ϕ_1
ϕ_2
GYRO A
GYRO B
GYRO C
HAND-SHAKE LOGIC
LOAD DATA
DATA REQUEST
DATA AVAILABLE
BAND PASS FILTER 5.03 KHZ Q = 5
5.555 KHZ FILTER
BAND PASS FILTER 6.14 KHZ Q = 5
PWR. AMP.
+45V DC
-45V DC
40V pk
180 ma pk
GYRO A
GYRO B
GYRO C
GYRO SIGNAL GENERATOR

Figure 4-8. Control Logic and Signal Generator

4.3.2 COMMON CONTROL CIRCUITRY

4.3.2.1 Digital Control

An integrated circuit crystal controlled oscillator produces the basic 4.0 MHz clock which is counted down to produce a family of lower frequency reference clocks. Figures 4-9 and 4-10 display the relative timing of these reference signals. Reference may be made to schematics of Data Item A004 of this contract for further details. Of particular interest is the fact that the gyro spin motor references are staggered in time to reduce the peak loading on the power supply.

4.3.2.2 Gyro Signal Generator

The signal generator excitation is derived from a 5.56 kHz logic level square wave, as shown in Figure 4-8. The logic signal is fed through a zener regulator resulting in a square wave with very precise amplitude. A stagger-tuned filter, consisting of two active band-pass filters in cascade, then passes only the fundamental frequency of the square wave, resulting in a sine wave which has a precise amplitude and is free of harmonics Stagger tuning tends to flatten off the peak gain as well as to reduce the change in phase shift with respect to frequency at the peak. The result is less deviation in gain and phase shift at the center frequency as the filter elements change frequency over temperature or age

The resulting operational amplifier level sine waves are then voltage amplified by discrete transistor circuitry to a 26.5 VRMS level, and capacitively coupled to the three gyro signal generator primaries.

4.3.3 PULSE TORQUED LOOP

Figure 4-11 displays the individual circuitry required for each channel of the gyro system. The spin motor drive logic contains additional control to guarantee that the transistor switch that is presently on will be turned off before the complementary off switch is turned on. It can be seen from the diagram that if both switches were on at the same instant, the ± 9 volt dc supplies would be momentarily shorted, causing shoot through currents.

An error in the null of the gyro will cause an a.c. voltage to appear at the output of the gyro signal generator. This signal is buffered within the IMU package, amplified again in the

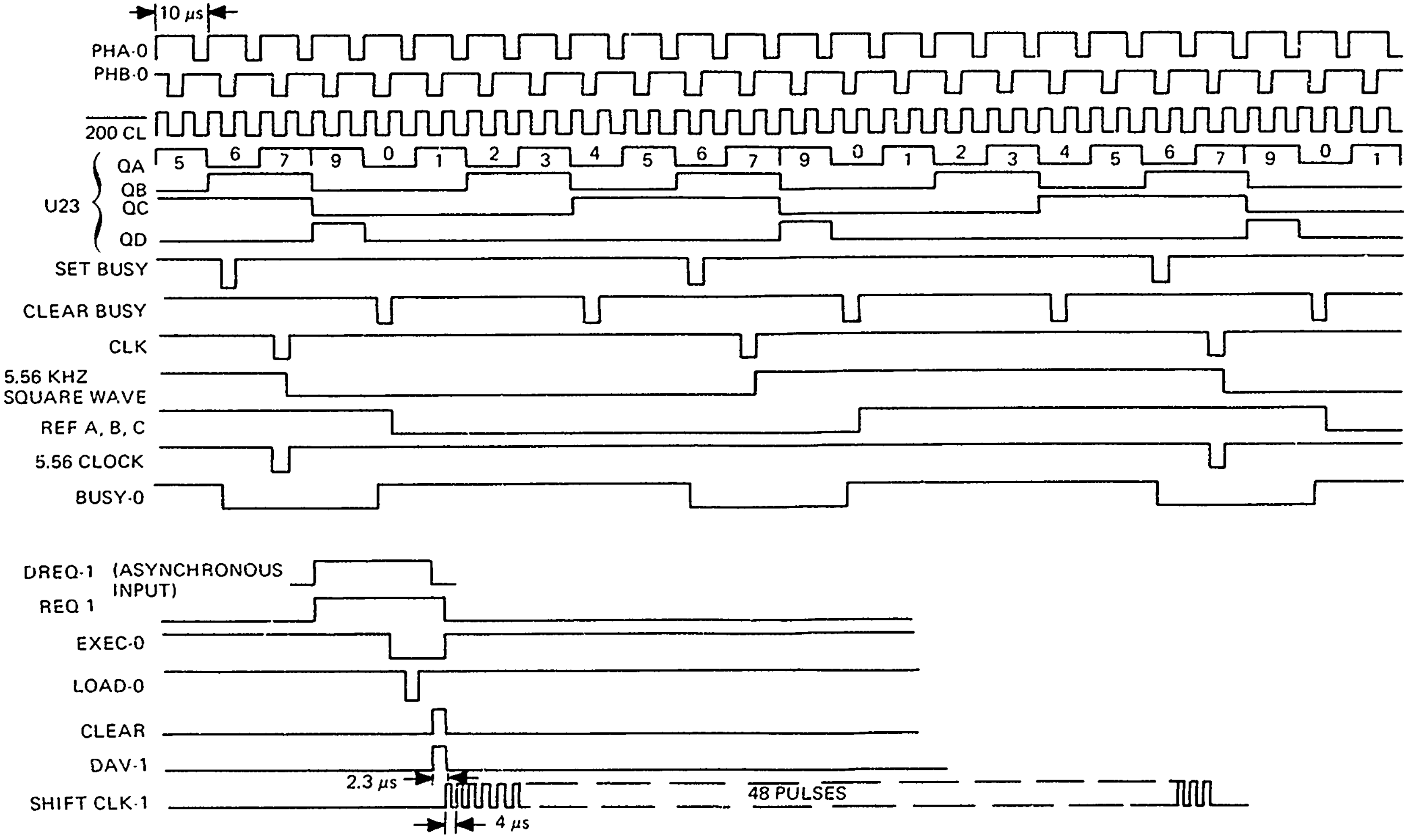
10 μs
PHA·0
PHB·0
200 CL
U23
QA
QB
QC
QD
5 6 7 9 0 1 2 3 4 5 6 7 9 0 1 2 3 4 5 6 7 9 0 1
SET BUSY
CLEAR BUSY
CLK
5.56 KHZ SQUARE WAVE
REF A, B, C
5.56 CLOCK
BUSY·0
DREQ·1 (ASYNCHRONOUS INPUT)
REQ 1
EXEC·0
LOAD·0
CLEAR
DAV·1
SHIFT CLK·1
2.3 μs
4 μs
48 PULSES

Figure 4-9. Timing and Control

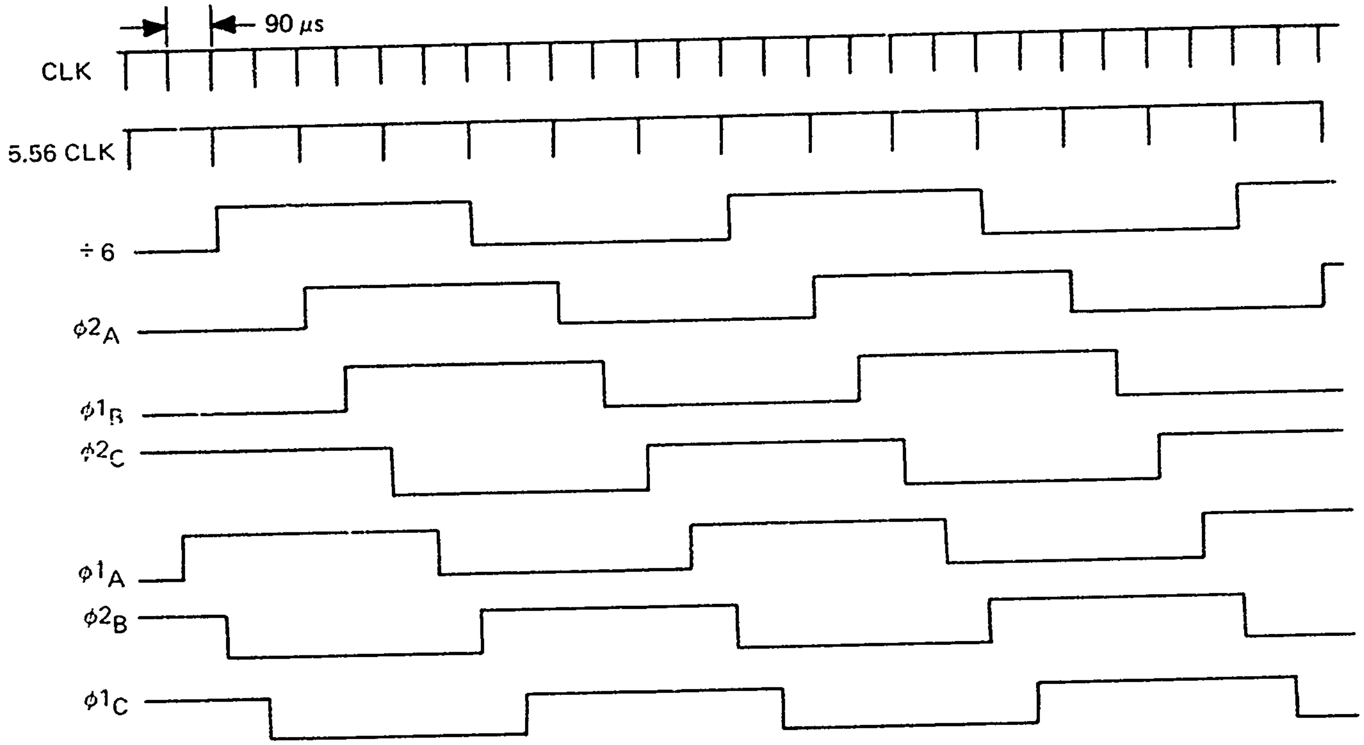
90 μs
CLK
5.56 CLK
÷ 6
φ2A
φ1B
φ2C
φ1A
φ2B
φ1C

Figure 4-10. Gyro Spin Motor Reference

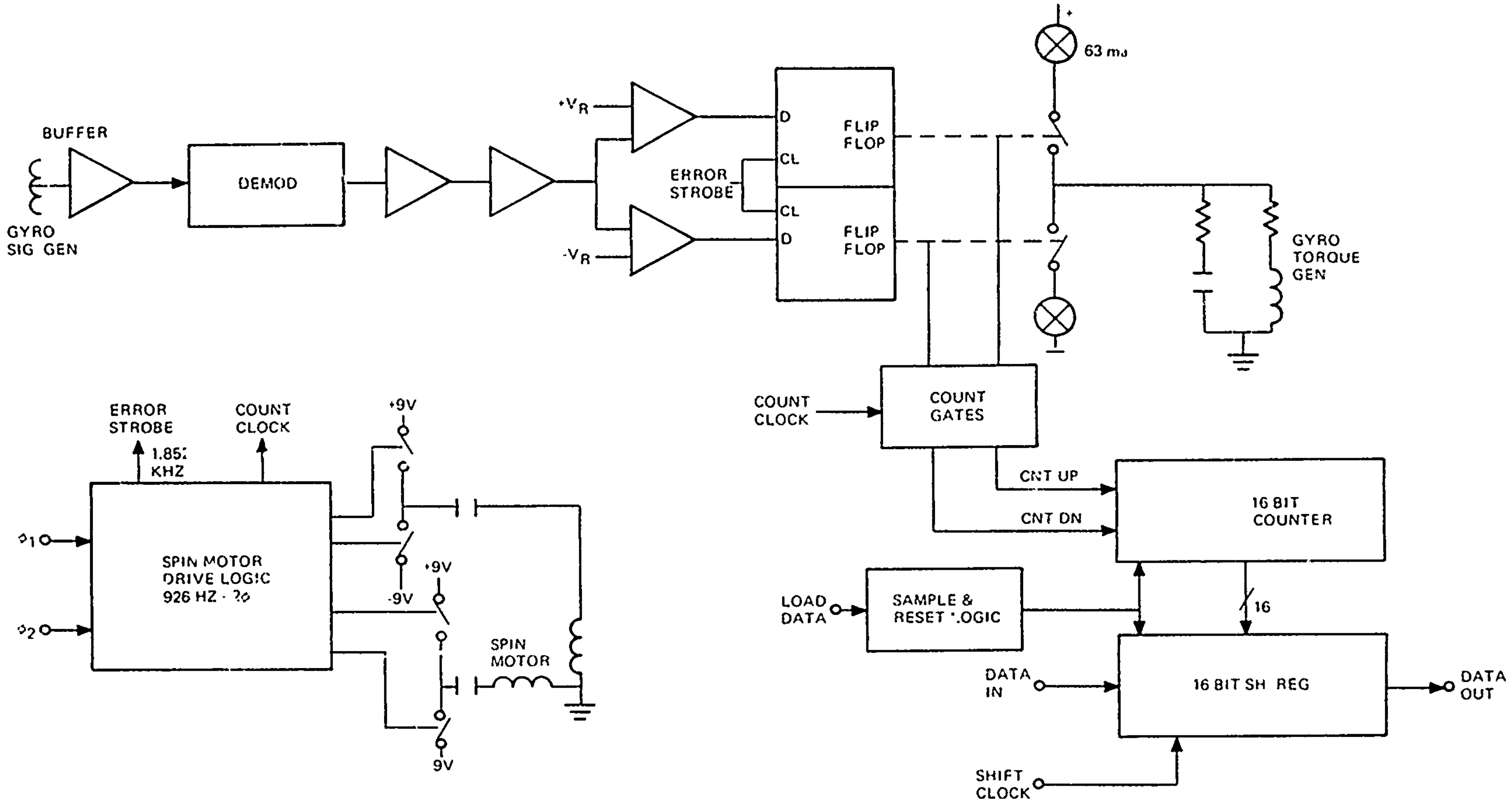
BUFFER
GYRO SIG GEN
DEMOD
+V_R
-V_R
D
CL
FLIP FLOP
ERROR STROBE
CL
D
FLIP FLOP
63 ma
GYRO TORQUE GEN
COUNT CLOCK
COUNT GATES
CNT UP
CNT DN
16 BIT COUNTER
16
LOAD DATA
SAMPLE & RESET LOGIC
DATA IN
16 BIT SH REG
DATA OUT
SHIFT CLOCK
ERROR STROBE
1.852 KHZ
COUNT CLOCK
φ1
φ2
SPIN MOTOR DRIVE LOGIC 926 HZ · 2φ
+9V
-9V
+9V
9V
SPIN MOTOR

Figure 4-11. Pulse Torqued Loop and Spin Motor Drive

Electronics Assembly, and demodulated. The 5.555 kHz demodulator reference is appropriately delayed to match the phase shifts developed by the stagger-tuned filter and the signal generator itself.

The demodulator output is filtered, and in particular a notch at 11.11 kHz greatly attenuates that component of the full wave rectified demodulator output. The resulting signal is fed to an amplifier which has high gain, but whose output is clamped to ± 0.7 volts. Limiting the output restricts the amplifier from going into saturation, which could cause time delays.

Figure 4-12 illustrates how the comparator pair, flip-flops, and current generator act as a three level contractor. If the absolute value of the limiter output is less than V_R, then both th switches of the 0.063A current generator are off, and no current is sent to the gyro torque generator coil. If the limiter exceeds V_R, however, the appropriate switch is turned on and precisely 0.063 amps flows into the torque generator in a direction to return the gyro to its null. The duration of the current pulse is controlled to be either the period of the error strobe (1 1852 Hz) or a multiple of it, and since the error strobe is derived from a crystal oscillator, it is very accurate. The threshold of the three level contractor, V_R, has been set to the level corresponding to the error that the gyro may have which may be corrected by one pulse of the torquer.

The commands for positive and negative current pulses are also sent to an up-down counter, which stores the net count. By now rotating the gyro through known angles, and monitoring the counters, the system may be calibrated. Details on calibration appear in subsection 6.3.

Upon commands from the control logic, the binary outputs of the counters are parallel loaded into 16 bit shift registers. The registers for the three channels are serially connected, as

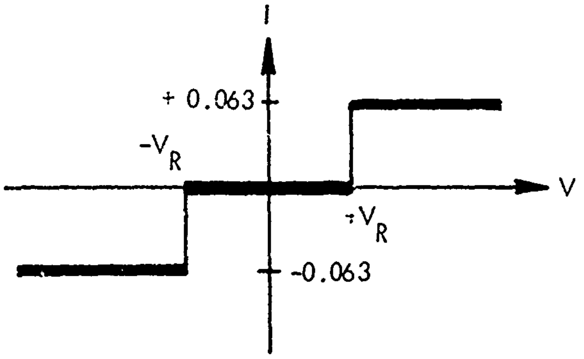

Figure 4-12. Three Level Contactor

shown in Figure 4-7, and a 48 bit clock train shifts out the data, which is transmitted to the CIU. The counters are reset to zero at the CIU sampling rate of 30 Hz.

4.3.4 ACCELEROMETER BUFFERS

Three accelerometers, orthogonally mounted in the Inertial Measurement Unit, are analog sensors for the Computer Interface Unit. To protect impedance levels over the long cables involved, buffer amplifiers are installed within the IMU itself. The buffers are low pass active filters with a 3 Hz bandpass, similar to the signal conditioners in the CIU for the other analog inputs. The accelerometer signals are conditioned with a simple decoupling network, in the CIU to eliminate any possible high frequency noise picked up in the cables.

Section 5
FLIGHT TEST PLAN

5.1. INTRODUCTION

The principal goal of the Closed Loop Fire Control System (CLFCS) flight test is to determine the feasibility of the concept for deployment in a combat environment. This goal is to be realized through a well balanced selection of flight test conditions, experimental data base, and analysis and interpretation of the test data, all of which account for the inherent limitations of the prototype CLFCS. Chief among these limitations are:

- The lack of a rangefinder, so that the bias error in the handset initial range is measured by observing the range component of bullet impact error.
- The imprecision of the sight, which means that the aircraft must be at an appreciable altitude above the target in order for the elevation (i.e., range) component of impact error to be observable.
- The sight deployment limits in train which constrain the maneuvers that may be executed during the engagement episode.

Whereas these limitations of the prototype system define a flight test envelope which falls inside the desired envelope of permissible engagements for a combat worthy CLFCS, it will be necessary to apply a certain amount of interpretation to the recorded test results in order to assess the feasibility of the CLFCS concept as it might ultimately be embodied.

Subordinate to the goal of assessing the overall feasibility of the CLFCS concept is that of assessing the performance in flight of its key subsystems (e g., the Inertial Measurement Unit, the computer hardware and software, etc.). Because of the limited capacity of the flight recorder, great care must be exercised in selecting the variables to be recorded for purposes of subsystem performance assessments. Moreover, the scope of such assessments which may be performed through post flight analysis will be understandably limited. A flexible utilization of the flight recorder is proposed whereby the number of variables recorded and the effective sampling rate are controlled by the CDC469 computer software.

As a procursor to the assessment of CLFCS effectiveness the optimization of certain parameters in the CDC 469 computer software may be desirable. Prominent among these are the following:

- The fraction of the observed range impact error which is applied to a range bias correction.
- The time constant of the first-order filter which is applied to the sight outputs during the period of bullet impact observation.

It is believed that these and the other adjustable coefficients in the state estimation and fire control software segments can be set at or near their optimum values prior to the flight test. However, the need to refine their values experimentally cannot be precluded at this point.

5.2. CLFCS FLIGHT TEST PHILOSOPHY

5.2.1 THE NEED FOR TRACKING ERROR DATA

The overall accuracy of a helicopter gunnery fire control system is significantly influenced by the accuracy with which the gunner is able to designate the target line-of-sight by tracking the target. In fact, gunner tracking error is often the dominant error source in such a system. Therefore, the flight test should include non-firing tracking error data runs to obtain a direct assessment of this improtant error source in the case of the prototype CLFCS.

5.2.2 THE ASSESSMENT OF THE GUNNER'S ABILITY TO MEASURE BURST IMPACT LOCATION

The unique capability of the CLFCS depends upon the gunner's ability to not only track the target accurately in preparation for firing, but also to obtain precise sighting measurements of the location of the first burst impacts. His ability to measure the burst location and the computer's ability to interpret that measurement are influenced by several factors:

- The altitude of the aircraft above the target plane.
- Departure of the ground plane from the horizontal in the vicinity of the target.
- Irregularities in and composition of the ground surface near the target.
- Foliation, haze, smoke, debris, wind, and other factors which degrade the gunner's ability to perceive the centroid of the burst.

As will become evident, there is some question as to how many of these factors can be encompassed by the initial flight test of the CLFCS due to consideration of the need to obtain quantiative bullet strikepoint data. However, ultimately the CLFCS should be tested with respect to all of them.

As part of the flight test of the prototype CLFCS, it is necessary that as complete records as possible be obtained of the accuracy with which the gunner measures the location of bursts. This requirement can be partially satisfied through sight camera film, which is also the medium for recording gunner tracking error. A more complete assessment could be obtained if aircraft position and attitude relative to a target coordinate set were recorded, along with the actual location of the bullet impacts in that same coordinate set. From these data, a reference sightline to the mathematical centroid of the burst could be computed in vehicle coordinates for comparison with the gunner's observation. Although desirable, this degree of rigor is probably beyond reach for the prototype CLFCS flight test because of the problems connected with recording aircraft attitude to the required precision.

5.2.3 THE CONFLICT BETWEEN TEST REALISM AND PRECISION OF STRIKEPOINT DATA

Several factors were enumerated above which affect the precision with which the closed loop fire control function can be implemented in actual practice. The realism of the prototype CLFCS flight test depends largely upon the degree to which these factors are encompassed by the flight test conditions. However, the introduction of realism in general will compromise the recording of precise, quantitative data on system performance.

Suppose, for example, that the target is located on an irregular ground surface composed of sand and gravel, and that it is surrounded by low brush; suppose also that the wind is blowing. These conditions are considered realistic in that they present a mild challenge to the CLFCS with respect to measuring the burst impact location. However, they also complicate the recording of the actual bullet strikepoints from directly above the target area, which will utilimately become the basis for judging overall system performance.

This conflict between realism and test data quality comes strongly into play in selecting the site of the prototype CLFCS flight test. The Yuma Proving Grounds affords a spectrum of target conditions, and generally allows a higher degree of realism to be injected into the tests. However, the recording of precise, quantitative data on bullet strikepoints is predicted to be relatively difficult. In contrast, the precision of strikepoint data afforded by the alternate Patuxent River site is very high, but the target engagement realism is poor.

At this stage in the CLFCS development it would seem preferable to emphasize precision of recorded data in preference to test condition realism so as to afford the greatest potential for post-flight analysis and also the best basis for modification of the system design in the future. There is also the fundamental question as to whether the gunner, equipped with the pantographic sight, can measure burst impact location under the most ideal conditions, let alone under conditions representative of a combat environment. Accordingly, the Patuxent River test site is favored for the prototype CLFCS flight tests.

At Patuxent River the target is water-borne. Bouys mark 25 m distances on either side of the target for the purpose of scaling the bullet strikepoint measurements. The waterspouts created by the bullet impacts are sharply defined, persistent, and relatively unaffected by wind in comparison with the dust clouds created by impacts on desert sand, for example Of the factors mentioned above which will present challenges to the CLFCS, the only one which can be addressed at Patuxent River is the effect of aircraft altitude. This suggests that a future flight test, perhaps of an improved CLFCS, be conducted at the Yuma Proving Grounds where the other factors can also be addressed, albeit with a possible reduction in strikepoint data precision.

5.3. RECOMMENDATIONS FOR FLIGHT TEST MANAGEMENT

It is proposed that the flight tests of the prototype CLFCS be conducted at Patuxent River and that they include the following elements:

- Hovering, straight-line, and veer-off aircraft flight.
- Various aircraft altitudes over the range of 200 to 1000 ft.
- Motion picture record of the bullet strikepoints taken from a helicopter orbiting directly above the target.
- Motion picture record through the gunner's sight showing the target tracking and bullet impact observation errors.
- Flight recording of key aircraft state and fire control variables for post-flight analysis and subsystem performance assessment.
- Range theodolite instrumentation of the aircraft's position and velocity relative to a target-centered coordinate set.

5.3.1 TARGET AND RANGE LAYOUT

It is proposed that essentially the same target and adjacent distance markers as those utilized during the Multi-Weapon Fire Control System (MWFCS) flight tests performed in 1973-1974 be a adopted for use in the CLFCS flight tests. Relative to the target, it is suggested that two courses be defined as illustrated in Figure 5-1. The factors which should be considered in selecting the geographic orientation of these courses are:

- Direction of winds
- Conditioning of the range theodolite solution for the aircraft's position and velocity
- Sun position

The second and third factors were of concern during the MWFCS tests; the first was evidently not, but is important in testing the CLFCS. Since part of the intended function of the CLFCS is to compensate for long correlation time wind velocity, it is recommended that alternate courses which orient the wind velocity entirely downrange and entirely crossrange be provided for. Since the winds over the Patuxent River test area appear to be predominantly out of the northwest and southwest, the courses shown in Figure 5-1 are selected.

5.3.2 AIRCRAFT FLIGHT CONDITIONS - ENGAGEMENT EPISODE EVENTS

It is assumed that the aircraft will be vectored to the initial point for the selected flight path (see Figure 5-1) by voice communication from the test controller, with the range theodolite data providing the basis for establishing aircraft position relative to the target. Commencement of target track at 2800 m is assumed. This would be the point at which the Action Switch would be depressed by the gunner, initiating Target State Estimator operation as well as the slewing of teh gun toward a position of alignment with the target line-of-sight. A fire control solution is developed and refined by the computer as tracking continues, with about 3 sec being the minimum elapsed time before actual firing should be commenced.

Based upon voice communication of the theodolite position data, the initial value of range for insertion into the Target State Estimator is precisely known. However, it will be desirable to deliberately introduce bias errors in this initial range to simulate the situation in which the crew must visually estimate its value.

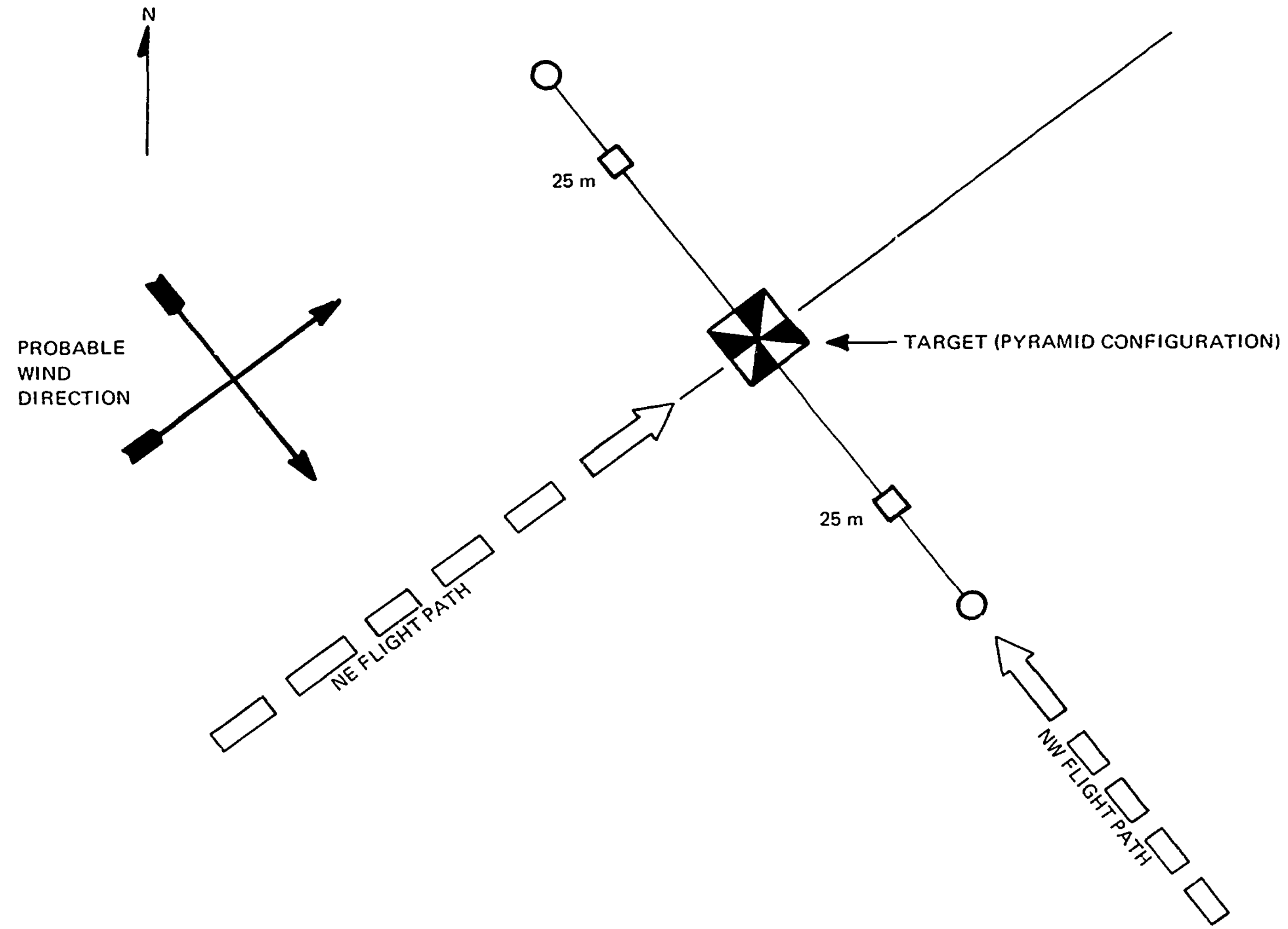
N
PROBABLE
WIND
DIRECTION
25 m
TARGET (PYRAMID CONFIGURATION)
25 m
NE FLIGHT PATH
NW FLIGHT PATH

Figure 5-1. Proposed Target/Flight Path Relationships

From the target track commencement point, three alternative flight paths are proposed:

- Hover - proceed along the selected target approach course (see Figure 5-1) to an appropriate firing range of approximately 5000 ft or 1524 m. Fire an initial, open-loop burst and subsequent closed-loop burst from a hovering flight condition. Altitude may be varied from run to run above and below a nominal value of 500 ft
- Straight-Line - proceed along a course about 10° to the right or left of the selected target approach course, thereby creating a 1600 ft or 486 m offset. A velocity of 100 to 120 knots is recommended. The open-loop burst may be fired at a slant range of about 6000 ft = 1829 m and a subsequent closed-loop burst, at a slant range of about 4000 ft = 1219 m. Altitude may be varied from run to run above and below the 500 ft nominal value.
- Veer-off - proceed in the same manner as in the straight-line course through the open-loop firing burst at 6000 ft = 1829 m. At a slant range of about 5000 ft, initiate a mild veer-off away from the target; speed may also be increased at this time. The closed-loop burst may be fired at a slant range of approximately 4000 ft = 1219 m. Altitude may be varied from run to run above and below the 500 ft nominal value.

These target engagement alternatives are illustrated in Figure 5-2.

5.3.3 INSTRUMENTATION AND DATA

The primary instrumentation for the CLFCS flight test will be a motion picture camera directed toward the target and carried by a helicopter orbiting above the target. The frame rate for this camera should be adequate to distinctly capture each bullet impact. These requirements are believed to be satisfied by the equipment and technique utilized during the MWFCS flight test.

Additional supporting instrumentation will be a sight motion picture camera which records gunner tracking and burst centroid observation activity, a magnetic tape flight recorder which records key aircraft state and fire control solution variables, and the range theodolite position and velocity data. Comments are in order relative to the information to be transmitted to the flight recorder and the usefulness of the range theodolite data.

5.3.3.1 Flight Recorder

The useof the information captured by the flight recorder will be to assess the performance of the CLFCS subsystems, as may be dictated at various points during the flight test program.

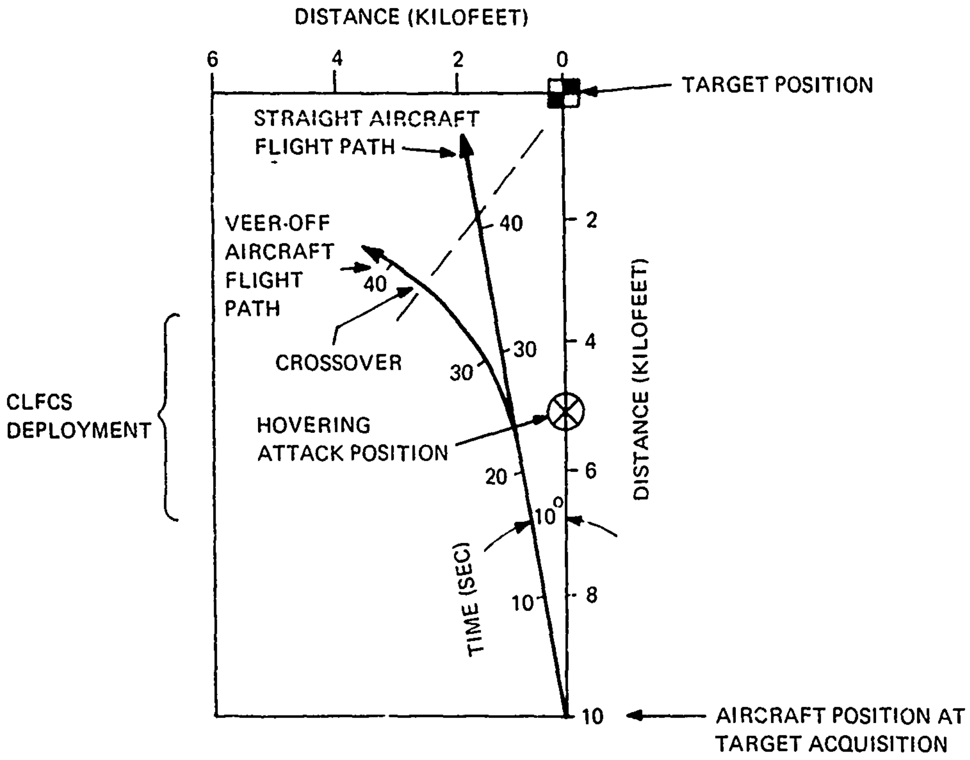
DISTANCE (KILOFEET)
6
4
2
0
TARGET POSITION
STRAIGHT AIRCRAFT FLIGHT PATH
VEER-OFF AIRCRAFT FLIGHT PATH
40
40
2
CROSSOVER
30
30
4
CLFCS DEPLOYMENT
HOVERING ATTACK POSITION
20
6
10°
TIME (SEC)
10
8
10
DISTANCE (KILOFEET)
AIRCRAFT POSITION AT TARGET ACQUISITION

Figure 5-2. Proposed Target Engagement Alternatives

Included in the general area of subsystem performance assessment is the detection of subsystem malfunctions which have contributed to anomalies in the behavior of the overall system. Thus, one kind of analysis which might be performed using this information is the post-flight reconstruction of the fire control solution versus time for comparison with that computed on board.

A sweeping solution to the selection of variables to be recorded is to say that all inputs to the Aircraft and Target State Estimators, all aircraft and target state components, and the variables involved in the open and closed loop fire control solutions be recorded. This would entail approximately 50 items of information. The writing speed of the flight recorder is such that this quantity of data could be captured for one computer frame out of seven, or 4.3 times per sec.

Because the need can be anticipated for a reduced set of system state variables to be captured more frequently than 4.3 times per sec, a flexible arrangement is recommended whereby the following requirements are met:

- Any quantity which exists as a defined variable in the CDC 469 computer can potentially be recorded.
- During a particular flight, the software segment which controls the interface with the flight recorder will be established so that up to a maximum of 50 selected variables, m, will be captured once every n computer frames.
- The recorder interface software will provide for the capturing of all the selected variables in a single computer frame. The recorder will then take a finite number of frames to write this information.
- Provision will also be made for independent selection of the parameters m and n above so that the number of variables captured, the capture rate, and the total elapsed time encompassed by the flight record can be traded off appropriately.

The final configuration for the recording mode is discussed in subsections 3.11, and 4.2.7.

5.3.3.2 Range Theodolite Data

The bearing and elevation of the aircraft is continuously recorded by each of several range theodolites, permitting a multi-angular solution for its position relative to the target, whose position is known relative to the theodolites. Time variation of position yields velocity in the target-fixed coordinate set.

If we designate the triad of geographic coordinates which are fixed in relation to the target as illustrated in Figure 5-3 by x, y, and z, then the theodolite data yields, effectively, $-R_{xyz}$ and V_{xyz}, which are the aircraft's position and velocity to the target in terms of their x y z components. Although this information is of some use, its utility in the prototype CLFS flight tests would be vastly increased if it were transformed into the aircraft coordinate set, which is designated u, v, and w (see Figure 5-3). This requires knowledge of aircraft attitude.

If $-R_{xyz}$ and V_{xyz} from the theodolite data could be transformed into u v w, direct comparison with the on-board measured and filtered values would be possible, permitting a rigorous assessment of the performance of the sensors, the computer, and the Aircraft and Target State Estimator software segments.

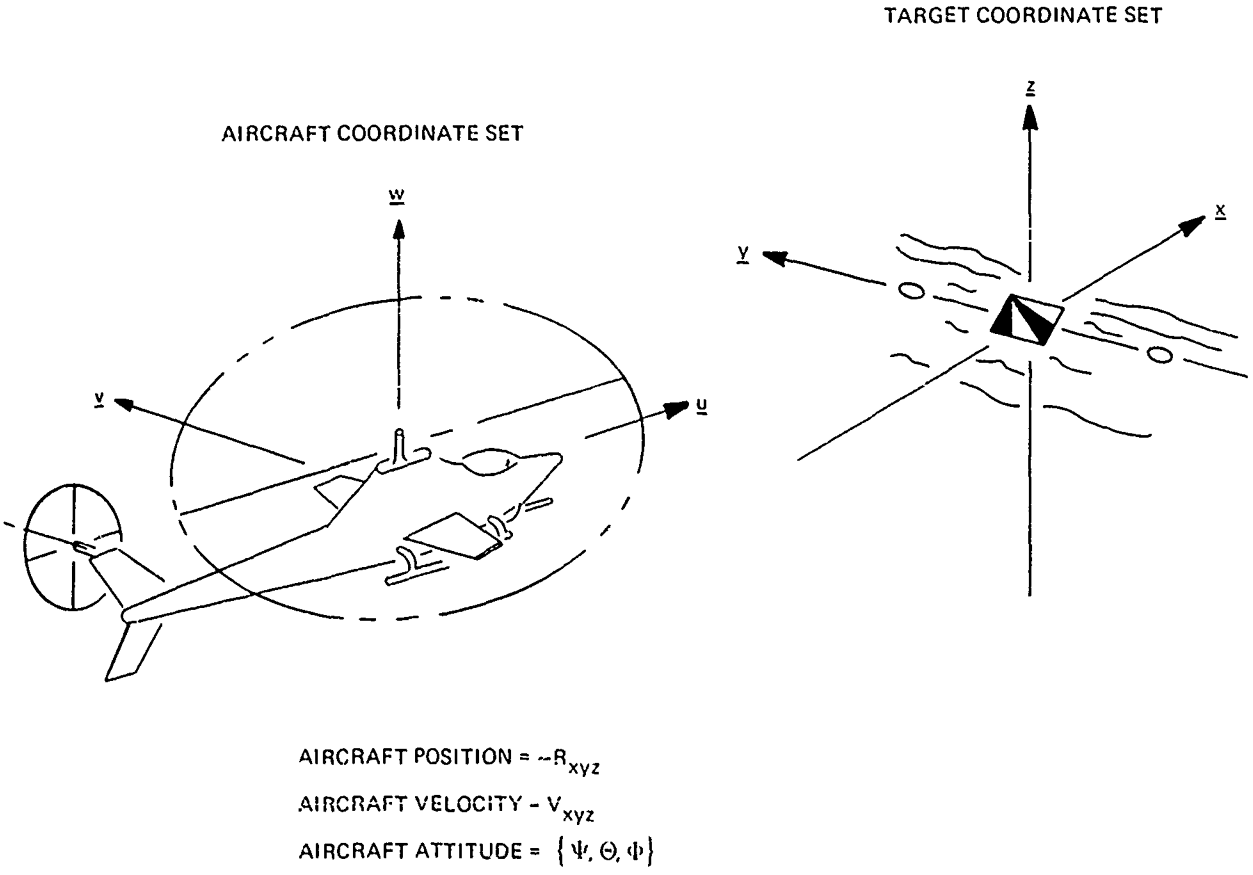
TARGET COORDINATE SET
z
x
y
AIRCRAFT COORDINATE SET
w
v
u
AIRCRAFT POSITION = $-R_{xyz}$
AIRCRAFT VELOCITY - V_{xyz}
AIRCRAFT ATTITUDE = $\{\Psi, \Theta, \Phi\}$

Figure 5-3. Target and Aircraft Coordinate Sets

5.4 OVERALL SYSTEM PERFORMANCE METRIC

The objective of the CLFCS concept is to substantially improve the kill probability of a second firing burst based upon an observation of where the first burst impacted in relation to the then current target line-of-sight estimate. Because the process of observing the first burst impact by the gunner and incorporating this into the fire control solution requires a finite time interval during the engagement episode, there is a definite time cost of this projected improvement in second burst effectiveness. There is also, obviously, a significant equipment cost. The principal goal of the prototype CLFCS flight test is to assess the feasibility of the concept in quantitative terms of the increment in target kill probability which is actually realized.

5.4.1 CLOSED LOOP VERSUS OPEN LOOP PERFORMANCE COMPARISONS

When the prototype CLFCS is delivered to the Army for flight test, the fire control system will potentially incorporate three levels of capability as illustrated in Figure 5-4. It is planned that the gunner will be able to control in flight which level of fire control capability is being used. Therefore, the effectiveness of each can be experimentally determined.

The Statement of Work for the CLFCS indicates that the open loop fire control configuration with which the CLFCS is to be compared is the Baseline System of Figure 5-4. However, General Electric believes that the Army will desire to compare all three configurations as part of the CLFCS flight test under the various conditions of aircraft flight, altitude, and wind discussed above.

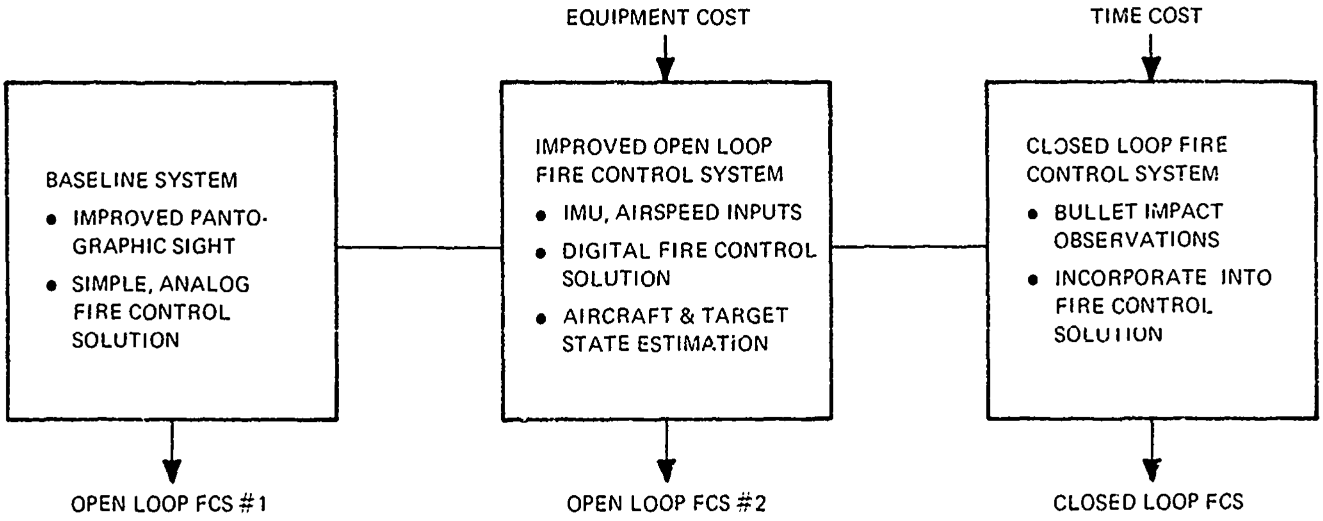
EQUIPMENT COST
TIME COST
BASELINE SYSTEM
• IMPROVED PANTOGRAPHIC SIGHT
• SIMPLE, ANALOG FIRE CONTROL SOLUTION
IMPROVED OPEN LOOP FIRE CONTROL SYSTEM
• IMU, AIRSPEED INPUTS
• DIGITAL FIRE CONTROL SOLUTION
• AIRCRAFT & TARGET STATE ESTIMATION
CLOSED LOOP FIRE CONTROL SYSTEM
• BULLET IMPACT OBSERVATIONS
• INCORPORATE INTO FIRE CONTROL SOLUTION
OPEN LOOP FCS #1
OPEN LOOP FCS #2
CLOSED LOOP FCS

Figure 5-4. Illustration of Three Potential System Comparison in the CLFCS Flight Test

5.4.2 PROBABILITY OF m HITS OUT OF n-ROUND BURSTS

The Statement of Work further indicates that the metric to be used for comparisons among these alternative fire control configurations is related to target kill probability versus time and rounds expended. This metric is particularized as follows:

- With the origin of the $\underline{x}\ \underline{y}\ \underline{z}$ target coordinate set as center (see Figure 5-3) define a pseudo target of radius $\bar{r}$ in the $\underline{x}$ - $\underline{y}$ plane.
- For each pass in an appropriately defined ensemble of passes, count the number of rounds which impact within the pseudo target area. This number will have to be adjusted according to the number of rounds actually expended or the length of time used in the pass so as to apply to a burst of a fixed number of rounds, n, or, alternatively, to a fixed length of time, τ (see Section 5.5). Let the number of hits for the ith pass in the ensemble, normalized by either n or τ, be designated h_i.
- Over the ensemble, determine the number of passes in which $h_i \geq m$ for $m = 1, 2, \ldots, 5$. Divide by the number of passes in the ensemble to compute the probability of at least 1 hit, 2 hits, etc.

The result of this analytical process is a histogram of the probability of at least m hits for $m = 1, 2, \ldots, 5$ which pertains to the particular set of conditions which characterize the ensemble, such as fire control system mode (Baseline Open Loop, Improved Open Loop, Closed Loop), altitude, wind, etc. The nature of the histogram is illustrated in Figure 5-5. The advantage of this form of presentation is that it removes the issue of a kill criterion as a matter of contention. It also distinguishes between a system or set of conditions which occasionally yields a large number of hits from one which frequently yields a few hits. The hit expectation for both of these could be equivalent, but the effectiveness in combat of the latter is substantially greater than that of the former.

5.5 WEAPON SYSTEM DEPLOYMENT

We have presented above a description of the proposed CLFCS flight tests, including the various conditions of aircraft maneuver, altitude, and wind which should be encompassed. The objective of the tests will be to compare the three fire control modes illustrated in Figure 5-4 using the performance metric of Figure 5-5.

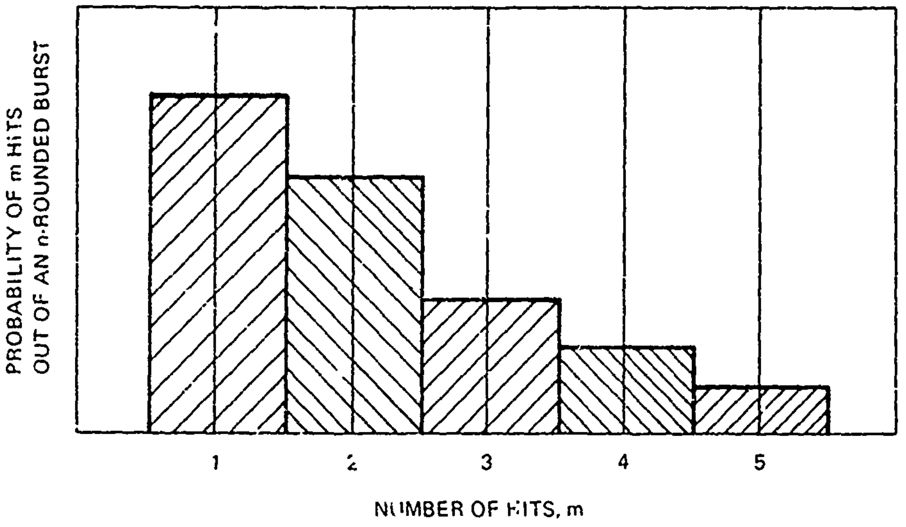

Figure 5-5. Performance Histogram for a Generic Ensemble of Passes

Because of the Statement of Work indicates that system effectiveness is to be evaluated versus time and ammunition expended, the issue of deployment strategy must also be addressed. Two distinctly different strategies are considered:

- High Value, Heavily Defended Target. An armed helicopter will occasionally be called upon to engage a target which poses a high level of threat to the survival of the helicopter. In this event, the strategy must be to defeat it in the shortest possible time (i.e., with minimized exposure to its defensive capability). The value of the target is such as to warrant the expenditure of a large fraction of the ammunition load so as to assure its destruction.
- Low Value Target, Mild Defenses. When the helicopter holds the fire power advantage in relation to the target's defensive capability and the value of the target is low, the strategy shifts to defeating the target with a minimum expenditure of ammunition.

5.5.1 CLFCS DEPLOYMENT STRATEGY

The tactical environment in which the CLFCS can be deployed to the greatest advantage in comparison with an open loop fire control system is in the Low Value Target/Mild Defenses scenario. The recommended strategy is to fire a short (< 1 sec), precisely aimed open loop burst, observe the impact centroid, incorporate the closed loop correction into the fire control solution, and fire a second, calibrated burst. Because the first burst is very short and the second burst has gun boresight, windage, and other long correlation time errors removed from it, the ratio of expected hits to rounds expended over the entire engagement is high in comparison with an open loop system deployed in a similar fashion.

In the case of the High Value, Heavily Defended Target scenarios, the CLFCS deployment strategy which appears to enhance helicopter survival is to open the attack with a prolonged burst of fire ($\leq$ 2 sec). If the first impacts are seen to be significantly in error, a burst centroid observation is made and incorporated into the fire control solution and a second, calibrated burst is fired.

Understanding that both of these deployment strategies must be further developed and refined during the flight test program, the objective of the flight test, in agreement with the original Statement of Work, ultimately involves the comparison of the performance of open and closed loop fire control under two engagement constraints:

- The total number of rounds expended during engagement, n, should be minimized. The hits recorded during each pass should be normalized so as to reflect a given value for n as explained in Section 5.4.2.
- The total elapsed time, τ , required to complete the engagement should be minimized, where τ is measured from the closing of the trigger switch at the beginning of the initial firing burst until the opening of that switch at the end of the last firing burst. A selected value of τ will be utilized for normalization purposes as explained in Section 5.4.2.

The particular values of n and τ used for normalization purposes, denoted n^* and τ^*, will be the average values of rounds expended and elapsed time, respectively, for the CLFCS operated over the ensemble of conditions tested.

The CLFCS is regarded as the pacing system configuration in that it requires a greater number of gunner fire control actions. Accordingly, when minimum - n and minimum - τ deployment strategies for the CLFCS have been developed, then the open loop fire control system (OLFCS) configurations will be tested in a manner which is compatible with the CLFCS tests. Specifically, the following guidelines will be used:

- In all instances, the OLFCS configurations will be deployed over the same spectrum of ranges as the CLFCS.
- In the case of a minimum - n engagement using an OLFCS, the gunner will be instructed to use discretion in the timing and duration of his firing bursts. If the aircraft is closing on the target, he should try to mimic the deployment of the CLFCS in firing a short burst at long range ($\approx$ 6000 ft) and another at short range

($\approx$4000 ft). He may exercise the option of firing a burst at medium range ($\approx$ 5000 ft). In any case, the fact should be impressed upon him that his hit score will be penalized for the expenditure of a large number of rounds.

- In case of a minimum - τ engagement using an OLFCS, the gunner will be instructed that elapsed time is of the essence and that he may lengthen his firing burst to assure a larger score. In other respects, he should mimic the CLFCS deployment strategy in distributing his firing burst over the 4000 - 6000 ft range spectrum when closing on the target.

Section 6
ACCEPTANCE TEST

6.0 INTRODUCTION

This section includes test plans and results for acceptance testing of the Closed Loop Fire Control System software and hardware. Also included is additional temperature and accuracy data taken on the major assemblies.

6.1 SOFTWARE TEST SUMMARY AND RESULTS

A numerical check problem is presented which demonstrates the performance of the closed loop fire control algorithm. It is based upon the same veer-off engagement which has been utilized heretofore (see Figure 6-1). The following event times have been selected:

t_0 = 21 sec (Acquire target, depress and hold action switch)

t_1 = 24 sec (Trigger depression for open loop firing burst)

t_2 = 25 1/3 sec (Break target track signal from computer to gunner)

t_3 = 27 sec (Acquire burst centroid)

t_4 = 28 sec (Re-acquire target)

t_5 = 30 sec (Trigger depression for closed loop firing burst)

In this problem, it is assumed that the open loop firing solution at $t_1 = 24$ sec is affected by a range bias error at the time of fire in combination with gun boresight errors in elevation and train as defined below:

ΔR = +930 ft (range estimated long)

$\Delta E_g = \Delta T_g = 0.010$ rad

As a consequence, the first burst flies long and to the right, as illustrated in Figure 6-1. Also shown in Figure 6-1, and on an expanded scale in Figure 6-2, is the fact that the closed

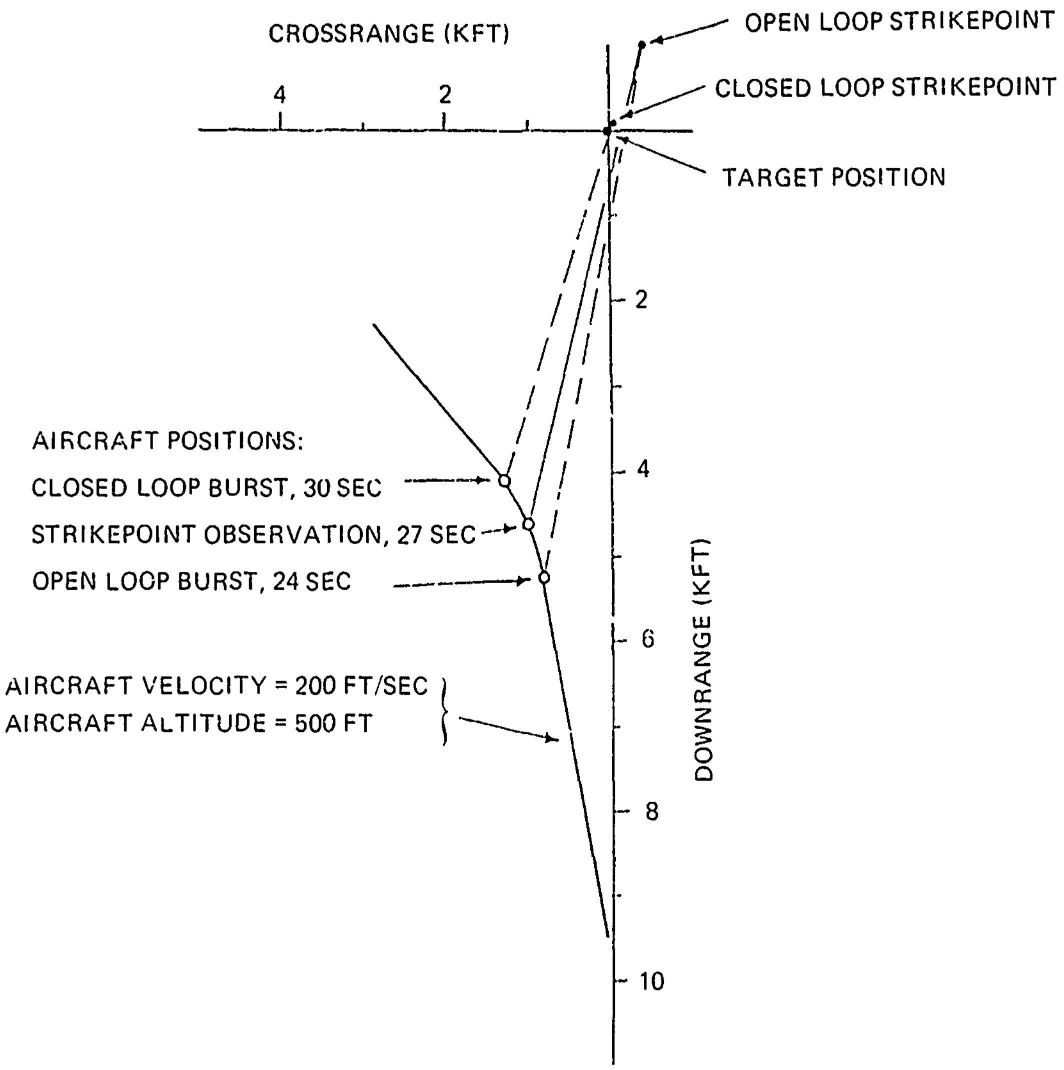
CROSSRANGE (KFT)
4
2
OPEN LOOP STRIKEPOINT
CLOSED LOOP STRIKEPOINT
TARGET POSITION
2
4
6
8
10
DOWNRANGE (KFT)
AIRCRAFT POSITIONS:
CLOSED LOOP BURST, 30 SEC
STRIKEPOINT OBSERVATION, 27 SEC
OPEN LOOP BURST, 24 SEC
AIRCRAFT VELOCITY = 200 FT/SEC
AIRCRAFT ALTITUDE = 500 FT

Figure 6-1. Illustration of Check Problem Geometry

loop fire control algorithm substantially removes the strikepoint error in the first burst, giving a strikepoint improvement ratio of 8.5 to 1 for the test case.

Table 6-1 provides a summary of the estimated uncertainties in the closed loop firing burst. The entry for "Mathematical approximations and numerical effects" reflects the inherent accuracy of the closed loop fire control algorithm and is based upon examination of a number of error combinations in the context of the veer-off engagement portrayed in Figure 6-1. The overall accuracy of the closed loop firing burst is expected to be approximately 10 mrad.

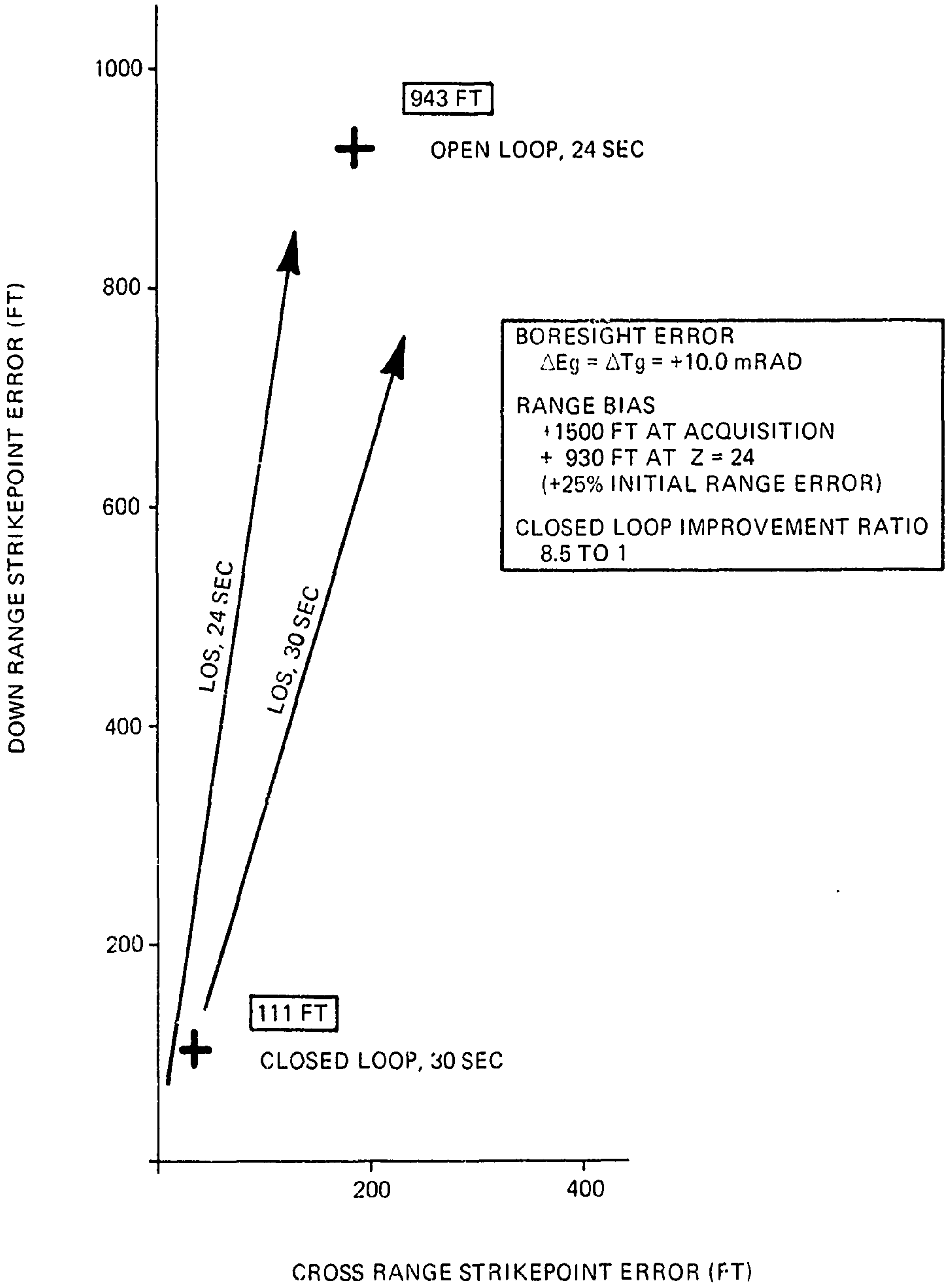

BORESIGHT ERROR
$\Delta E_g = \Delta T_g = +10.0$ mRAD

RANGE BIAS
+1500 FT AT ACQUISITION
+ 930 FT AT Z = 24
(+25% INITIAL RANGE ERROR)

CLOSED LOOP IMPROVEMENT RATIO
8.5 TO 1

Figure 6-2. CLFCS Effectiveness

TABLE 6-1
ACCURACY ASSESSMENT FOR THE CLOSED LOOP FIRING BURST

• Error in estimated target sightline at t_2 →	3.8 mrad
• Error in strikepoint sightline at t_3 →	4.2 mrad
• Error in target sightline at t_4 →	4.2 mrad
• Mathematical approximations and numerical effects →	7.2 mrad
• Estimated resultant RMS error →	10.1 mrad

6.2 SIMULATION METHOD FOR SOFTWARE TEST

Two software programs, TPATH and GQHIT, were written to implement the numerical check problem for the CDC closed loop fire control alogrithm. The information flow path relative to the CDC 469 software is shown in Figure 6-3. TPATH simulates the aforementioned veer-off engagement (Figure 6-1) with its corresponding event times. It computes true aircraft sensor values, with the exception of the range estimate signal, which includes a bias of +930 feet at the time of the first fire burst. Sensor values for each computer time frame of 1 30 second of the ten second engagement are put on paper tape by TPATH to be read into the CDC 469 via the CDC memory loader. The sensor values are continuously read into the CDC processor on a scaled time base to update the aircraft and line of sight estimators. At target acquisition time t_0 = 21 seconds the biased range estimate is inserted into the line of sight estimator. The open loop fire control algorithm uses outputs of range estimate, range rate, and relative air density to compute a set of gun orders which includes an open loop lead angle.

At the first fire time, t = 24 sec, the open loop gun position is recorded for input to the GQHit program. The GQHit program also inputs a boresight error (ΔTg, ΔEg) of +10 MR in train and elevation. Using these inputs and the M56 ballistics, a bullet strikepoint is computed in the horizontal target plane. The line of sight to the strikepoint is computed and recorded for input back to the CDC closed loop fire control algorithm for the Acquire Burst Centroid time of T = 27 sec. The closed loop algorithm uses the estimated target line of sight and the recorded estimated aircraft velocities and angular rates to compute by recursion an improved estimate of the target line of sight. Closed loop gun pointing corrections are computed by taking the difference between the estimated target line of sight and the measured strikepoint

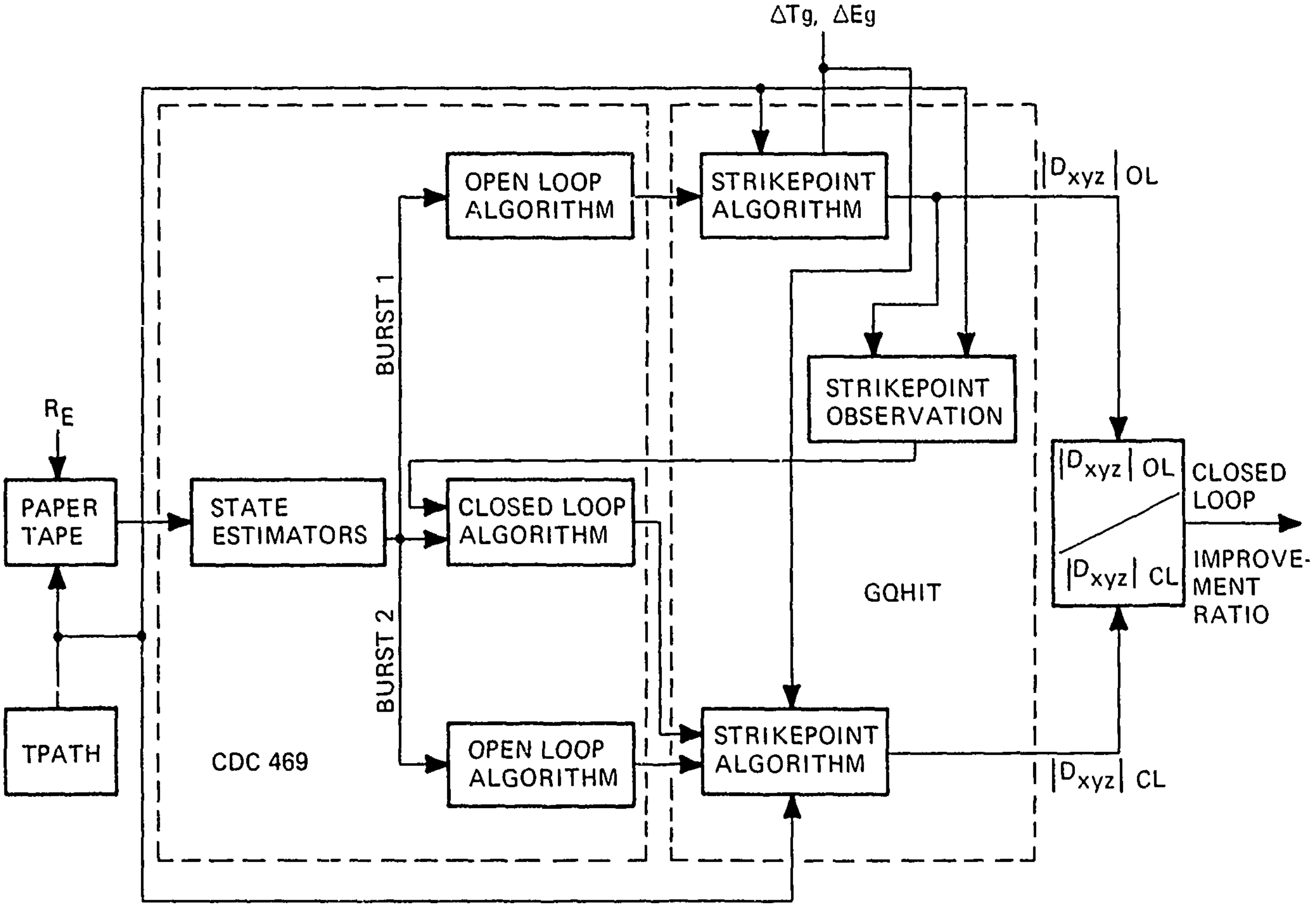

ΔTg, ΔEg
R_E
PAPER TAPE
TPATH
STATE ESTIMATORS
CDC 469
BURST 1
BURST 2
OPEN LOOP ALGORITHM
CLOSED LOOP ALGORITHM
OPEN LOOP ALGORITHM
STRIKEPOINT ALGORITHM
STRIKEPOINT OBSERVATION
STRIKEPOINT ALGORITHM
GQHIT
|Dxyz| OL
|Dxyz| CL
|Dxyz| OL / |Dxyz| CL
CLOSED LOOP IMPROVEMENT RATIO

Figure 6-3. Software Test Information Path

line of sight, which are factored into the total gun position values. This corrected gun position for time T = 30 sec, is then input to the GQHit program to compute a calibrated bullet strikepoint in the horizontal target plane. The ratio between the open loop strikepoint, error in feet and the closed loop strikepoint at T = 30 sec is the closed loop improvement ratio. Table 6-3 shows the results of the open loop and closed loop strikepoints.

In addition to TPATH and GQHIT, a third program, on time share, called GQGUN was written to check the validity of the CDC open loop algorithm. GQGUN uses true values of target sightline, range, and range rate, etc., from an offline version of TPATH and computes a gun position (including "lead angle") which should match CDC open loop computations. Listings for GQHIT and GQGUN are included in Appendix D. Also in the Appendix is a set of operating instructions for loading the paper tape reflecting TPATH into the CDC processor.

Verification of the open loop and closed loop software are listed in Tables 6-2 and 6-1 respectively. The recorded CDC processor data at selected times of interest is listed in Tables 6-4, 6-5, and 6-6.

TABLE 6-2
VERIFICATION OF OPEN LOOP FIRE CONTROL ACCURACY

```
GQGUN          03:55EST       11/23/76

FIRST FIRING CONDITION

OPEN LOOP FIRE CONTROL DATA
TARGET SIGHTLINE DIRECTION COSINES:
SH= 0.940513 RAD
SV=-0.335301 RAD
SN=-5.31038E-2 RAD
EST RANGE= 5351.23 FT
EST RANGE-RATE=-187.526 FT/SEC
DRAG COEF= 0.303177 1/SEC
EST TF= 2.35032 SEC
EST GRAV DROP= 110.331 FT
COMPUTED LEAD ANG.
DH=-8.83913E-3
DV=-2.03215E-2
DN= 1.31227E-2
COMPUTED GUNLINE DIRECTION COSINES:
GH= 0.933352 RAD
GV=-0.355729 RAD
GN=-3.29837E-2 RAD
GUN ELEV=-3.99243E-2 RAD
GUN TRAIN= 0.365507 RAD

STRIKEPOINT DATA
ACTUAL TF= 2.346 SEC
DRX= 1.05188 FT
DRY=-0.821959 FT
DRZ= 2.35596E-2 FT

HORIZ MISS= 1.13501 FT

ANGULAR MISS= 3.34572E-2 MRAD
```

TABLE 6-3

VERIFICATION OF CLOSED LOOP ALGORITHM

```
30HIT         09:02EST     11/23/76

FIRST FIRING CONDITION

OPEN LOOP FIRE CONTROL DATA
CDC 152 COMPUTED GUN ORDERS:
GH= 0.933625 RAD
GV=-0.357512 RAD
GR=-0.023006 RAD
GUN ELEV=-0.313008 RAD
GUN TRAIN= 0.375704 RAD


STRIKEPOINT DATA
ACTUAL TF= 3.93 SEC
DBX= 922.946 FT
DBY=-192.86 FT
DBZ=-7.13692E-2 FT

HORIZ MISS= 942.881 FT

ANGULAR MISS= 15.7659 MRAD

SECOND FIRING CONDITION

OPEN LOOP FIRE CONTROL DATA
CDC 469 COMPUTED GUN ORDERS:
GH= 0.595029 RAD
GV=-0.652011 RAD
GN=-0.169918 RAD
GUN ELEV=-0.4955 RAD
GUN TRAIN= 0.834159 RAD


STRIKEPOINT DATA
ACTUAL TF= 2.1152 SEC
DBX= 104.279 FT
DBY=-37.1401 FT
DBZ= 0.081543 FT

HORIZ MISS= 110.696 FT

ANGULAR MISS= 3.81752 MRAD
```

TABLE 6-4

FIRE CONTROL SOLUTION AT TIME T = 24 SECONDS
DATA BLOCK # 134_8

VARIABLE	LOCATION	OCTAL VALUE	SCALE	DECIMAL VALUE	DIMENSION
EGCL	266	0	B-1	0	RAD
TGCL	127	0	B-1	0	RAD
					-
Δ gv	137	176465	B-10	- 22.5	MR
Δ gu	140	177326	B-10	- 8.906	MR
Δ gw	141	1576	B-10	+ 28.781	MR
gu	217	72166	B-10	932.125	MR
gv	220	151547	B-10	-356.938	MR
gw	221	176421	B-10	- 22.969	MR
ρ / ρ_0	250	37420	B-1	.985352	-
R DOT	257	163644	B0	.191956	Kft/sec
RZ	261	16017	B-10	231.281	ft
Tf	317	40523	B-3	4.145	sec
Vu	335	62154	B-8	200.844	ft/sec
Vv	336	42	B-8	.266	ft/sec
Vw	337	4710	B-8	19.563	ft/sec
Zu	340	173271	B-10	74.219	MR
Zv	341	172626	B-10	83.313	MR
Zw	342	76070	B-10	993.750	MR
Su	343	72640	B-10	941.031	MR
Sv	344	153062	B-10	-334.375	MR
Sw	345	174623	B-10	- 51.750	MR
R	346	31430	B-4	6.4379	Kft.

TABLE 6-5

FIRE CONTROL SOLUTION AT TIME T = 27 SECONDS
DATA BLOCK # 256_8

VARIABLE	LOCATION	OCTAL VALUE	SCALE	DECIMAL VALUE	DIMENSION
EGCL	266	0	B-1	0	RAD
TGCL	127	0	B-1	0	RAD
Δ gv	137	175765	B-10	- 32.500	MR
Δ gu	140	176622	B-10	- 19.438	MR
Δ gw	141	243	B-10	5.719	MR
gu	217	63327	B-10	822.750	MR
gv	220	141350	B-10	488.844	MR
gw	221	156273	B-10	281.500	MR
ρ/ρ_0	250	37400	B-1	.984375	-
RDOT	257	164760	B0	- .1722107	Kft/sec
RZ	261	11524	B-10	160.125	ft
Tf	317	33030	B-3	3.4409	sec
Vu	335	64751	B-8	211.820	ft/sec
Vv	336	177634	B-8	- .781	ft/sec
Vw	337	5252	B-8	21.328	ft/sec
Zu	340	1365	B-10	23.656	MR
Zv	341	154114	B-10	-317.625	MR
Zw	342	73176	B-10	947.938	MR
Su	343	64505	B-10	842.188	MR
Sv	344	143363	B-10	-456.344	MR
Sw	345	156030	B-10	-287.219	MR
R	346	27242	B-4	5.87988	Kft

TABLE 6-6
FIRE CONTROL SOLUTION AT TIME T = 30 SECONDS
DATA BLOCK # 420_8

VARIABLE	LOCATION	OCTAL VALUE	SCALE	DECIMAL VALUE	DIMENSION
EGCL	266	177314	B-1	- 18.555	RAD
TGCL	127	177637	B-1	- 6.104	RAD
Δ gv	137	176007	B-10	- 31.906	MR
Δ gu	140	175411	B-10	- 39.719	MR
Δ gw	141	177540	B-10	- 4.469	MR
gu	217	45072	B-10	593.906	MR
gv	220	127244	B-10	-650.781	MR
gw	221	142521	B-10	-469.031	MR
ρ/ρ_o	250	37300	B-1	.980469	-
R	257	167435	B0	- .1315613	Kft/sec
RZ	261	7061	B-10	117.656	ft
Tf	317	27107	B-3	2.892	sec
Vu	335	67755	B-8	223.852	ft/sec
Vv	336	177453	B-8	- 1.664	ft/sec
Vw	337	5713	B-8	23.586	ft/sec
Zu	340	7142	B-10	115.063	MR
Zv	341	152226	B-10	347.313	MR
Zw	342	72126	B-10	930.688	MR
Su	343	47461	B-10	633.625	MR
Sv	344	131235	B-10	-618.875	MR
Sw	345	142761	B-10	-464.563	MR
R	346	25306	B-4	5.397949	Kft
Es	272	166434	B-	838.627 (u)	MR

6.3 DEMONSTRATION OF CLOSED LOOP FUNCTION ON AIRCRAFT

The following exercise is used to demonstrate the closed loop fire control function on board the aircraft as a ground check.

6.3.1 Select some simulated target and impact point separated by about 75 milliradians. Acquire the target and impact points with the sight and mark the respective turret positions; caution should be taken because the turret is active.

6.3.2 Acquire the target and depress ACTION. The INHIBIT FIRE light will flash momentarily until the computer has stabilized.

6.3.3 Depress FIRE momentarily and release, but continue to track the target.

6.3.4 After a preset time (≃time-of-flight) determined by the computer, the INHIBIT FIRE light will go on signaling the operator to break track. At this time, slew the sight to acquire the simulated impact point and depress and hold the ACQUIRE BURST CENTROID (ABC) switch.

6.3.5 Return the sight to the target and release the ABC switch. After a short period of time, the INHIBIT FIRE light will go out indicating that the computer has arrived at a closed loop solution and the turret has slewed to a new position to satisfy the revised gun orders.

6.3.6 Again taking caution with the active turret, mark the new turret position. Observe that the change in turret position relates to an amount equal and opposite to the distance from the target to the simulated impact point.

6.3.7 Release ACTION.

6.4 HARDWARE TEST OF COMPUTER INTERFACE UNIT

The following procedures were performed to demonstrate the performance of the Computer Interface Unit. CLFCS Test Set, GE 293E425, shown in Figure 6-4, was used to simulate inputs and measure outputs.

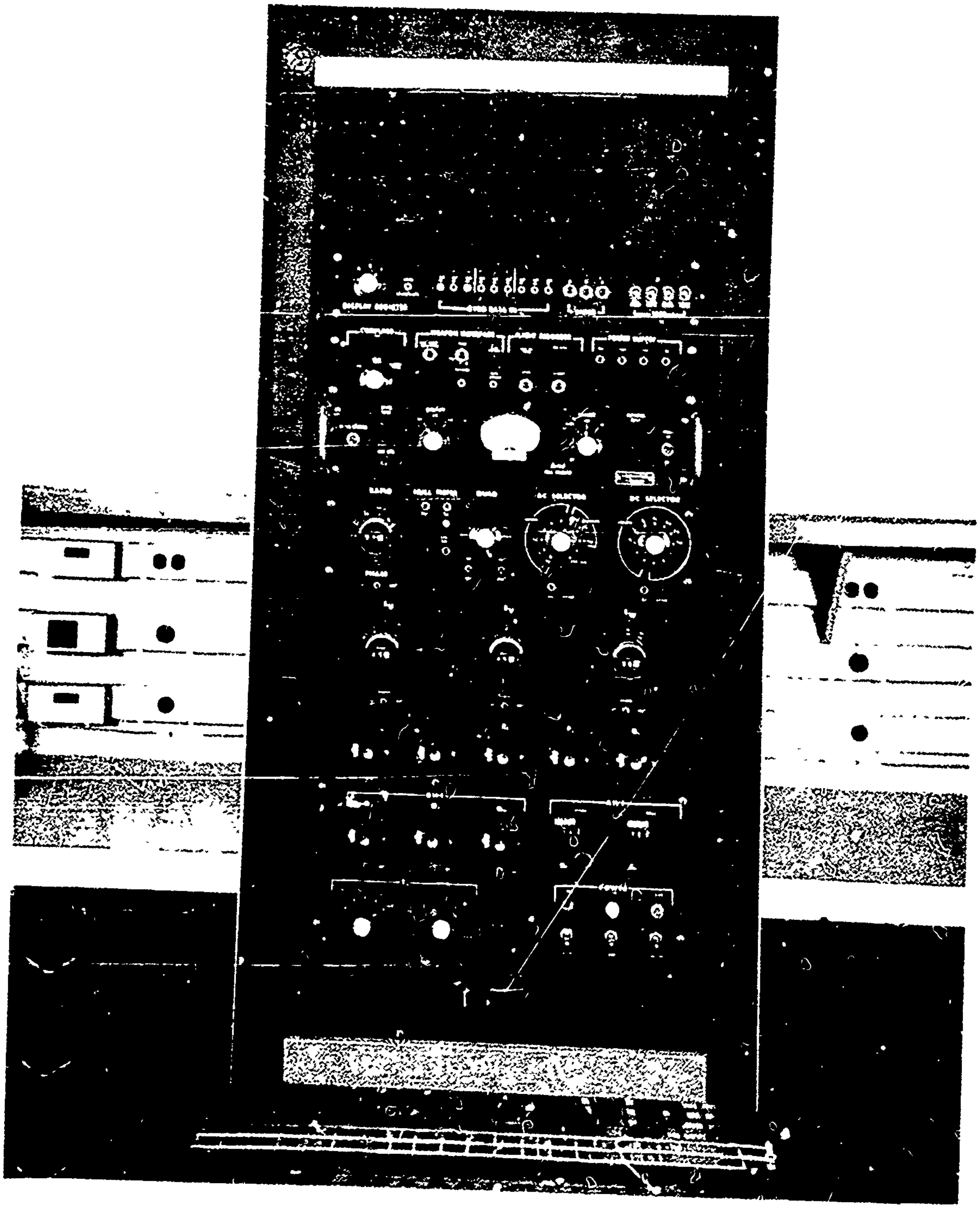

Figure 6-4. CLFCS Test Set

6.4.1 DISCRETES

Connect Computer Interface Unit (CIU) to the CIU Test Set and Console. Load in the Hardware Test Routine. Observe the Monitor Register 16 and/or the LED Display with Display Address set at 016. Observe that switching on the ACTION switch on the Test Set causes BIT 0 of Register 16 to become a "1". Observe that with ACTION on and Gun Error off, depressing the FIRE button causes BIT 1 to become a "1" and ABC causes BIT 2 to become a "1". Note that momentarily depressing TAPE START causes BIT 3 to become a "1" after approximately 2 seconds delay, and TAPE STOP returns BIT 3 to a "0". Observe that with the MODE switch set at OPEN LOOP, BIT 4 is a "0", and when set at CLOSED LOOP, BIT 4 is a "1". Observe that with GUN ERROR off, a "1" appears at BIT 5, and with GUN ERROR on, a "0" appears. BIT 6 and BIT 7 are "1"s and BIT 8 through BIT 15 are "0"s.

To demonstrate the output discrete, FIRE INHIBIT, first enter zeroes into Register 10, ones into Register 11. Direct execute the following instructions:

```
OUT 10B, 13B     145410
```

The FIRE INHIBIT light on the Test Set will go on. Then direct execute the following instructions:

```
Out 11B, 13B     145411
```

The FIRE INHIBIT light will go out.

6.4.2 A/D CONVERTER

The Hardware Test Routine causes the A/D to sample all 16 of its inputs dynamically. The desired channel number as listed in Table 6-7 is manually entered into Register 7, and the data for that channel is displayed in Register 17. Observe that a response occurs for each of the inputs by selecting the input and varying the corresponding analog function on the Test Set.

TABLE 6-7

ANALOG INPUTS

A/D CHANNEL	ANALOG INPUT
0	Fu
1	Fv
2	Fw
3	Sin Pitch
4	Cos Pitch
5	Sin Roll
6	Cos Roll
7	Ps
10	Ta
11	Pd
12	Su
13	Sv
14	Sw
15	Re
16	+10 VDC REF
17	Analog GND

This test if for demonstration only; accuracy will be demonstrated later.

6.4.3 SIMULATED GYRO INPUTS

The data link between the IMU and the CIU is digital. This interface is simulated in the CIU test set. Binary words may be set into the switch registers and loaded into the CIU by de depressing ENTER switches A, B, and C, as defined in Table 6-8. Observe that the binary word set in the switches occurs on the display monitor, shifted four binary points to the left. That is, the least significant bit on the test set will be worth octal 20 on the display.

TABLE 6-8

SIMULATED GYRO INPUT

CIU TEST SET CHANNEL	IMU AXIS	DISPLAY REGISTER
A	Pitch	13
B	Roll	14
C	Yaw	15

6.4.4 D/A CONVERTER

The Hardware Test Set Routine will output contents of Registers 10, 11, and 12 to D/A Converter channels U, V, and W, respectively. The 400 Hz analog outputs represent the direction cosines of the lead angle. Each 11 bit input is entered left justified into the registers, where full scale is equal to about 6.4 volts. Observe that a response occurs for each of the three channels by monitoring the output voltage on the CIU Test Set.

6.4.5 A/D AND D/A ACCURACY CHECK

The CLFCS System Software will now be loaded into the CDC 469. Its internal scaling, computation and normalization will demonstrate the accuracies of the analog converters. Enter the analog data from Table 6-9 into the CIU Test Sets. Monitor the internal locations and verify that the entries are within the specified limits of Table 6-10.

Since Estimated Range (Re) is sampled only at the start of ACTION Mode and is constantly being updated by velocity information, the following procedure should be used to capture its initial digital value.

1. Place computer in RUN, with ACTION off.
2. Key in the instruction 010007 at location 017407.
3. Turn ACTION on. Computer will start LOS Estimator, but will halt immediately after the initial Re value has been sampled.
4. Read value of Re stored in Register 5.
5. Place computer in STEP and turn ACTION off.
6. Restore instruction at location 017407 by entering 043501.
7. Place computer in RUN.

TABLE 6-9
ANALOG INPUT TEST SETTINGS

PARAMETER	ANALOG VALUE	TEST SET INPUT
Fu	+ 0.7441 Ft/sec^2	+0.051 VDC
Fv	- 4.7621 Ft/sec^2	+0.326 VDC
Fw	-37.4589 Ft/sec^2	-2.560 VDC
Sin P	- 0.074082	-4.25°
Cos P	0.997252	
Sin R	- 0.086629	-5.00°
Cos R	0.996241	
Ps	14.4452 PSI	+4.223 VDC
Ta	2[illegible].007°K	+2.835 VDC
Pd	0.329402 PSID	+2.534 VDC
Su	+940.613 munits	+0.940613
Sv	-335.301 munits	+0.335301
Sw	- 53.109 munits	+0.053109
Re	5.625 Kft	+1.715 VDC

The CLFCS System Software will also be used to check the accuracy of the D/A converter, but it will be used in the STEP Mode so that the D/A inputs may be controlled. The procedure is as follows:

1. Depress MASTER CLEAR. Depress STEP four times. Insert 11473 into register 0. This will leave the interrupt system disabled.
2. Enter digital data in the indicated locations as listed in the table.
3. Step the program counter through location 11505. This will transfer the data to digital latches in the D/A converters.
4. Observe that the D/A outputs as measured on the CIU Test Set agree with the output specified in Table 6-11 within 0.62 milliunits.

TABLE 6-10

SPECIFIED RESULTS FROM A/D INPUTS

PARAMETER	LOCATION	NOMINAL	VARIANCE	OCTAL		SCALING
				MAX	MIN	
Fu	102	+ 0.7441	±0.2125	000752	000420	B-6
Fv	103	- 4.7621	±0.2125	004431	004762	B-6
Fw	104	- 37.4389	±0.2125	132614	132263	B-6
Z_u = + Sin P	361	- 74.082	±4.0	173476	173076	B-10
Z_v = Cos P Sin R	362	- 86.391	±4.4	172700	172247	B-10
Z_w = Cos P Cos R	363	993.503	±4.4	076275	075643	B-10
Ps	254	14.4452	±0.0150	001635	001633	B-9
Ta	315	287.007	±0.280	043722	043656	B-9
Pd	255	0.329402	±0.001900	000523	000517	B-5
Su	276	940.613	±1.500	072703	072543	B-10
Sv	277	-335.301	±1.500	153107	152747	B-10
Sw	300	- 53.109	±1.500	174615	174454	B-10
Re	360	5.625	± .050	026126	025616	B-4

TABLE 6-11

SPECIFIED D/A OUTPUTS

D/A CHANNEL	LOCATION	DATA ENTRY (milliunits)	SCALE	OCTAL INPUT	NOMINAL OUTPUT (milliunits)
DELGUG	142	+ 16	B-10	001000	+ 16.000
DELGVG	143	-128	B-10	170000	+128.000
DELGWG	144	+256	B-10	020000	-256.000

6.4.6 TEMPERATURE DATA

Additional data was taken on the A/D and D/A converters to determine their linearity and also temperature dependance over a limited range of temperature. The accuracy data is tabulated in Tables 6-12 through 6-17. During the testing it was determined that the maximum allowable operating ambient (cockpit) is 100°F. This ambient results in a 122°F or 50°C CDC 469 processor chassis temperature, which is the maximum the vendor recommends.

6.5 ALIGNMENT AND CALIBRATION OF CLFCS INERTIAL MEASUREMENT UNIT

6.5.1 ALIGNMENT FIXTURE

An assembled Inertial Measurement Unit (IMU), GE Dwg. 123D6654 was mounted to an alignment fixture as depicted in SK RC 42776. The IMU has three machined orthogonal surfaces, to which the gyros and accelerometers are mounted, within a perpendicularity error of 0.3 MR. Three accelerometers mounted to the machined surfaces have their sensitive axis perpendicular to their mounting flange within 2.0 MR and the gyros have their OA perpendicular to 1.5 MR MAX. or 1 MR RSS. The alignment of the gyro IA was accomplished on an Inland rate table model 823 with servo controller model 403 and the aid of the alignment fixture. The fixture has three orthogonal planes each defined by three pads .75 inch in diameter which are lapped to produce a perpendicularity error less than 5 sec. of arc (0.024 MR). An interface block is used to adapt the IMU to the alignment fixture and is not attached to the fixture with any high degree of accuracy. The alignment of the IMU to the alignment fixture was done optically by using the crobolox reflecting target, which has a wedge angle of < 0.0022 MR, as the reference surface for the IMU and adjusting the leveling screws on the IMU. This was done with an error of less than 0.33 MR.

Before alignment of the gyro IA's could be pursued, an interface plate had to be attached to the rate table. The plate has three pads which correspond to the pads on each of the three orthogonal surfaces on the alignment fixture. When the plate was belted to the rate table, a run out of 0.03 MR was attained. The fixture with the IMU could be bolted to the interface plate on each of its sides to align the IA's.

TABLE 6-12
A/D TEST DATA -D.C. INPUTS

A/D CHANNEL	PARAM-ETER	REAL WORLD	CIU INPUT, V	CALC. DECIMAL	CALC. OCTAL	-10° F		ROOM TEMP		100° F	
						MEASURED	ERROR	MEASURED	ERROR	MEASURED	ERROR
0	-Au	-16.0 FT S^2	- 1.0941	- 3584	171000	171020	-1	171000	0	171000	0
		0	0.0000	0000	000000	000000	0	000000	0	177760	-1
		-16.0	- 1.0941	- 3584	7000	006760	-1	006760	-1	006760	-1
1	Av	-16.0 FT/S^2	- 1.0941	- 3584	171000	171040	-2	171020	-1	171000	0
		0	0.0000	0000	000000	000000	0	000000	0	177760	-1
		-16.0	- 1.0941	- 3584	7000	006760	-1	006760	-1	006760	-1
2	-Aw	-48.0 FT/S^2	- 3.2823	-10736	153020	153060	-2	153060	-2	153060	-2
		-32.1725	- 2.200	- 7200	161740	162000	-2	161760	-1	161760	-1
		-16.0	- 1.0941	- 3584	171000	171020	-1	171020	-1	171020	-1
7	P_s	-14.0 PSI	- 4.0000	26192	63120	062760	-6	063060	-2	063060	-2
		-15.0	- 4.5000	29472	71440	071720	-7	071360	-3	071400	-2
8	T_a	0° C	- 2.1053	6895	15360	015340	-1	015400	-1	015340	-1
		25	- 3.4211	11200	25700	025660	-1	025700	0	025660	-1
		70	- 5.7895	18960	45020	044740	-3	045020	0	045000	-1
9	Q_c	0 PSID	0.0000	0000	00000	000000	0	000000	0	177760	-1
		0.100	- 0.7692	2512	4720	004720	0	004720	0	004700	-1
		1.000	- 7.6923	25184	61140	061000	-6	061060	-3	061100	-2
13		1500 M	1.5000	4912	11460	011460	0	011460	0	011140	-1
13	Re	2000	2.0000	6544	14620	014620	0	014600	-1	014600	-1
		2500	2.5000	8176	17760	017760	0	017760	0	017760	0
14	-10 Vr	-10.0V	-10.0V	32751	077760	077700	-3	077760	0	077760	0
15	0V	0V	0V	0	000000	000400	-2	000020	-1	177760	-1

TABLE 6-13

A/D TEST DATA - PITCH AND ROLL, POSITIVE ANGLES

ANGLE DEG P	R	TEMP A/D CHAN SIGNAL	-10°F				RM TEMP				100°F			
			3 SIN P	4 COS P	5 SIN R	6 COS R	3 SIN P	4 COS P	5 SIN R	6 COS R	3 SIN P	4 COS P	5 SIN R	6 COS R
		IDEAL	.000000	1.000000	.000000	1.000000	.000000	1.000000	.000000	1.000000	000000	1.000000	000000	1.000000
		$RECORDED_8$	177760	067200	17[illegible]00	067340	177740	066160	177700	066240	177720	067220	177760	067240
0	0	$RECORDED_{10}$	- 80	28288	- 128	28384	- 32	27760	- 64	27808	- 48	28304	- 16	28320
		NORMALIZED	- .002830	999996	- 004510	.999990	- .001153	.999999	- .002301	999997	- .001696	999999	- 000565	1.000000
		ERROR NORM	- .002830	- .000004	- .004510	- .000010	- .001153	- .000001	- 002301	- .000003	- 001696	- .000091	- .000565	.000000
		ERROR MR	-2 83		-4.50		-1 22		-2.27		-1.70		-0.56	
		IDEAL	.034899	.999391	.034899	.999391	034899	.999391	.034899	.999391	.034899	.999391	034899	.999391
		$RECORDED_8$	001620	067160	001540	067300	001640	066140	001620	066220	001640	067200	001560	067240
2	2	$RECORDED_{10}$	912	28272	864	28352	928	27744	912	27792	928	28288	880	28320
		NORMALIZED	.032241	.999480	.030460	.995360	.033430	999441	032796	.999422	.032788	.998870	.031058	.999518
		ERROR NORM	- .002658	.000089	- .004439	- .004031	- .001469	.005531	- 002103	.000031	- .002111	- .000521	- .003841	.000127
		ERROR MR	-2.62		-4 36		-1.40		-2.09		-2.09		-3.84	
		IDEAL	087156	.996195	.087156	.996195	087156	.996195	.087156	.996195	.087156	.996195	.087156	.996195
		$RECORDED_8$	004520	067020	004460	067160	004500	066000	004460	066060	004560	067040	004500	067100
5	5	$RECORDED_{10}$	2384	28176	2352	28272	2368	27648	2352	27696	2416	28192	2368	28224
		NORMALIZED	.084310	.996140	.082905	.996557	.085336	.996352	084580	.995970	.085385	.996348	.083606	.996499
		ERROR NORM	- 002846	000245	- .004251	000362	- .001820	.000157	- 002576	- .000225	- .001771	.000153	- .003550	.000304
		ERROR MR	-2.79		-4.19		-1 75		-2.62		-1.78		-3.56	
		IDEAL	173648	.984808	173648	984808	.173648	.984808	.173648	.984808	.173648	.984808	.173648	.984808
		$RECORDED_8$	011420	066320	011300	066460	011260	065300	011240	065400	011400	066340	011340	066400
10	10	$RECORDED_{10}$	4880	27856	4800	27952	4784	27328	4768	27392	4864	27872	4832	27904
		NORMALIZED	.172559	.984999	169246	985574	172436	985021	.171461	985038	.171914	985112	.170626	.985336
		ERROR NORM	- .001089	.000191	- .004402	.000766	- 001212	.000213	- 002187	.000230	- 001734	000304	- .003022	.000528
		ERROR MR	-1.05		-4.54		-1.22		-2.27		-1 76		-3.07	
		IDEAL	.342020	939693	342020	.939693	.342020	.939693	342020	.939693	342020	.939693	.342020	939693
		$RECORDED_8$	022640	063740	022600	064040	022360	062740	022360	063020	022620	063740	022600	064000
20	20	$RECORDED_{10}$	9632	26592	9600	26656	9456	26080	9456	26128	9616	26592	9600	26624
		NORMALIZED	.340562	940222	338839	940844	340863	.940113	.340309	.940314	340062	.940403	.339200	.940714
		ERROR NORM	- .001458	000529	- 003181	001151	- .001157	000420	- .001711	000621	- 001958	.000710	- .002820	.001021
		ERROR MR	-1 57		-3 32		-1.22		-1.75		-2 08		-3.00	
		IDEAL	500000	866025	500000	866025	.500000	866025	.500000	.866025	500000	.866025	500000	.866025
		$RECORDED_8$	033520	057660	033420	069900	033040	056740	033040	057040	033420	057700	033400	057740
30	30	$RECORDED_{10}$	14160	24496	14096	24576	13856	24032	13856	24096	14096	24512	14112	24544
		NORMALIZED	50047	865762	497537	867443	499489	.866320	498660	867184	.498514	.866882	.498297	.866653
		ERROR NORM	000457	- 000263	- 002463	.001418	- 000511	000295	- 001340	.001159	- 001486	.000857	- 001703	.000628
		ERROR MR	-0 52		-2.79		-0.52		-1 75		-1 72		-1 79	

TABLE 6-14

A/D TEST DATA - PITCH AND ROLL, NEGATIVE ANGLES

ANGLE DEG P	ANGLE DEG R	TEMP A D CHAN SIGNAL	-10°F 3 SIN P	-10°F 4 COS P	-10°F 5 SIN R	-10°F 6 COS R	RM TEMP 3 SIN P	RM TEMP 4 COS P	RM TEMP 5 SIN R	RM TEMP 6 COS R	100°F 3 SIN P	100°F 4 COS P	100°F 5 SIN R	100°F 6 COS R
0	0	IDEAL	.000000	1.000000	.000000	1.000000	.000000	1.000000	000000	1 000000	.000000	1.000000	.000000	1.000000
		RECORDED$_8$	177640	067200	177600	067320	177740	066140	177700	066240	177720	067220	177640	067260
		RECORDED$_{10}$	- 96	28288	- 128	28368	- 32	27744	64	27808	- 48	28304	- 96	28336
		NORMALIZED	- .003394	.999994	- .004512	.999990	- .001153	.999999	- .002301	.999997	- .001696	.999999	- .003388	.999994
		ERROR NORM	- .003394	- .000006	- .004512	- .000010	- .001153	- .000001	- .002301	- 000003	- .001696	- .000001	- 003388	- .000006
		ERROR MR	-3 39		-4.5		-1.22		-2.27		-1.69		-3.38	
-2	-2	IDEAL	- .034899	.999391	- .034899	999391	- 034899	.999391	- .034899	999391	- .034899	999391	- .034899	.999391
		RECORDED$_8$	175700	067160	175620	067300	175767	066140	175740	066200	175720	067200	175660	067260
		RECORDED$_{10}$	- 1088	28272	- 1136	28352	- 1033	27744	1056	27776	- 1072	28304	- 1104	28336
		NORMALIZED	- .038455	.999260	- .004004	.999198	- 037207	999308	- .037991	999278	- .037847	.999284	- .038932	999242
		ERROR NORM	- .003556	- .000131	.030895	- .000193	- 002308	- .000083	- .003092	- .000113	- .002948	- .000107	- .004033	- .000149
		ERROR MR	-3.49		-5 06		-2.27		-2.18		-2.97		-4.01	
-5	-5	IDEAL	- 087156	.996195	- 087156	996195	- .087156	.996195	- .087156	.996195	- 087156	.996195	- .087156	.996195
		RECORDED$_8$	172760	067000	172700	067160	173120	066000	173100	066060	173040	067040	172740	067100
		RECORDED$_{10}$	- 2576	28160	- 2624	28272	- 2480	27648	- 2496	27696	- 2528	28192	- 2592	28224
		NORMALIZED	- .091097	.995842	- .092415	995721	- .089340	.996001	- .089758	.995964	- 089312	.996004	- .091452	.995809
		ERROR NORM	- 003941	- .000353	- .005259	- .000474	- .002184	- .000194	- .002602	- .000231	.002156	- .000191	- .004296	- .000386
		ERROR MR	-4.01		-5 24		-2.27		-2.62		-2 09		-4 36	
-10	-10	IDEAL	- 173648	.984808	- .173648	984808	- 173648	984808	- 173648	984808	- 173648	.984808	- .173648	.984808
		RECORDED$_8$	166140	066300	166100	066440	166400	065300	166340	065400	166240	066320	166100	066400
		RECORDED$_{10}$	- 5024	27840	- 5056	27936	- 4864	27328	- 4896	27392	- 4960	27856	- 5056	27904
		NORMALIZED	- .177591	.984104	- 178092	.984014	- .175268	.984527	- .175950	.984399	- .175301	.984515	- .178290	.983978
		ERROR NORM	- .003943	- .000704	- .004444	.000794	- .001620	- .000281	- .002302	- .000499	.348949	- .000293	- .004642	- .000830
		ERROR MR	-4 01		-4.54		-1.57		-2.27		-1.75		-4.71	
-20	-20	IDEAL	- .342020	939693	- 342020	.939693	- 342020	.939693	- 342020	939693	- 342020	.939693	- .342020	939693
		RECORDED$_8$	154660	063700	154600	064040	155060	062740	155220	063020	155000	063740	154640	064000
		RECORDED$_{10}$	- 9808	26560	- 9856	26656	- 9552	26080	- 9584	26128	- 9728	26592	- 9824	26624
		NORMALIZED	- 346412	.938082	- 346801	.937939	- .343916	.939000	- .344373	.938833	- .343557	.939132	- .346176	.938170
		ERROR NORM	- .004392	- .001611	- 004781	- .001754	- 001896	- .000693	- .002353	- 000860	- .001537	- .000561	- .004156	- .001523
		ERROR MR	-4 71		-5.06		-2.09		-2 44		-1.57		-4.36	
-30	-30	IDEAL	- 500000	.866025	- .500000	.866025	- 500000	866025	- 500000	.866025	- 500000	866025	- 500000	.866025
		RECORDED$_8$	144020	057620	143760	060000	144600	056720	144520	057020	144140	057700	144020	060000
		RECORDED$_{10}$	- 14320	24464	- 14352	24576	- 13952	24016	- 14000	24080	- 14240	24512	- 14320	24576
		NORMALIZED	- 505169	.863020	- 504290	863534	- .502330	.864616	- .502620	.864507	- .502326	864678	- 503451	864024
		ERROR NORM	00.169	- 003005	- 004290	- 002491	- 002330	- .001349	- .002620	- 001518	- .002326	- 001347	- 003451	- 002001
		ERROR MR	-5 93		-4 88		-2 62		-2 97		-2 62		-4 01	

TABLE 6-15

A/D TEST DATA - SIGHTLINE DATA, ZERO ELEVATION ANGLE

ANGLE T E	TEMP A D CHAN SIGNAL	-10°F			RM TEMP			100°F		
		12 Su	13 Sv	14 Sw	12 Su	13 Sv	14 Sw	12 Su	13 Sv	14 Sw
0° 0°	IDEAL	0.999999	0.000000	0.000000	0.999999	0.000000	0.000000	0 999999	0.000000	0 000000
	RECORDED$_8$	067100	000020	000000	067140	177760	177760	067340	177760	177760
	RECORDED$_{10}$	282244	16	0	28256	- 16	- 16	28384	- 16	- 16
	NORMALIZED	1.000000	-0.000567	0.000000	1.000000	-0.000566	-0.000566	1.000000	-0.000564	-0 000564
	ERROR UNITS	0 000000	-0.000567	0.000000	0.000001	-0.000566	-0.000566	0.000001	-0.000564	-0.000564
	ERROR T, E MR	0.57	0.00		-0.57	-0.57		-0.57	-0.57	
30° 0°	IDEAL	0.866025	0.500000	0.000000	0.866025	0.500000	0.000000	0.866025	0.500000	0.000000
	RECORDED$_8$	057600	033460	000000	057640	033440	177760	057740	033500	177760
	RECORDED$_{10}$	24446	14128	0	24480	14112	- 16	24544	14144	- 16
	NORMALIZED	0.865827	0.500344	0.000000	0.866355	0 499428	-0 000566	0.864712	0.498309	0.000564
	ERROR UNITS	-0.000327	-0.099656	0.000000	0.000330	-0.000572	-0.000566	-0.001313	-0.001691	0.000564
	ERROR T, E MR	0.40	0.00		-0.66	-0.57		-0.81	-0.51	
60° 0°	IDEAL	0.500000	0.866025	0.000000	0.500000	0.866025	0.000000	0.500000	0.866025	0.000000
	RECORDED$_8$	033440	057620	000020	033460	057560	177760	033540	057660	177760
	RECORDED$_{10}$	14112	24464	16	14128	24432	- 16	14176	24996	- 16
	NORMALIZED	0 499673	0.866214	0.000567	0.500589	0.366685	-0.000567	0 500880	0.865516	-0.000565
	ERROR UNITS	-0.000327	0.000189	0.000567	0.000589	-0.000340	-0.000567	0.000880	-0.000509	-0.000565
	ERROR T, E MR	0.38	0.57		-0 68	-0 57		-1.02	-0.57	
90° 0°	IDEAL	0.000000	0.999999	0.000000	0.000000	0.999999	0.000000	0.000000	0.999999	0.000000
	RECORDED$_8$	000000	067100	000020	177760	067040	177760	177760	067100	177760
	RECORDED$_{10}$	0	28224	16	- 16	28192	- 16	- 16	28224	- 16
	NORMALIZED	0.000000	1.000000	0.000567	-0.000568	1.000000	-0.000568	-0.000567	1.000000	-0.000567
	ERROR UNITS	0.000060	0.000000	0.000567	-0.000568	0.000001	-0.000568	-0.000567	0.000001	-0.000567
	ERROR T, E MR	0.00	0.57		-0.57	-0.57		-0.57	-0.57	
-30° 0°	IDEAL	0.866025	-0.500000	0.000000	0.866025	-0.500000	0.000000	0 866025	-0.500000	0.000000
	RECORDED$_8$	057600	144360	000000	057640	144340	177760	057740	144320	177740
	RECORDED$_{10}$	24448	- 14096	0	24480	- 14112	- 16	24544	- 14128	- 32
	NORMALIZED	0.866318	-0.499493	0.000000	0.866355	-0 499428	-0.000568	0.866674	-0.498874	-0.001130
	ERROR UNITS	0.000293	0 000507	0.000000	0.000300	0.000572	-0.000568	0.000649	0.001126	-0.001130
	ERROR T, E MR	0.58	0.00		0.66	-0.57		1.30	-1.13	
-60° 0°	IDEAL	0.500000	-0.866025	0.000000	0.50000	-0.866025	0.000000	0.500000	-0.866025	0.000000
	RECORDED$_8$	033440	120220	000000	033460	120220	177740	033540	120160	177740
	RECORDED$_{10}$	14112	- 24432	0	14128	- 24432	- 32	14176	- 24464	- 32
	NORMALIZED	0.500164	-0.865931	0.000000	0.500589	-0.865684	-0.001134	0.501371	-0.865232	0.001132
	ERROR UNITS	0.000164	0.000094	0.000000	0.000589	0.000341	-0.001134	0.001371	0.000793	0.001132
	ERROR T, E MR	0.19	0.00		0.68	-1.13		1.58	-1.13	
-90° 0°	IDEAL	0.000000	-0.999999	0.000000	0.000000	-0 999999	0.000000	0.000000	-0.999999	0.000000
	RECORDED$_8$	000000	110660	000000	177760	110720	177740	177760	110640	177720
	RECORDED$_{10}$	0	28240	0	- 16	- 28208	- 32	- 16	- 28256	- 48
	NORMALIZED	0.000000	1.000000	0.000000	-0.000567	-0.999999	-0.001134	-0.000566	-0.999998	0.001699
	ERROR UNITS	0 000000	0.000000	0.000000	-0.000567	0.000000	-0.001134	-0.000566	0.000001	0.001699
	ERROR T, E MR	0.00	0.00		-0.57	-1.13		0.57	-1.17	

TABLE 6-16

A/D TEST DATA - SIGHTLINE DATA, NON ZERO ELEVATION ANGLE

ANGLE T E	TEMP A/D CHAN SIGNAL	-10°F 12 Su	-10°F 13 Sv	-10°F 14 Sw	RM TEMP 12 Su	RM TEMP 13 Sv	RM TEMP 14 Sw	100°F 12 Su	100°F 13 Sv	100°F 14 Sw
0° 5°	IDEAL	0.996195	0.000000	0.087156	0.996195	0.000000	0.087156	0.996195	0.000000	0.087156
	RECORDED$_8$	066740	000020	004620	066740	177760	004620	067000	177760	004600
	RECORDED$_{10}$	28128	16	2448	28128	-16	2448	28160	-16	2432
	NORMALIZED	0.996234	0.000567	0.086703	0.996234	-0.000567	0.086703	0.996291	0.000566	0.026043
	ERROR UNITS	0.000039	0.000567	-0.000453	0.000039	-0.000567	-0.000453	0.000096	0.000566	-0.001113
	ERROR T E MR	0.57	-0.45		-0.57	-0.46		0.57	-1.10	
60° 5°	IDEAL	0.498097	0.862730	0.087156	0.498097	0.862730	0.087156	0.498097	0.862730	0.087156
	RECORDED$_8$	033360	057460	004660	033340	057400	004620	033360	057400	004640
	RECORDED$_{10}$	14064	24368	2480	14048	24320	2448	14064	24320	2464
	NORMALIZED	0.497939	0.862755	0.087805	0.498293	0.862649	0.885832	0.498695	0.862363	0.087371
	ERROR UNITS	-0.000158	0.000025	0.000649	0.000196	-0.000081	0.000324	0.000598	-0.000367	0.000215
	ERROR T E MR	0.15	0.64		-0.21	-0.33		-0.70	0.215	
0° -5°	IDEAL	0.996195	0.000000	-0.087156	0.996195	0.000000	-0.087156	0.996195	0.000000	-0.087156
	RECORDED$_8$	066720	000020	173140	066720	177760	173140	067000	177760	173140
	RECORDED$_{10}$	28112	16	-2464	28112	-16	-2464	28160	-16	-2464
	NORMALIZED	0.995312	0.000566	-0.087239	0.996181	-0.000567	-0.087315	0.996194	0.000567	-0.037371
	ERROR UNITS	-0.000883	0.000566	0.000083	-0.000014	-0.000567	-0.000159	-0.000001	0.000567	-0.000215
	ERROR T E MR	0.57	0.082		-0.57	-0.16		0.57	-0.215	
60° -5°	IDEAL	0.498097	0.862730	-0.087156	0.498097	-0.862730	-0.087156	0.498097	0.862730	-0.087156
	RECORDED$_8$	033360	057460	173160	033340	120400	173120	033360	057400	173160
	RECORDED$_{10}$	14064	24368	-2448	14048	-24320	-2480	14064	24320	-2448
	NORMALIZED	0.497989	0.862840	-0.086681	0.498224	-0.862564	0.087959	0.498720	0.862405	-0.086808
	ERROR UNITS	-0.000108	0.000110	0.000475	0.000147	0.000166	0.000803	0.000623	-0.000325	0.000348
	ERROR T E MR	0.15	0.475		0.21	-0.58		-0.70	0.35	
-30° 10°	IDEAL	0.852869	-0.492404	0.173648	0.852869	-0.492404	0.173648	0.852869	-0.492404	0.173648
	RECORDED$_8$	057020	144700	011420	057000	144720	011400	057020	144740	011400
	RECORDED$_{10}$	24080	-13888	4880	24064	-13872	4864	24080	-13856	4864
	NORMALIZED	0.853208	-0.492081	0.172909	0.853373	-0.491937	0.172490	0.853765	-0.491269	0.172455
	ERROR UNITS	0.000339	0.000323	-0.000739	0.000504	0.000467	-0.001158	0.000896	0.001135	-0.001193
	ERROR T E MR	0.46	-0.74		0.67	1.20		1.45	-1.19	
-30° -10°	IDEAL	0.852869	-0.492404	-0.173648	0.852869	-0.492404	-0.173648	0.852869	-0.492404	-0.173648
	RECORDED$_8$	057020	144700	166320	057000	144720	166320	057020	144740	166300
	RECORDED$_{10}$	24080	13888	-4912	24064	-13872	-4912	24080	-13856	-4928
	NORMALIZED	0.853037	-0.491984	-0.174008	0.853121	-0.491792	-0.174141	0.853428	-0.491076	-0.174655
	ERROR UNITS	0.000168	0.000420	-0.000360	0.000252	0.000612	-0.000493	0.000559	-0.001328	-0.001007
	ERROR T E MR	0.45	-0.36		0.67	-0.50		1.45	-1.01	
-90° -10°	IDEAL	0.000000	-0.984808	-0.173648	0.000000	-0.984808	-0.173648	0.000000	-0.984808	-0.173648
	RECORDED$_8$	000000	111560	166300	177760	111640	166300	177760	111640	166300
	RECORDED$_{10}$	0	27792	-4928	-16	-27744	-4928	-16	-27744	-4928
	NORMALIZED	0.000000	-0.984641	-0.174594	-0.000568	-0.984588	-0.174887	0.000568	-0.984588	-0.174887
	ERROR UNITS	0.000000	0.000167	-0.000946	-0.000568	0.000220	-0.001239	0.000568	0.000220	-0.001239
	ERROR T E MR	0.09	-0.95		0.58	-1.20		0.58	-1.24	

TABLE 6-17

D/A CONVERTER TEST DATA - LEAD ANGLE OUTPUTS

INPUT		CHANNEL U					CHANNEL V					CHANNEL W				
			-10°F		100°F			-10°F		100°F			-10°F		100°F	
OCTAL	DECIMAL	V_o/V_{ref} DESIRED	V_o/V_{ref} MEASURED	ERROR Mrad	V_o/V_{ref} MEASURED	ERROR Mrad	V_o/V_{ref} DESIRED	V_o/V_{ref} MEASURED	ERROR Mrad	V_o/V_{ref} MEASURED	ERROR Mrad	V_o/V_{ref} DESIRED	V_o/V_{ref} MEASURED	ERROR Mrad	V_o/V_{ref} MEASURED	ERROR Mrad
077760	32752	0.64268	0.64100	-1.68	0.64071	-1.97	0.64124	0.63956	-1.68	0.63915	-2.09	0.64113	0.63922	-2.11	0.63917	-1.96
037760	16368	0.32131	0.32079	-0.55	0.31916	-2.18	0.32062	0.32000	-0.62	0.31846	-2.14	0.32057	0.32000	-0.57	0.31842	-2.15
000600	384	0.00785	0.00790	0.55	0.00798	0.13	0.00783	0.00790	0.07	0.00792	0.09	0.00783	0.00770	-0.13	0.00773	-0.10
000160	112	0.00251	0.00260	0.09	0.00269	0.18	0.00250	0.00260	0.10	0.00259	0.09	0.00250	0.00243	-0.07	0.00250	0.00
000000	0	0.00031	0.00039	0.08	0.00047	0.16	0.00031	0.00039	0.08	0.00040	0.09	0.00031	0.00025	-0.06	0.00026	-0.05
177620	- 112	-0.00188	-0.00186	0.02	-0.00186	0.02	-0.00188	-0.00186	0.02	-0.00189	-0.01	-0.00188	-0.00186	0.02	-0.00181	0.07
177200	- 384	-0.00722	-0.00726	-0.04	-0.00722	0.00	-0.00720	-0.00719	0.01	-0.00722	-0.02	-0.00720	-0.00712	0.08	-0.00722	-0.02
140020	-16368	-0.32071	-0.32000	0.71	-0.31974	0.97	-0.32000	-0.31937	0.63	-0.31902	0.98	-0.31994	-0.31937	0.57	-0.31905	0.89
100020	-32752	-0.64206	-0.64051	1.55	-0.64287	-0.81	-0.64062	-0.63912	1.50	-0.64133	-0.71	-0.64051	-0.63900	1.51	-0.64133	-0.82

6.5.2 GYRO ALIGNMENT AND CALIBRATION TEST SET-UP

Gyro alignment and calibration was performed on the Inland controls direct drive rate table:

Table	-	Model No. 823, Serial No. 6316-1;
Controller	-	Model No. 403, Serial No. 7;
Amplifier	-	Model No. 1500 CP, Serial No. 19.

The gyro output was measured using the gyro calibration unit (GCU) and a photocell pickoff. An up/down counter in the GCU counts the net number of torque pulses applied to the gyro torque coil during an interval of time. The time interval is determined either by a thumbwheel switch on the front panel of the GCU for fixed time intervals or with the photocell pickoff for 1 revolution time intervals. When the photocell pickoff is used, a tab on the rate table interrupts the light projecting on the photocell, producing a pulse which resets and enables the up/down counter. After producing a second pulse which disables the up/down counter and displays the net torque pulse count on the GCL LED readout.

Figure 6-5 is a sketch of the alignment and calibration test set-up.

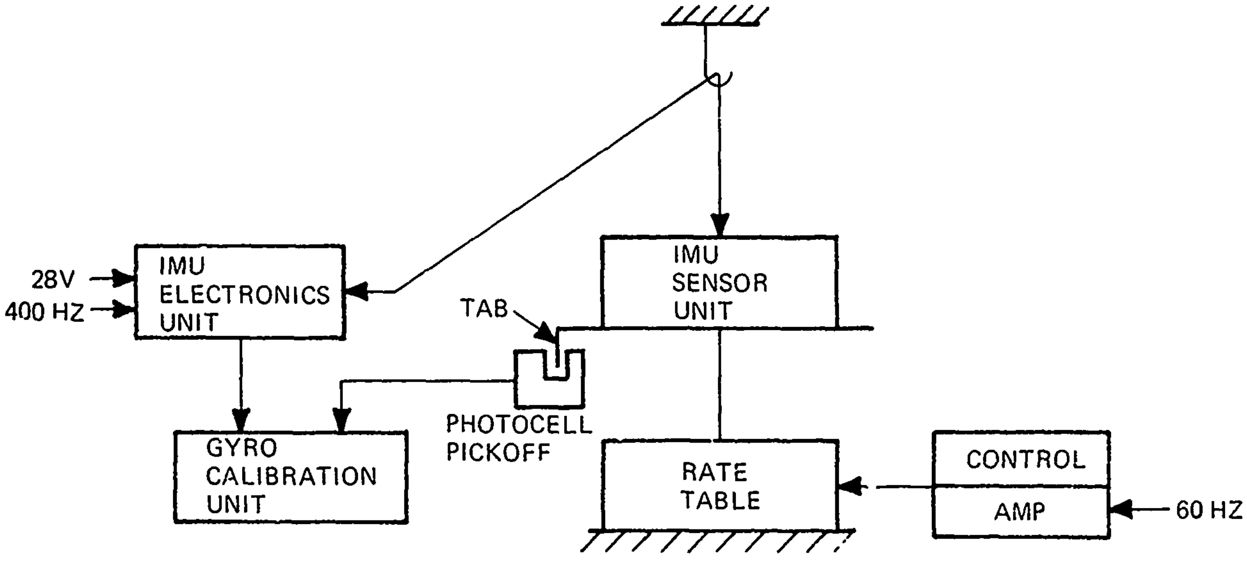
28V
400 HZ
IMU ELECTRONICS UNIT
TAB
IMU SENSOR UNIT
PHOTOCELL PICKOFF
GYRO CALIBRATION UNIT
RATE TABLE
CONTROL
AMP
60 HZ

Figure 6-5. Calibration and Alignment Test Setup

6.5.3 GYRO ALIGNMENT

The gyro input axis was aligned by mounting the sensor unit and its calibration fixture to the adapter plate on the rate table with the spin axis parallel to the table axis. With this orientation, the gyro output will be nearly zero when it is correctly aligned. Using the GCU and photocell pickoff, the gyro output for 360° rotation of the rate table was noted. The gyro was repeatedly repositioned and rotated until the output was less than 11 counts, which is equivalent to a misalignment of < 1 MR.

6.5.4 GYRO CALIBRATION

The gyro calibration test set-up was the same as used for gyro alignment. Calibration data were recorded for one revolution at various rates, Table 6-18, and for 60 seconds at various rates, Table 6-19. Two data points were recorded at each test condition to demonstrate repeatability.

In obtaining the one revolution calibration data, the maximum gyro rate was determined by increasing the table turning rate until the gyro count for one revolution decreased. The maximum rate is approximately 58° sec.

The gyro drift is recorded in Table 6-19 under the heading 0°/sec. Gyro drift was recorded with the rate table stationary in one position and again in a second position 180° from the first.

6.5.5 GYRO SCALE FACTORS

A statistical analysis of the gyro data was made which resulted in the gyro output scaling listed in Table 6-20 and alignment data in Table 6-21. This scaling is mechanized in the CLTCS software.

Additional data was taken on the yaw gyro to determine its scale factor's dependence upon temperature. The results of this data are shown in Figure 6-6. The curve shows that the gyro output is 0.27% lower at 30°F than at 70°F, when rotated at 15°/second. This error relates to a 7 milliradian error in integrated yaw angle over a 10 second interval at a turning rate of 15°/second. If desired, the scaling in the software may be revised to reflect some average temperature in the aircraft cockpit (the IMU sensor environment), but since the cockpit is heated/air conditioned, it would not appear necessary.

TABLE 6-12

IMU DATA - ONE REVOLUTION AT VARIOUS RAT...

TABLE 6-12

IMU DATA - ONE REVOLUTION AT VARIOUS RATES

RATE	10°/Sec		20°/Sec		30°/Sec		40°/Sec		50°/Sec		5[illegible] Sec		59°/Sec
DIRECTION	CW	CCW	CW	CCW	CW	CCW	CW	CCW	CW	CCW	CW	CCW	CCW
PITCH GYRO													
Pitch	11425	-11431	11425	-11423	11427	-11423	11427	-11423	11427	-11427	11430	-11427	-11316
Rotation	11430	-11434	11429	-11429	11429	-11429	11431	-11423	11423	-11427	11429	-11427	
Roll	0	-2	0	-2	0	0	0	-1	-1	0	1	-2	-1
Rotation	1	-2	0	-2	1	-1	0	-2	0	1	-1	-1	
Yaw	0	-2	1	-2	0	-2	-1	-3	0	-2	0	-2	-3
Rotation	1	-1	0	-1	0	-3	0	-2	0	-1	0	0	
ROLL GYRO													
Pitch	3	-4	5	-2	5	-5	2	-7	3	-7	4	-6	-7
Rotation	3	-3	4	-3	5	-4	3	-7	5	-5	6	-7	
Roll	11433	-11433	11434	-11436	11433	-11437	11436	-11437	11436	-11437	11435	-11436	-11311
Rotation	11432	-11441	11434	-11436	11434	-11435	11436	-11437	11436	-11437	11435	-11436	
Yaw	3	-1	5	-1	0	-1	2	-4	2	-3	2	-3	-3
Rotation	2	-2	[illegible]	-2	2	-4	2	-3	1	-1	2	2	
YAW GYRO													
Pitch	2	6	1	3	-1	0	1	0	-1	1	0	1	0
Rotation	3	6	0	3	-1	1	0	0	-2	1	0	0	
Roll	3	0	6	0	5	0	5	0	0	-1	4	1	-1
Rotation	[illegible]	[illegible]	0	1	5	-1	5	0	4	-1	5	[illegible]	
Yaw	11441	-11423	11439	-11434	11440	-11436	11441	-11441	11441	-11442	11440	-11442	[illegible]
Rotation	11441	-11437	11433	-11436	11441	-11433	11441	-11439	11439	-11441	11440	-11441	

TABLE 6-19

IMU DATA - VARIOUS RATES FOR 60 SECOND INTERVALS

	0°/Sec		10°/Sec		20°/Sec		30°/Sec		40° Sec		50° Sec		58° Sec	
	0°	180°	CW	CCW	CW	CCW	CW	CCW	CW	CCW	CW	CCW	CW	CCW
PITCH GYRO														
Pitch	5	5	19044	-19018	38079	-38037	57118	-57061	76146	-76080	95181	-95100	110408	-110316
Rotation	5	6	19045	-19017	38080	-38039	57113	-57062	76149	-76081	95183	-95100	110410	-110311
Roll	-3	0	-1	-1	0	-3	-1	-6	-1	1	-1	-2	1	-1
Rotation	-3	2	-1	-1	0	-1	1	-4	-1	-2	1	-1	-1	1
Yaw	-5	-3	0	-5	0	-6	2	-14	1	-17	3	-19	4	-23
Rotation	-2	-3	0	-4	3	-8	2	-11	2	-15	1	-19	4	-4
ROLL GYRO														
Pitch	2	11	16	-4	19	-13	16	-30	27	-44	38	-59	45	-67
Rotation	1	12	11	-3	20	-16	17	-29	20	-43	33	-56	52	-69
Roll	9	9	19061	-19039	38122	-38083	57167	-57116	76227	-76171	95282	-95224	110511	110439
Rotation	7	8	19062	-19039	38111	-38082	57168	-57126	76220	-76170	95282	-95224	110513	110444
Yaw	6	-3	7	-7	6	-12	9	-10	15	-18	19	-23	18	-21
Rotation	5	-5	3	-5	8	-10	11	-13	13	-17	14	-20	20	-22
YAW GYRO														
Pitch	6	15	7	9	3	8	3	6	-1	3	1	3	-2	2
Rotation	5	14	7	9	6	10	2	6	1	6	1	5	-1	5
Roll	1	11	15	1	20	-1	25	1	33	-1	39	0	47	-5
Rotation	2	11	13	-1	20	1	27	1	34	1	39	-1	47	-7
Yaw	8	9	19075	-19026	38129	-38076	57196	-57137	76234	-76170	95285	-95206	110544	-110473
Rotation	7	8	19081	-19020	38127	-38077	57142	-57135	76239	-76173	95276	-95205	110548	-110476

TABLE 6-20

SUMMARY OF GYRO CALIBRATION DATA

AXIS	AVERAGE COUNTS/REV	SCALE FACTOR MRAD/COUNT	STANDARD DEVIATION COUNTS	PER CENT OF MEAN OUTPUT
Pitch	11428.46	0.54978	1.8	0.016
Roll	11435.71	0.54944	1.9	0.016
Yaw	11438.46	0.54930	3.7	0.032

TABLE 6-21

SUMMARY OF GYRO ALIGNMENT DATA

GYRO IA AXIS	MISALIGNMENT IN MILLIRADIANS RELATIVE TO		
	U AXIS	V AXIS	W AXIS
Pitch	0.456	N.A.	-0.080
Roll	N.A.	0.055	0.255
Yaw	0.182	0.087	N.A.

6.5.5 ACCELEROMETER CALIBRATION

Accelerometer calibration data is recorded in Table 6-23. This data was recorded at the same time as the gyro data with the rate table stationary and level.

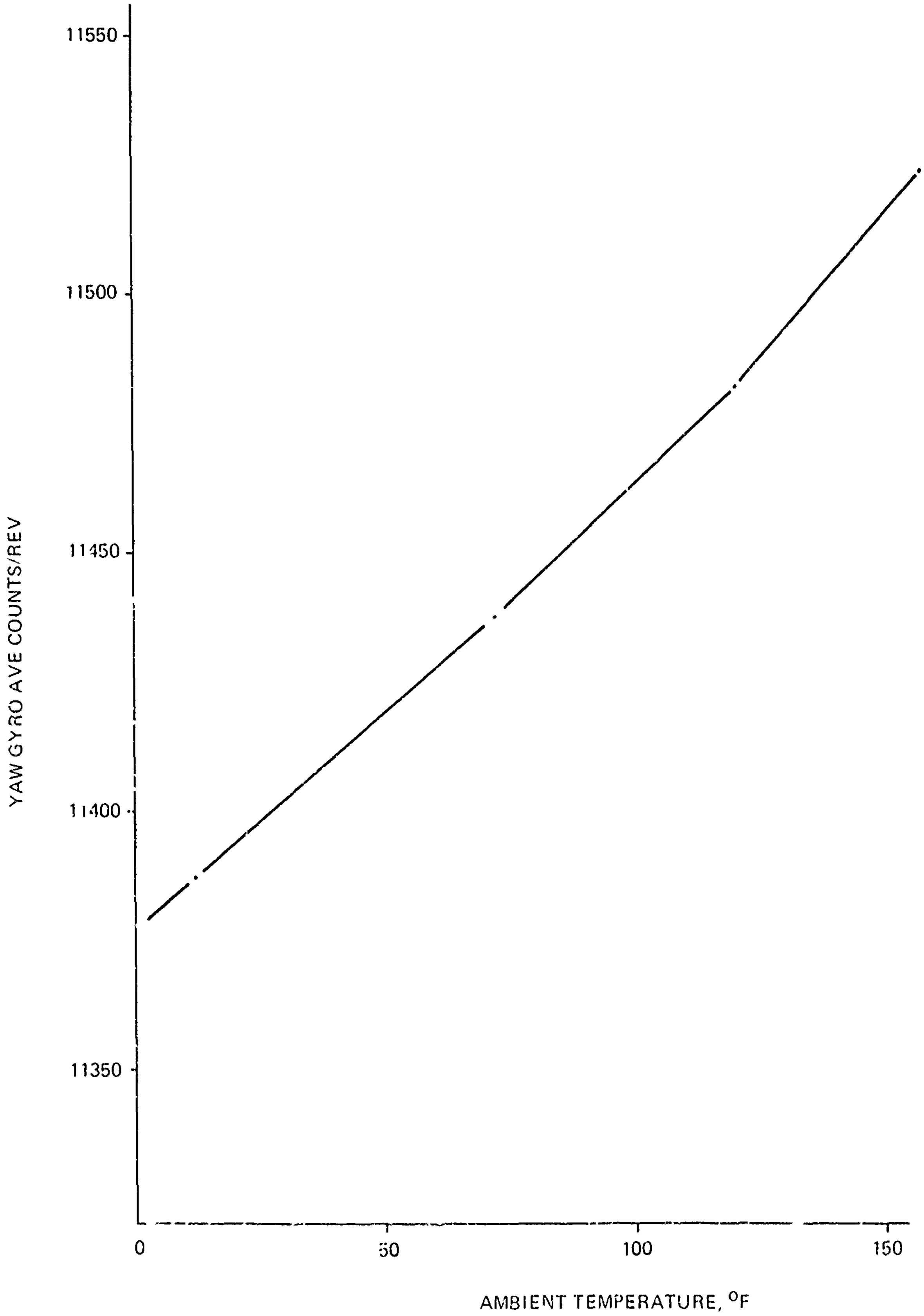

Figure 6-6. Yaw Gyro Average Counts/Rev at 15°/Sec vs Temperature

TABLE 6-22

IMU DATA - BUFFERED ACCELEROMETER OUTPUTS (VOLTS)

	U	V	W
Pitch Axis Vertical	.0033	-2.204	.0081
Roll Axis Vertical	-2.185	- .0018	.0073
Yaw Axis Vertical	.0072	- .0045	-2.201

Section 7

ELECTROMAGNETIC INTERFERENCE REPORT

7.0 INTRODUCTION

This section is a summary of the design criteria for meeting the electromagnetic interference requirements of the CLFCS, specifically to meet the requirements of MIL-I-6181. Experience was drawn from the design critieria and resulting performance of the Multi-Weapon Fire Control System, another armed helicopter contract with Frankford arsenal. Although no EMI testing was required on the CLFCS contract, the contractor is confident that the CLFCS will meet the customer's requirements.

7.1 GROUNDING SYSTEM

7.1.0 PHILOSOPHY

A uni-point ground system, which isolates all subsystem grounds from each other, was chosen by the contractor for the Closed Loop Fire Control Subsystem. The primary power ground is isolated from the secondary power or circuit ground. All the individual ground systems are treated as branches from a central ground point. The central ground point for the CLFCS was selected as a bus bar located beneath the CLFCS circuit breakers mounted to the right of the pilot's seat. This is the only location in the system where the individual ground systems are connected together. Therefore, the only coupling that exists between the individual ground systems is capacity coupling.

Since each ground system is floating above the central ground point, the impedance of this connection is the only impedance which is common to all of them. Current flow through this common impedance causes all systems to rise or fall relative to absolute "zero" volts. Therefore, the entire system sees only a change in the absolute zero voltage level, which has no effect on the operation of the system.

The uni-point ground system has the advantage of ground loop control. A complete ground system can be checked for isolation from all other ground systems by lifting the single point ground connection. Ground loop paths can still occur, however, through the capacity of filters, etc.

A disadvantage to this technique occurs if one particular package does not adhere to the uni-point ground system, since all the rest of the systems current flow in the overall ground system can pass through its multi-point grounds. This has been the case in the CLFCS, where part of the system already existed and is not of the uni-point ground design. This problem is aleviated by the use of differential input analog buffer amplifiers in the Computer Interface Unit (CIU), where the impedance connecting two grounds is substantially high so as to minimize loop current. The CIU analog outputs present a problem, however, because the turret presents a single input load, and it becomes necessary to connect the return signals to ground, although the high side of the output signals are capacitively coupled to their respective loads.

7.1.1 A.C. POWER GROUND

The A.C. primary power is grounded at its source. Isolation from the secondary power is maintained by transformers. Power line filters are used in both the high side and the return side of the input power.

7.1.2 D.C. POWER GROUND

The D.C. primary power is also grounded at its source. It is isolated from other ground systems, and is filtered with a line filter as well as is the hot line. Number 16 wire is used to adequately carry the 3 amp input current.

7.1.3 D.C. SECONDARY GROUND

The D.C. secondary ground system is isolated from the D.C. primary ground by virtue of transformers in the power supply chopper circuit. Line filters are placed at the output of the power supply, to attenuate noise produced by the chopper.

The analog signal lines are differential pair inputs where possible, with the return grounded at the source's D.C. secondary ground bus.

Digital signals transmitted outside an LRU are in complementary format in line driver/receiver pairs, so that neither line is grounded, and good LRU isolation is maintained.

7.1.4 ANALOG SHIELD GROUNDS

Shields are used on susceptible analog circuit connecting lines for protection against cross-talk in the cables. The shields are grounded to chassis ground at the source end only, which eliminates conduction of low frequency currents through the shield. The analog shields are otherwise isolated from each other, and are carried to, but not connected to, the chassis in which the load resides. In the case of the low level gyro error signals, the signals are further protected by carrying the shield through the LRU connectors and into the chassis to as close as possible to their respective source and load circuits.

7.1.5 INTERFERENCE SHIELDS

Interference shields are required for digital signals transmitted between LRU's to prevent radiation of high frequency interference from the interconnecting lines. The shield grounds are connected to chassis ground at both ends of the cable, and the shield is considered to be an extension of the chassis.

7.2 SUPPRESSION DEVICES

7.2.1 LINE FILTERS

Line filters specified as attenuating radio frequency interference by 70 db were utilized in conditioning the D. C. and A. C. primary power to the LRU's, as well as the D. C. secondary power from the modular, chopper power supply. Control lines brought into the power supply cavity to operate relays were also conditioned by line filters.

7.2.2 DECOUPLING CAPACITORS

In the Computer Interface Unit large electrolytic capacitors were placed across the individual D. C. secondary power supply buses to signal ground. These help absorb any surge loads that should occur, although their primary use is to hold up the secondary lines during power shutdown for a long enough period (50 us) for the processor to properly shut down without destroying memory.

For each printed circuit wiring board, each secondary power connection typically has one 3.3 μf tantalum and ten 0.1 uf ceramic capacitors to decouple a wide range of frequencies. The tantalum is placed at the bottom of the board as near as possible to the connector input power pins, and the ceramics are distributed evenly about the board. Critical analog circuits are protected by R-C networks which further isolate power connections to the amplifiers.

Decoupling networks of the R-C type are used across switch contacts that are activated during a target engagement episode. Discretes for infrequently changing signals such as mode control, etc., are not protected.

7.2.3 DIODE SUPPRESSION

Transients from the switched inductive loads of relay coils are suppressed by placing a diode directly across the coil. When the source voltage is removed from the coil, a back EMF is generated, but this reverse voltage is clamped to about -0.5 volts by the diode, which circulates the coil discharge current until the energy is dissipated as heat in the coil. If it were not for the diode, a -150 to -200 volt surge with high frequency content would occur.

The diode delays the actual drop-out of the relay by a few milliseconds, but this is not a problem in this application.

7.3 CABLE DESIGN

The signal cables are grouped according to their interference and susceptibility levels. Within the chassis, the secondary power lines run perpendicular to the signal lines, and the digital lines are clustered next to the power bus, while the analog lines are clustered separately on the opposite side of the chassis. Analog lines are twisted pairs, as are digital signals leaving the LRU. All lines are maintained close to the chassis so that capacitive coupling will reduce the radiation capability.

The signal grouping is carried on into the LRU connectors. Sub-groups of nearby pins are chosen, to the extent that pins for shields are chosen to segregate the sub-groups from each other, thus reducing possible crosstalk. Where twisted pairs exist within the chassis, twisted shielded pairs exist in the cables, with shield grounding rules following that of paragraphs 7.1.4 and 7.1.5.

7.4 PACKAGE SHIELDING

Each LRU of the CLFCS is essentially a closed package of sheet aluminum, which will give adequate shielding of the electric fields that may be present either within or without the LRU.

Metal RFI gaskets, wide flanges with indentations, and adequate attachment of hardware reduce any leakage through the seams of the covers.

Perforated screens provide an air opening for the power supply cooling fan. The perforations result in a reduced opening size, which allows the intercepted electromagnetic wave to be conducted to the chassis. Critical leads are routed away from these openings to reduce a direct radiation path.

Test connectors exist on the CIU and the IMU Electronics. During normal operation a metal dust cap is attached to the test connectors to seal off this path of radiation.

7.5 SPECIAL CIRCUITS

7.5.1 INTERFACE CIRCUITS

Where digital information flows between LRU's, a high degree of isolation is obtained by the use of line driver/receiver pairs, which use complementary pair signals. For receivers in the CIU which connect to the peripheral equipment, a control line is used to disable them during normal flight operation, so that they will not ambiguously detect the open input lines.

The analog inputs to the CIU are differentially received to limit ground loops and buffered to isolate the time variable (chopping) A/D input impedance. The signals are filtered with a bandpass of 3 Hz, well below the A/D sampling rate of 30 Hz.

The CIU analog output is a capacitively coupled A. C. signal sent to the turret subsystem.

7.5.2 POWER SUPPLY MONITOR

The CIU contains a power supply monitor circuit which properly initializes or shuts down the CDC 469 processor during turn-on or power off operations.

In particular, during shutdown, the monitor circuit allows the processor to complete the present instruction and shutdown without losing memory. At power on, the monitor also detects whether the power interruption was for more or less than 2 seconds, and accordingly selects an alternate starting address for the resumption of operation.

7.5.3 GYRO SERVO AMPLIFIER

The demodulator of the gyro servo amplifier uses a sampling time which is out of phase with the motor switching transients, thus giving itself a relatively noise free operational environment.

Section 8
RELIABILITY REPORT

8.1 RESULTS

A reliability prediction has been computed for each of the three major assemblies of the Closed Loop Fire Control System. The total subsystem failure rate resulted in 1329.9 failures per 10^6 hours, or 751.9 hours MTBF.

8.2 ASSUMPTIONS

All units will be on board an AH-1G helicopter for the purpose of feasibility testing of the closed loop fire control concept. The Computer Interface Unit and the Inertial Measurement Unit are airborne inhabited, the IMU Electronics Assembly is airborne uninhabited. A maximum component temperature of 80°C is assumed.

For the purpose of reliability study, a generic parts list is utilized to assign failure rates based upon the listings of MIL-Handbook-217B, Section 3, with the exeception of assigned failure rates noted in the tabulation.

The government furnished CDC 469 processor, which is a part of the Computer Interface Unit, is not included within the reliability analysis.

8.3 DISCUSSION OF RESULTS

The resulting subsystem failure rate of 1329.9 failures per 10^6 hours (751.9 hours MTBF) represents a "conservative" predicition. Had detailed component temperature and electrical stress data been available, the indicated failure rates might have been less since the generic failure rates of MIL-Handbook-217B, Section 3, are average case condition.

8.4 ANALYSIS

The method of Parts Count Reliability Prediction was used to determine the results. The general expression for equipment failure rate with this method is

$$\lambda_{EQUIP} = \sum_{i=1}^{i=1} N_i (\lambda_G \pi_Q)_i$$

for a given equipment environment where:

λ_{EQUIP} = total equipment failure rate (failures 10^6 hr.)

λ_G = generic failure rate for the ith generic part (failures 10^6 hr.)

π_Q = quality factor for the ith generic part

N_i = quantity of ith generic part

n = number of different generic part categories.

8.4.1 COMPUTER INTERFACE UNIT

The required information for determining the failure rate of the Computer Interface Unit is tabulated in Table 8-1. For the 35 items.

$$\lambda_{EQUIP} = 606.3 \ f/10^6 \text{ hours.}$$

or MBTF = 1649.4 hours.

The parts count is

$$\sum_{i=1}^{i=35} N_i = 1006.$$

and therefore the failure rate per part is

$$\frac{\lambda_{EQUIP}}{\Sigma N_i} = 0.603 \ f/10^6 \text{ hours. part.}$$

8.4.2 IMU ELECTRONICS ASSEMBLY

The required information for the IMU Electronics Assembly is in Table 8-2, and

$$\lambda_{EQUIP} = 566.0 \ f/10^6 \text{ hours,}$$

$$\text{MBTF} = 1766.8 \text{ hours,}$$

$$\sum_{i=1}^{i=31} N_i = 739,$$

and

$$\frac{\lambda_{EQUIP}}{\Sigma N_i} = 0.766 \ f/10^6 \text{ hours/part}$$

8.4.3 INERTIAL MEASUREMENT UNIT

The required information for the Inertial Measurement Unit is in Table 8-3, and

$$\lambda_{EQUIP} = 157.6 \ f/10^6 \text{ hours,}$$

$$\text{MTBF} = 6345 \text{ hours,}$$

$$\sum_{i=1}^{i=13} N_i = 95 \text{ parts,}$$

and

$$\frac{\lambda_{EQUIP}}{\Sigma N_i} = 0.723 \ f/10^6 \text{ hours/part.}$$

8.4.4 TOTAL SUBSYSTEM

The total prediction for the 3 assemblies is

$$\lambda \text{ EQUIP} = 1329.9 \text{ f}/10^6 \text{ hours,}$$

$$\text{MBTF} = 751.9 \text{ hours,}$$

$$\sum_{i=1}^{i=79} N_i = 1840 \text{ parts,}$$

and

$$\frac{\lambda \text{ EQUIP}}{\Sigma \quad N_i} = 0.723 \text{ f}/10^6 \text{ hours/part.}$$

TABLE 8-1
COMPONENT FAILURE RATES FOR THE COMPUTER INTERFACE UNIT

ITEM i	QTY N	FAMILY	π_Q	λ	N_λ
1	8	Connector Sets - 70 Pin PW BD, Airborne, Solder Cup	1.0	1.7	13.6
2	9	Double Sided Printed Wire Board	1.0	.024	.216
3	24	Linear Microckt, Military	5.0	.24	28.8
4	14	Linear Hybrid Microckt, Military	5.0	.27	18.9
5	61	TTL Microckt, 5400 Series	5.0	.14	42.7
6	81	CMOS Microckt, 54C00 Series	5.0	.14	56.7
7	1	CMOS Multiplexer, H1506A	5.0	.14	.70
8	3	CMOS D/A Conv., MN412H	5.0	.14	2.1
9	1	TTL A/D Conv., MN5205H	5.0	.14	.70
10	6	FIFO Memory Microckt - AM2812ADM	5.0	.99	29.7
11	1	C0-238A 3 MHz XTAL Oscillator	1.0	.2	.2
12	16	NPN Transistor - Jan	1.0	2.0	32.0
13	5	PNP Transistor - Jan	1.0	3.2	16.0
14	25	Diode - Jan	1.0	1.6	40.0
15	21	Capacitor, M39003/01-, Level m	1.0	.26	5.46
16	2	Capacitor, M39003/02-, Level m	1.0	.26	.52
17	12	Capacitor, M39014/01-, Level m	1.0	.11	1.32
18	183	Capacitor, M39014/02-, Level m	1.0	.11	20.1
19	5	Capacitor, M39018/01-, Level m	1.0	6.9	34.5
20	1	Capacitor, Polycarbonate	1.0	.012	.012
21	263	Resistor, RCR07G	1.0	.018	4.73
22	257	Resistor, RNC55H	1.0	.063	14.3
23	2	Trimpot, RJ26FX102	1.0	27.0	54.0
24	1	Connector, 25 Pin Micro-dot	1.0	1.7	1.7
25	2	Connector, 51 Pin Micro-dot	1.0	1.7	3.4
26	1	Panel Connector, 10 Pin	1.0	1.7	1.7
27	4	Panel Connector, 55 Pin	1.0	1.7	6.8
28	17	Power Cube Module	1.0	5.0	85.0
29	1	Magnetic Demod 930C725P1	1.0	20.0	20.0
30	1	Time Meter MS17321-10	N.A.	N.A.	N.A.

TABLE 8-1. (Continued)

ITEM i	QTY N	FAMILY	π_Q	λ	N_λ
31	2	EMI Filter - 28 VDC Feed Thru, 539D919P5	1.0	.11	.22
32	2	EMI Filter - 115 VAC Feed Thru	1.0	.11	.22
33	2	Power Relay, 539D940P2	1.0	5.7	11.4
34	1	Fan, 115 VAC 400 Hz, 11 Watt	1.0	50.0	50.0
35	1	Thermal Switch	1.0	8.6	8.6

TABLE 8-2. COMPONENT FAILURE RATES FOR THE IMU ELECTRONICS ASSY

ITEM i	QTY N	FAMILY	π_Q	λ	N_λ
1	6	Connector Sets - 70 Pin PW BD, Solder Cup Airborne	1.0	1.7	10.2
2	7	Double Sided Printed Wire Board	1.0	.024	.168
3	17	Linear Microckt, Military	5.0	.24	20.4
4	5	TTL Microckt, 5400 Series	5.0	.14	3.5
5	75	CMOS Microckt, 54C00 Series	5.0	.14	52.5
6	1	C0-238A\ 4 MHz XTAL Oscillator	1.0	.2	.2
7	25	NPN Transistor - Jan	1.0	2.0	50
8	48	PNP Transistor - Jan	1.0	3.2	153.6
9	51	Diode - Jan	1.0	1.6	81.6
10	28	Capacitor, M39003′01-, Level m	1.0	.26	7.28
11	28	Capacitor, M39014 01-, Level m	1.0	.11	3.08
12	85	Capacitor, M39014, 02-, Level m	1.0	.11	9.35
13	4	Capacitor, M83421.′01-, Level m	1.0	.012	.048
14	145	Capacitor, RCR07G	1.0	.018	2.61
15	157	Resistor, RN55H	1.0	.063	9.891
16	9	Resistor, RNC70H	1.0	.063	.567
17	2	Resistor, RWR 81S2R21FM	1.0	.26	.52
18	15	Power Cube Module	1.0	5.0	75
19	1	Time Meter MS17321-10	N.A.	N.A.	N.A.
20	2	EMI Filter - 28 VDC Feed Thru, 539D919P5	1.0	.11	.22

TABLE 8-2. (Continued)

ITEM i	QTY N	FAMILY	π_Q	λ	N_λ
21	2	Power Relay, 539D940P2	1.0	5.7	11.4
22	1	Fan, 115 VAC 400 Hz, 11 Watt	1.0	50	50
23	1	Thermal Switch	1.0	14	14
24	12	Resistor RNC65H	1.0	.063	.756
25	1	Capacitor, Polycarbonate	1.0	.012	.012
26	6	Fuse, GEA 6/10	1.0	.10	.6
27	1	Connector, 22 Pin, MS27508E12B22S	1.0	1.7	1.7
28	1	Connector, 10 Pin, MS27508E12B98PA	1.0	1.7	1.7
29	1	Connector, 37 Pin, MS27508E14B37P	1.0	1.7	1.7
30	1	Connector, 26 Pin, MS27508E16B26S	1.0	1.7	1.7
31	1	Connector, 42 Pin, MS27508E16B42S	1.0	1.7	1.7

TABLE 8-3

COMPONENT FAILURE RATE . OR THE INERTIAL MEASUREMENT UNIT

ITEM i	QTY N	FAMILY	π_Q	λ	N_λ
1	1	Printed Wire Board - Single Side	1.0	.012	.012
2	6	Linear Microckt, Military	5.0	.24	7.20
3	24	Capacitor, M39014/02-, Level m	1.0	.11	2.64
4	6	Capacitor, M39014/01-, Level m	1.0	.11	.66
5	2	Capacitor, M39003/01-, Level m	1.0	.26	.52
6	3	Capacitor, MC71A3R3K	1.0	.11	.33
7	24	Resistor, RNC55H	1.0	.063	1.51
8	18	Resistor, RCR07G	1.0	.018	.324
9	1	Connector, 22 Pin, MS27508E12B22P	1.0	1.7	1.7
10	1	Connector, 37 Pin, MS27508E14B37P	1.0	1.7	1.7
11	3	Connector, 17 Pin, Matrix Science 90231-17	1.0	1.7	5.1
12	3	Gyro Assy, Honeywell GG1111LC02*	1.0	42.5	127.5
13	3	Accelerometer, Sundstrand QA-1000-S5**	1.0	2.8	8.4

* Supplier supplied Failure Rate 42.5 f/10^6 hours.

** Accelerometer Failure Rate Assigned 2.8 f/10^6 hours.

APPENDIX A

KALMAN ESTIMATOR TERMINOLOGY
PROCESS EQUATIONS
AND
COMPUTATIONAL FLOW

A.1 LIST OF DEFINITIONS

k = CURRENT COMPUTER FRAME DESIGNATOR

Δt = LENGTH OF EACH COMPUTATIONAL FRAME (SEC)

t = $k \Delta t$

= DURATION OF ESTIMATOR OPERATION MEASURED FROM THE INITIATION OF THE FIRST FRAME TO THE CLOSE OF THE kth FRAME

x_k = TRUE STATE VECTOR FOR FRAME k HAVING $m \times 1$ ELEMENTS

y_k = ACTUAL OBSERVATIONS RECEIVED DURING FRAME k HAVING $n \times 1$ ELEMENTS

u_k = RANDOM STATE EXCITATION FOR FRAME k OF DIMENSION $\leq m$

v_k = RANDOM OBSERVATION NOISE FOR FRAME k OF DIMENSION $\leq n$

Φ = STATE TRANSITION PROCESS FUNCTIONAL CONSISTING OF m EQUATIONS CONNECTING x_{k+1} TO x_k

A = LINEARIZED STATE TRANSITION MATRIX HAVING $m \times m$ ELEMENTS

$$\begin{bmatrix} \frac{\partial \Phi_1}{\partial x_1} & \frac{\partial \Phi_1}{\partial x_2} & \cdots & \frac{\partial \Phi_1}{\partial x_m} \\ \frac{\partial \Phi_2}{\partial x_1} & \frac{\partial \Phi_2}{\partial x_2} & \cdots & \frac{\partial \Phi_2}{\partial x_m} \\ \vdots & \vdots & & \vdots \\ \frac{\partial \Phi_m}{\partial x_1} & \frac{\partial \Phi_m}{\partial x_2} & \cdots & \frac{\partial \Phi_m}{\partial x_m} \end{bmatrix}$$

B = STATE EXCITATION PROPAGATION MATRIX

Γ = STATE TO OBSERVATION CONVERSION PROCESS FUNCTIONAL

C = LINEARIZED STATE TO OBSERVATION CONVERSION MATRIX HAVING n x m ELEMENTS

$$\begin{bmatrix} \frac{\partial \Gamma_1}{\partial x_1} & \frac{\partial \Gamma_1}{\partial x_2} & \cdots & \frac{\partial \Gamma_1}{\partial x_m} \\ \frac{\partial \Gamma_2}{\partial x_1} & \frac{\partial \Gamma_2}{\partial x_2} & \cdots & \frac{\partial \Gamma_2}{\partial x_m} \\ \vdots & \vdots & & \vdots \\ \frac{\partial \Gamma_n}{\partial x_1} & \frac{\partial \Gamma_n}{\partial x_2} & \cdots & \frac{\partial \Gamma_n}{\partial x_m} \end{bmatrix}$$

D = OBSERVATION NOISE PROPAGATION MATRIX

K = COVARIANCE MATRIX FOR u_k

L = COVARIANCE MATRIX FOR v_k

$\hat{x}_k$ = ESTIMATED STATE FOR FRAME k

$\bar{x}_{k+1}$ = EXPECTED OR FORECAST STATE FOR FRAME k+1

$\bar{y}_k$ = EXPECTED OBSERVATIONS = $\Gamma(\bar{x}_k)$

z_k = INNOVATION = $y_k - \bar{y}_k$

Q_k = COVARIANCE MATRIX FOR z_k

G_k = GAIN MATRIX

$\Delta\hat{x}_k$ = ERROR IN ESTIMATED STATE = $\hat{x}_k - x_k$

$\hat{P}_k$ = COVARIANCE MATRIX FOR $\Delta\hat{x}_k$

$\Delta\bar{x}_{k+1}$ = ERROR IN EXPECTED STATE = $\bar{x}_{k+1} - x_{k+1}$

$\bar{P}_{k+1}$ = COVARIANCE MATRIX FOR $\Delta\bar{x}_{k+1}$

A.2 PROCESS EQUATIONS

TRUE STATE PROCESS - $x_{k+1} = \Phi(x_k) + Bu_k$

OBSERVATION PROCESS - $y_k = \Gamma(x_k) + Dv_k$

ESTIMATION PROCESS - $\bar{y}_k = \Gamma(\bar{x}_k)$

$z_k = y_k - \bar{y}_k$

$\hat{x}_k = \bar{x}_k + G_k z_k$

$\bar{x}_{k+1} = \Phi(\hat{x}_k)$

ESTIMATION ERROR COVARIANCE - $\hat{P}_k = (I - G_kC)\bar{P}_k(I - G_kC)^T + G_kDLD^TG_k^T$

$\bar{P}_{k+1} = A\hat{P}_kA^T + BKB^T$

INNOVATION COVARIANCE - $Q_k = C\bar{P}_kC^T + DLD^T$

KALMAN GAIN MATRIX - $G_k = \bar{P}_kC^TQ_k^{-1}$

A.3 ESTIMATOR COMPUTATIONAL FLOW

k = CURRENT FRAME DESIGNATOR

k+1 = SUBSEQUENT FRAME DESIGNATOR

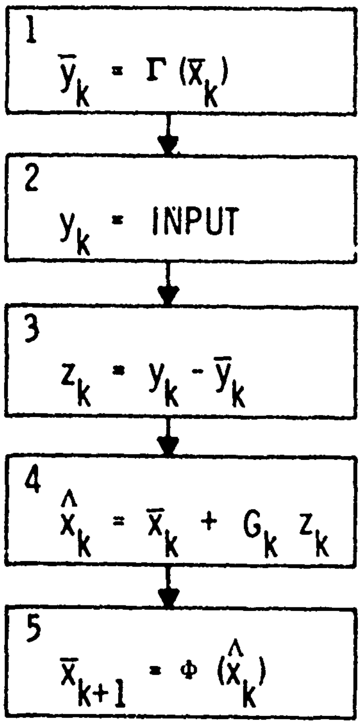
1
$\bar{y}_k = \Gamma(\bar{x}_k)$
2
y_k = INPUT
3
$z_k = y_k - \bar{y}_k$
4
$\hat{x}_k = \bar{x}_k + G_k z_k$
5
$\bar{x}_{k+1} = \Phi(\hat{x}_k)$

EXPECTED OBSERVATIONS FOR FRAME k

OBTAIN ACTUAL OBSERVATIONS FROM INPUT BUFFERS

INNOVATION VECTOR FOR FRAME k

NEW ESTIMATED STATE FOR FRAME k

EXPECTED STATE FOR ENTRY INTO FRAME k+1

A.4 GAIN COMPUTATIONAL FLOW

k = CURRENT FRAME DESIGNATOR
k+1 = SUBSEQUENT FRAME DESIGNATOR

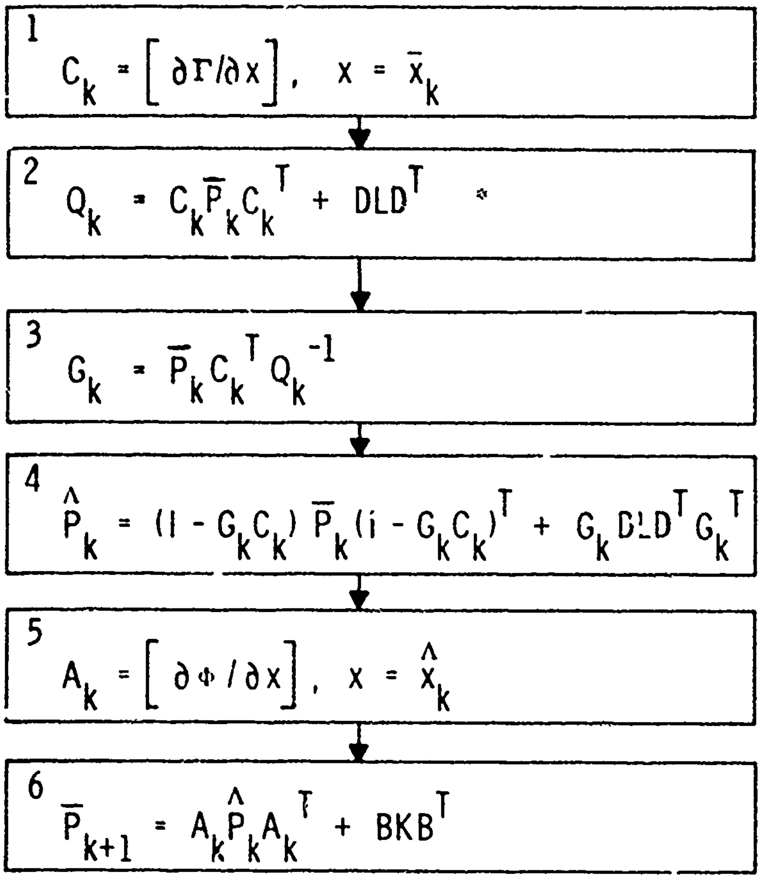

1 $C_k = \left[\partial r/\partial x\right], \quad x = \bar{x}_k$ CONVERSION MATRIX

2 $Q_k = C_k\bar{P}_kC_k^T + DLD^T$ * INNOVATION COVARIANCE

3 $G_k = \bar{P}_kC_k^TQ_k^{-1}$ GAIN MATRIX

4 $\hat{P}_k = (I - G_kC_k)\,\bar{P}_k(I - G_kC_k)^T + G_kDLD^TG_k^T$ FILTERED STATE ERROR COVARIANCE

5 $A_k = \left[\partial\Phi/\partial x\right], \quad x = \hat{x}_k$ TRANSITION MATRIX

6 $\bar{P}_{k+1} = A_k\hat{P}_kA_k^T + BKB^T$ EXPECTED STATE ERROR COVARIANCE

---

* $\bar{P}_1$ DEFINED TO INITIATE GAIN COMPUTATION.

A.5 DISCUSSION

The separation of the computational flows for the estimator and gain algorithms in Section A.3 and A.4 is significant in relation to an airborne computer mechanization. The source of the gain matrix G_k utilized in Step 4 of the estimator algorithm may be any one of the following:

- A fixed gain matrix, computed in non-real time according to Section A.4 until the steady-state values are reached. These are then stored in the airborne computer's memory.
- An explicitly varying gain matrix, developed by fitting a non-real time computation of the Kalman gains according to Section A.4. The empirical relations for generating the approximate time-varying gain elements would be mechanized in the airborne computer.
- A Kalman gain matrix, computed in real-time according to Section A.4, but possibly at a reduced update rate.

Computing the Kalman gain matrix in real-time but at a reduced update rate in comparison with the main frame rate of the airborne computer distributes the time consuming covariance propagation algorithms of Section A.4 over several main frame iterations. The result is potentially a significant reduction in computational burden at the expense of a minor sacrifice in accuracy. This is due to the fact that the dynamics of the gain process are frequently slow in comparison with the computer bandwidth appropriate to a fire control problem.

Figure A-1 illustrates in block diagram form the estimator computational flow. It is noted that the outputs for computer frame k include both the filtered state array, $\hat{x}_k$, and the expected or forecast state array, $\bar{x}_{k+1}$. Figure A-2 presents a partial time-line of events in successive frames k and k+1. The numbers in the segments of frame k refer to the steps in the estimator algorithm shown in Section A.3. The output $\hat{x}_k$ is linked in time to the occurrence of Step 2, when the airborne computer's input buffers are filled with new sensor data. It is assumed that the length of time actually required for this operation is very short in comparison with the frame length, Δt, so that the observations y_k can be regarded as pertaining to a specific instant of time. Likewise, the output $\bar{x}_{k+1}$, also available during the kth frame, is linked to the observation input event in frame k+1. This places in evidence the fact that interpolation between $\hat{x}_k$ and $\bar{x}_{k+1}$ can potentially realize a state output x_k^* with optimum phasing for control purposes.

$$x_k^* = (1-\alpha)\,\hat{x}_k + \alpha\,\bar{x}_{k+1}$$

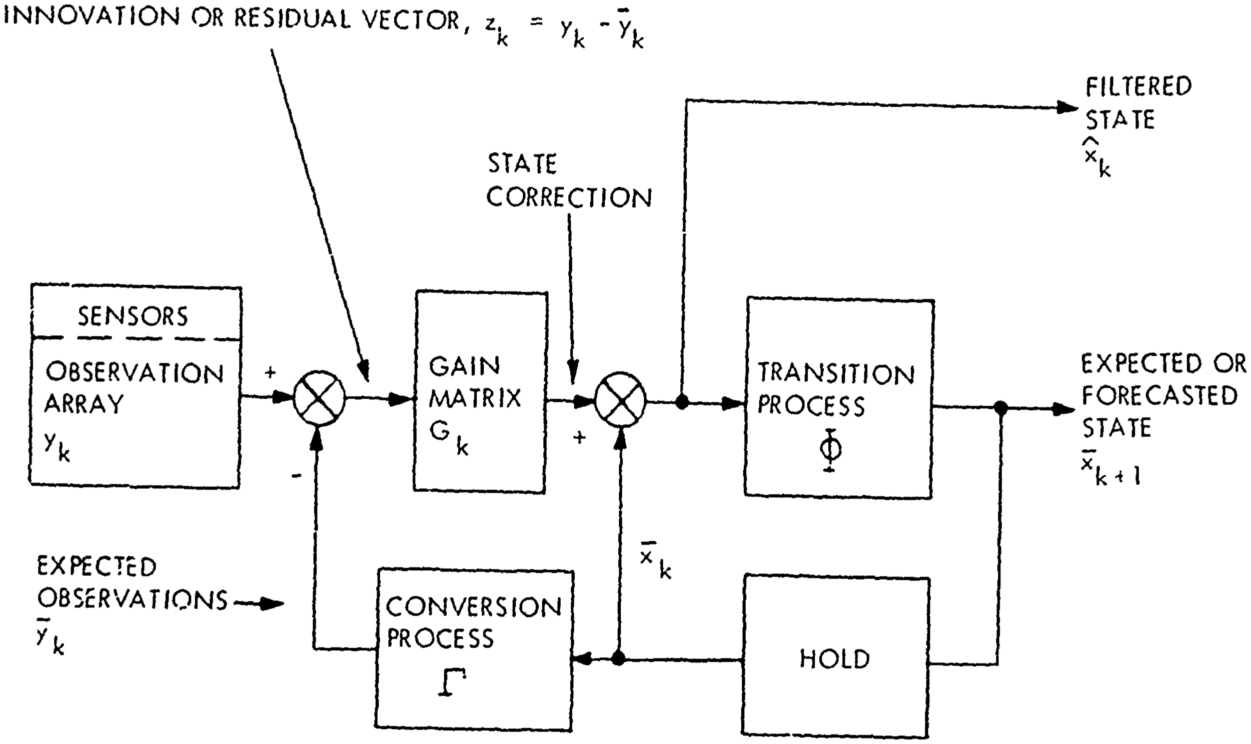
INNOVATION OR RESIDUAL VECTOR, $z_k = y_k - \bar{y}_k$
FILTERED STATE $\hat{x}_k$
STATE CORRECTION
SENSORS
OBSERVATION ARRAY y_k
+
-
GAIN MATRIX G_k
+
TRANSITION PROCESS Φ
EXPECTED OR FORECASTED STATE $\bar{x}_{k+1}$
$\bar{x}_k$
EXPECTED OBSERVATIONS $\bar{y}_k$
CONVERSION PROCESS Γ
HOLD

Figure A-1. Kalman Estimator Block Diagram

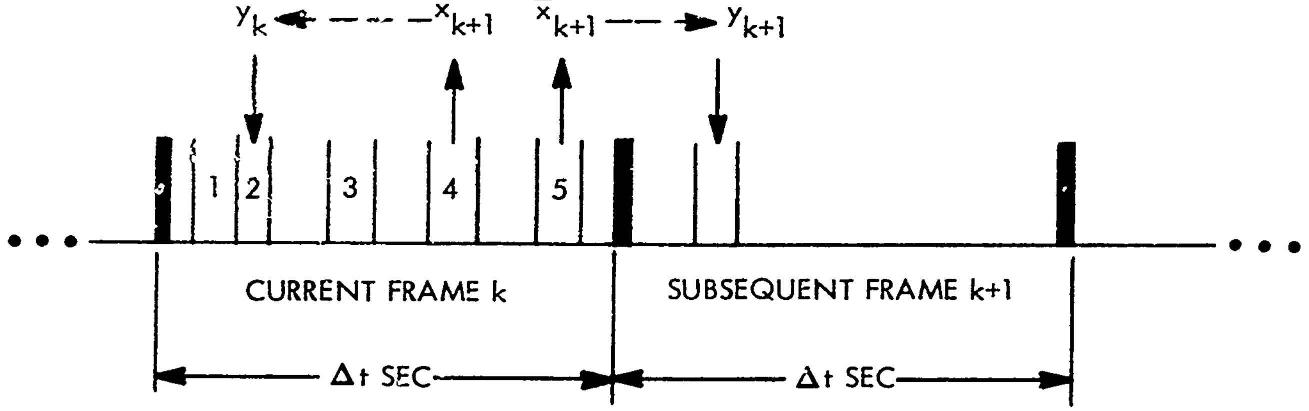

y_k
$\hat{x}_{k+1}$
$\bar{x}_{k+1}$
y_{k+1}
1
2
3
4
5
CURRENT FRAME k
SUBSEQUENT FRAME k+1
Δt SEC
Δt SEC

Figure A-2. Illustration of Computer Frame Timing

APPENDIX B

KALMAN ESTIMATOR ANALYSIS PROGRAM (KEAP-II)

The Kalman Estimator Analysis Program, KEAP-II, is an analytic tool for evaluating the performance of a state estimation system, using the Kalman estimation technique. It can be used to generate the time histories of the state estimates and predict the statistical accuracy of these estimates. It uses a discrete form of the extended, or nonlinear Kalman equations. A perturbation method is used to generate the local derivatives of the state transition and state to observation conversion processes when they cannot be assumed to be constant.

The program permits switching between two or more modes of operation in any sequence desired. Such modes can represent, for example, loss of sensor signals, change in sensor noise characteristics, cyclic computation changes, change of basic configuration, etc. In addition, provision is made for calculating the estimator gains at a lower frequency than the estimation frequency. In this case, the propagation of the estimation error continues at the higher rate, showing the build up of error.

In many cases, the primary output of interest is the computed error variance or RMS error. Provision is made to use true state in the determination of the transition function derivatives if desired. In this manner, the error variance is typical of an ensemble of runs, having the true state as a mean. In such use, the estimate of state time histories are primarily of value in determining the settling of initial conditions.

The noise characteristics of states and observations can be simulated by augmenting the state vector with auxiliary states, which are then used to shape the white noise to the proper frequency spectrum via digital filtering techniques.

The program is written in FORTRAN IV for the HIS 600/6000 computers. It makes extensive use of variable dimensioning in the subroutines to save computer core as different sizes of systems are evaluated. A special set of subroutines for matrix and vector operations, including variable format matrix read and write, are provided. Extensive optional printout is available during initial runs of a new problem, as well as a special summary printout of time histories in simplified form. Detailed printouts can be obtained at any point or series of time points and can include the complete gain and covariance matrices. Printout identification can be specified in common words as desired.

The specific system being evaluated is defined by FORTRAN statements inserted into four subroutines. Subroutine PHIF contains the definition of the state transition process, or the predicted transition from one point in time to the next point in time. Subroutine GAMMAF contains the expressions defining the predicted observation values in terms of the current estimates of the states. Subroutine YF includes equations defining the true observations as functions of the true states, and subroutine XTF contains the definition of the values of the true states as functions of previous values of true state and time.

The basic program can be modified to evaluate non-optimal gain systems by minor revisions to the main program, describing the desired gains.

APPENDIX C

HELICOPTER FLIGHT PATH SIMULATION

As part of the analysis of the CLFCS aircraft and target state estimators, and also in support of the checkout of the CDC 469 computer software, the generation of the ideal aircraft and target states versus time for straight-line and veer-off engagements was desired. There follows a listing of the Computer Program "TPATH" written for this purpose. In Table C-1 are listed the values of the ideal state components versus time for the two target engagements described in Section 2.3.3 (see Table 2-9).

TABLE C-1

TABULATION OF IDEAL AIRCRAFT AND TARGET STATES VS TIME

Time (sec)	ω_u (mrad/sec)	ω_v (mrad/sec)	ω_w (mrad/sec)	a_u (ft/sec^2)	a_v (ft/sec^2)	a_w (ft/sec^2)	V_u (ft/sec)	V_v (ft/sec)	V_w (ft/sec)	z_u (mrad)	z_v (mrad)	z_w (mrad)	s_u (mrad)	s_v (mrad)	s_w (mrad)	R (kft)	Total LOS Angle (deg)	Altitude (ft)	Yaw Path Angle (deg)	Pitch Path Angle (deg)
21	0	0	0	0	0	0	199.2	0	17.6	- 88.1	0	996.1	956.1	-292.8	- .040	5.93	17.0	500	-10.0	0
24	-125.5	-26.4	26.4	1.64	7.54	5.48	200.5	0	18.0	- 74.1	- 86.4	993.5	940.6	-335.3	- 53.1	5.36	19.8	501	-11.3	0.8
27	- 18.3	-49.9	49.9	2.95	10.9	10.9	210.9	0	21.0	21.9	-316.1	948.5	837.7	-461.8	-291.5	4.82	33.1	540.5	-21.8	6.59
28	- 7.43	-50.0	50.0	2.88	10.9	11.2	214.9	0	22.3	53.0	-329.3	942.7	780.5	-515.5	-353.6	4.65	38.7	568.9	-25.6	8.56
30	- 1.61	-50.0	50.0	2.75	11.2	11.6	222.6	0	25.0	113.0	-345.0	931.8	631.4	-619.9	-465.3	4.36	50.8	549.4	-33.2	12.4

```
C     CLFCS TEST FLIGHT PATH GENERATION          4/10/76        REM
C         BASED ON PROGRAM PBPATH OF 1/17/75
C
C     NOTE BASIC CONCEPT  OUTPUT AT TIME T IS STATUS AT THAT TIME.
      REAL K,M1,M2,M3,M
      DIMENSION X(16),GY(3),SF(3),EF(4),SC(3),Y(17),SY(17)
      DIMENSION IOCT(17),NOCT(17),SFACT(17),NOCTG(3),SQY(17),CY(17)
      DIMENSION IXBAR(12),IZRO(1)
      DATA IOCT/17*-15/
      DATA SFACT/223.9627,-223.9627,223.9627, 28449.,28449.,28449.,
     +           28449.,3275.2,172.3789,25194.,28.33048,-28.33048,
     +           -28.33048, 998.284,512.,512.,512./
      DATA IACE/170000/,ILOS/70000/,IFIRE/30000/,IABC/50000/
      NOD=108
      WRITE(NOD,104)
  104 FORMAT(1H1)
      K=57.295780
C
C     INITIAL POSITION RELATIVE TO TARGET AND SPEED
      D1=-10000.
      D2=0.
      D3=500.
      V=200.
C
C     INITIAL RANGE ESTIMATE FOR TRANSFER TO LOS ESTIMATOR
      REST=5.92944
      REST=REST+1.5
C
C     INITIAL CRAFT ATTITUDE AS EULER ANGLES - YAW,PITCH,ROLL
      A1=-.1745
      A2=-.08821
      A3=0.
      P=0.
      Q=0.
      R=0.
      SAVE1=0.
      SAVE2=0.
      SAVE3=0.
C
C     CONSTANTS DEFINING THE PATH
      T1=22.5
      T2=3.
      R4=-.05
      R5=.05
      R6=4.02
      C=.05
C
C     COMPUTATION OF INITIAL ANGLE OF ATTACK AND RESOLVED SPEED
      A4=(-2.103E-2*V +8.32E-5*V**2 -5.22E-7*V**3)/K
      V1=V*COS(A4)
      V2=0.
      V3=-V*SIN(A4)
C
C     INITIALIZE AND DEFINE FINAL ITERATION
      IZRO(1)=0
      T=0.
      T3=0.
      TT3=1./2.
      TT3=1./20.
      ITER=0
      ITERP=0
      ITERF=900
C
C     ESTABLISH OUTPUT MODE AND PRINTOUT ITERATIONS
C         MODE 1 - PRINT EVERY 1/2 SECOND, NO OCTAL OUTPUTS
C         MODE 2 - PRINT EVERY ITERATION FROM IP1 TO IP2, WITH OCTAL
C         MODE 3 - PRINT EVERY 1/2 SECOND, PBPATH OUTPUTS ONLY
      MODE=1
      MODE=3
      MODE=2
C     UNDER MODE 2  M2T=0 - NO TAPE, M2T=1 - CDC TAPE, M2T=2 - BINARY TAPE
      M2T=2
      M2T=0
      M2T=1
      IP1=629
      IP2=900
      ITPP=1
      ITPP=15
      ITPP=30
C
C     ESTABLISH FRAMES FOR SYSTEM MODE CHANGES (DISCRETES CHANGE)
      ID1=629
      ID2=630
      ID3=719
      ID4=720
      ID5=721
      ID6=809
      ID7=810
      ID8=840
      ID9=900
C
C     IF M2T=2 PUNCH INITIALIZING VALUES FOR A/D AND GYROS
      IF(M2T.NE.2)GO TO 1050
      QY(1)=2.7862
      QY(2)=0.
      QY(3)=-32.0768
      QY(4)=-.088298
      QY(5)=.996029
      QY(6)=0.
      QY(7)=.299965
      QY(8)=14.4416
      QY(9)=286.985
      QY(10)=.325157
      QY(11)=958.967
      QY(12)=-282.946
      QY(13)=3.389
      QY(14)=5.610
      QY(15)=0.
      QY(16)=0.
      QY(17)=0.
      WRITE(104) QY
 1050 CONTINUE
C
C     IF M2T=1 PUNCH INITIALIZING VALUES FOR A/D AND GYROS IN OCTAL
      IF(M2T.NE.1) GO TO 1100
      NOCT(1)=176620
      NOCT(2)=000000
      NOCT(3)=016020
      NOCT(4)=173060
      NOCT(5)=067260
      NOCT(6)=000000
      NOCT(7)=067440
      NOCT(8)=066000
      NOCT(9)=022100
      NOCT(10)=020000
      NOCT(11)=065040
      NOCT(12)=017520
      NOCT(13)=177640
      NOCT(14)=012740
      NOCTG(1)=0
      NOCTG(2)=0
      NOCTG(3)=0
C     THIS PART OF TAPE IS TO BE LOADED BEFORE STARTING CDC INITIALIZING.
      CALL CDCTO(014514,NOCT,14,17)
      CALL CDCTO(000225,NOCTG,3,3)
      CALL CDCTO(021212,IZRO,1,1)
C
C     IF M2T=1 PUNCH INITIAL XBAR VALUES TO BE READ ALONG WITH THE
C     FIRST FRAME'S SET OF A/D AND GYROS WHICH WILL BE PUNCHED LATER.
      IXBAR(1)=0
      IXBAR(2)=0
      IXBAR(3)=0
      IXBAR(4)=0
      IXBAR(5)=0
      IXBAR(6)=0
      IXBAR(7)=61766
      IXBAR(8)=0
      IXBAR(9)=4644
      IXBAR(10)=172366
      IXBAR(11)=0
      IXBAR(12)=76203
      CALL CDCTO(014550,IXBAR,12,12)
 1100 CONTINUE
C
C     START TIME LOOP
C       INITIAL ITERATION WITH DELTA T ZERO IS TO OUTPUT INITIAL VALUES
C
C     ESTABLISH MANEUVER FACTOR
 1150 F=0.
      T=ITER*T3+.0001
      IF(T.LT.T1) GO TO 1200
      F=1.-EXP(-(T-T1)**2/T2)
      IF(T.LT.(T1+10)) GO TO 1200
      F=F-(1.-EXP(-(T-T1-10.)**2/T2))
C
C     COMPUTE EULER ANGLE RATES FROM PREVIOUS CRAFT RATES AND ATTITUDES
 1200 CONTINUE
 1220 R1=-R*COS(A3)/COS(A2)-Q*SIN(A3)/COS(A2)
      R2=-Q*COS(A3)+R*SIN(A3)
      R3=P-(Q*SIN(A3)+R*COS(A3))*SIN(A2)/COS(A2)
 1230 CONTINUE
C
C     INTEGRATE TO GET EULER ANGLES AT END OF TIME STEP
      A1=A1+R1*T3
      A2=A2+R2*T3
      A3=A3+R3*T3
C
```

```
C     SAVE VEHICLE AXIS RATES EXISTING AT START OF TIME STEP
      PST=P
      QST=Q
      RST=R
C
C     RESOLVE CRAFT VELOCITIES AT START OF TIME STEP TO EARTH AXES
      U1=X1*V1+X3*V3
      U2=Y1*V1+Y3*V3
      U3=Z1*V1+Z3*V3
C
C     INTEGRATE VELOCITIES TO GET POSITIONS AT END OF TIME STEP
      D1=D1+U1*T3
      D2=D2+U2*T3
      D3=D3+U3*T3
C
C     COMPUTE LOS RANGE AND DIRECTION COSINES/ EARTH AXES
      D=SQRT(D1**2+D2**2+D3**2)
      S1=-D1/D
      S2=-D2/D
      S3=-D3/D
C
C     INTEGRATE ACCELERATION TO GET NEW SPEED
      V=V+F*R6*T3
C
C     COMPUTE ANGLE OF ATTACK AND RESOLVE SPEED TO CRAFT AXES VELOCITIES
      A4=(-2.103E-2*V +8.32E-5*V**2 -5.22E-7*V**3)/K
      V1=V*COS(A4)
      V2=0.
      V3=-V*SIN(A4)
C
C     COMPUTE THE EARTH/CRAFT TRANSFORMATION MATRIX FOR FOR NEW ATTITUDE
      X1=COS(A1)*COS(A2)
      Y1=-SIN(A1)*COS(A2)
      Z1=SIN(A2)
      X2=SIN(A1)*COS(A3)-COS(A1)*SIN(A2)*SIN(A3)
      Y2=COS(A1)*COS(A3)+SIN(A1)*SIN(A2)*SIN(A3)
      Z2=COS(A2)*SIN(A3)
      X3=-SIN(A1)*SIN(A3)-COS(A1)*SIN(A2)*COS(A3)
      Y3=-COS(A1)*SIN(A3)+SIN(A1)*SIN(A2)*COS(A3)
      Z3=COS(A2)*COS(A3)
C
C     COMPUTE ANGLE BETWEEN LOS AND CRAFT U AXIS
      M1=S2*Z1-S3*Y1
      M2=S3*X1-S1*Z1
      M3=S1*Y1-S2*X1
      M=SQRT(M1**2+M2**2+M3**2)
      CA5=X1*S1+Y1*S2+Z1*S3
      A5=ATAN2(M,CA5)*K
C
C     COMPUTE CRAFT AXES ANGULAR RATES
      Q=F*R4
      R=F*R5
      P=-C*(R*V1+32.17*Z2)
C
C     COMPUTE LATERIAL SPECIFIC FORCE IN G'S
      F2=-Z2+(-R*V1+P*V3)/32.17
C
C     COMPUTE AND PRINT OUTPUT WHEN DESIRED
C     NOTE  THE REMAINDER OF THE PROGRAM IS OUTPUT AND DOES NOT ALTER
```

```
C      THE BASIC PATH GENERATION PROCESS IN ANY WAY.
       GO TO (1750,1740,1750,1740), MODE
 1740  IF((ITER.GE.IP1).AND.(ITER.LE.IP2)) GO TO 1760
       GO TO 2000
 1750  IF((ITER.NE.ITERP).AND.(ITER.NE.0)) GO TO 2000
       ITERP=ITERP+ITPP
 1760  CONTINUE
       X(1)=1000.*P
       X(2)=1000.*Q
       X(3)=1000.*R
       X(4)=Q*V3+F*R6*COS(A4)
       X(5)=R*V1-P*V3
       X(6)=-Q*V1-F*R6*SIN(A4)
       X(7)=V1
       X(8)=V2
       X(9)=V3
       X(10)=1000.*Z1
       X(11)=1000.*Z2
       X(12)=1000.*Z3
       X(13)=1000.*(X1*S1+Y1*S2+Z1*S3)
       X(14)=1000.*(X2*S1+Y2*S2+Z2*S3)
       X(15)=1000.*(X3*S1+Y3*S2+Z3*S3)
       X(16)=D/1000.
       A6=K*ATAN(-U2/U1)
       A7=K*ATAN(U3/SQRT(U1**2+U2**2))
C
C      OUTPUT OF PRPATH  QUANTITIES TO MATCH TABLE C-1, IF MODE 3 CHOSEN
       IF(MODE.NE.3) GO TO 1880
       WRITE(NOD,100) T,X,A5,D3,A6,A7
  100  FORMAT(F7.3,//,3F10.3,3F10.4,3F10.3,3F10.4,//,3F10.4,F10.5,F10.4,
     +        F10.2,2F10.4,/)
       GO TO 2000
C
C      COMPUTATION OF SIMULATED OBSERVATIONS
C      SEQUENCE IS A/D CHANNELS 0 - 13 THEN GYROS
 1880  DO 1900 I=1,3
       Y(I)=-X(I+3)-32.17*X(I+9)*.001
 1900  Y(I+10)=X(I+12)
       Y(4)=SIN(A2)
       Y(5)=COS(A2)
       Y(6)=SIN(A3)
       Y(7)=COS(A3)
       Y(8)=14.694-.0004965*D3
       Y(9)=273.+15.-.001981*D3
       Y(10)=8.257E-6*EXP(-D3/33000.)*V**2
       Y(14)=REST
C
C      COMPUTE GYRO ANGLES INCLUDING RESIDUE FROM PREVIOUS DIGITAL VALUE
       Y(15)=PST*T3*1000.+SAVE1
       Y(16)=QST*T3*1000.+SAVE2
       Y(17)=RST*T3*1000.+SAVE3
       GT1=PST*T3*1000.
       GT2=QST*T3*1000.
       GT3=RST*T3*1000.
C
C      AT ABC INSERT IMPACT COSINES X 1000
       IF(ITER.NE.810) GO TO 1905
       Y(11)=840.053
       Y(12)=-468.636
```

```
      Y(13)=-273.298
 1905 CONTINUE
C
C     CHECK THAT COMPUTED STATIC AND DYNAMIC PRESSURES AND ABSOLUTE
C     TEMPERATURE GIVE THE DESIRED AIRSPEED.   STANDARD DAY ASSUMED.
      VCK=SQRT(6177.6*Y(9)*Y(10)/Y(8))
C
C     SCALE TO COMPUTER INPUT SCALING FOR SIMULATING OBSERVATION INPUTS
      DO 1910 I=1,17
 1910 SY(I)=Y(I)*SFACT(I)
      SY(8)=SY(8)-19651.2
      SY(9)=SY(9)-40190.15
C
C     OUTPUT OBSERVATIONS IF MODE 1 OR 2
 1930 WRITE(MOD,102) T,(Y(I),I=1,10)
  102 FORMAT(F7.3,3F11.4,4F11.6,F11.4,F11.3,F11.6   )
C
C     CALCULATE OCTAL AND QUANTITIZED DECIMAL IF IN MODE 2
      IF(MODE.NE.2) GO TO 1950
      DO 1940 I=1,17
      CALL BSOCT(SY(I),IOCT(I),NOCT(I))
C
C     FORCE THE 4 LOW ORDER BITS TO ZERO TO SIMULATE THE RESULT OF
C     THE 11BIT A/D AND THE WAY DATA IS TRANSFERED TO THE CDC CORE.
      NOCT(I)=NOCT(I)/10*10
      IOCT2=NOCT(I)/10-NOCT(I)/100*10
      IF((FLOAT(IOCT2/2)).NE.(FLOAT(IOCT2)/2.)) NOCT(I)=NOCT(I)-10
 1940 CONTINUE
C
C     CONVERT OCTAL BACK TO DECIMAL AND REVERSE SCALING PROCESS
      DO 1942 I=1,17
 1942 CALL SOCTD(NOCT(I),IOCT(I),SQY(I))
      SQY(8)=SQY(8)+19651.2
      SQY(9)=SQY(9)+40190.15
      DO 1944 I=1,17
 1944 QY(I)=SQY(I)/SFACT(I)
C
C     WRITE A/D SCALED DECIMAL, B-15 SCALED OCTAL AND QUANTITIZED DECIMAL
      WRITE(MOD,118) (SY(I), I=1,10)
  118 FORMAT(7X,10F11.0  )
      WRITE(MOD,106) (NOCT(I),IOCT(I), I=1,10)
  106 FORMAT(7X,10(I8,I3))
      WRITE(MOD,122) (QY(I),I=1,10)
  122 FORMAT(7X,3F11.4,4F11.6,F11.4,F11.3,F11.6,/)
C
C     SAVE DIFERENCE BETWEEN GYRO ANGLE AND DIGITAL REPRESENTATION.
      SAVE1=Y(15)-QY(15)
      SAVE2=Y(16)-QY(16)
      SAVE3=Y(17)-QY(17)
C
C     WRITE SECOND PART OF OUTPUT INCLUDING DISCRETES AND VELOCITY CHECK
      IF(ITER.EQ.ID1) IDESC=IACE
      IF((ITER.GE.ID2).AND.(ITER.LE.ID3)) IDESC=ILOS
      IF(ITER.EQ.ID4) IDESC=IFIRE
      IF((ITER.GE.ID5).AND.(ITER.LE.ID6)) IDESC=ILOS
      IF(ITER.EQ.ID7) IDESC=IABC
      IF((ITER.GE.ID8).AND.(ITER.LE.ID9)) IDESC=ILOS
 1950 WRITE(MOD,108) (Y(I), I=11,17),IDESC,V,VCK
  108 FORMAT(7X,3F11.3,F11.3,3F11.4,I11,2F11.3   )
```

```
      IF(MODE.EQ.2) WRITE(NOD,120) (SY(I), I=11,17)
  120 FORMAT(7X,7F11.0   )
      IF(MODE.EQ.2) WRITE(NOD,110) (NOCT(I),IOCT(I), I=11,17)
  110 FORMAT(7X,7(I8,I3))
      IF(MODE.EQ.2) WRITE(NOD,124) (GY(I),I=11,17) ,GT1,GT2,GT3
  124 FORMAT(7X,3F11.3,F11.3,4F11.4,/)
C
C     IF MODE 2 AND M2T=2  PUNCH BINARY TAPE FOR INPUT TO A/C E[illegible]OR
      IF(M2T.NE.2) GO TO 1955
      WRITE(104) GY
      GO TO 2000
C
C     IF MODE 2 AND M2T=1 PUNCH CDC TAPE TO SIMULATE A/D, GYROS,AND DISCRETES
 1955 IF(M2T.NE.1) GO TO 2000
      DO 1960 I=1,3
 1960 NOCTG(I)=NOCT(I+14)
      CALL CDCTO (014514,NOCT,14,17)
      CALL CDCTO (000225,NOCTG,3,3)
      CALL CDCTO(000247,IDFSC,1,1)
      CALL CDCTO(021212,IZRO,1,1)
C     NOTE ADDRESS 021212 IS USED TO STOP THE TAPE WHEN READ.
C
C     UPDATE ITERATION COUNT, SET T3 TO TRUE T3 AFTER ITERATION ZERO
 2000 ITER=ITER+1
      IF(ITER.EQ.1) T3=TT3
      IF(ITER.LE.ITERF) GO TO 1150
      WRITE(NOD,104)
      STOP
      END
C     SUBROUTINE TO CONVERT DECIMAL NUMBERS TO OCTAL WITH A SPECIFIED
C     BINARY POINT SCALING.  THIS VERSION FOR 16 BIT FRACTIONAL BINARY.
C     SCALING CONVENTION IS N = BINARY POINT LEFT  SHIFT WHEN CONVERTING
C     SCALED VALUES TO NON SCALED VALUES.       1/20/76    REM
C
      SUBROUTINE BSOCT(DD,N,NOCT)
      INTEGER DIGIT(7),NUM(7)
      D=DD
C     SAVE SIGN
      ISGN=SIGN(1.,D)
C     SCALE
      D=AINT(ABS(D)*FLOAT(2**(18+N))+0.5)
      IF(D .GE. 262144.) GO TO 40
C     FIND OCTAL DIGITS
      DO 10 I=1,6
      DIGIT(I)=AMOD(D,8.)
   10 D=AINT(D/8.)
C     ROUND
      IF(DIGIT(1) .LE. 4) GO TO 20
      DIGIT(2)=DIGIT(2)+1
      DO 15 I=2,6
            IF(DIGIT(I) .LE. 7) GO TO 20
      DIGIT(I)=0
   15 DIGIT(I+1)=DIGIT(I+1)+1
C     COMPLEMENT IF NEGATIVE
   20 IF(ISGN .EQ. 1) GO TO 30
      DO 22 I=3,6
   22 NUM(I)=7
      DO 24 I=2,6
      MI=I
      IF(DIGIT(I) .NE. 0) GO TO 26
   24 NUM(I)=0
      GO TO 30
   26 NUM(I)=8
      DO 28 I=2,6
   28 DIGIT(I)=NUM(I)-DIGIT(I)
      DIGIT(7)=1
      GO TO 32
C     CONVERT DIGITS TO INTEGER NUMBER
   30 DIGIT(7)=0
   32 NOCT=0
      DO 34 I=2,7
   34 NOCT=NOCT+DIGIT(I)*10**(I-2)
      RETURN
   40 IF(ISGN .NE. 1) GO TO 45
      NOCT=77777
      RETURN
   45 NOCT=100000
      RETURN
      END
C     SUBROUTINE TO CONVERT SCALED OCTAL TO DECIMAL   5/9/76   KEP
      SUBROUTINE SOCTD(NOCT,N,DD)
C
C     RENAME OCTAL NUMBER TO AVOID RETURNING AN ALTERED VALUE
      MOCT=NOCT
C     COMPLEMENT BACK IF NEGATIVE
      IF(MOCT.LE.77777) GO TO 48
      NUMC=177777
      DO 45 J=1,5
      IF((MOCT/10**(J-1) -MOCT/(10**J)*10).NE.0) GO TO 46
   45 NUMC=NUMC-7*10**(J-1)
      DD=-32768.
      GO TO 50
   46 NUMC=NUMC+10**(J-1)
      MOCT=-(NUMC-MOCT)
C     CONVERT TO DECIMAL AND REVERSE BINARY SCALING
   48 DD=0.
      DO 49 J=1,5
   49 DD=DD+FL   ((MOCT/10**(J-1)-MOCT/(10**J)*10)*8**(J-1))
   50 DD=DD/2**(15+N)
      RETURN
      END
C     SUBROUTINE TO PUNCH TAPE TO LOAD CDC CLFCS COMPUTER   4/22/76  RLA
C     EACH CALL LOADS ONE ARRAY,STARTING AT A GIVEN ADDRESS THEN SIGNALS
C     THE READER TO STOP. A 10 SPACE LEADER WILL OCCUR BETWEEN CALLS.
      SUBROUTINE CDCTO (IADDR,IOCT,N,MAXD)
      DIMENSION IOCT(MAXD),IBUF(555),IHEX(4)
      DATA IBUF(1) /8Z80808080/, IBUF(2) /8Z808080FF/,ISTOP /8Z8F808080/
C     LOAD LEADER WORD AND START ADDRESS TRIGGER VIA DATA STATEMENT
      I=3
      NOCT=IADDR
C     MODIFY AND LOAD INTO OUTPUT VECTOR THE ADDRESS, THEN DATA
C         CONVERT OCTAL INTO DECIMAL
    4 NDEC=0
      DO 6 J=1,6
      IF(NOCT.EQ.0) GO TO 8
      NDEC=NDEC+(NOCT-NOCT/10*10)*8**(J-1)
    6 NOCT=NOCT/10
    8 CONTINUE
```

```
C           CONVERT DECIMAL TO HEX ELEMENTS AND ADD BIT IN 5TH PLACE
C           WHEN NOT 1,2,3 OR 4 TO GIVE BLIND CODE.
      DO 10 J=1,4
      IHEX(J)=MOD(NDEC,16)
      IF((IHEX(J).EQ.0).OR.(IHEX(J).GT.4)) IHEX(J)=IHEX(J)+16
   10 NDEC=NDEC/16
C           SHIFT HEX AND COMBINE
      IBUF(I)=IHEX(1)+ISL(IHEX(2),8)+ISL(IHEX(3),16)+ISL(IHEX(4),24)
C           OR IN THE CONSTANT MASK BITS TO COMPLETE BLIND CODE
      IBUF(I)=IOR(IBUF(I),IBUF(1))
C     INCREMENT COUNTER AND TEST FOR LAST OF DATA
      I=I+1
      IF(I-4-N) 20,22,22
   20 NOCT=IOCT(I-3)
      GO TO 4
   22 IBUF(I)=ISTOP
C     DUMP OUTPUT ON TAPE
      CALL BUFFOUT(104,1,IBUF,I)
   30 CALL ICHECK(104,IND)
      IF(IND.NE.2) GO TO 30
      RETURN
      END
```

APPENDIX D

OPEN AND CLOSED LOOP FIRE CONTROL SIMULATION

For the purpose of verifying the accuracy of the open and closed loop fire control algorithms presented in Sections 2.5 and 2.6, it was necessary to generate the fire control solutions arising from ideal state variable input conditions, as well as from input conditions incorporating selected bias errors. The time shared computer programs "GQGUN" and "GQHIT", whose listing appears on the following pages, were prepared for this purpose.

Also included in this appendix is a set of operating instructions particular to loading the paper tape generated from TPATH (see Appendix C) and recording selected data for acceptance test.

OPERATING INSTRUCTIONS FOR SOFTWARE DEMONSTRATION

1. Load program tape (S.A. = 7237) and load any system patch tapes (S.A. = 7314_8).
2. Key in:

ADDR	INST		
010445	043247	Discretes	
011633	007700	Gyros	
010433	007700	A/D	
010444	007700	A/D	
011657	000400		
011660	013720		
013720	042625	LDR	225, 5
013721	062430	STR	30, 5
013722	042626	LDR	226, 5
013723	062431	STR	31, 5
013724	042627	LDR	227, 5
013725	062432	STR	32, 5
013726	047420	LDR	TEMP, 17B
013727	000017	RTN	17B

```
ADDR      INST
007343    010143 ⎫ Loader Jmp
007143    000400 ⎬ to Start of
007144    010400 ⎭ Main Prog.
011453    042756   LDR    356, 5  ⎫
011454    002420   DJP    $, 5    ⎬     dec. counter
011455    062756   STR    356, 5  ⎭
011456    000105   NZS
011457    010057   ENP    *
011460    000400 ⎫
011461    007314 ⎭  Jmp to Loader
000304    025004   KTF  ≈  1/3
007353    010326
007475    020436   MUL SGX,1
007476    060625   STR GYRO X, 1
007501    020437   MUL SGY, 1
007502    060626   STR GYRO Y, 1
```

3. Read (single step mode) the initialization block of test tape (STOP CODE = R1 = 021212).
    a. execute (single step) program locations 10436_8 to 10317_8, 10322_8 - 10326_8.
4. Read and execute 92_{10} (134_8) blocks of data = FIRE time (T = 24).
    a. enter 134_8 in loc. 356_8
    b. enter 7314_8 in program counter (location 0)
    c. Run - tape stops after 92nd frame is executed
    d. step mode - record data
5. Read and execute 90_{10} (132_8) blocks of data - ABC time (T = 27)
    a. enter 132_8 in location 356_8
    b. enter 7314_8 in program counter (location 0)
    c. run mode - tape stops after 90th frame executed
    d. step mode - record data

6. Read and execute 30_{10} (36_8) blocks of data - Release ABC (last ABC frame = T = 27.967) time (T = 28.000).
   a. enter 37_8 in location 356_8
   b. enter 7314_8 in program counter (location 0)
   c. run mode - tape stops after $\underline{37_8}^{th}$ frame executed
   d. stop mode - record data

7. Read and execute 11_{10} (13_8) blocks of data - end of recursion.
   a. enter 13_8 in location 356_8
   b. enter 7314_8 in program counter (location 0)
   c. run mode - tape stops after $\underline{13_8}^{th}$ frame executed
   d. stop mode - record data

8. Read and execute 49_{10} (61_8) blocks of data - calibrated fire (T = 30)
   a. enter $\underline{61}$ in location 356_8
   b. enter 7314_8 in program counter (location 0)
   c. run mode - tape stops after $\underline{61}^{st}$ frame executed
   d. step mode - record data

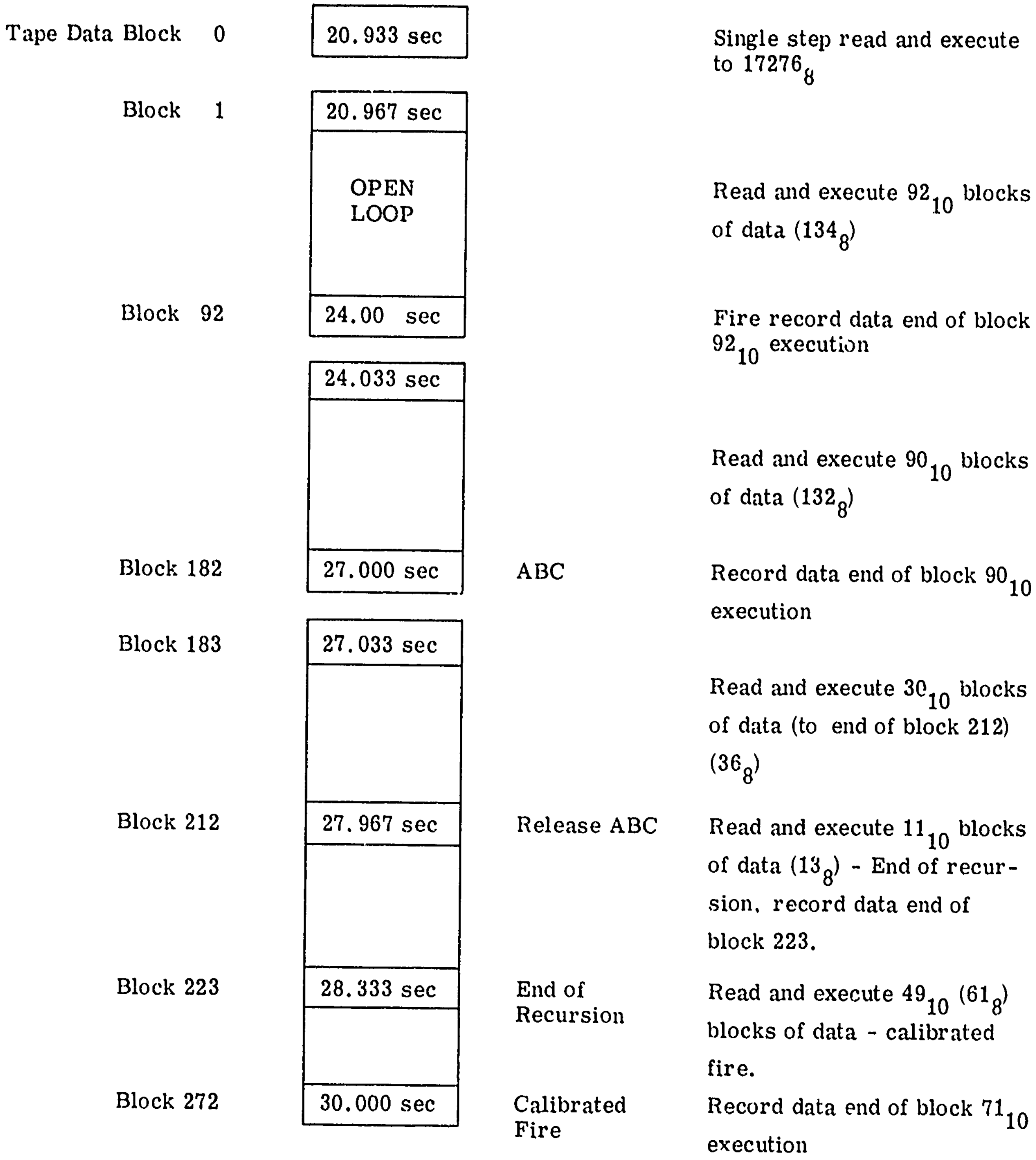

Tape Data Block 0	20.933 sec		Single step read and execute to 17276_8
Block 1	20.967 sec OPEN LOOP		Read and execute 92_{10} blocks of data (134_8)
Block 92	24.00 sec		Fire record data end of block 92_{10} execution
	24.033 sec		Read and execute 90_{10} blocks of data (132_8)
Block 182	27.000 sec	ABC	Record data end of block 90_{10} execution
Block 183	27.033 sec		Read and execute 30_{10} blocks of data (to end of block 212) (36_8)
Block 212	27.967 sec	Release ABC	Read and execute 11_{10} blocks of data (13_8) - End of recursion, record data end of block 223.
Block 223	28.333 sec	End of Recursion	Read and execute 49_{10} (61_8) blocks of data - calibrated fire.
Block 272	30.000 sec	Calibrated Fire	Record data end of block 71_{10} execution

Figure D-1. Outline of Software Test

```
GOGUN       08:57EST     11/23/76

1000 REM CLOSED LOOP FIRE CONTROL ANALYSIS PROGRAM
1010 REM INCORPORATES M-56 BALLISTICS - P.BRIGGS - 7/8/76
1020 READ P5, A6, A7
1030 S4=0
1040 S5=0
1050 S6=0
1060 B4=0
1070 B5=0
1080 B6=0
1090 PRINT "FIRST FIRING CONDITION"
1100 PRINT
1110 READ B, C1, C2, Q1, Q2
1120 READ A1, A2, A3
1130 READ V1, V2, V3
1140 READ P1, P2, P3
1150 GOSUB 2530
1160 P7=SQR(P1^2+P2^2+P3^2)
1170 S1=-(X1*P1+Y1*P2+Z1*P3)/P7
1180 S2=-(X2*P1+Y2*P2+Z2*P3)/P7
1190 S3=-(X3*P1+Y3*P2+Z3*P3)/P7
1200 V7=-(V1*S1+V2*S2+V3*S3)
1210 C3=(C1/2)*C2*SQR(B-V7)
1220 T1=(P5+P7)/((B-V7)-C3*(P5+P7))
1230 Q=Q1-Q2*C2*T1
1240 P6=(Q/2)*(T1^2)
1250 C4=Q*T1*(1+C3*T1)/(2*B)
1260 G1=S1+C4*Z1-(V1+V7*S1)/B
1265 D1=G1-S1
1270 G2=S2+C4*Z2-(V2+V7*S2)/B
1275 D2=G2-S2
1280 G3=S3+C4*Z3-(V3+V7*S3)/B
1285 D3=G3-S3
1290 C5=1/SQR(G1^2+G2^2+G3^2)
1300 G1=C5*G1
1310 G2=C5*G2
1320 G3=C5*G3
1330 PRINT "OPEN LOOP FIRE CONTROL DATA"
1340 PRINT "TARGET SIGHTLINE DIRECTION COSINES:"
1350 PRINT "SU="; S1; "RAD"
1360 PRINT "SV="; S2; "RAD"
1370 PRINT "SW="; S3; "RAD"
1380 PRINT "EST RANGE="; P5+P7; "FT"
1390 PRINT "EST RANGE-RATE="; V7; "FT/SEC"
1400 PRINT "DRAG COEF="; C3; "1/SEC"
1410 PRINT "EST TF="; T1; "SEC"
1420 PRINT "EST GRAV DROP="; P6; "FT"
1421 PRINT "COMPUTED LEAD ANG."
1422 PRINT "DU="; D1
1423 PRINT "DV="; D2
1424 PRINT "DW="; D3
1430 PRINT "COMPUTED GUNLINE DIRECTION COSINES:"
1440 PRINT "GU="; G1; "RAD"
1450 PRINT "GV="; G2; "RAD"
1460 PRINT "GW="; G3; "RAD"
1470 A4=ATN(G3/SQR(G1^2+G2^2))
1480 A5=ATN(-G2/G1)
1490 PRINT "GUN ELEV="; A4; "RAD"
1500 PRINT "GUN TRAIN="; A5; "RAD"
1510 PRINT
```

```
1520 U1=X1*V1+X2*V2+X3*V3
1530 U2=Y1*V1+Y2*V2+Y3*V3
1540 U3=Z1*V1+Z2*V2+Z3*V3
1550 V1=U1
1560 V2=U2
1570 V3=U3
1580 IF ABS(S4)>.1 THEN 1640
1590 U1=0
1600 U2=0
1610 U3=0
1620 U4=0
1630 GO TO 1680
1640 U1=ATN(S6/SQR(S4^2+S5^2))
1650 U2=ATN(S5/SQR(S4^2+S5^2))
1660 U3=ATN(-S5/S4)
1670 U4=ATN(-B5/B4)
1680 A4=A4+A6+U1-U2
1690 A5=A5+A7+U3-U4
1700 S1=COS(A4)*COS(A5)
1710 S2=-COS(A4)*SIN(A5)
1720 S3=SIN(A4)
1730 IF ABS(S4)<.1 THEN 1840
1740 PRINT "CLOSED LOOP FIRE CONTROL DATA"
1750 PRINT "ES="; U1; "RAD"
1760 PRINT "ER="; U2; "RAD"
1770 PRINT "TS="; U3; "RAD"
1780 PRINT "TR="; U4; "RAD"
1790 PRINT "ELEV CORRECTION="; U1-U2; "RAD"
1800 PRINT "TRAIN CORRECTION="; U3-U4; "RAD"
1810 PRINT "CORRECTED GUN ELEV="; A4; "RAD"
1820 PRINT "CORRECTED GUN TRAIN="; A5; "RAD"
1830 PRINT
1840 GOSUB 2630
1850 V=V1*S1+V2*S2+V3*S3
1860 C3=(C1/2)*C2*SQR(B+V)
1870 T1=.5
1880 T2=.1
1890 PRINT "STRIKEPOINT DATA"
1900 T1=T1+T2
1910 D=D1-D2*C2*T1
1920 R=1/(1+C3*T1)
1930 B1=R*(B*S1+V1)*T1
1940 B2=R*(B*S2+V2)*T1
1950 B3=R*(B*S3+V3)*T1-(D/2)*(T1^2)
1960 B7=SQR(B1^2+B2^2+B3^2)
1970 IF ABS(B3+P3)>.1 THEN 2150
1980 PRINT "ACTUAL TF="; T1; "SEC"
1990 PRINT "DBX="; B1+P1; "FT"
2000 PRINT "DBY="; B2+P2; "FT"
2010 PRINT "DBZ="; B3+P3; "FT"
2020 B4=(X1*B1+Y1*B2+Z1*B3)/B7
2030 B5=(X2*B1+Y2*B2+Z2*B3)/B7
2040 B6=(X3*B1+Y3*B2+Z3*B3)/B7
2050 PRINT
2060 PRINT "HORIZ MISS="; SQR((B1+P1)^2+(B2+P2)^2); "FT"
2070 PRINT
2080 H1=S2*B6-S3*B5
2090 H2=S3*B4-S1*B6
2100 H3=S1*B5-S2*B4
2110 H4=H1^2+H2^2+H3^2
2120 H5=(1+H4)*SQR(H4)
2130 PRINT "ANGULAR MISS="; 1000*ATN(H5); "MRAD"
2140 PRINT
2150 IF ABS(B3+P3)<.1 THEN 2210
2160 IF (B3+P3)>0 THEN 1900
2170 T1=T1-T2
```

```
2180 T2=.1*T2
2190 IF T2<1E-6 THEN 2520
2200 GO TO 1900
2210 D1=B1+P1
2220 D2=B2+P2
2230 D3=B3+P3
2240 READ P1, P2, P3
2250 IF P1=0 THEN 2520
2260 B1=-P1+D1
2270 B2=-P2+D2
2280 B3=-P3+D3
2290 B7=SQR(B1^2+B2^2+B3^2)
2300 READ A1, A2, A3
2310 GOSUB 2530
2320 H1=(X1*B1+Y1*B2+Z1*B3)/B7
2330 H2=(X2*B1+Y2*B2+Z2*B3)/B7
2340 H3=(X3*B1+Y3*B2+Z3*B3)/B7
2350 PRINT "STRIKEPOINT OBSERVATION DATA"
2360 READ S4, S5, S6
2370 PRINT "TARGET SIGHTLINE DIRECTION COSINES:"
2380 PRINT "SH="; S4; "RAD"
2390 PRINT "SV="; S5; "RAD"
2400 PRINT "SW="; S6; "RAD"
2410 PRINT "STRIKEPOINT SIGHTLINE DIRECTION COSINES:"
2420 PRINT "BH="; H1; "RAD"
2430 PRINT "BV="; H2; "RAD"
2440 PRINT "BW="; H3; "RAD"
2450 PRINT
2460 PRINT "SECOND FIRING CONDITION"
2470 PRINT
2480 B4=H1
2490 B5=H2
2500 B6=H3
2510 GO TO 1110
2520 STOP
2530 X1=COS(A1)*COS(A2)
2540 Y1=-SIN(A1)*COS(A2)
2550 Z1=SIN(A2)
2560 X2=SIN(A1)*COS(A3)-COS(A1)*SIN(A2)*SIN(A3)
2570 Y2=COS(A1)*COS(A3)+SIN(A1)*SIN(A2)*SIN(A3)
2580 Z2=COS(A2)*SIN(A3)
2590 X3=-SIN(A1)*SIN(A3)-COS(A1)*SIN(A2)*COS(A3)
2600 Y3=-COS(A1)*SIN(A3)+SIN(A1)*SIN(A2)*COS(A3)
2610 Z3=COS(A2)*COS(A3)
2620 RETURN
2630 H1=X1*G1+X2*G2+X3*G3
2640 H2=Y1*G1+Y2*G2+Y3*G3
2650 H3=Z1*G1+Z2*G2+Z3*G3
2660 G1=H1
2670 G2=H2
2680 G3=H3
2690 RETURN
2700 DATA 0.,0.,0.
2710 DATA 3320, .0104, .98541, 27.6476, .176772
2720 DATA -.139954, -.074149, -.086737
2730 DATA 200.4541, 0, 17.9523
2740 DATA -5272.016, 835.125, 501.160
2750 DATA -4680.559, 1007.375, 540.543
2760 DATA -.350779, .021910, -.321706
2770 DATA .838627,-.460672,-.290665
2780 DATA 3320, .0104, .98114, 27.6476, .176772
2790 DATA -.542697, .113263, -.354657
2800 DATA 222.646, 0, 24.0967
2810 DATA -4110.242, 1305.873, 649.375
2820 DATA 0, 0, 0
2830 END
```

```
GOHIT        09:03EST     11/23/76

1000 REM CLOSED LOOP FIRE CONTROL ANALYSIS PROGRAM
1010 REM INCORPORATES M-56 BALLISTICS - R.BRIGGS - 7/3/75
1020 READ P5, A6, A7
1030 S1=0
1040 S5=0
1050 S5=0
1060 R1=0
1070 B5=0
1080 B5=0
1090 PRINT "FIRST FIRING CONDITION"
1100 PRINT
1110 READ B, C1, C2, D1, D2
1120 READ A1, A2, A3
1130 READ V1, V2, V3
1140 READ P1, P2, P3
1150 GOSUB 2530
1160 P7=SQR(P1^2+P2^2+P3^2)
1170 S1=-(X1*P1+Y1*P2+Z1*P3)/P7
1180 S2=-(X2*P1+Y2*P2+Z2*P3)/P7
1190 S3=-(X3*P1+Y3*P2+Z3*P3)/P7
1200 V7=-(V1*S1+V2*S2+V3*S3)
1210 C3=(C1/2)*C2*SQR(B-V7)
1220 T1=(P5+P7)/((B-V7)-C3*(P5+P7))
1230 D=D1-D2*C2*T1
1240 P6=(D/2)*(T1^2)
1250 G1=D*T1*(1+C3*T1)/(2*B)
1260 READ G1,G2,G3
1270 READ E,T
1280 C5=1/SQR(G1^2+G2^2+G3^2)
1300 G1=C5*G1
1310 G2=C5*G2
1320 G3=C5*G3
1330 PRINT "OPEN LOOP FIRE CONTROL DATA"
1430 PRINT "COC 469 COMPUTED GUN ORDERS:"
1440 PRINT "GU="; G1; "RAD"
1450 PRINT "GV="; G2; "RAD"
1460 PRINT "GW="; G3; "RAD"
1470 A4=ATN(G3/SQR(G1^2+G2^2))
1480 A5=ATN(-G2/G1)
1481 A4=A4+A6+E
1482 A5=A5+A7+T
1483 G1=COS(A4)*COS(A5)
1484 G2=-COS(A4)*SIN(A5)
1485 G3=SIN(A4)
1490 PRINT "GUN ELEV="; A4; "RAD"
1500 PRINT "GUN TRAIN="; A5; "RAD"
1510 PRINT
1520 U1=X1*V1+X2*V2+X3*V3
1530 U2=Y1*V1+Y2*V2+Y3*V3
1540 U3=Z1*V1+Z2*V2+Z3*V3
1550 V1=U1
1560 V2=U2
1570 V3=U3
1580 H1=0
1600 H2=0
1610 H3=0
1620 J1=0
1630 PRINT
1640 GOSUB 2630
```

```
1850 V=V1*G1+V2*G2+V3*G3
1860 C3=(C1/2)*C2*SQR(B+V)
1870 T1=.5
1880 T2=.1
1890 PRINT "STRIKEPOINT DATA"
1900 T1=T1+T2
1910 Q=Q1-Q2*C2*T1
1920 R=1/(1+C3*T1)
1930 B1=R*(B*S1+V1)*T1
1940 B2=R*(B*S2+V2)*T1
1950 B3=R*(B*S3+V3)*T1-(G/2)*(T1^2)
1960 B7=SQR(B1^2+B2^2+B3^2)
1970 IF ABS(B3+P3)>.1 THEN 2150
1980 PRINT "ACTUAL TF="; T1; "SEC"
1990 PRINT "DBX="; B1+P1; "FT"
2000 PRINT "DBY="; B2+P2; "FT"
2010 PRINT "DBZ="; B3+P3; "FT"
2020 B4=(X1*B1+Y1*B2+Z1*B3)/B7
2030 B5=(X2*B1+Y2*B2+Z2*B3)/B7
2040 B6=(X3*B1+Y3*B2+Z3*B3)/B7
2050 PRINT
2060 PRINT "HORIZ MISS="; SQR((B1+P1)^2+(B2+P2)^2); "FT"
2070 PRINT
2080 H1=S2*B6-S3*B5
2090 H2=S3*B4-S1*B6
2100 H3=S1*B5-S2*B4
2110 H4=H1^2+H2^2+H3^2
2120 H5=(1+H1)*SQR(H4)
2130 PRINT "ANGULAR MISS="; 1000*ATN(H5); "(RAD)"
2140 PRINT
2150 IF ABS(B3+P3)<.1 THEN 2210
2160 IF (B3+P3)>0 THEN 1900
2170 T1=T1-T2
2180 T2=.1*T2
2190 IF T2<1E-5 THEN 2520
2200 GO TO 1900
2210 D1=B1+P1
2220 D2=B2+P2
2230 D3=B3+P3
2240 READ P1, P2, P3
2250 IF P1=0 THEN 2520
2260 B1=-P1+D1
2270 B2=-P2+D2
2280 B3=-P3+D3
2290 B7=SQR(B1^2+B2^2+B3^2)
2300 READ A1, A2, A3
2310 GOSUB 2530
2320 H1=(X1*B1+Y1*B2+Z1*B3)/B7
2330 H2=(X2*B1+Y2*B2+Z2*B3)/B7
2340 H3=(X3*B1+Y3*B2+Z3*B3)/B7
2460 PRINT "SECOND FIRING CONDITION"
2470 PRINT
2480 B4=H1
2490 B5=H2
2500 B6=H3
2510 GO TO 1110
2520 STOP
2530 X1=COS(A1)*COS(A2)
2540 Y1=-SIN(A1)*COS(A2)
2550 Z1=SIN(A2)
2560 X2=SIN(A1)*COS(A3)-COS(A1)*SIN(A2)*SIN(A3)
2570 Y2=COS(A1)*COS(A3)+SIN(A1)*SIN(A2)*SIN(A3)
2580 Z2=COS(A2)*SIN(A3)
2590 X3=-SIN(A1)*SIN(A3)-COS(A1)*SIN(A2)*COS(A3)
2600 Y3=-COS(A1)*SIN(A3)+SIN(A1)*SIN(A2)*COS(A3)
2610 Z3=COS(A2)*COS(A3)
```

```
2520 RETURN
2530 H1=X1*G1+X2*G2+X3*G3
2540 H2=Y1*G1+Y2*G2+Y3*G3
2550 H3=Z1*G1+Z2*G2+Z3*G3
2560 G1=H1
2570 G2=H2
2580 G3=H3
2590 RETURN
2700 DATA 1075.63,.01,.01
2710 DATA 3320, .0101, .28541, 27.6476, .176772
2720 DATA -.139951, -.074149, -.036737
2730 DATA 200.4541, 0, 17.2523
2740 DATA -5272.016, 335.125, 501.160
2745 DATA .932125,-.356933,-.022962
2746 DATA 0,0
2750 DATA -4680.559, 1007.875, 510.513
2760 DATA -.350772, .021210, -.321706
2780 DATA 3320, .0101, .28111, 27.6476, .176772
2790 DATA -.512597, .113253, -.351557
2800 DATA 222.645, 0, 24.2267
2810 DATA -4110.242, 1305.373, 512.375
2815 DATA .523995,-.550731,-.159031
2816 DATA -.016303,-.006902
2820 DATA 0, 0, 0
2830 END
```

APPENDIX E
SAFETY STATEMENT

This appendix lists the CLFCS Safety Statement. Originally issued on June 17, 1976, paragraph 4, Sequence of Operations, has been modified to reflect the recently revised closed loop fire control algorithm.

1.0 INTRODUCTION

This statement is submitted to Frankford Arsenal as a supplement to the requirements of Contract DAAA25-74-C0609, so that the user will be aware of any potential hazards associated with the Closed Loop Fire Control Subsystem on the AH-1G airframe and its interface with the associated GFE equipment. It is emphasized that the contract did not require a system safety engineering program and, therefore, there is no strict relationship between this report and the other reports and documents as so stated by AR 700-51, Item 13-003.

2.0 SYSTEM DESCRIPTION

The Closed Loop Fire Control Subsystem (CLFCS) consists of:

- Computer Interface Unit (CIU)
- Inertial Measurement Unit (IMU)
- IMU Electronics Unit
- Control Panel (Pilot)
- Sensors
- Modified XM-197 Turret/Sight

The purpose of the subsystem is to provide a lead angle for gun aiming utilizing a digital computation and analog conversions within the Computer Interface Unit. The Inertial Measurement Unit and IMU Electronics Unit provide angular rates and linear accelerations to the CIU. The sensors provide environmental inputs to the CIU. In addition to the open loop fire control solution, the system also incorporates first burst strikepoint observations to make an improvement on the second burst effectiveness.

3.0 CONCLUSIONS

A potential hazard that exists in the Closed Loop Fire Control Subsystem is the possibility of the gun being misdirected relative to the line-of-sight due to an electrical failure in the Computer Interface Unit or due to improper inputs to the CIU. This hazardous condition can occur in three areas:

a. The lead angle signals of the CIU consist of three AC outputs, each of which normally varies between 6.4 VAC in-phase and 6.4 VAC out of phase, and is in sync with the system 10 VAC 400 Hz reference. Should this reference (due to shorts, etc.) appear as an output signal, it could cause the gun line to deviate from the line-of-sight by an angle up to 180°.

b. Should the sensors (including the IMU) functionally fail or if the sensors have not been turned on, the CIU will not have proper inputs, and will arrive at an improper solution for its lead angle output. A component failure in the CIU interface circuitry or in the GFE computer itself should also be placed in this category. Such a condition could tend to cause the 6.4 VAC output to oscillate slowly, perturbing the gunline within a $\pm 33^{\circ}$ envelope about the line-of-sight.

c. When the CLFCS peripheral equipment is attached to the CIU in the airframe, lead angles may be directed to the gun by hand entries directly from the console. This would result in the gun slewing to its new position, which would be within 33° of the line-of-sight.

These conditions are considered hazardous both in view of a firing situation and a ground handling situation. The gun barrel has a five foot length and the slew rate of the turret is faster than human reflexes; personal injury could result if one is within the five foot spherical radius of the turret.

Conditions (a) and (b) can be identified by running a preflight ground observation of the gun being slaved to the sight. In flight, the gun is not easily observable, and a failure may not be detected. For a close support mission, this could be a Category IV hazard. During test of the development vehicle, the range should be clear of ground personnel. Any chase ship activity should be restricted to an altitude above the test vehicle, outside any possible pointing angle of the gun.

Condition (c) can be controlled by proper use of the peripheral equipment coupled with an appropriate sequence of operations.

4.0 SEQUENCE OF OPERATIONS

The following sequence should be observed in operating the system either during ground test or for pre-flight test. The sequence simulates the exercise of the closed loop algorithm and may be used as a gross check of system operations.

a. Prior to this sequence of operations, check that all CLFCS switches are in the OFF position, in particular the ARMED and the SERVO POWER switch. Keep personnel clear of turret area. Use normal procedures to power up the DC, AC, and battery bus on the aircraft.

b. Turn on vertical reference gyro.

c. Turn on circuit breakers for the turret, sight, CIU, and IMU. Do not turn on turret SERVO POWER.

d. Place ARMED switch in SAFE position.

e. Place COMPUTER MODE switch in CLOSED LOOP position. This will apply power to the CIU and to the IMU and other sensors. The FIRE INHIBIT light will be energized by the CIU for approximately 5 seconds to allow the IMU gyro motors to get up to speed. Set RANGE potentiometer on Control Panel to 2000 meters.

f. Clear personnel from immediate turret area. Turn on turret SERVO POWER.

g. Direct sight at some point, depress ACTION. Turret should slew to the line-of-sight with the addition of a lead angle.

h. Release ACTION SWITCH.

CAUTION

DO NOT PROCEED PAST THIS POINT DURING ANY GROUND TESTING IF AMMUNITION HAS BEEN LOADED.

i. Place ARMED switch in ARMED position.

j. Select some simulated target and impact point separated by about 75 milliradians. Acquire the target and impact points with the sight and mark the respective turret positions; caution should be taken because the turret is active.

k. Acquire the target and depress ACTION. The INHIBIT FIRE light will flash momentarily until the computer has stabilized.

l. Depress FIRE momentarily and release, but continue to track the target.

m. After a preset time (time-of-flight) determined by the computer, the INHIBIT FIRE light will go on signaling the operator to break track. At this time, slew the sight to acquire the simulated impact point and depress and hold the ACQUIRE BURST CENTROID (ABC) switch.

n. Return the sight to the target and release the ABC switch. After a short period of time, the INHIBIT FIRE light will go out indicating that the computer has arrived at a closed loop solution and the turret has slewed to a new position to satisfy the revised gun orders.

o. Again taking caution with the active turret, mark the new turret position. Observe that the change in turret position relates to an amount equal and opposite to the distance from the target to the simulated impact point.

p. Release ACTION.

Once airborne, there is no automatic indication of a gun aiming error during operation. If there is any reason to suspect such a condition, it is possible to traverse the sight to a position to the side, where the gun will become observable, to check for gross errors.

5.0 FAILURE MODE ANALYSIS

While it is assumed that the probability of failure is small, no detailed analysis has been performed to date.

Failure mode (a) has never occurred in any tests made to date; the CIU has accumulated 400 hours of laboratory testing.

Failures of the type in mode (b) have occurred in three instances, none of which occurred when the turret was being driven. Two of these were in the GFE computer. The third was in the CIU interface circuitry and occurred during the early part of system test.

6.0 REFERENCES

Reference should be made to the safety statement, written in the Final Technical Report, August 1973, prepared by the General Electric Company, Burlington, Vermont, under contract number DAAF03-73-C0098.